Crown Ethers as Potential Lead(II) Specific Probes

A thesis submitted for the Degree of
Doctor of Philosophy

by

Daniela Caiazza
B.Sc.(Hons) *Flinders*

The Department of Chemistry
The University of Adelaide

March 1999

Errata

p. 10, bot. n line: should read 'The time required for the release of all the lead....'.

p. 20, line 5 from bottom: omit the word 'all'.

p. 21, top line: 'had' should be 'has'. Line 20: 'VO' should be 'VO^{2+}'.

p. 23, line 6: the definition should read '....containing oxygen and possibly also one or more nitrogen and/or sulfur atoms'.

p. 24, line 8: 'has' should be 'have'.

p. 27, line 10: omit the word 'ions'.

p. 31, line 3: 'As ligands **1** and **3-6** all contain the two....' should read 'As ligands **1**, **3** and **4** contain two....'.

p. 33, sub-heading: should read '....1(35),5(10), 6,8....'.

p. 34, sub-heading: should read '....octa-deca-2,11....'.

p.80, Equation 3.37: '$SbCl_3$' should be '$SbCl_5$' (twice).

p. 83, line 11: stability order should read '....$[Pb\mathbf{1}]^{2+} > [Pb\mathbf{2}]^{2+}$'.

p. 85, line 15: stability order should read '....$[Cd\mathbf{2}]^{2+} \approx [Cd\mathbf{1}]^{2+}$'.

p. 107, line 9: omit the word 'the'. Line 20: should read '....are directed out of the macrocyclic ring cavity'.

p.116, line 8: should read '....silver(I)-oxygen and -sulfur....'.

To Mum and Dad

Table of Contents

Abstract vi

Abbreviations vii

Declaration x

Acknowledgements xi

1 Introduction 1

1.1 Historical overview 1

1.2 Chemical and physical properties of lead 2

1.3 Toxicity of lead and its compounds 3

1.4 The biochemical and cellular aspects of lead toxicity 4

1.5 The health effects of lead poisoning 5

1.5.1 Haematological effects 5

1.5.2 Neurological effects 6

1.6 Metal chelation therapy 6

1.7 Current methods of measuring lead(II) concentrations 8

1.7.1 Sampling procedures 9

1.7.2 Atomic Absorption Spectroscopy (AAS) 10

1.7.3 Anodic Stripping Voltammetry (ASV) 10

1.7.4 Analytical validity 11

1.8 A potential new method for lead(II) detection 12

1.9 Fluorescent probes 12

1.9.1 Fluorescent intracellular ion indicators 13

	1.9.2	Properties of fluorescent intracellular ion indicators	13
1.10	Fluorescent probes for the detection of intracellular calcium(II) ions		14
1.11	Fluorescent indicators for transition metal and heavy metal ions		16
1.12	Zinc(II) fluorophoric probes		17
1.13	Lead(II) fluorophoric probes		18
1.14	Macrocyclic crown ether chemosensors		20
	1.14.1	Introduction	20
	1.14.2	Ion-specific macrocyclic ether chemosensors	23
	1.14.3	Lead(II)-specific macrocyclic ether chemosensors	24
	1.14.4	Design strategies	25
1.15	Fluorescent probes for other metal ions		26
1.16	Work described in this thesis		27
2	**Design and syntheses of trial ligands**		28
2.1	Target molecules		28
2.2	Crown ether ligand syntheses		31
	2.2.1	Introduction	31
	2.2.2	Synthesis of *3,12,20,29-Tetraoxa-35,36-diaza pentacyclo-[29.3.1-1.^{14,18}0.^{5,10}-0.22,27]-hexatriaconta-1(35),6,8,14,16-18(36),-22(27),23,25,31,33 -dodecaene, 1*	33
	2.2.3	Synthesis of *2,3,11,12-Bis(4'-methylbenzo)-1,4,10,13-tetrathia-7,16-dioxacyclo-octa-2,11-diene, 2*	34

	2.2.4	Synthesis of *7,16-Diaza-1,4,10,13-tetraoxa-2,3,11,12-dibenzo-cyclo-octadeca-2,11-diene,* ***3***	40
	2.2.5	Synthesis of *2-[19-(2-hydroxy-2-phenylethyl)-7, 8, 9, 10, 18, 19,20,21-octahydro-6H,17H-dibenzo[b,k][1,4,10,13,7,16]-tetra-oxadiazacyclo octadecin-8-yl]-1-phenyl-1-ethanol,* ***4***	51
	2.2.6	Synthesis of *2-[16-(2-hydroxy-2-phenylethyl)-1,4,10,13-tetraoxa-7,16-diazacyclo-octadecanyl]-1-phenyl-1-ethanol,* ***6***	53
2.3	Conclusions		54
3	**Equilibrium studies of crown ether complexes**		56
3.1	Introduction		56
3.2	Pioneering methods for the determination of stability constants		56
3.3	The potentiometric titration technique		58
	3.3.1	Direct titrations	61
	3.3.2	Competitive titrations	63
	3.3.3	Determination of stability constants by curve fitting	65
3.4	Results and Discussion		74
	3.4.1	Complexation of ligands **1**, **2**, **5** and **6** with silver(I) ions	76

	3.4.2	Complexation of ligands **1**, **2**, **5** and **6** with lead(II) ions	78
	3.4.3	Complexation of ligands **1**, **2**, **5** and **6** with zinc(II) ions	83
	3.4.4	Complexation of ligands **1**, **2**, **5** and **6** with cadmium(II) ions	85
3.5	UV-visible spectroscopy		88
3.6	Conclusions		91
4	**Gas phase studies**		93
4.1	Mass spectrometric methods for the assessment of metal complexation by crown ether ligands		93
4.2	The electrospray ionisation mass spectrometry technique		96
	4.2.1	Results and Discussion	98
4.3	Gas phase versus solution phase studies		103
4.4	*Ab initio* calculations		105
	4.4.1	Results and Discussion	107
4.5	Conclusions		130
5	**Summary and Conclusions**		131

6	**Experimental**		135
6.1	Synthetic methods		135
	6.1.1	General	135
	6.1.2	Syntheses	136
6.2	Physical methods		152
	6.2.1	Non-aqueous titrations	152
	6.2.2	Standardisation of metal ion solutions	153
	6.2.3	Electrospray ionisation mass spectrometry	154
	6.2.4	*Ab initio* calculations	155
	6.2.5	UV-visible spectroscopy	155

Appendix A X-ray crystallographic data 157

Appendix B Potentiometric titration data 162

References 173

Abstract

The monitoring of lead(II) ion concentrations in the environment and in biological media is a research area of great topical interest. This thesis describes a comprehensive study of a select but informative set of crown ether ligands that may potentially be used in the development of a fluorescent lead(II)-specific probe.

The synthesis of a series of macrocyclic ligands that contain various combinations of oxygen, nitrogen and sulfur donor atoms is described. The dibenzo-dipyridyl-22-crown-6 derivative **1**, the bis(4-methylbenzo)tetrathia-18-crown-6 derivative **2**, and the dibenzo-diaza-18-crown-6 derivative **3** were synthesised by a convergent synthetic strategy that culminated in the 1:1 condensation reaction between the appropriate components of the target macrocycle under low to moderate dilution conditions. The molecular structure of **1** was confirmed by X-ray crystallography. Phenylhydroxyethyl pendant arms were incorporated into the parent diaza-18-crown-6 derivatives **3** and **5** to afford the *N,N'*-substituted derivatives of dibenzo-diaza-18-crown-6 **4** and diaza-18-crown-6 **6**, respectively.

The stabilities and selectivities of the macrocyclic ligands **1**, **2**, **5** and **6** toward lead(II), zinc(II) and cadmium(II) ions were determined by potentiometry in *N,N'*-dimethylformamide (DMF) solution using a silver(I)-ion selective electrode. The presence of pendant phenylhydroxyethyl arms in **6** substantially enhances complexation of large cations such as lead(II) and cadmium(II). This is confirmed by the observation that ligand **6** forms a stable complex with lead(II) and cadmium(II) ions, with a log $K_S > 7.52$ for both complexes, but exhibits no affinity toward zinc(II) ions. Ligand **5** complexes lead(II) (log $K_S = 6.71 \pm 0.12$) more strongly than cadmium(II) and zinc(II) ions (log $K_S = 5.92 \pm 0.02$ and log $K_S = 4.30 \pm 0.07$, respectively). Ligands **1** and **2** complex lead(II) less strongly than **5** (log $K_S([Pb\mathbf{1}]^{2+}) = 2.62 \pm 0.01$; log $K_S([Pb\mathbf{2}]^{2+}) = 2.38 \pm 0.21$), and cadmium(II) (log $K_S([Cd\mathbf{2}]^{2+}) < 2$) and zinc(II) (log $K_S([Zn\mathbf{2}]^{2+}) < 2$) are weakly complexed by **2**. These low stabilities are most likely due to the large macrocyclic cavity of ligand **1**, although the poor stability and selectivity of ligand **2**, with four sulfur donor atoms, toward the softer

acid metal ions are attributable to a free ligand conformation which is unsuitable for complexation. All four ligands form stable complexes with silver(I) ions (log $K_s([Ag\mathbf{1}]^+)$ = 5.50 ± 0.04; log $K_s([Ag\mathbf{2}]^+)$ = 6.49 ± 0.02; log $K_s([Ag\mathbf{5}]^+)$ = 9.42 ± 0.13; log $K_s([Ag\mathbf{6}]^+)$ = 7.52 ± 0.01), consistent with the more covalent nature of the metal-ligand interactions anticipated for the soft acid silver(I).

Electrospray ionisation mass spectrometry (ESI-MS) was used to probe the coordination properties of ligands **1 - 6** with silver(I), lead(II), zinc(II) and cadmium(II) ions. As noted in the solution studies, strong complexation between each of the ligands and silver(I) ions also occurs in the gas phase. Ligand **6** forms a very stable lead(II) complex in the gas phase, as does ligand **2**. Ligands **5** and **6** both form stable complexes with cadmium(II) ions in the gas phase. Ligand **5** is more selective toward silver(I) ions than cadmium(II) ions in both the solution and gas phase. Ligand **6** is highly selective toward cadmium(II) ions over silver(I) and lead(II) ions in the gas phase. ESI-MS studies clearly demonstrate the destabilizing effects of the rigid aromatic moieties of ligands **3** and **4** which lower their affinities toward lead(II), zinc(II) and cadmium(II) ions. Complementary *ab initio* calculations were carried out to predict gas phase structures for the free ligands and selected complexes.

In conclusion, ligand **6** is the most promising candidate for use as a prototype in the development of a fluorescent lead(II)-ion specific probe. The high affinity of this ligand for lead(II) and cadmium(II) ions was observed in DMF solution although, under gas phase conditions, ligand **6** was found to be more selective for cadmium(II). Furthermore, there was sufficient discrimination observed by ligand **6** toward softer acid metal ions when compared to biologically more prevalent ions such as the borderline hard acid zinc(II).

Abbreviations

Å	Ångström (10^{-10} m)
Bis(4-methylbenzo)-tetrathia-18-crown-6	2,3,11,12-Bis(4'-methylbenzo)-1,4,10,13-tetrathia-7,16-dioxacyclo-octa-2,11-diene
calc.	calculated
δ	chemical shift (ppm)
Diaza-18-crown-6	4,7,13,16-tetraoxa-1,10-diazacyclooctadecane
Dibenzo-18-crown-6 hexaoxacyclooctadeca-	2,3,11,12,dibenzo-1,4,7,10,13,16-2,11-diene
Dibenzo-diaza-18-crown-6 cyclo-	7,16,Diaza-1,4,10,13-tetraoxa-2,3,11,12-dibenzo-octadeca-2,11-diene
Dibenzo-dipyridyl-22-crown-6	3,12,20,29-Tetraoxa-35,36-diazapentacyclo-[29.3.1-1.^{14,18}0.^{5,10}-0.22,27]-hexatriaconta-1(35),6,8,14,16,-18(36),22(27),23,25,31,33-dodecaene
DMF	*N,N'*-dimethylformamide
DMSO	dimethyl sulfoxide
D_N	Gutmann donor number
E	electrode potential (volts)
e.m.f.	electromotive force (volts)
E_0	standard electrode potential (volts)
EI-MS	electron ionisation mass spectrometry
ESI-MS	electrospray ionisation mass spectrometry
expt.	experimental
FAB-MS	fast atom bombardment mass spectrometry
HPLC	high performance liquid chromatography
HSAB	hard-soft acid-base
I	ionic strength
K_s	stability (equilibrium) constant
L	unspecified ligand
ln	natural logarithm (base e)
log	decadic logarithm (base 10)

M^{n+}	unspecified metal ion
$[ML]^{n+}$	unspecified metal complex
ν	wavenumber (cm^{-1})
n.m.r.	nuclear magnetic resonance
ppm	parts per million
THP	tetrahydropyranyl
t.l.c.	thin layer chromatography
tosyl (Ts)	*p*-toluene sulfonyl

Declaration

This work contains no material which has been accepted for the award of any other degree or diploma in any university or other tertiary institution and, to the best of my knowledge and belief, contains no material previously published or written by another person, except where due reference has been made in the text.

I give consent to this copy of my thesis, when deposited in the University Library, being available for loan and photocopying.

Daniela Caiazza

March, 1999

Acknowledgements

I would like to express my sincere appreciation to Dr A. D. Ward and Prof. S. F. Lincoln for their supervision, guidance and encouragement throughout my postgraduate research. I am particularly grateful for their special effort in proofreading this thesis.

I am most grateful to Dr Mark Buntine for his time and effort spent on the *ab initio* work over the past few years. His valuable advice and interest in this work are greatly appreciated. I am very grateful to Dr Edward Tiekink for his efforts spent on the X-ray diffraction work and, particularly, for the generous loan of his colour printer.

I am very grateful to Sonia Whitbread for her kind assistance with the potentiometric studies. A special thanks to Kym Hendrickson for her advice with the data analysis. Many thanks to Lee West for his assistance with certain synthetic procedures. A special thank-you to Bruce May for his generous advice in many matters.

I am very appreciative of Paul Wabnitz's time and effort spent on the ESI-MS work. Thank-you to Tom Blumenthal, Dr Karl Cornelius and Ben Hall for assistance with preliminary FAB and ESI-MS work. A special thank-you to Wendy Holstein for her kind assistance with data analysis and her helpful advice regarding the final (crucial!) ESI-MS sample. Many thanks to Stephen Blanksby for his assistance with endless computational matters.

I am extremely indebted to Dr John Valente for his cherished friendship. I thank him for his generous assistance and encouragement in all areas of this research project. I also thank Danielle Gracanin for her patience and kind friendship.

Many thanks to colleagues (past and present) in the Department of Chemistry, in particular Dr Yanni Papageorgio, Dr Kathy Kociuba, Dr Caroline Ward, Dr Wayne Pearce, Dr Adrian Clark, Dr John Hevko, Steffen Creaser, Brian Chia, and Tom Avery for their valued friendship.

My sincere gratitude to my parents for all their love, guidance, encouragement and support throughout my entire education. Thank-you to Ornella and Eric for their support, kind generosity and humour. It appears the time has come, Eric!

Finally, a special thank-you to Lou for his interest and valuable advice with regard to my research work and particularly for his patience and support throughout the writing of this thesis. I also thank Lou for his complete love and devotion.

1 Introduction

This chapter presents an overview describing the rationale behind the development of a lead(II)-specific fluorophore. It includes a historical overview of the uses of lead and its compounds; the discovery of their toxic effects, and a discussion of the biochemical and cellular aspects of lead(II) toxicity; methods for treatment of lead(II) poisoning, in particular the use of metal chelation therapy; and details on the currently used methods for the measurement of lead(II) concentrations in biological and environmental systems. Recent literature describing the use of fluorescent probes for the detection of various metal ions in aqueous media is also presented. An emphasis is placed on these studies describing the use of fluorescent intracellular ion indicators that target transition metal and heavy metal ions, in particular lead(II) ions.

An introduction into macrocyclic chemistry, with particular emphasis on macrocyclic crown ether compounds, is also presented. The use of macrocyclic crown ether ligands as ion-selective chemosensors is discussed, and the viability of these systems as a basis for the rational design of a lead(II)-specific probe is introduced.

1.1 Historical overview

Lead has been an important metal in human societies over many thousands of years.[1] It is the most abundant of the heavy metals in the Earth's crust (14 ppm), occurring chiefly as the sulfide ore, galena (PbS). The ease of extraction of the metal from its ores, good malleability, ductility, corrosion resistance and poor conductivity account for the use of lead as a versatile construction material throughout history.[1,2] Ancient Phoenician, Egyptian, Greek, Indian and Chinese civilizations are known to have smelted and used lead for cooking vessels, roofs, water ducts, utensils, ornaments and weights. Throughout the Roman Empire, lead pipes were used extensively for the transport of water.[1] Lead compounds such as coloured lead oxides were used as pigments in glazes and cosmetics by a number of ancient civilizations.[2]

The symptoms associated with lead poisoning parallel its use throughout human history. The earliest description of lead poisoning was reported in 300 BC by the physician Hippocrates, who reported a case of colic in a metal worker, thought to have been working on the extraction of lead from its ore.[3] Even though Hippocrates' initial description of lead poisoning was considered far from conclusive, in the first century AD the philosopher and physician Dioscorides accurately described lead colic and discussed the paralysis that developed after swallowing solid lead or inhaling lead fumes.[4] Other early records and descriptions of lead poisoning were thought to be related to the contamination of beverages. Throughout the Middle Ages, lead acetate ("sugar of lead") was used as a sweetening agent in wine and for promoting acid fermentation in wine production. Such uses led to numerous cases of lead poisoning,[3,4] particularly throughout France where this sweetening method was customary.[4] Further outbreaks of lead poisoning from contaminated water supplies in Europe, rum in the Caribbean, and cider in South-western England were all reported in the eighteenth century as the use of lead piping and lead sheet became more widespread.[3] However, it was the advent of the Industrial Revolution that caused a major proliferation in the use of lead and its compounds.[3] Mass industrialisation and the introduction and development of the motor vehicle led to a dramatic increase in lead consumption owing to its use in lead-acid storage batteries (Pb metal and PbO_2), and as an "anti-knock" agent in leaded petrol (Pb tetraalkyls).[2]

1.2 Chemical and physical properties of lead

Lead is classed as a heavy metal, belonging to the Group 14 elements of the Periodic Table. Lead is an electropositive element, and it shows true cationic character in the +2 oxidation state. Conversely, lead exhibits a strong tendency for covalent bonding in the +4 oxidation state.[5,6] In its interactions with Lewis bases, lead(II) is classified as an intermediate Lewis acid that lies between typical hard and soft acids, such as sodium(I) and mercury(I) respectively.[7-9] A hard acid is characterised by a high positive charge density and a low polarizability and electronegativity. All of these features favour the formation of ionic bonds by hard acids. The opposite is true for soft acids, which exhibit

high polarizability, high electronegativity, lower positive charge density and thus, exhibit a strong tendency for the formation of covalent bonds.[7-10] With the exception of the insolubility of lead salts, such as the halides, hydroxides, sulfates and phosphates in aqueous media, lead tends to possess a chemistry similar to the divalent alkaline earth group metals, rather than share the properties of elements in its own group.[5,6]

1.3 Toxicity of lead and its compounds

As human exposure to compounds of lead is of great concern, the biogeochemical cycling of lead and routes for human exposure have been widely studied.[2,3,11-13]

The organometallic tetraalkyl lead compounds, such as the tetramethyl ($PbMe_4$) and the tetraethyl ($PbEt_4$) species, are lipid soluble and are easily absorbed by the respiratory and gastrointestinal tracts, and the skin. Tetraethyl lead was the first alkyl lead compound introduced into petrol in 1923.[2] Its introduction was fundamental in the efficient development of the high-compression internal combustion engine.[11] By the 1960s, further development of alkyl lead compounds had resulted in the introduction and use of tetramethyl and mixed tetramethyl-ethyl lead compounds as anti-knock additives. About 70-75% of the lead in petrol is discharged into the atmosphere in exhaust gases,[14,15] and these gasoline additives constitute the majority of organolead compounds found in the environment.

Inorganic sources of lead compounds include paints and primers, eye cosmetics, medicinal preparations and hair-darkening products.[16] Major industrial sources of inorganic lead include smelters, storage batteries, cable sheathing and lead alloys.[12,17] The prime medium for lead mobilisation is air. The metal tends to form fine particulates, especially when heated by industrial high-temperature sources, and it may travel long distances before deposition.[1,4,14] Lead particles that accumulate on soil surfaces eventually become mixed into the surface soil layer and may be taken up directly by grazing animals.[4] Thus, lead uptake by humans may occur either by the direct absorption of lead compounds or lead contaminated sources *via* the gastrointestinal tract or, alternatively, by the absorption

of airborne particles by the lungs and skin.[2,17] The direct absorption of lead compounds or lead-contaminated sources is of particular concern when considering children suffering from the disorder pica, the compulsive consumption of non-food items, may be exposed directly to lead contaminated sources, such as paint chips, dust and dirt particles, in their daily life. Fortunately, since most inorganic lead compounds are insoluble *in vivo*, only small amounts are able to be absorbed directly through the gastrointestinal tract. Once absorbed, however, accumulation of lead deposits occurs in the liver, kidneys, and bones owing to the slow excretion of the ingested lead from the body.[17] The absorption of airborne particles of inorganic lead sources by the lungs and skin is a much greater threat to adults and children. Particularly, the inhalation of lead carbonate and lead sulfate dusts causes rapid accumulation in the lungs, which is followed by gradual dispersion of the metal to the blood and bones.[17]

Once lead enters the blood, approximately 97% is taken up by erythrocytes.[3,17] Although firmly bound to the erythrocytes with a half life of two to three weeks, the equilibrium is reversible and a redistribution of lead to other soft tissues throughout the body, namely the liver and kidneys, takes place.[3,17] Lead may also be carried to the brain, spleen and heart.[17] Ultimately some of the soft tissue lead is excreted in the urine or bile, however approximately 90% of the absorbed lead accumulates in calcified tissues, bones and teeth.[12,16] Lead resembles calcium in its deposition in and remobilization from the skeletal structures of the body.[6] Generally, accumulation in the calcified tissues is progressive and life-long whereas soft tissue lead binding is reversible and short-lived.[3]

1.4 The biochemical and cellular aspects of lead toxicity

Lead has no known function as an essential trace element in any organism.[2] The biochemical basis for the multiple toxic effects of the metal is its ability to form strong bonds with a number of donor sites present within proteins. Such ligands include the sulfhydryl groups in a number of proteins and enzymes (typically cysteine residues), imidazole groups in histidine residues, carboxyl groups in glutamic and aspartic acid residues and the phosphate groups of nucleic acids.[2,13,18] As a result of such binding, lead

interferes with the normal synthesis and function of proteins and enzymes in cells.[13,18] In general, this interference may be attributed to significant structural changes induced by the lead within the protein or enzyme, or by binding of the lead to the active sites of certain enzymes, thus disrupting the formation of normal enzyme-substrate complexes. Lead also exhibits a strong affinity for mitochondria. The majority of binding sites are in the protein portion of the mitochondrial membrane, causing a number of disturbances and interferences to normal mitochondrial metabolism.[2,13] Lead also has the potential to enter the matrix of the mitochondria and bind the reactive groups of certain amino acid residues.[2]

1.5 The health effects of lead poisoning

The health effects associated with exposure to lead can range from mild, reversible effects to that of permanent damage, chronic disease, and in extreme situations, even death.[19] The various biochemical and physiological changes observed in individuals exposed to excessive levels of lead have been widely reported in the literature.[2,3,13,18-22]

1.5.1 Haematological effects

Lead poisoning in humans is accompanied by marked abnormalities in porphyrin metabolism.[18] This leads to the haematological effects caused by excessive exposure to the metal. Lead is well known to interfere with the synthesis of haem by the inhibition of several mitochondrial enzymes in the haem pathway, particularly porphobilinogen synthetase and haem synthetase.[5,13,19] Exposure to lead reduces haem production and causes accumulation and excessive excretion of several porphyrin intermediates throughout the pathway.[18,19] Lead also affects the synthetic pathway of the globin protein through its antagonism of iron.[18-20] Interference and inhibition of the body's ability to synthesise haemoglobin leads to a decreased production of red blood cells. This disorder is shown clinically as anaemia.

1.5.2 Neurological effects

The toxicity of lead to the peripheral and central nervous systems has been recognised for nearly 200 years.[2] However, it is recognised that neurological involvement of lead occurs only after extreme and prolonged exposure to excessive levels of the metal.[2,3,23] The peripheral nervous system tends to be principally involved in adults, with early reports showing that optical atrophy (degradation of optical nerves), tremors and wrist drop were all common neurological symptoms that were diagnosed in adult industrial workers who were exposed to excessive lead levels.[2,3] However, young children tend to be more susceptible than adults to the neuropathic effects of lead.[23] It is well established that even low-level exposure to lead levels affects growth and development at the foetal, infant or young child stage. It has been shown that exposure to lead(II) affects the stature, growth rate, and intellectual development in children, and the birthweight, gestational age, and congenital abnormalities in the foetus.[24] The intellectual underdevelopment observed in children between the ages of 1 - 4 years is of particular interest, with many studies strongly supporting the hypothesis that lead, even at very low doses, causes significant lowering of IQ levels and thus impairs a child's intellectual performance.[23-27] The physiological damage associated with this lower level of exposure appear to be irreversible.[24] An eleven year follow up study of children with 'minor' neurobehavioural dysfunctions, due to low level exposure in their early childhood, has been published.[28] The authors reported that such children demonstrated a higher risk of reading disabilities, absenteeism, poor eye-hand coordination and other deficits contributing to school failure and drop-out later in life.[24,28] The overall pattern of these studies suggest that any threshold for the effects of lead on the foetus or young child is so low to be inconsequential,[24,27] and all children with elevated levels of lead in the blood, even relatively 'mild' increases, should be treated for lead poisoning.

1.6 Metal chelation therapy

During the early 1950s, Hardy *et al.*[29] investigated the use of citrates and citric acid as potential lead(II) sequestering agents. Initial results showed an increase in both urine and

faecal excretion of lead. However, this method of lead sequestering was found to be inefficient because large, intolerable doses of citrates and citric acid were required for a worthwhile treatment.[29] In 1954, the powerful chelating agent calcium ethylenediaminetetraacetic acid (Ca_2EDTA) was introduced. This compound was found to be of immediate therapeutic benefit by dramatically increasing lead excretion, returning porphyrin and haemoglobin levels to normal in a matter of days, and by relieving the clinical signs and symptoms of lead toxicity.[4] Other agents with metal binding properties have also been investigated and used in the treatment of lead poisoning.[3,4,17] These include: N-(2-hydroxyethyl) ethylenediaminetriacetic acid (HEDTA); a combination of EDTA and the thiol-containing ligand 2,3-dimercapto-1-propanol (BAL, British Anti-Lewisite); sodium 2,3-dimercapto-1-propanesulfonate (DMPS); *(d)*-penicillamine; N-(2-mercapto-propionyl)glycine; and 2,3-dimercaptoglycine. The chemical structures of these agents are shown in Figure 1.1.

EDTA

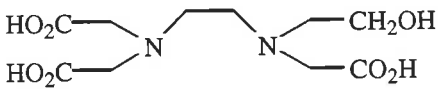

HEDTA

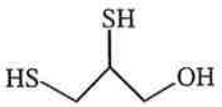

BAL

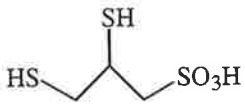

DMPS

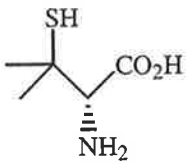

***(d)*-penicillamine**

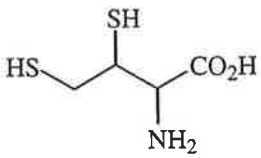

2,3-dimercaptoglycine

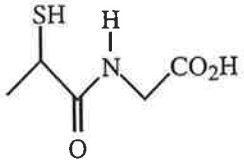

N-(2-mercaptopropionyl)glycine

Figure 1.1 *Common chelating agents used for the treatment of lead(II) poisoning.*

The dose and type of chelating agent used in the treatment of lead poisoning are highly dependent on the severity of the exposure.[4,17] Although blood lead(II) levels are rapidly reduced by chelating drugs, some rebound may occur after the initial course. This is due to an internal redistribution of lead(II) from sites which are inaccessible to the chelating agent.[4] More severe and adverse properties of these chelating agents, however, are their nonspecificity and relative toxicity. These agents are selective for lead(II) ions, but they also exhibit a high selectivity for other essential trace-elements (e.g. copper(II), zinc(II), and iron(II)) found in the body. The chelating agents also exhibit a selectivity for calcium(II) ions, interfering and disturbing their balance throughout the body. Trace-metal supplements complement the use of these chelating agents in the treatment of lead poisoning.[17,29] An additional adverse effect of these chelating agents is renal damage.[4,5] In an attempt to overcome these adverse side-effects, recent work by Raymond *et al.*[17] has led to the development of thiohydroxamic acid ligands as powerful, selective chelating agents for lead(II). Preliminary studies showed that the stability of the lead(II)-thiohydroxamato complex was higher than the stability of the lead(II)-EDTA complex, and also quite different to the stability with the 'harder' metal ions, which comprise many of the trace elements.[17,30] Although research into the development of powerful and selective chelating agents of lead(II) ions still continues, a non-toxic, highly stable and specific lead(II) chelating agent has yet to be developed.[30]

1.7 Current methods of measuring lead(II) concentrations

The toxic effects of lead(II) depend on its location within the body.[25] Lead has a half-life of approximately thirty days in the blood. The brain retains lead(II) for a much longer period than blood, a fact that may explain the particular susceptibility of the central nervous system to the metal. Lead(II) stored in the skeletal system of adults has a half-life of more than ten years. The half-life is less in children due to the intense remodelling of the skeleton in the growing body.[25] Since lead(II) is stored to differing extents in various tissues, the measurement of lead(II) levels must be interpreted in relation to the retention time of the lead(II) in a particular tissue.[25]

1.7.1 Sampling procedures

For the assessment of lead(II) levels in the body, the most widely used method is the measurement of lead(II) in whole blood.[2,3,16,25,26] Other sites of assessment include urine analysis, teeth samples and hair samples. Such assessments are not as favourable, however, due to the intrusive, difficult and multiple sample collection techniques required for the urine and teeth samples. Further, teeth samples are a better measure of long-term lead(II) retention in the body, rather than the short-term.[25]

The technique of measuring lead(II) concentrations in whole blood samples is problematic. A standardised procedure must be used for the collection, storage, transport and analysis of blood to avoid contamination and other errors. Venous blood samples are more difficult to obtain, but are preferred in place of capillary samples, as they are generally less susceptible to contamination.[24-27] For trace analysis of lead(II), the main problem is to avoid contamination by lead(II) present in the everyday environment. Particular storage methods must be employed between the time of sampling and the time of detection of lead(II) in the sample to avoid any possibility of external contamination.[25,31] The preparation of the sample for analysis is also of prime importance. The blood sample must be completely digested for the determination of the total lead(II) content, generally by wet ashing techniques at low temperatures.[31,32] The homogeneous sample is then analysed for lead(II), usually by means of atomic absorption spectrophotometry (AAS) or anodic stripping voltammetry (ASV). These methods are the two most common techniques used for the detection of nanogram amounts of lead(II) ions in biological samples,[2,3,23,25] but the technique of isotopic dilution mass spectrometry (IDMS) is the definitive method for lead(II) analysis in whole blood.[23,24] This method offers analyses to be carried out at the highest levels of accuracy and precision. However, IDMS is a time consuming and expensive technique that requires high levels of operator expertise.[23,24] This method is rarely used for routine testing and primarily serves as a confirming or validating method for samples analysed by other means.

1.7.2 Atomic Absorption Spectroscopy (AAS)

Two different versions of AAS are employed. In the original form, a volume of the sample solution is injected into a flame causing atomisation of the lead present in the matrix. The sample's lead-atom population then absorbs light radiation, at one of lead's characteristic wavelengths, either from a lead-specific hollow cathode lamp or an electrodeless discharge lamp. This absorption is then registered by a photocell. This method allows lead(II) to be measured in biological systems as a concentration of the total element, derived from a calibration curve.[23] However, aspirating the lead(II) analyte solution directly into the flame is generally unsatisfactory for trace analysis of lead(II) because of larger sample sizes that are required and lower sensitivity.[23]

Over the last 10-15 years, a flameless-atomic absorption method has become the most popular analytical variant of AAS.[23,24] Much lower detection limits can be obtained by this procedure,[23-25] and the sensitivity is one thousand times that of the conventional aspiration flame analysis.[23] Generally, this method utilizes an electrothermally heated graphite tube or platform, into which a volume of the sample matrix is placed and heated to predetermined temperatures (suitable for drying, ashing and atomisation of the sample) by passing an electric current through the graphite.[25] This flameless method is a very reliable form of AAS analysis, with the added advantage of speed and adaptability to automated operation, and it is the method most likely to be employed for the determination of lead(II) levels in biological samples.[24]

1.7.3 Anodic Stripping Voltammetry (ASV)

The electrochemical technique of AVS for the analysis of trace elements has been available for two decades.[23] AVS is based on a two step principle for lead analysis. First, the lead(II) ions liberated from the sample matrix are deposited by a two electron reduction onto a negatively charged cathode, as a function of time and negative voltage. Second, the current is reversed at the characteristic electrochemical potential, and the deposited lead is re-oxidised and released from the cathode.[31] The time required for the release all the lead

into solution is proportional to the amount of lead(II) ions originally present in the solution.[25] As with other electrochemical techniques, the ASV process collects all the metal of interest at the deposition step. Thus, ASV is a measure of the total quantity of lead(II) in the sample, offering high operational sensitivity.[24] An obvious requirement for this technique is adequate liberation of the lead(II) ions into a chemical matrix that permits deposition and stripping without interference.[23] Early methods involved chemical degradation of the organic matrices in whole blood.[23,25,33-36] However, even though this approach ensures mineralization, it is a time consuming process and the risk of contamination is high.[31] Alternatively, decomplexation using an ion-exchange reagent containing a mixture of competitive ions, including chromium and mercury, has been found to liberate lead(II) ions from binding sites by competitive binding.[25,37]

In general, the advantages of both the flame and flameless AAS techniques, and the AVS technique for measuring lead(II) levels in biological samples include: straightforward methods requiring modest analyst expertise; commercially available, relatively inexpensive equipment; and the collection of satisfactory results offering sufficient accuracy and precision.[23]

1.7.4 Analytical validity

The variability in the analysis of lead levels by AAS or ASV techniques originate from differing methods of sample collection, and storage and preparation procedures, particularly with respect to controlling external contamination.[25] The analyses are usually performed in duplicate or triplicate, and the resulting signal is compared to a signal elicited by a known reference standard. The quality of the calibration standard is then of upmost importance, and must be of the highest accuracy and precision. Numerous studies have shown inconsistencies and large variations in both accuracy and precision, when comparing inter- and even intra-laboratory analysis of the same blood sample.[23,25] The tediousness and labour intensive procedures required to measure samples of such low concentrations causes discrepancies and inconsistencies even when analyses are handled by the most experienced analyst. Also, these procedures are not considered the most

viable nor efficient when dealing with large sample sizes. A more reliable, efficient and inexpensive universal screening method for the determination of lead(II) ions of biological samples is desired. This may offer a faster, more readily accessible alternative for the monitoring of lead(II) concentrations in the blood. This is of particular importance in the determination of lead(II) poisoning in remote, high risk populations.

1.8 A potential new method for lead(II) detection

The research work presented in this thesis describes the proposed development of a lead(II)-specific probe which offers an efficient, accessible method for the determination of lead(II) ion concentrations in biological media. By implementation of a particular class of organic substrates, namely crown ether compounds, it is envisaged that an appropriate system that selectively and specifically targets lead(II) ions in biological media may be developed. We endeavour to study systems that will be elaborated in such a way that upon the selective binding of the ligand to lead(II) ions, a sufficient optical response is promoted, which allows for the direct detection of lead(II) levels in biological and environmental systems. Since the detection of the fluorescence signal of a ligand, or probe, is often the most sensitive technique for measuring ion concentrations in a number of biological systems,[38] it is envisaged that the incorporation of fluorescent groups into the appropriate lead(II) specific ligands will offer a new and rapid route of monitoring lead(II) levels in biological and environmental systems.

1.9 Fluorescent probes

The availability of sensitive and selective fluorescent indicators or probes for living and fixed cells has opened new horizons in cell biochemistry.[38] In combination with an appropriate fluorescent probe, use of the modern epifluorescence microscope[38] or the video intensification microscope[38] has allowed fluorescent-labelled molecules or specific metal-ion concentrations in living systems to be visualised, measured and recorded in real-time.[38] The resultant fluorescence signal permits sharper analysis of cytological detail than previously observed with stained specimens in ordinary light, enabling cell

organisation and function to be analysed with unprecedented precision and clarity.[38] With the addition of the confocal ultraviolet laser fluorescence microscope, which has an almost planar field of focus, thus allowing fluorescence of a single cell in one particular plane to be observed at a given time, the precise optical sectioning and analysis of living and fixed cells are possible.[38]

1.9.1 Fluorescent intracellular ion indicators

During the past decade, the development of fluorescent indicators or probes that selectively respond to biologically important ions has received a great upsurge of interest.[38] These probes incorporate photoresponsive molecular or supramolecular systems that possess a binding site, a fluorophore, and a mechanism for communication between the two, enabling real-time *in situ* monitoring of the flux of specific ions in individual living cells. The most widely used and successful fluorescent probes have been employed for the measurement of hydrogen ions (pH) and intracellular calcium ions (Section 1.9).[38-43] Fluorescent probes for the detection of other biologically important ions including the alkali (sodium, potassium) and alkaline-earth (magnesium) metal cations, have featured predominately in the literature.[38,41,43,44,45] However, only a few examples of fluorescent probes that target transition metal and heavy metal ions have been reported to date.[39,44,46-53] This may not be altogether unexpected, as these ions (excluding copper, iron and zinc) are not biologically prevalent species and thus, methods for the analysis of these species was not of great concern historically. However, as the role of these metal ions in biology and in the environment become more apparent, the design of photoresponsive probes that target such ions is an area of great topical interest.

1.9.2 Properties of fluorescent intracellular ion indicators

In developing new metal-specific photoresponsive probes, the molecular system under investigation must possess certain characteristics:

(i) It is essential that the molecular system displays a preferential selectivity toward the desired metal ion of interest, especially over biologically prevalent cations. The specificity

ensures that the recorded optical signal is directly attributed to the binding of the metal ion. Competing equilibria that affect the signal must be considered in the design of the probe and, where such effects cannot be eliminated, their interference to binding must be considered and, if possible, minimised.

(ii) The molecular probe must be designed to function within the typical biological cell environment. It must possess the potential to cross the outer membrane of a cell, enter and remain within the cell for a sufficient period so as to allow complexation to occur. It must be soluble within the aqueous media of the cell and function at physiological pH (7.4) and under conditions of constant ionic strength (0.1 M).

(iii) An optimal molecular probe must exhibit a significant, measurable change in its optical fluorescence upon ion binding. This change in indicator fluorescence, from the free to the complexed state, can be measured by a shift in the excitation wavelength and the corresponding shift in the fluorescence emission wavelengths, or as an increase (or decrease) in the quantum yield or extinction co-efficients of the indicator.[38] Additionally, it is preferable if the molecular probe is weakly or non-fluorescent in its free, unbound form, to ensure that no interference results from any free probe.

1.10 Fluorescent probes for the detection of intracellular calcium(II) ions

To date, the most successful fluorescent probes that have been developed are those which monitor free intracellular calcium(II) concentrations.[38,39] A large number of calcium(II) probes are known and, in general, all are fluorescent derivatives containing the octadentate ligand BAPTA (1,2-bis(2-aminophenoxy-ethane)-*N,N,N',N'*-tetraacetic acid) (Figure 1.2), itself an aromatic analogue of the calcium-selective chelating ligand EGTA (ethyleneglycol-bis(β-aminoethylether)-*N,N,N',N'*-tetraacetic acid).[38,41,42]

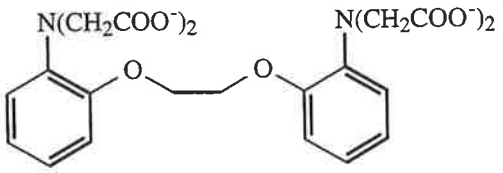

Figure 1.2 *The structure of BAPTA.*

The first fluorescent method for the measurement of calcium(II) levels in mammalian cells was reported by Tsien.[42,43,54-56] The method involved monitoring the fluorescence of the indicator known as Quin2 (Figure 1.3). Even though Quin2 offered valuable insights into the role of calcium(II) as an intracellular messenger, it has always had a number of severe limitations.[42] Over the next five years, by extension and development of his initial work, Tsien *et al.*[38,41,42] introduced the calcium(II) selective indicators, Indo-1 and Fura-2 (Figure 1.3). On exposure to ultraviolet light, these compounds were found to exhibit enhanced fluorescence, in the presence of calcium(II), as compared to the Quin2 prototype.[41,42] Further extensions of this work led to the development of Fluo-3 (Figure 1.3), a fluorescent calcium(II) indicator that is excited by visible light. Fluo-3 eliminated the problems associated with laser excitation in the UV region such as the potential to injure the cell, autofluorescence of the cell, and the release of bound calcium(II) at UV wavelengths.[38,41] The calcium(II) complex of Fluo-3 is 40-fold more fluorescent than the free dye, a fluorescence enhancement that is the greatest reported for any fluorescent calcium(II) indicator to date.[41] Even though Fluo-3 forms stable complexes with manganese(II) and zinc(II), the fluorescence of these complexes is much lower than that of the calcium(II) complex.[41]

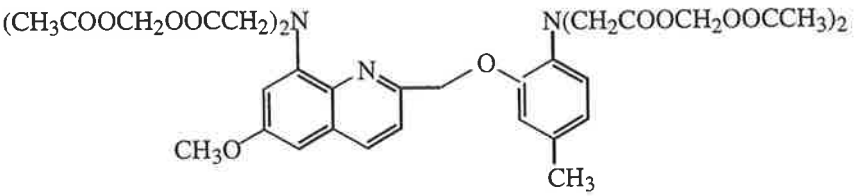

Quin2

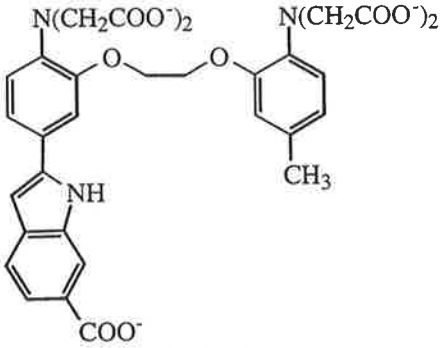

Indo-1

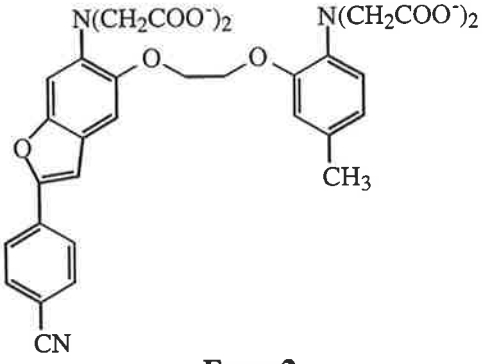

Fura-2

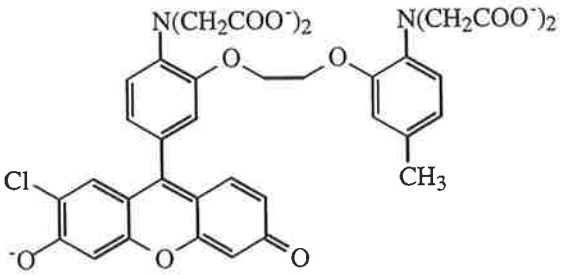

Fluo-3

Figure 1.3 *The structures of commonly used fluorophoric probes for the determination of intracellular calcium(II) ions.*

1.11 Fluorescent indicators for transition metal and heavy metal ions

The use of fluorescent sensor molecules that target submicromolar concentrations of transition or heavy metal cations in biological or environmental samples has been an emerging research area over the past decade. The most studied metals include zinc(II),[40,44,50,51,53] copper(II)/(I),[40,48,50,52,57,58] iron(III)/(II),[39,40] gallium(III),[39,40] nickel(II),[40,50] mercury(II),[40,44,52] lead(II),[40,44,51,57] cadmium(II),[40,44,53,57] and silver(I).[44,46,47]

A number of problems are generally associated with the use of fluorescent probes for the detection of transition metal ions. These include: competitive binding of more abundant biological cations, including calcium(II) and magnesium(II); most transition metals absorb UV-visible light but very few re-emit the energy in the form of UV or visible emissions, owing to strong coupling of their electronic excited states with those of other molecules (e.g. water) *via* the ligand field effect resulting in an efficient de-excitation mechanism;[59] reduced functionality for these systems in aqueous media owing to weaker metal-ion complexation, and generally smaller or insignificant changes in fluorescence as compared to non-aqueous solutions.[60]

1.12 Zinc(II) fluorophoric probes

Zinc(II) features significantly in many processes associated with cell activation and growth.[61-66] Work by our research group has involved the design and development of a highly fluorescent sensor molecule that is used to measure zinc(II) flux within living cells.[53] The fluorescent probe, ethyl(2-methyl-8-p-toluenesulfonamido)-6-quinolyloxy acetate, also referred to as Zinquin E, allows simultaneous *in vivo* detection of zinc(II) ions in a range of intracellular sites.[53] Upon loading, Zinquin E readily traverses the cell membrane and is hydrolysed, by cellular esterases, to the charged carboxylate form, 2-methyl-8-(toluene-p-sulfonamido)-6-quinolyloxyacetic acid, Zinquin A (Scheme 1.1). The anionic nature of Zinquin A prevents leakage of the fluorophore back across the cell membrane. Zinquin A is now able to chelate the readily exchangeable, free zinc(II) ions within the cell and, upon fluorometric excitation, gives an intensely fluorescent signal.

The interactions of Zinquin A with cobalt(II), nickel(II), copper(II), magnesium(II), calcium(II) and cadmium(II) ions have also been investigated.[53] The fluorophore was found to coordinate to all these metal ions, excluding calcium(II) and magnesium(II), but no increase in fluorescence was observed for the complexes of copper(II), nickel(II) and cobalt(II). The cadmium(II) complex showed an increase in fluorescence over the free ligand, but the intensity of the fluorescence signal was lower than that observed for the zinc(II) species.[53]

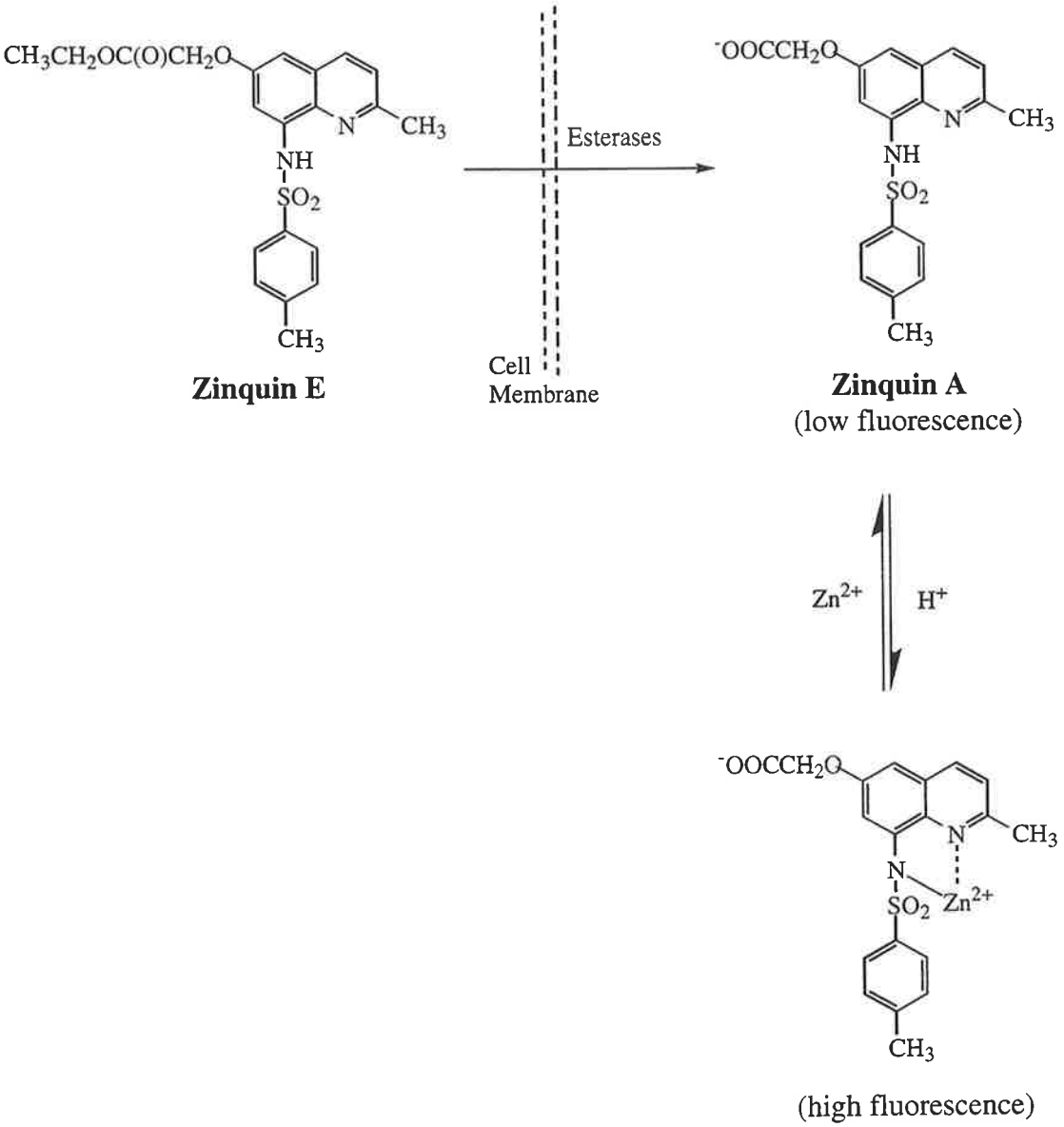

Scheme 1.1 *Diagrammatical representation of free Zinquin E and Zinquin A forms, and Zn^{2+} - Zinquin A complexed species formed within cells.*

Furthermore, the cadmium(II) levels in the body are not significant enough to interfere with the monitoring of the more prevalent zinc(II) ions. Thus, Zinquin A exhibits the appropriate selectivity and fluorophoric characteristics that make it a successful fluorescent probe of zinc(II) ions in biological samples.

1.13 Lead(II) fluorophoric probes

Following on from the research into the development of a fluorophoric probe that successfully targets intracellular zinc(II) ions, our research group has had a keen interest in

developing fluorophoric probes that can target other biologically- or environmentally-relevant metal cations. In particular, it is envisaged that a quantitative, accurate method for determining lead(II) levels in biological and environmental samples may potentially be achieved by the rational design of a lead(II) specific fluorophoric probe.

Very few fluorophoric probes that can selectively target lead(II) ions are known. The commercially available probe known as Phen Green (Figure 1.4) is a phenanthroline-based indicator, sensitive enough to measure large fluorescence (quenching) changes produced by submicromolar ion concentrations of lead(II) ions in aqueous samples.[40] The disadvantage of Phen Green is that it is a general purpose heavy metal sensor, capable of detecting a broad range of metal ions. Furthermore, Phen Green is unsatisfactory for measuring lead(II) levels in biological samples.[40] Phen Green diacetate (Figure 1.4) may be useful for loading into cells, however its response to intracellular metal ions has not yet been reported.[40]

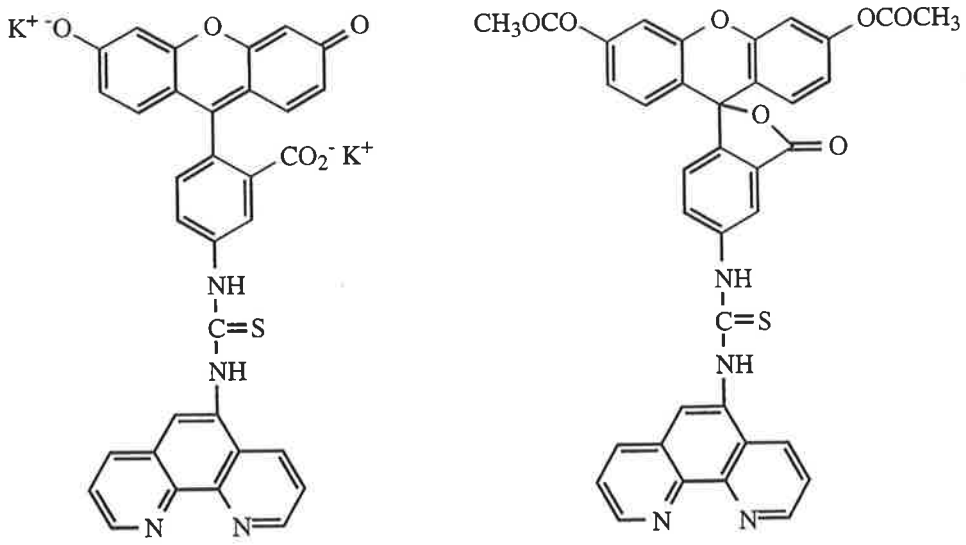

Phen Green

Phen Green Diacetate

Figure 1.4 *The structures of Phen Green and Phen Green Diacetate.*

Czarnik[44] has discussed the use of an anthracene thiohydroxamate derivative as a chelation-enhanced fluorescence (CHEF) chemosensor for the determination of lead(II) ions in aqueous media (Equation 1.1). Thiohydroxamic acids exhibit a well-known affinity for lead(II).[17,44] Even though the thiohydroxamate group itself is found to be strongly

fluorescence quenching, *via* photoinduced electron-transfer from the nitrogen to the anthracene ring system,[44,50,60,67] Czarnik envisioned that upon coordination to the less strongly quenching lead(II) ions, a net CHEF would be achieved. Total complexation of lead(II) was found to induce a 13-fold enhancement of fluorescence for the complexed state, as compared to the free ligand (Equation 1.1). Even though there is a measurable increase in fluorescence, the overall fluorescence of this molecular system is too weak for it to be considered as a viable fluorophore for monitoring lead(II) levels in aqueous media.[44]

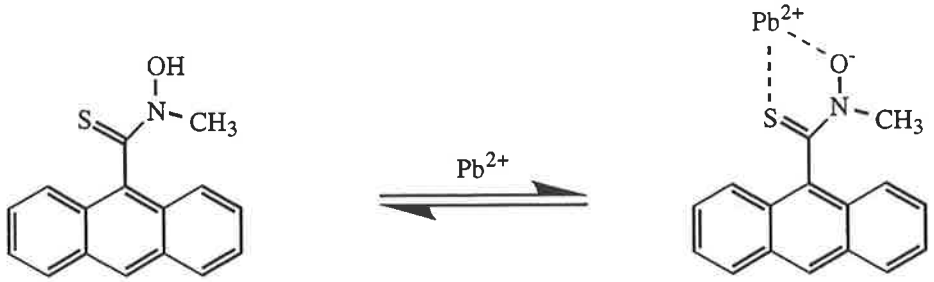

Low fluorescence High fluorescence

Equation 1.1 *Equilibrium reaction between an anthracene thiohydroxamate system and lead(II) ions.*

1.14 Macrocyclic crown ether chemosensors

1.14.1 Introduction

Over the last 50 years, a large number of synthetic macrocyclic compounds, capable of binding cations, anions and neutral molecules have appeared in the literature. It is well established that the interest in these synthetic systems stems from the fact that many important biological processes involving coordination of one specific metal ion all contain some variant of a macrocyclic ligand.[68,69] The importance of such complexes is readily exemplified by the transportation of dioxygen in mammalian and other respiratory systems by the iron(II)-containing haem proteins; the chlorin complex of magnesium(II) in chlorophylls and its importance in photosynthesis; and the complexation of cobalt(II) by a

corrin ring in Vitamin B_{12}.[69-71] Furthermore, it had been demonstrated that various naturally-occurring macrocyclic antibiotics (e.g. valinomycin and nonactin) selectively complex alkali metal cations, such as sodium(I) and potassium(I), and exhibit an ability to transport these ions across cell membranes. It is the biological relevance of all of these processes that provides the motivation for studies into the chemistry of not only these naturally occurring systems, but also synthetic macrocyclic ligand systems in general. Indeed, early research in this field was aimed at the possibility of using synthetic macrocycles as simple models for studies of these complex biological processes.[69,71]

A major aspect of macrocyclic chemistry includes the many studies of crown ether compounds and their derivatives, such as the cryptands (cage-type bicyclic crown compounds), of which the more complex include the spherands and the carcerands, and the lariat ethers (substituted crown ethers).[71-73] These macrocycles typically contain central hydrophilic cavities encircled by various donor atoms, and exterior flexible frameworks exhibiting hydrophobic behaviour. Thus, recognition by these organic substances (hosts) for metal cations, anions or neutral molecules (guests), is at present a topic of fundamental importance in both supramolecular chemistry and biochemistry.

Pederson's seminal publication appeared in 1967 and it reported the synthesis and complexation properties of a large number of unique, novel macrocyclic polyethers.[74] Whilst studying the effects of bi- and multi-dentate phenolic ligands on the catalytic properties of the vanadyl (VO) group, Pederson attempted the synthesis of the bis[2-(*o*-hydroxyphenoxy)ethyl] ether by reacting bis(2-chloroethyl)ether with 2-(*o*-hydroxyphenoxy)tetrahydropyran under basic conditions in *n*-butanol (Equation 1.2). Even though Pederson obtained the desired quinquedentate ligand bis[2-(*o*-hydroxyphenoxy)ethyl]ether, a small amount of white, fibrous crystals was also isolated. This by-product was found to be 2,3,11,12-dibenzo-1,4,7,10,13,16-hexaoxa-cyclooctadeca-2,11-diene, now more commonly known as dibenzo-18-crown-6, and its formation was attributed to the presence of approximately 10% unreacted catechol in the reaction mixture (Equation 1.2). Investigating the solubility properties of this polyether, Pederson rapidly

discovered its potential for producing stable polyether-metal complexes with many salts of the alkali and alkaline earth metals.[74,75] This particular class of compounds became known as "crown" ethers, due to the appearance of their molecular models and their ability to "crown" or "uncrown" cations, without chemical damage to the ligand.[71] The trivial nomenclature of crown polyethers includes the number and type of substituent groups on the ring; the total number of atoms in the polyether ring; the class of compound; and the number of oxygen atoms in the polyether ring (e.g. compound 2,3,11,12-dibenzo-1,4,7,10,13,16-hexaoxa-cyclooctadeca-2,11-diene is trivially named dibenzo-18-crown-6 as **dibenzo** (number and type of substituents on ring) **-18-** (total number of atoms in ring) **crown** (class) **-6** (number of oxygen atoms in ring)).

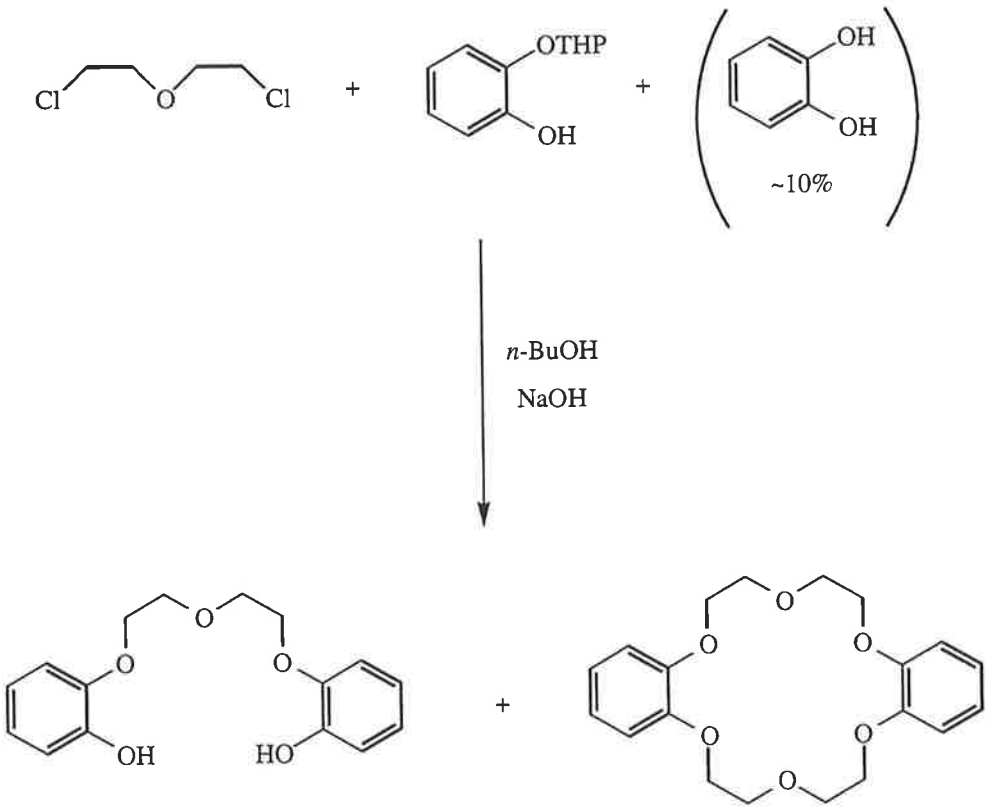

Equation 1.2 *Formation of bis[2-(o-hydroxyphenoxy)ethyl]ether (left) and the crown ether dibenzo-18-crown-6 (right).*

Pederson's paper marked the beginning of a new and major development in the study of the metal-ion chemistry of macrocyclic ligands, and it led to a proliferation of research into the synthesis of new crowns and crown-like compounds. Common lines of enquiry for these

systems included the synthesis of new and unique crown ethers in order to understand and appreciate the limits of possible ring sizes and heteroatom content, and investigations into the types of species that could be bound or complexed by these novel macrocycles.[69,71] The development of a wide variety of mixed donor macrocycles, incorporating nitrogen (polyaza crown compounds) and sulfur (polysulfide crown compounds) donor atoms in the rings, in addition to the ether oxygen atoms, rapidly surfaced in the literature.[76] As the field of macrocyclic chemistry has now grown so broad, the only true definition of a crown ether that remains accurate is that the molecules are cyclic systems that contain one or more macrocyclic rings, generally with nine or more ring atoms, containing oxygen, nitrogen or sulfur as donor atoms.[71,72]

The number of crown ether compounds that has been reported in the literature to date is enormous, and discussions into the synthesis and complexation chemistry of all the possible structural variants is far beyond the scope of this thesis. However, comprehensive reviews that summarise the synthesis of novel crown ether compounds and their derivatives, and their binding affinities (kinetic and thermodynamic) with cations, anions and neutral guest molecules have figured prominently throughout the literature.[77-85] These works offer a concise and quantitative base for understanding the effects of macrocycle and guest interactions for a large number of structures, based on the kinetic and thermodynamic properties of the resulting complexes. These surveys can assist one in the rational design of new macrocycles, and reasonable predictions can be made regarding their effectiveness in forming host-guest complexes with desired thermodynamic stabilities.[84,86]

1.14.2 Ion-specific macrocyclic ether chemosensors

The application of supramolecular receptors to fluorescence sensing was first described by Sousa in 1977.[87] When naphthalene is functionalised with a crown ether moiety, the association of alkali earth metals is signalled by changes in the naphthalene fluorescence. Subsequent reports by Bouas-Laurent and Lehn,[88,89] Wolfbeis,[90] de Silva,[91] Street,[92] and Czarnik[44,51,93] all built on this original premise, in which binding of metals to crowns and azacrowns has been coupled to the emission changes of covalently-attached fluorophores.

1.14.3 Lead(II)-specific macrocyclic ether chemosensors

It is well established in the literature that structurally mixed-donor crown ether compounds form stable complexes with the transition metal and heavy metal cations, while their complexes with the alkali metals are thermodynamically less stable.[74,83,84,86] It is this property that makes crown ether compounds, containing a mixture of oxygen, nitrogen or sulfur donor atoms, promising candidates in the development of lead(II) ion-selective probes.

Only a few examples exist in the literature that describe the study of lead(II)-specific macrocyclic chemosensors in aqueous solution. Czarnik *et al.*[44,51] has taken the general cyclic polyaza-cryptand (Figure 1.5), with selectivity for lead(II) reported by Hancock *et al.*[94] and synthesised the conjugated anthrylhemicryptand derivative (Figure 1.5). Upon complexation of the derivative with lead(II), a weak net quenching of fluorescence was observed, a result that is most likely attributed to the heavy atom effect.[10] Furthermore, the anthryl derivative was found to be ineffective at binding lead(II) at the micromolar chemosensor concentrations employed owing to its low binding affinity in aqueous solution.

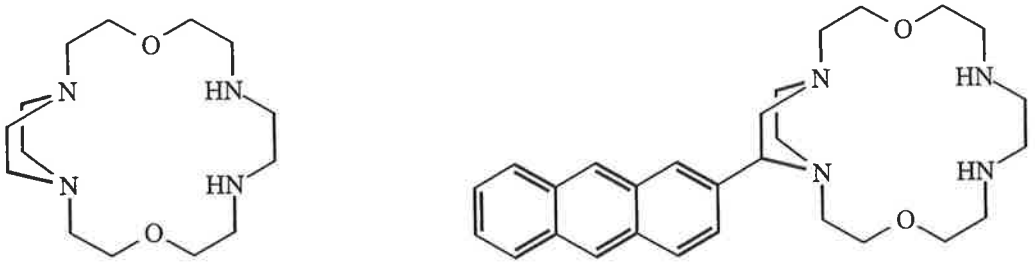

Figure 1.5 *Polyaza-cryptand (left) and its anthrylhemicryptand derivative (right).*

Bartsch and Porter *et al.*[49] introduced the diprotonic chromophoric and fluorophoric crown polyethers presented in Figure 1.6, as potential reagents for the selective extraction and determination of heavy metal ions, including lead(II), mercury(II), cadmium(II), copper(II) and barium(II). Both ligands were found to have an unprecedented selectivity for mercury(II) and, to a lesser extent, a selectivity for lead(II) over the other divalent cations

studied. However, upon complexation of the fluorophoric ligand with lead(II) or mercury(II) ions, a quenching rather than an enhancement of fluorescence was observed, attributed to the heavy atom effect.[10]

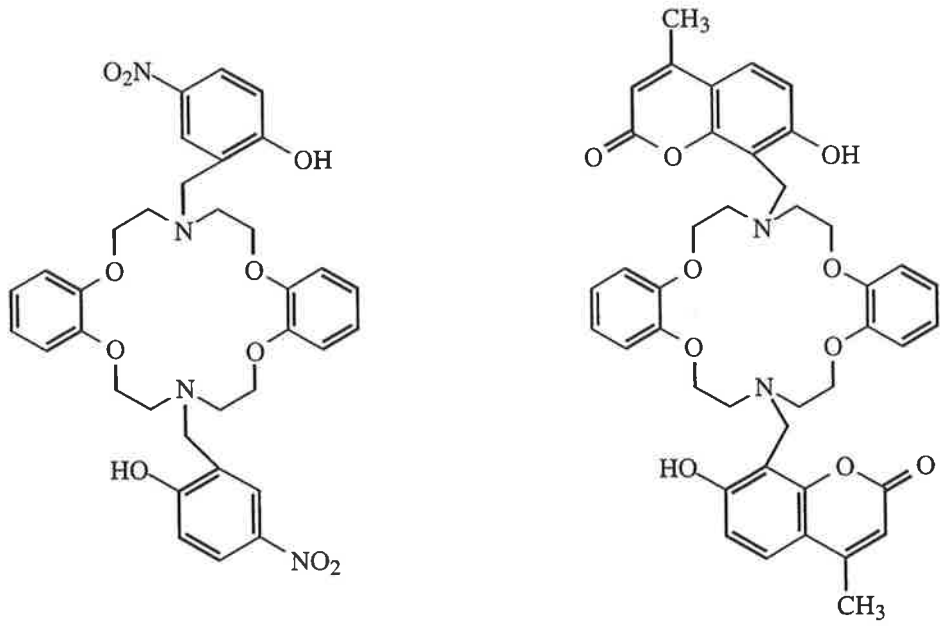

Fig. 1.6 *Chromophoric (left) and fluorophoric (right) crown polyether derivatives.*

1.14.4 Design strategies

Many factors affect the formation and thermodynamic stabilities of ion-macrocycle complexes, and all need to be addressed properly in the design of potential ligands for specific metal ion recognition. Such factors include: (i) the type(s) of donor atoms and binding sites in the ring, (ii) the number of binding sites in the ring, (iii) the relative sizes of the ion and the macrocyclic cavity, (iv) the physical placement of the binding sites, (v) the steric hindrance within the ring, (vi) the solvent and extent of solvation of the ion and the binding sites, and (vii) the electrical charge of the ion.[77,86] Even though one can make adequate generalisations based on these factors alone, it is still a difficult task to predict whether specific ion recognition will be obtained by a particular ligand or series of ligands of interest.

In the first stages in the rational design of ligands for specific metal ion recognition, a macrocyclic ligand that may exhibit a favoured coordination toward one metal ion of interest is prepared. The choice of the initial ring system is usually intuitive, or it may be based on analogy with the known complexation characteristics of structurally-related ligands.[86] Upon synthesis of the desired ligand system, its coordination chemistry is then examined. This may include; (i) the determination of thermodynamic stability constants for the desired complexes, generally by means of potentiometric or calorimetric methods; (ii) kinetic studies of complex formation and/or dissociation; (iii) X-ray structural analysis where possible; (iv) spectroscopic solution studies and, finally, (v) molecular modelling studies using gas-phase *ab initio* or molecular mechanics calculations.[84,86,95] Using these results, the system under investigation can be assessed for any relevant metal-ion discrimination. Once the factors influencing this discrimination are established, the original ring system may be structurally modified in an attempt to enhance any observed discrimination toward the particular metal ion.[86]

1.15 Fluorescent probes for other metal ions

Our interest in the study of the coordination properties of macrocyclic ligands toward lead(II) has been clearly described in this chapter, however, their affinity towards zinc(II) and cadmium(II) ions is also considered relevant to this investigation. Zinc(II) is a biologically prevalent cation that tends to show considerable affinity for mixed-donor, macrocyclic ligand families.[84,85,95] The binding affinities of macrocyclic ligands for zinc(II) ions must be investigated in order to quantify the stabilities of the ligands toward zinc(II) ions and thus, establish the likelihood for zinc(II) interference when the ligands are used as probes for lead(II) ions in biological media. Investigations into the affinity of the macrocyclic ligands toward cadmium(II) ions is also of interest to this study. Even though the effects of cadmium(II) pollution on human and environmental sources are not considered to be as widespread as lead(II) contamination, the acknowledged increase in the levels of the heavy metal, particularly in natural aquatic environments, has led to much concern over its adverse effects on biological systems.[6,18,20,96] Only a few cadmium(II)

probes exist in the current literature and, therefore, investigations into the development of a cadmium(II)-specific fluorescent probe would also be of considerable benefit.

1.16 Work described in this thesis

The established strategies that are summarized above will be followed in this work for the investigation of crown ether compounds as potential lead(II)-specific fluorophores. A series of macrocyclic ligands were chosen for this study, and details of their syntheses are presented in Chapter 2. A rationale for the choice of the ligands investigated in this study is also presented. This thesis is mainly concerned with the synthesis of the series of ligands and the assessment of their selectivity and stability towards a series of metal ions including lead(II), zinc(II) and cadmium(II) ions. The interaction of these ligands with the relevant metal ions is discussed in Chapter 3, and the various factors that were found to influence any observed discrimination are also reported. This preliminary work would form the basis of an elaborate sequence in the development of a lead(II)-specific probe. It is envisaged that those macrocyclic ether ligands which exhibit the most promising coordination behaviour, either because they form the most stable complexes with lead(II) or they show the greatest selectivity toward lead(II) ions over the other metal ions, would be structurally modified in an attempt to incorporate the desired properties of a fluorophoric probe.

2 Design and Syntheses of Trial Ligands

2.1 Target Molecules

This investigation commenced by selecting the series of crown ether compounds shown in Figure 2.1. It was envisaged that ligands **1 - 6** would offer a select but informative group of crown ether ligands which would provide a means of determining the type of ligand that would have the greatest potential to be developed into a lead(II)-specific probe. Ligands **1 - 6** contain a combination of oxygen, nitrogen and sulfur donor atoms. It is well established in the literature that macrocyclic polyether ligands (i.e. those containing only oxygen donor atoms) show a high selectivity towards the alkali and alkali-earth metal ions.[69,74,75,79,97] However, it is also acknowledged that replacement of the oxygen atoms with nitrogen or sulfur atoms in these systems leads to a significant increase in the selectivity of the resultant ligands toward transition and heavy metal ions.[69,98] Since this investigation is primarily concerned with the development of ligand systems that show particular stability toward lead(II) and cadmium(II), with sufficient discrimination for the heavy metals over the biologically prevalent zinc(II) ions, it seemed logical that our investigation should commence with a series of macrocyclic ligands containing mixed donor-atom systems.

When developing a macrocyclic ligand system that is specifically designed to target a particular metal ion or metal ion series, the classification of the metal ions (acids) and the donor atoms (bases) as hard, soft or intermediate is a useful starting point in donor atom selection.[7-10] The Hard and Soft-Acid and Base (HSAB) classification of both the donor atoms and metal ions relevant to this investigation indicates that the hardness of the Lewis bases (donor atoms) decreases as one moves from oxygen to nitrogen to sulfur. The hardness of the Lewis acids (metal ions) decreases as one moves from the borderline hard zinc(II) to lead(II) to cadmium(II).[7-10] Even though the HSAB classification will provide a preliminary guide for donor atom selection in the ligand series, more detailed considerations of the various parameters influencing the complexation properties of the

ligands need to be addressed. In most cases, such considerations can only be established experimentally.

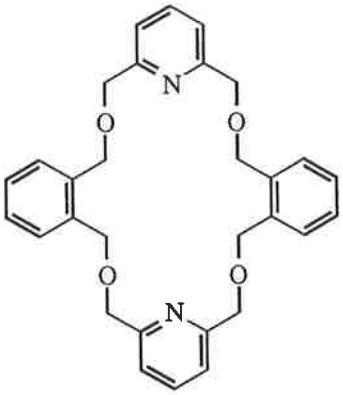

1

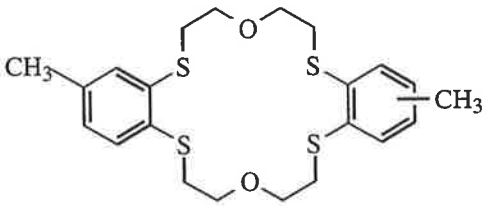

2

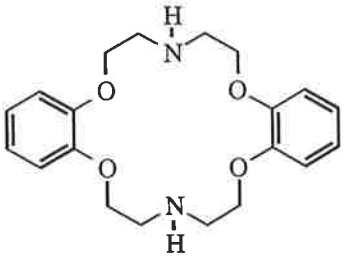

3

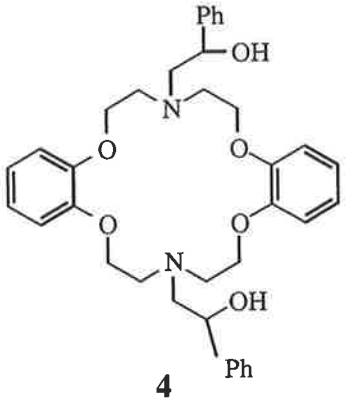

4

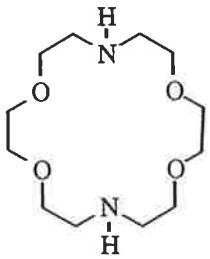

5

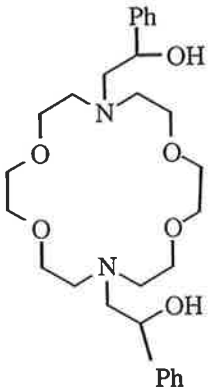

6

Figure 2.1

The selectivity of macrocyclic ligands that contain nitrogen, or a combination of nitrogen and oxygen donor atoms, toward transition and heavy metal ions is well described in the literature.[69,98,99] Each of the ligands **1**, **3** and **5** contain four oxygen and two nitrogen donor atoms in the macrocyclic ring system. Ligands **4** and **6** possess an identical crown ether structure with four oxygen and two nitrogen donor atoms, in addition to the two additional neutral oxygen donor atoms that are present within the pendant arms of compounds. Ligands **4** and **6** are of particular interest to this study with respect to their potential selectivity toward lead(II) ions. It is well established in the recent literature that as the number of neutral oxygen atoms in the ligand system increases, regardless of whether or not the oxygen donor atoms are part of the ring system, the greater the selectivity of the ligand toward large metal ions.[94,98,100,101] It was envisaged, therefore, that major increases in selectivity towards lead(II) ions would be observed as one moves from compound **3** to **4** and from compound **5** to **6**. Ligands **3** and **5** were specifically chosen as preliminary target molecules since they possess the potential for further structural modification, namely by the addition of pendant groups on either or both of the nitrogen atoms in the molecule. These modifications would enable the selectivity of the ligands to be tailored specifically toward a particular metal ion of interest.

Ligand **2** is of particular interest to this study. Even though lead(II) is considered to be intermediate in hardness between hard and soft acids, its high binding affinity towards ligands that contain soft sulfur atoms is reported in the literature.[17,30] Thus, it was expected that ligand **2**, with the presence of the four soft sulfur donor atoms, would exhibit a useful selectivity for the large lead(II) and cadmium(II) ions.

Even though ligand **1** is structurally related to ligands **3** - **6**, with respect to the number and type of donor atoms present in the crown ether ring, a few significant differences are obvious. The nitrogen atom is sp^2-hybridized in ligand **1** and sp^3-hybridized in the remaining compounds **3** - **6**. Such a difference may be important when one compares both the binding affinities and the fluorescence characteristics of the ligands. Provided that the available pyridyl nitrogen donor atoms of ligand **1** can coordinate to the metal ion, it was

postulated that a greater change in the UV-visible absorbance spectrum, and possibly the fluorescence, would result for those complexes of ligand **1** owing to the direct effect of coordination on the chromophoric (pyridyl) moiety of the system. As ligands **1** and **3 - 6** all contain the two aromatic substituents, it was assumed that any chromophoric changes that are induced by binding of the metal ion to the oxygen atoms would be comparable for all such ligands.

Another requirement of the ligands chosen for this study includes the incorporation of, or the potential for the incorporation of, chromophoric groups into the molecule, generally in the form of aromatic rings. It is established in the literature that the presence of electron-withdrawing aromatic groups in many types of crown ether ligands reduces the Lewis basicity of the nearby donor atoms,[69] and causes an overall increase in the steric strain and rigidity of the cyclic systems.[98,100,102] Moreover, this effect improves ligand preorganisation towards particular ions and thus markedly enhances its metal ion selectivity as the rigidity inhibits the cyclic ligand from undergoing the considerable structural changes that are required to accommodate differently-sized ions.[83,86,100] The incorporation of aromatic groups into the ligand system is also considered important with respect to the chromophoric properties that they impose. It is feasible that ligands **1 - 4** and **6** may contain sufficient chromophoric properties to promote significant changes in the absorbance maxima upon complexation. Furthermore, the use of simpler chromophoric moieties will provide valuable information on general methods of incorporation of aromatic systems into crown ether ligands; an important consideration, particularly in later syntheses, when the incorporation of more highly conjugated derivatives is required.

2.2 Crown ether ligand syntheses

2.2.1 Introduction

The preparative methodology for some of the crown ether ligands presented in Figure 2.1 is discussed in the literature.[76,103-106] However, it is widely acknowledged that these apparently conventional syntheses are far from straightforward.[71,106,107]

Generally, the preparative procedures for the synthesis of crown ethers can be subdivided into two major categories; (i) direct macrocycle syntheses and (ii) metal-ion template syntheses.[69,71] The first group of reactions involves a convergent synthetic strategy that culminates in the 1:1 condensation reaction between the appropriate components, under low to moderate dilution conditions, to afford the target macrocycle. This direct method may also be performed under high-dilution conditions to enhance the formation of the desired intramolecular condensation product and reduce the potential for oligomerization or polymerization. Alternatively, low- to moderate-dilution conditions may be employed where certain mechanisms, such as metal-ion template formation or the presence of bulky leaving groups, may operate in assisting the cyclization step of the particular ligand system.[69] Both methods have been found to afford high yields of the desired cyclized products. However, yields have been found to be reliant on the particular system studied and the specific conditions employed in the procedure. The majority of the crown ether ligands prepared in this study were synthesised by direct methods under moderate dilution conditions.

The second group of reactions involves metal-ion template syntheses. The high affinities of crown ethers for certain metal ions allows one to exploit what is termed the "template effect", which involves metal ion organisation of the transition state that ultimately leads to the formation of the desired macrocycle.[106] Pederson's initial isolation of dibenzo-18-crown-6 (Equation 1.2) was accomplished in concentrated solution, and it is now generally accepted that the presence of the sodium(I) ion (introduced into the solution in the form of sodium hydroxide) contributed to the formation of the crown polyether.[71,74] Many procedures that utilise the template effect for the synthesis of macrocyclic crown compounds have been described in the literature,[69,108-110] but it is also generally acknowledged that the process has not been investigated systematically in all cases.[69,71] In some instances, it was found that even where no templating cation was present, the same high yields of the desired macrocycles were obtained.[71] Thus, the definitive rules concerning this important principle and the general understanding of such effects have yet

to be formulated precisely,[69,71] and invocation of the template effect is to be made with some discretion.[71]

2.2.2 Synthesis of *3,12,20,29-Tetraoxa-35,36-diazapentacyclo-[29.3.1.1.^{14,18}0.^{5,10}-0.22,27]-hexatriaconta-1(35),6,8,14,16,18(36),22(27),23,25,31,33-dodecaene, 1.*

The synthesis of ligand **1** was achieved using the reaction shown in Equation 2.1.[105]

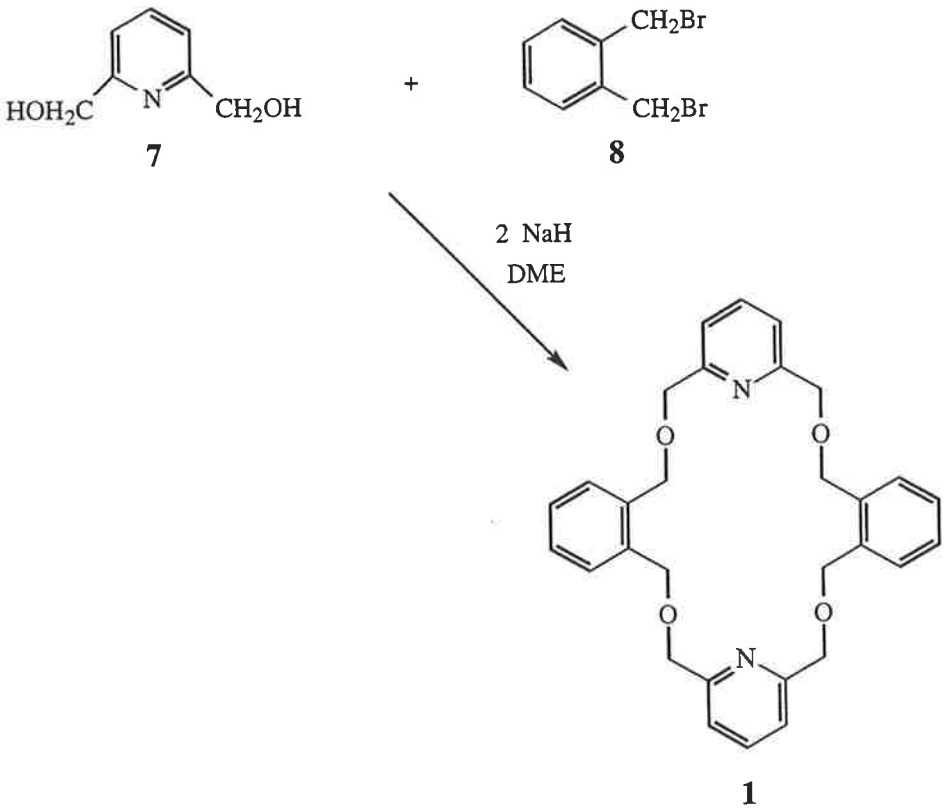

Equation 2.1

The precursor pyridine derivative **7** was prepared by the sodium borohydride reduction of dimethyl 2,6-pyridinedicarboxylate in dry methanol, using a standard literature method (Equation 2.2).[111] The product was obtained as white prisms in good yield.

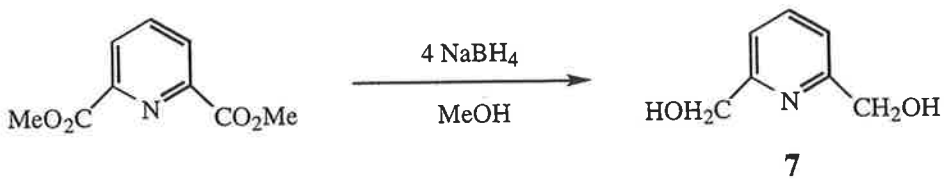

Equation 2.2

Compound **8** was synthesised by the bromination of *o*-xylene using *N*-bromosuccinimide (NBS), with a catalytic amount of benzoyl peroxide to initiate the reaction (Equation 2.3). The dibromide **8** was obtained as fine white needles in good yield. The mass spectrum of **8** displayed a molecular ion peak at *m/z* 264 and a base peak at *m/z* 185, corresponding to M-Br fragmentation.

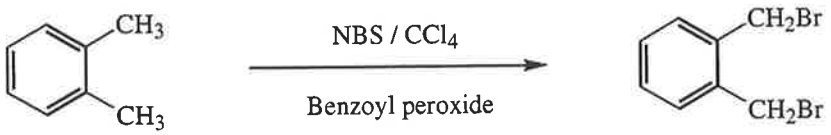

8

Equation 2.3

The coupling of compounds **7** and **8** in the presence of sodium hydride in dry dimethoxyethane (Equation 2.1) afforded a crude reaction mixture. Purification by flash chromatography using a gradient solvent system, from a 1:1 ethyl acetate/hexane mixture to a 3:1 ethyl acetate/hexane mixture, afforded a crude fraction which was recrystallised from ethanol to afford the desired product **1** as white needles, in an average yield of 35-40%. The molecular structure of **1** was confirmed by X-ray crystallography (Appendix A).

2.2.3 Synthesis of *2,3,11,12-Bis(4'-methylbenzo)-1,4,10,13-tetrathia-7,16-dioxacyclo-octa-2,11-diene, 2.*

The synthesis of compound **2** was first attempted by using a similar method to that outlined by Pederson[76] in 1971, involving the one-pot coupling reaction between toluene-3,4-dithiol and bis(2-chloroethyl) ether in dry DMF, in the presence of sodium hydride (Scheme 2.1). The reaction involves the initial generation of the mono-anionic species of toluene-3,4-dithiol, followed by the dropwise addition of one-half equivalent of the bis(2-chloroethyl) ether to afford the intermediate species **9**. This intermediate was not isolated, but it was further reacted with two equivalents of hydride and another one equivalent of bis(2-chloroethyl) ether to afford the cyclized product **2**.

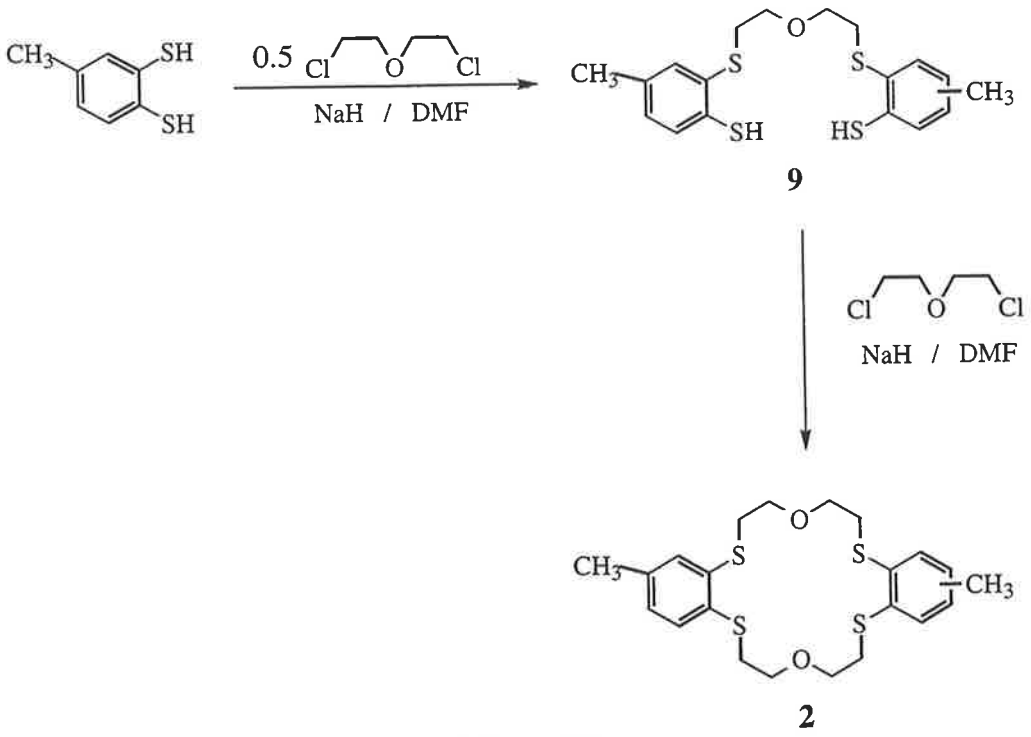

Scheme 2.1

Initial attempts at this procedure afforded a highly viscous, pink paste, which on t.l.c. analysis (dichloromethane) showed the presence of at least four products. The purification method outlined by Pederson[76] involved the extraction of the paste with *n*-heptane, followed by acetone, and combination and concentration of these organic fractions to afford the desired cyclized product **2** as white, shiny crystals. However, our attempts at purification of the crude product by this method were to no avail. On each occasion an oily paste was obtained, and the same mixture of compounds was observed when analysed by t.l.c.

Regardless of the low final yields of product reported by Pederson (*ca.* 6%),[76] numerous attempts at purifying the crude, pink paste by flash chromatography using both silica and neutral alumina were undertaken, all of which proved to be unsuccessful. T.l.c analysis showed significant smearing of the crude mixture on the t.l.c. plate, even when a number of solvent systems were utilised. ^{1}H n.m.r. analysis of the crude paste showed evidence for the formation of the desired product **2**, with the characteristic signals for the methylene groups adjacent to the sulfur and oxygen atoms appearing at δ 2.97 - 3.1 and δ 3.59 - 3.91, respectively. However, the amount of desired product in the mixture was very low.

As purification of this crude mixture proved to be very difficult and the amount of the desired product expected from this reaction sequence was at best questionable, it was considered that this method was not viable in the efficient synthesis and isolation of the ligand **2**, particularly when the high cost of the toluene-3,4-dithiol precursor was considered.

An improved method for the synthesis of **2** is shown in Scheme 2.2. 2-(2'-chloroethyloxy) ethanol was converted to its tetrahydropyranyl ether under standard conditions, using 3,4-dihydro-2*H*-pyran in the presence of acid.[112] The crude residue was purified by Kugelrohr distillation to yield compound **10** as a colourless oil in good yield.

The coupling of toluene-3,4-dithiol and two equivalents of **10** was performed in dry n-butanol, in the presence of sodium hydride. The first step involved the *in situ* reaction of sodium hydride with *n*-butanol to form the butoxide anion, which in turn reacted with toluene-3,4-dithiol to generate the disulfide-anion species. The electrophile **10** was then added slowly to the solution containing the anionic species and heated to 100°C for 24 hours. T.l.c. analysis (10% ethyl acetate / hexane) of the reaction mixture showed two products, which were assumed to be the mono- and di-alkylated products of the toluene-3,4-dithiol starting material. The reaction mixture was heated for a further 24 hours in an attempt to drive the reaction further to completion. After this extended period of heating, t.l.c. analysis did not show any change in the product ratio. The crude reaction mixture containing **11** was directly treated with $HCl_{(aq)}$ in order cleave the tetrahydropyranyl protecting groups. Purification by flash chromatography using a 10% acetone / dichloromethane solution, followed by gradual increases in solvent polarity, afforded the desired product **12** as a pale yellow oil in very good yield.

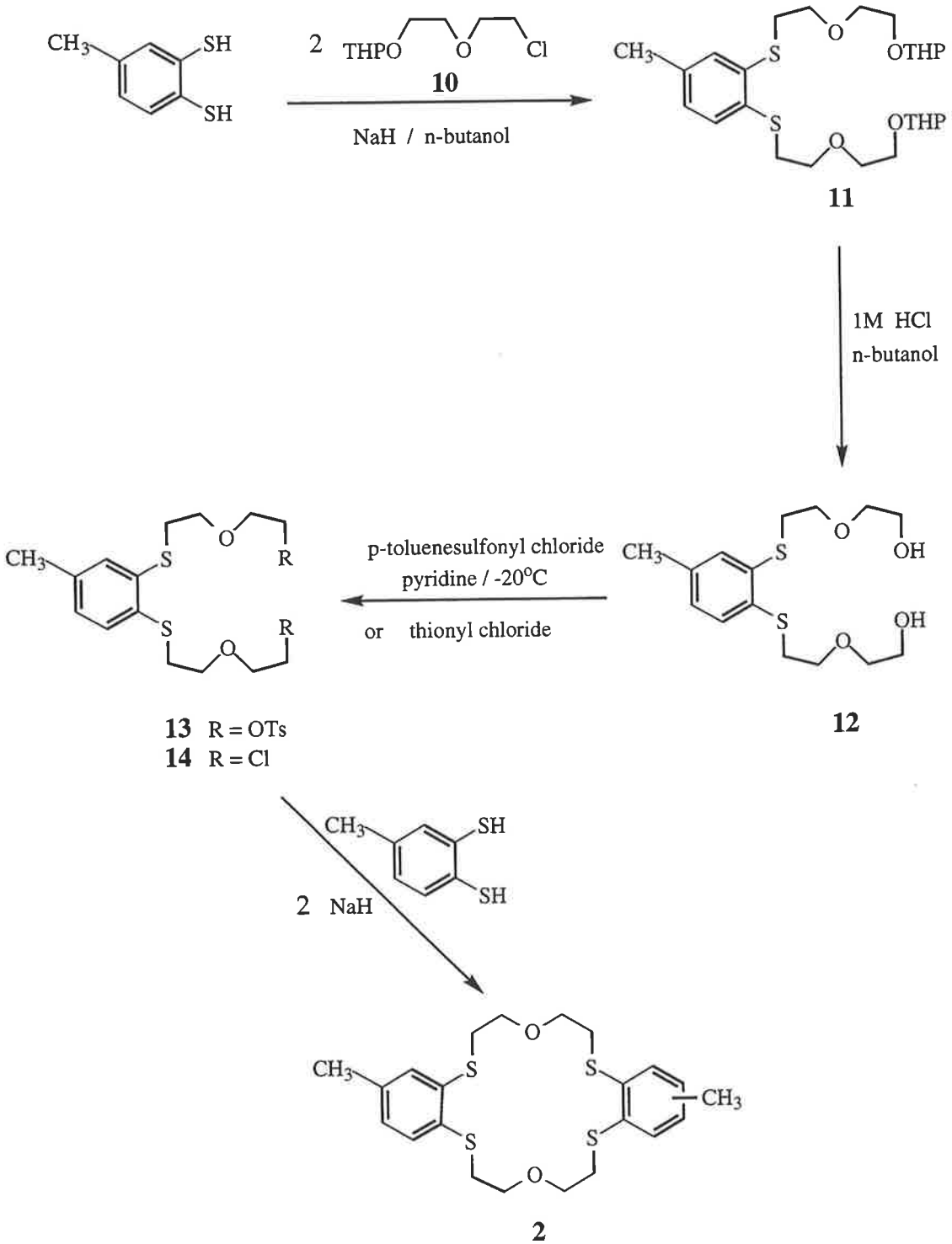
CH3
SH
SH
2
THPO
O
Cl
10
NaH / n-butanol
CH3
S
O
OTHP
S
O
OTHP
11
1M HCl
n-butanol
CH3
S
O
OH
S
O
OH
12
p-toluenesulfonyl chloride
pyridine / -20°C
or thionyl chloride
CH3
S
O
R
S
O
R
13 R = OTs
14 R = Cl
CH3
SH
SH
2 NaH
CH3
S
O
S
CH3
S
S
O
2

Scheme 2.2

Compound **12** showed ^{1}H n.m.r. resonances at δ 2.97 - 3.08 and δ 3.44 - 3.66 for the methylene protons adjacent to the sulfur and oxygen atoms, respectively. The mass spectrum of **12** showed a molecular ion at 332, and peaks at *m/z* 271 and *m/z* 243 corresponding to M-$C_2H_5O_2$ and M-$C_4H_9O_2$ fragmentations, respectively. Infra-red analysis of **12** showed the characteristic O-H stretch at 3416 cm^{-1}.

The crude mixture contained approximately 20% of the mono-tetrahydropyranyl ether of **12**. This material was obtained as a pale yellow oil and it was characterised by ^{1}H n.m.r. spectroscopy. The ^{1}H n.m.r signals of the mono-cleaved product appear in almost identical positions to those of **12**, with the exception of a multiplet at δ 3.76 - 3.81 which is assigned to the methylene protons adjacent to the tetrapyranyl group. In addition, the signals of the characteristic 2-CH proton of tetrahydropyranyl moiety were observed at δ 4.6.

The next step in the reaction sequence (Scheme 2.2) involved the conversion of the diol **12** to either the ditosylate **13** or the dichloride **14**. The tosylation of **12** was achieved under standard conditions,[113] using *p*-toluenesulfonyl chloride in pyridine. Purification of the crude reaction mixture by flash chromatography (30% ethyl acetate / hexane) afforded the desired product **13** as a pale yellow oil in 75% yield. The characteristic tosyl AB quartet was observed at δ 7.80 and δ 7.30 in the ^{1}H n.m.r spectrum of **13**. Mass spectral analysis confirmed the structure of **13** with a molecular ion peak at *m/z* 640 and a peak at *m/z* 469, corresponding to a M-$C_7H_7SO_3$ fragmentation. In addition to **13**, a small amount (< 10%) of the mono-tosylated species was also obtained from the reaction mixture and its structure was indicated by ^{1}H n.m.r. analysis.

It is interesting to note that in the event of the tosylation reaction warming above 0°C, an elimination reaction of **13** led to the facile formation of the alkene species **15**. This product was isolated exclusively from a reaction mixture that was allowed to stir for 12 hours at room temperature. The structure was confirmed by ^{1}H n.m.r. analysis with the characteristic alkene signals observed at δ 5.09 - 5.29 and δ 5.78 - 5.86.[114] The isolation of

the by-product **15** was not unexpected in the tosylation reaction as Amabilino *et al.*[106] acknowledged the importance in maintaining lower temperatures during the tosylation of related diol systems.

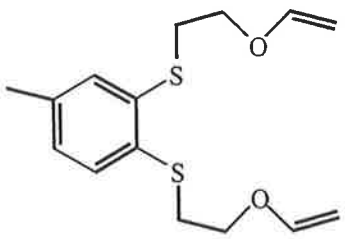

15

Compound **14** was prepared by the treatment of **12** with neat thionyl chloride. The crude product was purified by flash chromatography to afford compound **14** as an dark-orange oil, whose structure was confirmed by ^{1}H n.m.r. spectroscopy, mass spectroscopy and infra-red analysis. As expected, the ^{1}H n.m.r. spectrum of **14** did not greatly differ from the spectrum obtained for the starting diol **12**, except for the absence of the broad OH signal. The mass spectrum of **14** showed a molecular ion peak at *m/z* 369 and fragmentations at *m/z* 333.5 and *m/z* 298, which correspond to the M-Cl and M-2Cl, respectively. The infra-red analysis of **14** showed the characteristic C-Cl stretch at 746 cm^{-1}.

Even though compound **14** was successfully isolated, the total yield of reaction after chromatography was 25%. It was thought that the mediocre yield was due to the tendency of **14** to bind irreversibly to the acidic silica column, most probably because of displacement of the chloro groups of **14** by the nucleophilic oxygen sites present in the silica. During chromatography the entire length of the silica column became visibly coated with the orange oily residue which was unable to be removed, even with solvents of high polarity.

The cyclization step of the reaction sequence was achieved by a nucleophilic substitution reaction between the anionic derivative of toluene-3,4-dithiol and either ditosylate **13** or dichloride **14**. Upon purification of the crude reaction products, compound **2** was isolated

in an average yield of 34% as fine, white needles, with melting point 140-144°C, literature[76] 147°C. Microanalytical data confirmed the formula of **2**, and the mass spectrum showed a molecular ion signal at *m/z* 452. In addition, the ultraviolet spectrum of **2** recorded in methanol showed an absorbance maximum at 256 nm, in exact agreement with the literature value.[76] It is clear that, when compared to Pederson's original method,[76] the step-wise synthesis described above greatly improves the yield of the desired tetrasulfide ligand **2**.

2.2.4 Synthesis of *7,16-Diaza-1,4,10,13-tetraoxa-2,3,11,12-dibenzocyclo-octadeca-2,11-diene, 3.*

Investigations into the synthesis of compound **3** began by using the procedure first described by Högberg and Cram in 1975.[104] The first step of the procedure is outlined in Equation 2.4, and it involves the one-pot cyclization reaction between the tosyl-protected diethanolamine derivative **16** and pyrocatechol. The tosylation of diethanolamine was readily achieved under standard conditions to afford **16** in good yield. The subsequent reaction of **16** with pyrocatechol under basic conditions in DMF afforded a fine, white powder, which was found by t.l.c. analysis to contain a mixture of the required cyclized species **17** and the mono-cyclized species **18**. Mass spectral analysis showed two strong $(M+H)^+$ signals at *m/z* 667 and *m/z* 334, corresponding to compounds **17** and **18**, respectively. The ^1H n.m.r data showed characteristic signals at δ 3.16 and δ 4.15 for the methylene protons adjacent to the nitrogen and oxygen atoms, respectively. As expected, both compounds **17** and **18** gave identical ^1H n.m.r spectra.

Attempts at separating the mixture of products containing **17** and **18** by flash chromatography, using a variety of solvent systems, proved to be unsuccessful. Purification by fractional crystallisation was also unsuccessful, and attempts at the isolation of either **17** or **18** by the selective complexation with sodium(I) ions in an ethanol solution was also found to be an unsuitable method for purification.

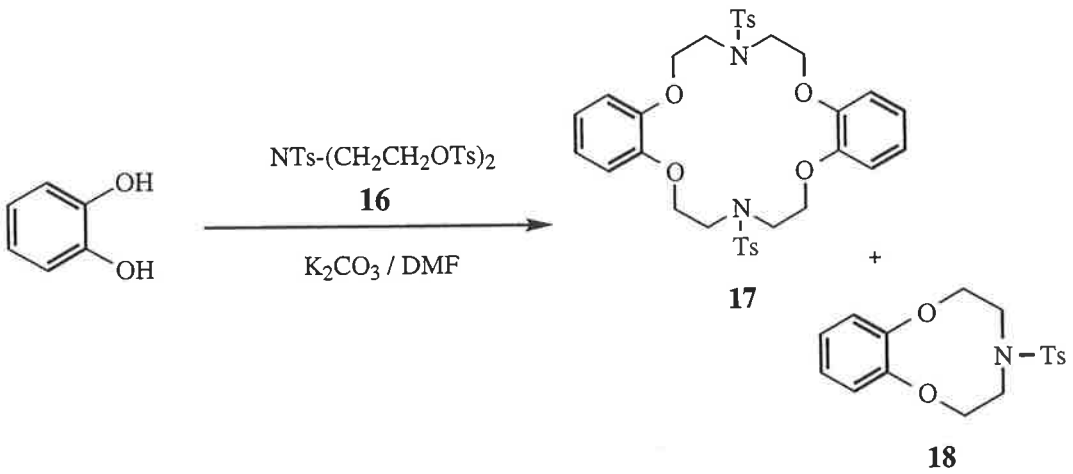

Equation 2.4

In addition to the difficulties encountered in the separation of the product mixtures containing **17** and **18**, another point of concern regarding this method was whether compound **17** could be obtained from the reaction mixture in a significant yield. Mass spectral evidence suggested that the mono-cyclized ligand **18** was present in greater amounts than that of the desired product **17**; a result which is in accordance with that reported by Högberg and Cram[104] who quoted a 40% isolated yield for **18**, but only a 10% yield for **17**. Unfortunately, the purification methods employed by Högberg and Cram[104] were not reported. Despite the questionable yield of the desired product **17** in the mixture, it was decided that a detosylation reaction would be attempted on the crude mixture containing both **17** and **18**.

The removal of the tosyl groups from **17** and **18** would afford a mixture of amino compounds **3** and **19** respectively, as shown by Equation 2.5. It was envisaged that this mixture of ligands may have been more readily separable than their precursors, possibly by ion-exchange methods utilising the protonated species.

The robustness of these types of crown ether systems toward detosylation reactions is well known,[49,115] and it is generally attributed to the steric bulk of the macrocyclic ring, particularly the presence of the aromatic moieties, that prevent the efficient removal of the tosyl-protecting groups.

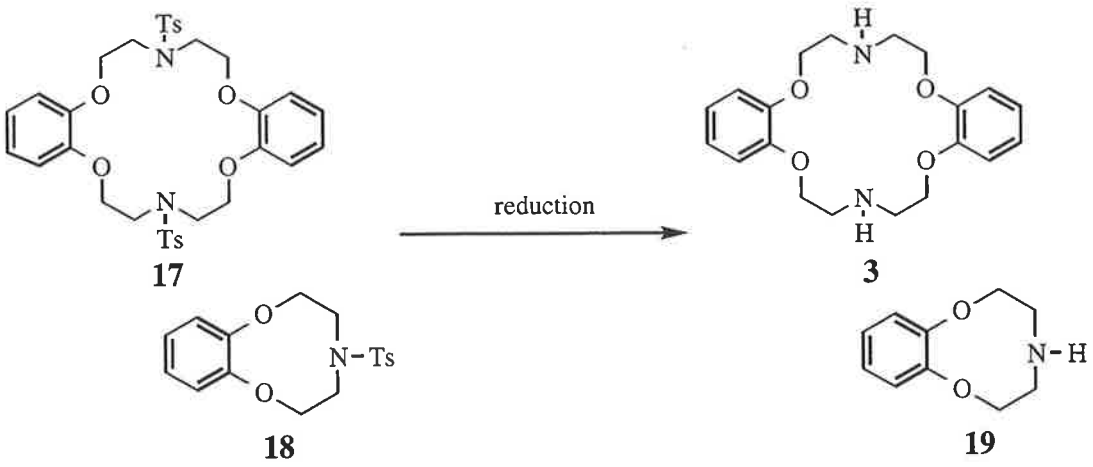

Equation 2.5

Attempts at hydrolysing the sulfonamide groups by using either a solution of glacial acetic acid / hydrobromic acid / 5M phenol[104] or a concentrated sulfuric acid solution[116] were unsuccessful. Despite extending the reaction time and increasing the reaction temperature, the detosylation reaction was never observed under these conditions, and compounds **17** and **18** were recovered intact from the reaction mixtures. Attempts at the reductive cleavage of the sulfonamide groups using the sodium / naphthalene method[117,118] in dimethoxyethane were also unsuccessful.

As numerous methods for the cleavage of these types of sulfonamide groups were found to be unsuccessful, and an efficient method for the isolation of the desired cyclized species, as either the ditosylate **17** or the diamine **3**, was yet to be established, it was concluded that this pathway was not a viable route for the synthesis of compound **3**. Furthermore, as mentioned previously, it was anticipated that even if the detosylation reaction was successful and the subsequent isolation of compound **3** was achieved, the overall yield of **3** was anticipated to be very low. An alternative route for the synthesis of compound **3** was required.

A step-wise approach to the synthesis of the desired dibenzo-diaza-18-crown-6 derivative **3** was employed.[103] It was postulated that the two halves of the macrocycle, namely the ditosylate species **20** and the carbamate species **21** presented in Equation 2.6, could be constructed separately and then combined in the final cyclization step to afford the ligand

22 containing the two benzylcarbamate groups. Since methods for the removal of benzylcarbamate moieties involve facile reactions that are well described in the literature,[103,113] it was envisaged that the cyclized product **22** would be an appropriate precursor for the formation of **3**, and that this step-wise reaction sequence would offer a more viable and efficient synthesis of the desired compound. Furthermore, the step-wise pathway presented in Equation 2.6 would eliminate the possibility of the formation of the mono-cyclized material **19** and perhaps lead to a better overall yield of **3**.

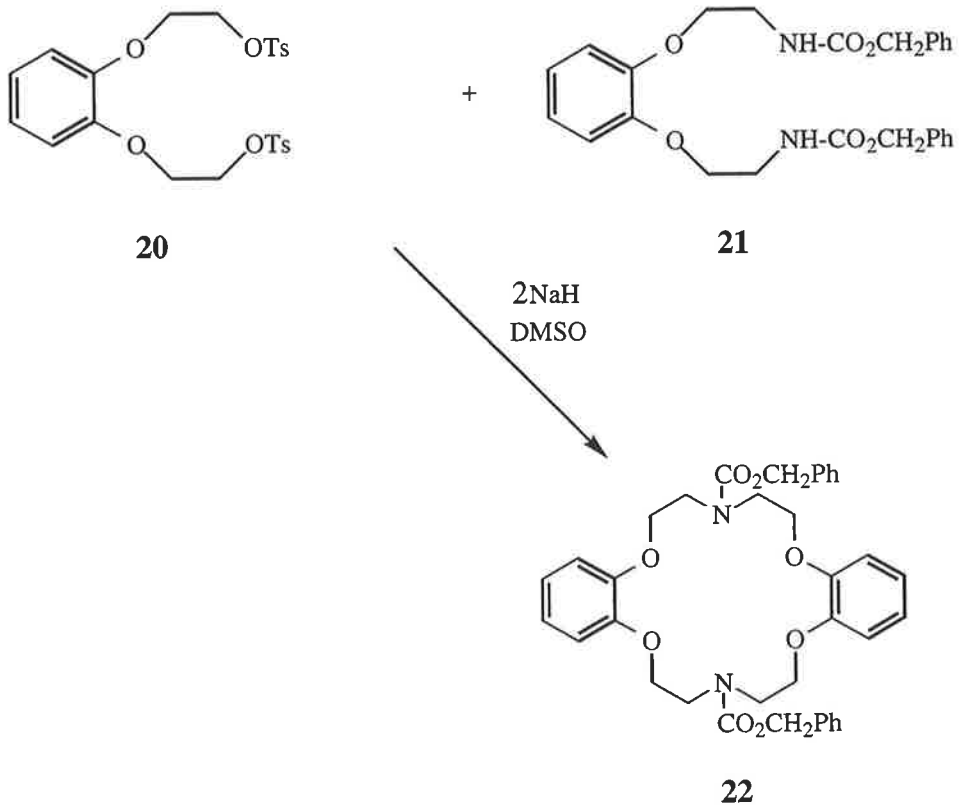

20 **21** **22**

Equation 2.6

The three-step synthesis of **20** began with the generation of the diester derivative **23** by the reaction between pyrocatechol and ethylbromoacetate under basic conditions in dry acetone (Equation 2.7).

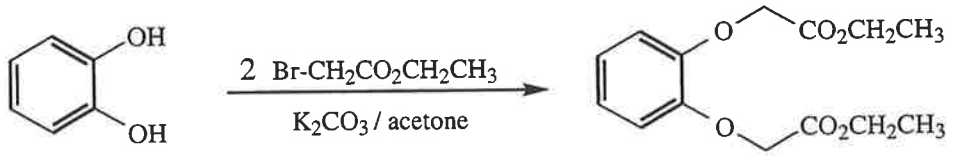

23

Equation 2.7

The crude residue was obtained as an orange oil which, when purified by Kugelrohr distillation, afforded **23** as a colourless, viscous oil in good yield. The structure of **23** was confirmed by ^{1}H n.m.r spectroscopy, with the characteristic ethyl ester signals observed at δ 1.29 and δ 4.26. In addition, the mass spectrum gave a molecular ion peak at *m/z* 282 and a fragmentation peak at *m/z* 135, corresponding to M-$C_6H_{10}O_4$. The infra-red spectrum of **23** showed a strong carbonyl absorbance at 1756 cm^{-1}.

The next step in the synthesis involved the reduction of the diester **23** to the diol species **24**, under standard conditions employing lithium aluminium hydride in dry diethyl ether (Equation 2.8).

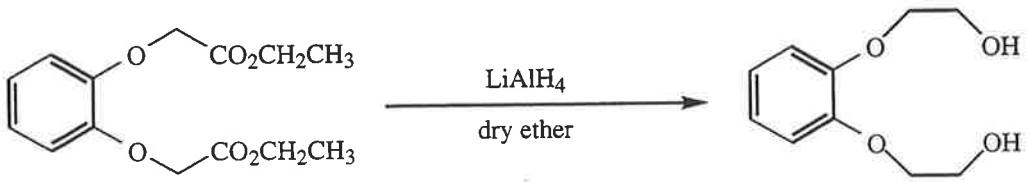

23 **24**

Equation 2.8

Removal of the inorganic salts from the reaction product by vacuum filtration, and evaporation of the resulting filtrate gave **24** as a crude solid, which upon crystallization from hexane afforded the desired compound as white needles in good yield. The formation of the diol was confirmed by the disappearance of the ester signals in the ^{1}H n.m.r spectrum, and the appearance of a broad signal centred at δ 3.55 corresponding to the hydroxyl protons. This assignment was confirmed by a deuterium oxide exchange reaction. A broad infra-red band located at 3504 cm^{-1} was assigned as the hydroxyl stretch. The mass spectrum of **24** showed a molecular ion signal at *m/z* 198. Despite the inconsistency found between the experimental melting point of the diol **24** (79 - 80°C), with that reported in the literature (93 - 94°C),[103] the analytical data described above were all consistent with the structure of **24**.

The procedure described by Landini *et al.*[119] offers an alternative method for the synthesis of **24**. Rather than preparing compound **24** by the two-step sequence *via* the diester **23**, it

can be obtained directly by the reaction of pyrocatechol and 2-chloroethanol in dry ethanol (Equation 2.9).

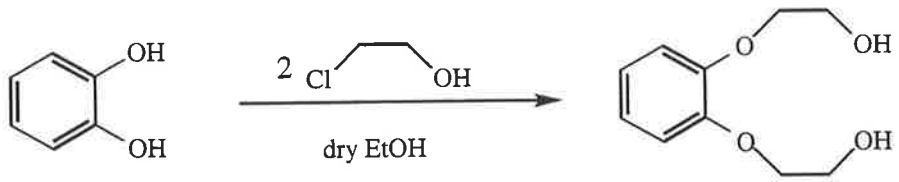

24

Equation 2.9

Crystallization of the crude product from benzene / petroleum ether afforded the diol **24** as white crystals in 50% yield. The ^{1}H n.m.r, mass spectral and infra-red data were in accordance with those quoted above. The melting point of **24** was found to be 78 - 80°C, which corresponded exactly with that reported by Landini *et al.*[119]

The final step in the sequence requires the conversion of the diol **24** to the ditosyl-protected species **20**. The tosylation reaction was achieved under standard conditions using *p*-toluenesulfonyl chloride, either in the presence of dry pyridine acting as both solvent and base, or in the presence of triethylamine in dry dichloromethane (Equation 2.10).

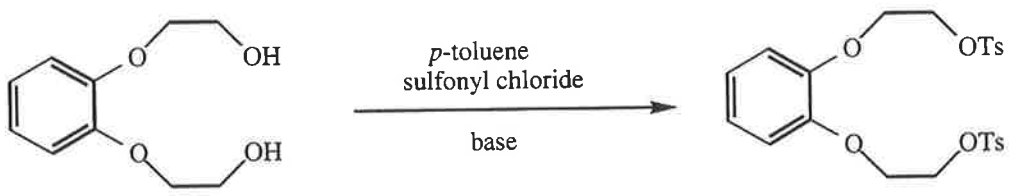

24 **20**

Equation 2.10

Both methods afforded, after crystallisation from ethyl acetate / hexane, the desired product **20** as fine, white needles in average yields of 75%. The structure of **20** was supported by ^{1}H n.m.r analysis which confirmed the disappearance of the broad hydroxyl signal, and the appearance of the characteristic AB quartet at δ 7.83 and δ 7.36 corresponding to the tosyl aromatic protons. In addition, the mass spectrum of **20** showed

a $(M+H)^+$ signal at *m/z* 507 and a fragmentation signal at *m/z* 197, corresponding to the loss of both tosyl groups ($M-C_{14}H_{14}S_2O_4$).

Numerous routes for the synthesis of the carbamate **21** were investigated. One potential synthetic pathway is outlined in Scheme 2.3, and it involves the conversion of the ditosylated species **20** to the diazide species **25**. It was anticipated that reduction of the diazide to the corresponding diamine **26**, followed by dialkylation of **26** with benzyl chloroformate, would afford the desired carbamate species **21.**

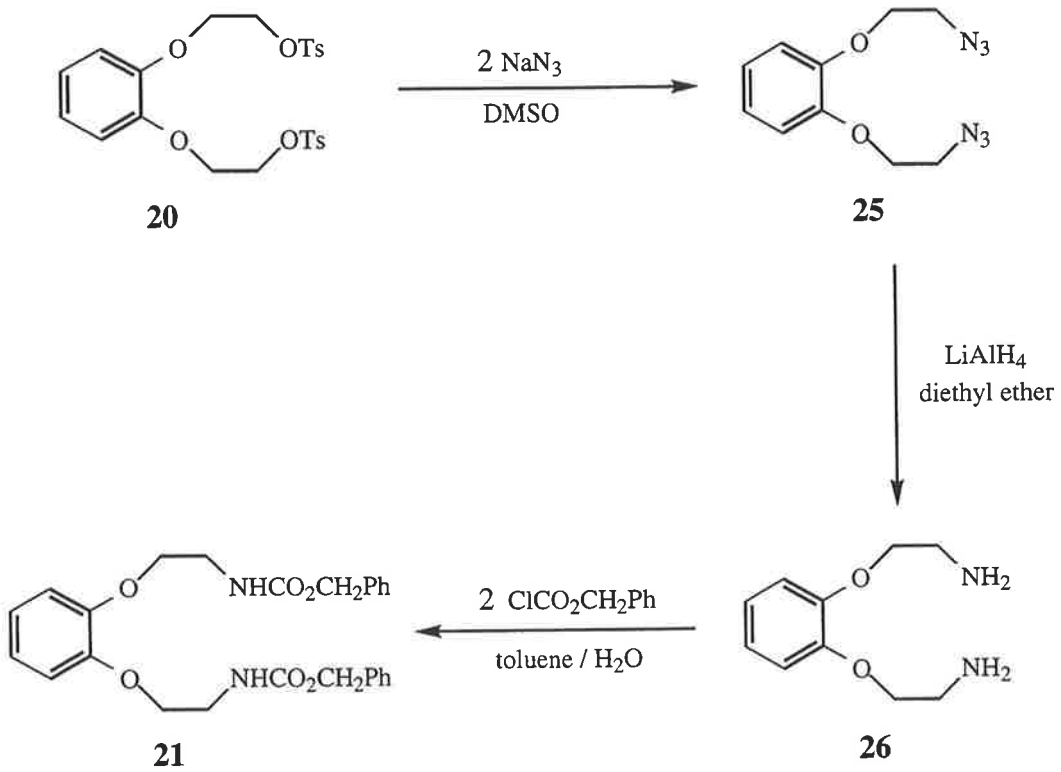

Scheme 2.3

Using standard conditions of sodium azide in dry dimethyl sulfoxide, compound **20** was rapidly converted to the diazide **25** in almost quantitative yield. Compound **25** was obtained as white crystals, and its structure is consistent with infra-red data which showed the characteristic N_3 stretch at 2108 cm^{-1}. The mass spectrum of **25** showed a molecular ion peak at *m/z* 248 and a fragmentation peak at *m/z* 136, corresponding to $M-C_2H_4N_6$.

The reduction of **25** to **26** using lithium aluminium hydride proved to be quite difficult. The reaction was attempted a number of times with different batches of the reducing agent,

however, the reaction could not be reproduced as efficiently as stated in the literature.[120] Hodgkinson *et al.*[120] reported an isolated yield of 64% for **26**, however, this yield was never realised in our hands, and an average yield of only 30% was obtained for this product. ^{1}H n.m.r spectroscopy provided evidence of broad N-H signals, consistent with the structure of **26**. However, as the overall yield of reaction could not be optimised it was thought that this method was not the most viable route for the synthesis of **26**.

An alternative method was attempted for the conversion of the diazide **25** to the corresponding diamine **26**. The method involved the use of sodium borohydride as the reducing agent, rather than lithium aluminium hydride, under phase-transfer conditions utilising a heterogeneous solvent mixture of toluene and water.[121] Initial attempts at the conversion under mild conditions involved stirring the reaction mixture at room temperature for 12 hours. However, t.l.c. analysis showed that no diamine product **26** had formed. Much more vigorous reaction conditions, which involved heating the reaction mixture to 100°C for 24 hours, were then applied. ^{1}H n.m.r analysis of the crude reaction mixture showed that only approximately one-third of the diazide had been reduced to the desired product **26**. Increasing the reaction time to 36 hours did not affect the product ratio of **26** : **25** obtained by this method.

As it was clear that the direct conversion of the diazide **25** to the diamine **26** was not facile, an alternative, independent method for the synthesis of **26** was investigated. The diester **23** was converted to the diamide derivative **27** as shown in Equation 2.11. The procedure involved the dropwise addition of **23** into a vigorously stirred solution of aqueous ammonia, which caused an instant precipitation of diamide **27** to occur. The structure of **27** was confirmed by its infra-red spectrum, which showed the two characteristic N-H stretches of the amide at 3384 and 3188 cm^{-1}, in addition to the strong C=O stretch at 1656 cm^{-1}. The ^{1}H n.m.r spectrum of **27** displayed singlet resonances at δ 4.49 and δ 6.96, attributed to the methylene and aromatic protons, respectively. More importantly, its ^{1}H n.m.r spectrum showed the disappearance of the ethyl ester signals found in the spectrum of **23**. The mass spectrum of **27** produced a significant $(M+H)^+$ signal at *m/z* 225.

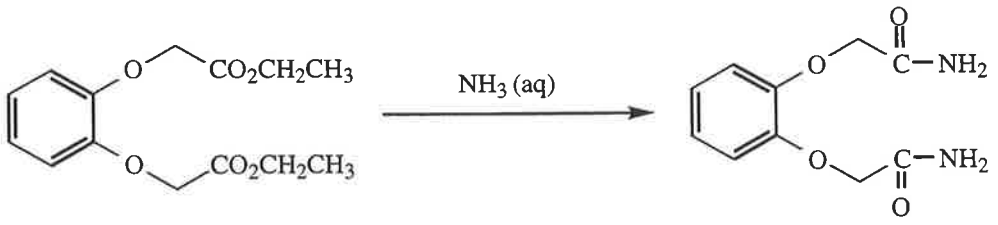

23 **27**

Equation 2.11

Even though the procedure for the conversion of the diester **23** to the diamide **27** was successful (Equation 2.11), a more direct synthesis of **27** was attempted. It was envisaged that the diamide **27** could be synthesised by the one-step reaction of pyrocatechol with two equivalents of the iodomethylformamide, in the presence of potassium carbonate (Equation 2.12). Upon extraction of the crude reaction mixture with dichloromethane, a significant amount of the pyrocatechol precursor was re-isolated.

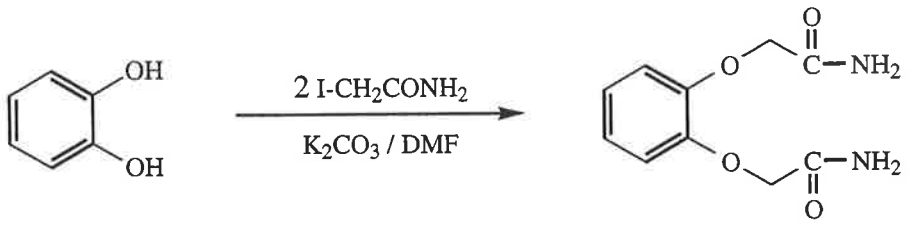

27

Equation 2.12

As the formation of **27** by this one-step method proved to be unsuccessful under various reaction conditions, no further reactions were attempted and the reaction outlined by Equation 2.11 was used exclusively for the synthesis of the diamide **27**.

The next step involved the conversion of the diamide **27** to the diamine **26** (Equation 2.13). This was achieved using diborane as the reducing agent, generated *in situ* by the reaction between sodium borohydride and boron trifluoride-etherate in dry dimethoxyethane. This method afforded **26** as a colourless oil in average yields of 80%, which was used without further purification. ^{1}H n.m.r analysis confirmed the structure of **26** by the presence of the characteristic methylene proton signals at δ 3.10 and δ 4.05, corresponding to the protons adjacent to the nitrogen and oxygen atoms, respectively. Additionally, infra-red analysis

of the product showed the appearance of the strong absorbance signal at 3384 cm^{-1}, indicative of an alkyl amine (N-H) stretch.[114] The mass spectrum produced a $(M+H)^+$ signal at *m/z* 197 and a fragmentation peak at *m/z* 153, corresponding to a $M-C_2H_6N$ fragmentation.

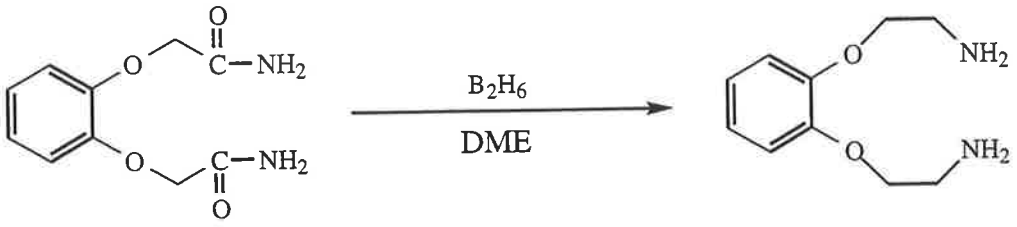

27 **26**

Equation 2.13

The final step in the preparation of one of the precursors required for the formation the desired cyclized crown ether ligand **3** involved the synthesis of the carbamate derivative **21** from the diamine compound **26** (Equation 2.14). This route involves a straightforward reaction between **26** and two mole equivalents of benzyl chloroformate under basic conditions. After purification of the crude product by recrystallization, the carbamate **21** was obtained in good yield as fine, white needles with melting point 102 - 104°C (literature[103] 103 - 104°C). The ^1H n.m.r spectrum of **21** showed the appropriate signals as reported for compound **26,** in addition to the sharp singlets at δ 5.09 corresponding to the methylene protons adjacent to the phenyl rings, and at δ 7.32 corresponding to the ten aromatic protons of the benzyl-carbamate substituents. The infra-red spectrum of **21** further confirmed its structure, with the characteristic pair of bands at 3436 and 3344 cm^{-1}, indicative of amide N-H stretches.[114] Additionally, a strong C=O stretch was observed at 1726 cm^{-1}.

The ethoxycarbonyl derivative **28** was also synthesised according to a similar method to that used for **21**, except that two mole equivalents of ethyl chloroformate was used in place of benzyl chloroformate (Equation 2.14). After purification by flash chromatography and recrystallization, compound **28** was obtained as white crystals in 75% yield. The ^1H n.m.r.

spectrum supported the structure of **28**, with the appearance of the characteristic signals at δ 1.25 and δ 4.16 corresponding to the ester hydrogen atoms.

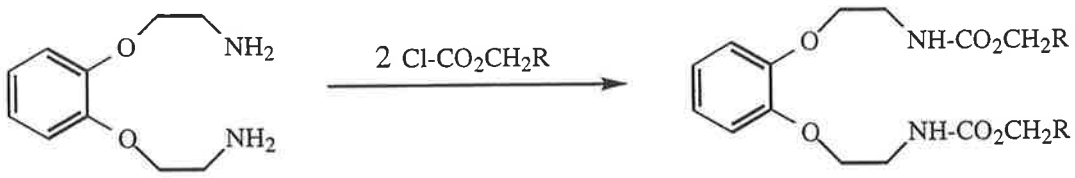

26

21 R=Ph
28 R=CH_3

Equation 2.14

The key step of the reaction sequence (Equation 2.6) involved the reaction between the anionic species of **21**, formed by the reaction of **21** with the *in situ*-generated butoxide-anion, and the ditosylate species **20.** The desired cyclized product **22** was obtained as white needles in an average yield of 52%, with melting point 221-224°C (literature[103] 221-224°C). The structure of **22** was confirmed by its ^{1}H n.m.r and ^{13}C n.m.r spectra, both of which agreed with those reported by Hodgkinson *et al.*[103] In addition, the mass spectrum of **22** produced a $(M+H)^+$ signal at *m/z* 627, and fragmentations signals at *m/z* 583 and *m/z* 492, which correspond to M-CO_2 and M-$C_8H_7O_2$, respectively.

The final step in the reaction sequence to afford the desired derivative **3** involved the removal of the two benzylcarbamate groups from compound **22** (Equation 2.15). This was readily achieved by heating **22** with a 50% hydrogen bromide / glacial acetic acid solution for a few minutes at 100°C. The desired diamine **3** was obtained as a pale yellow solid in excellent yield. The structure of **3** was confirmed by ^{1}H n.m.r. analysis with a broad singlet observed at δ 2.55, indicative of the amine protons,[113] and by the sharp triplets located at δ 3.16 and δ 4.15, corresponding to the methylene protons adjacent to the nitrogen and oxygen atoms, respectively. Furthermore, the mass spectrum of **3** showed a strong $(M+H)^+$ signal at *m/z* 359.

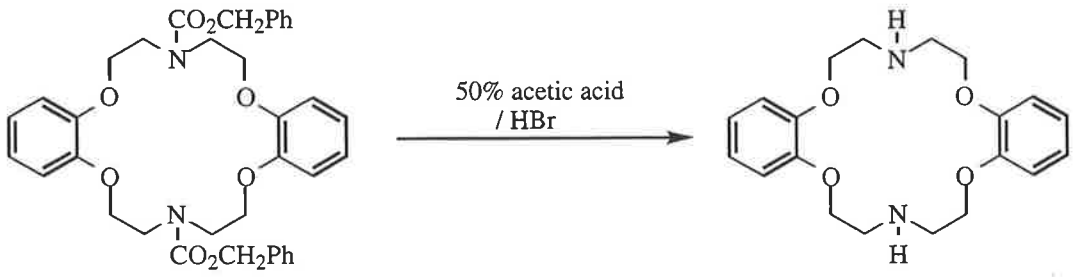

22 **3**

Equation 2.15

2.2.5 Synthesis of *2-[19-(2-hydroxy-2-phenylethyl)-7, 8, 9, 10, 18, 19, 20, 21-octahydro-6H, 17H-dibenzo[b, k][1,4,10,13,7,16]tetraoxadiazacyclooctadecin-8-yl]-1-phenyl-1-ethanol, 4.*

The synthesis of ligand **4** was achieved according to Equation 2.16. The dibenzo-diaza-18-crown-6 derivative **3** was treated with an excess of *(R)*-styrene oxide in dry dimethylformamide, and the mixture was heated to 80°C for ten days.

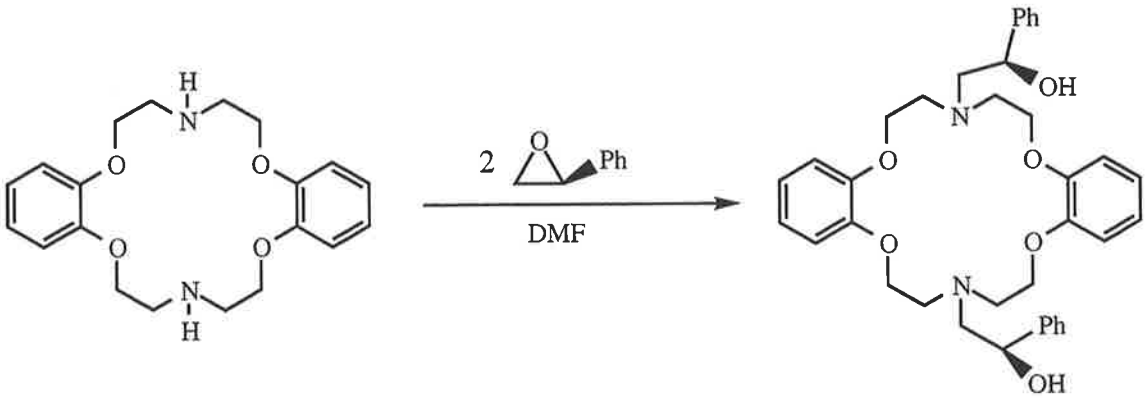

3 **4**

Equation 2.16

Throughout the duration of the reaction, t.l.c. analysis of the crude reaction mixture showed the disappearance of the crown ether starting material at R_f = 0.34, and the appearance of a two new chromophoric products, one at R_f = 0.23 and the other at R_f = 0.09. The product with the higher R_f value appeared within the first few days of the reaction and it was assumed to be the mono-alkylated species. As the reaction progressed,

this product disappeared, and a new product with a lower R_f value appeared. This product was thought to be the desired dialkylated product **4**, and it was formed exclusively after the reaction mixture was heated for ten days. Such an extended reaction period is most likely required due to the steric bulk and inflexibility of the crown ether ligand. A similar type of dialkylation reaction involving compound **3** has been reported in the literature, with lengthy periods required for the reaction to reach completion.[49]

The excess *(R)*-styrene oxide was removed under reduced pressure to afford an orange oil, but attempts at purifying the crude product by Kugelrohr distillation were unsuccessful. Even under extreme temperatures and low pressures, e.g. 180°C at 0.02 mmHg, the desired product could not be isolated. However, compound **29** was isolated by the distillation procedure. This compound is formed by the hydrolysis of the precursor *(R)*-styrene oxide and its structure was confirmed by ^{1}H n.m.r spectroscopy.

29

Purification of the crude material by flash chromatography gave the desired product **4** as a pale yellow oil. Crystallization from DMF / water afforded compound **4** as a pale yellow solid. The structure of ligand **4** was confirmed by ^{1}H n.m.r and ^{13}C n.m.r spectroscopy and mass spectrometry. Its ^{1}H n.m.r spectrum shows the characteristic proton signals at δ 3.32 and δ 4.15, corresponding to the methylene groups adjacent to the nitrogen and oxygen atoms, respectively. These signals mirror those observed for the related protons of the parent crown ether ligand **3**. Additionally, the signals observed for the protons present in the pendant arm include a multiplet at δ 4.65 - 4.67 representing the single proton on the chiral carbon, and a multiplet at δ 4.65 - 4.67 representing the diastereotopic protons of the methylene group. ESI-MS analysis of **4** afforded a strong $(M+Na)^+$ base peak at *m/z* 621, and a strong $(M+H)^+$ signal at *m/z* 599, with a relative intensity of 56%.

2.2.6 Synthesis of *2-[16-(2-hydroxy-2-phenylethyl)-1,4,10,13-tetraoxa-7,16-diazacyclo-octadecanyl]-1-phenyl-1-ethanol, 6.*

The synthesis of ligand **6** involved treating the commercially available 1,10-diaza-18-crown-6 derivative **5** with two equivalents of *(R)*-styrene oxide in dry DMF (Equation 2.17), in a related procedure to that described for the synthesis of ligand **4**. A reaction time of 14 hours was required for the synthesis of ligand **6**, which is in stark contrast to that required for the preparation of **4** (10 days). It is clear, therefore, that the inflexible nature and steric bulk associated with the parent crown ether **3**, as imposed by the aromatic moieties, greatly affects the rate of the dialkylation reaction when compared to the simpler crown ether **5**.

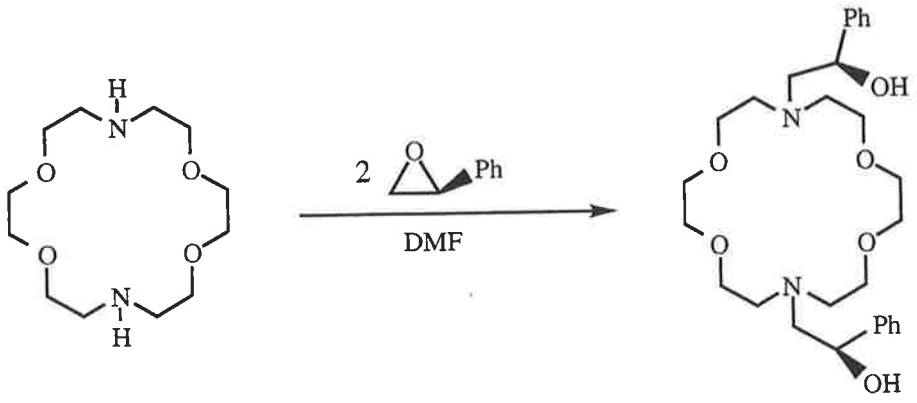

5 **6**

Equation 2.17

The excess *(R)*-styrene oxide was removed under reduced pressure to give the crude residue as a dark, orange oil. The crude material was purified using ion-exchange chromatography and afforded the desired product **6** as a colourless oil, in average yields of 60 - 70%. The structure of **6** was consistent with its ^{1}H n.m.r spectrum. The characteristic methylene signals observed at δ 2.58 - 2.75 and δ 3.57 - 3.76 correspond to the protons located adjacent to the nitrogen and oxygen atoms, respectively, as observed for the parent crown ligand **5**. Additionally, the multiplet observed at δ 4.67 - 4.73 is consistent with the proton present on the chiral carbon in the pendant arm, and the diastereotopic methylene protons of the pendant arm are located as a multiplet at δ 2.91 - 3.07. The electrospray

ionisation mass spectrum of compound **6** produced a strong $(M+Na)^+$ base peak observed at *m/z* 525.5, and a $(M+H)^+$ peak at *m/z* 503, with a relative intensity of 8%.

2.3 Conclusions

In conclusion, our target ligands (**1 - 4** and **6**) were prepared in moderate to good overall yields using the methods detailed in this chapter. Ligand **5** was obtained commercially.

Ligand **1** was synthesised by a modification of the convergent method outlined by Newkome *et al.*[105] Reaction of 2,6-(dihydroxymethyl)pyridine and α,α'-dibromo-*o*-xylene afforded **1** in an overall yield of 35-40%. The molecular structure of **1** was confirmed by X-ray crystallography (Appendix A).

A new method was used for the synthesis of ligand **2**. It involved a 1:1 condensation reaction between the electrophilic ditosyl derivative **13** or the dichloro derivative **14** with 3,4-dimercaptotoluene, which incorporated the required fragments of the target molecule **2**. Ligand **2** was obtained in an overall yield of 20%, a marked improvement over that obtained by the method described by Pederson.

The synthesis of the desired dibenzo-diaza-18-crown-6 derivative **3** was attempted by following the procedure outlined by Hodgkinson *et al.*[103] Significant modifications to the original synthetic pathway were required, particularly when difficulties were encountered in reproducing several key steps of the scheme. As found in the synthesis of ligands **1** and **2**, the convergent method offered a viable route to the synthesis of **3** by the construction of the two fragments of the molecule, namely the ditosylate derivative **20** and the carbamate derivative **21**, prior to their condensation in the final cyclization step to afford the desired ligand.

Compound **4** was synthesised by the reaction of **3** with excess *(R)*-styrene oxide. A reaction time of ten days was required for the exclusive formation of **4**. The lengthy period was most likely attributed to the steric bulk of the crown ether system, owing to the

inflexible nature of the compound as a result of the aromatic rings. After lengthy purification, compound **4** was isolated albeit in a low yield.

Compound **6** was synthesised in a similar manner to ligand **4** by the reaction of **5** with two equivalents of *(R)*-styrene oxide. A reaction time of 14 hours was required for the formation of **6**, in stark contrast to the lengthy time required for the formation of the analogous ligand **4**. This result clearly demonstrates the considerable steric influence of the aromatic rings on the rate of reaction. Purification of **6** using ion-exchange chromatography afforded the desired product in an overall yield of 65%.

Once the syntheses of the target macrocyclic ligands had been achieved, their thermodynamic binding affinities toward lead(II), zinc(II), cadmium(II) and silver(I) ions were investigated. These results are presented in detail in Chapter 3.

3 Equilibrium studies of crown ether complexes

3.1 Introduction

Understanding the interactions of macrocylic polyethers and their derivatives, such as polyamines and polythioethers, with metal cations requires an understanding of the various parameters that govern the complexation reactions.[83] Detailed compilations of data exist that include both the thermodynamic and kinetic aspects of many metal ion-macrocycle interactions.[77,83-85] General parameters that affect the formation and thermodynamic stability of the complexes include the structure and size of the macrocyclic system, the number, type and arrangement of their donor atoms, the nature of the metal ions, and the nature of the solvent.[77]

The use of stability (or equilibrium) constants for metal complex formation involving macrocyclic ligands has long been employed as a quantitative measure of the affinity of a ligand for a metal ion in solution.[122] When a ligand coordinates to a metal ion, an equilibrium is established between the solvated metal ion (M^{n+}), the ligand (L), and the resulting complex $[ML]^{n+}$. This equilibrium is represented by Equation 3.1,

$$M^{n+} + L \underset{}{\overset{K_s}{\rightleftharpoons}} [ML]^{n+} \qquad \textbf{3.1}$$

where the concentration stability constant, K_s, is defined by Equation 3.2.

$$K_s = \frac{[[ML]^{n+}]}{[M^{n+}][L]} \qquad \textbf{3.2}$$

3.2 Pioneering methods for the determination of stability constants

Some of the earliest measurements of stability constants for crown ether metal complexes were reported by Izatt *et al.*[80,123,124] This early work discussed the use of a calorimetric technique to study the interaction of several mono- and di-valent alkali and alkaline-earth metal ions, including potassium(I), silver(I), ammonium(I), magnesium(II) and barium(II), with the dicyclohexyl-18-crown-6 ligand **30** in aqueous solution. A relative stability sequence for the complexes formed with this ligand was established.[80]

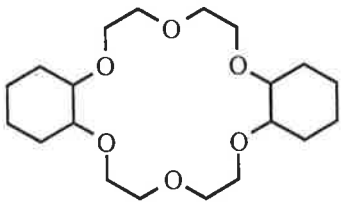

30

One of the first implementations of spectroscopic methods for the determination of stability constants of crown ethers was reported by Wong *et al.*[125] By using n.m.r. and UV-visible spectroscopy, the complexation of the cyclic dimethyldibenzo-18-crown-6 polyether **31** with fluorenyl alkali metal salts was investigated in ethereal and pyridine solvent systems. The selectivity exhibited by this crown ether toward alkali metal ions was found to be highly dependent on the nature of the solvent.[125] These spectroscopic methods were developed by extension of Pederson's[74,126] initial findings that reported the change in the absorbance spectra for the dibenzo-18-crown-6 polyether (Section 1.14) upon addition of sodium(I) ions to a methanol solution.[124]

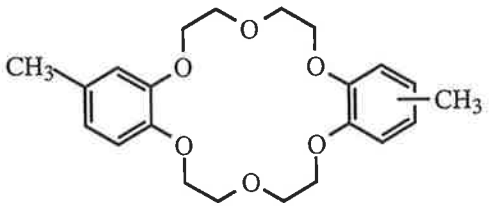

31

Frensdorff[97] was the first to perform a comprehensive study of the stability constants of 1:1 complexes of 22 different macrocyclic polyether compounds, containing between 12- and 60-membered ring systems with a varying number of donor atom substituents, and a series of univalent cations by the implementation of potentiometric titration methods using cation-selective electrodes. The stability constant determinations were conducted in both methanol and aqueous solvent systems. These results were the first to offer significant evidence for the importance of solvation effects on the stability of macrocyclic crown ether complexes. A large increase, of almost three to four orders of magnitude, was observed for the respective complexes in methanol as compared to aqueous systems.[97] Additionally, evidence emerged for the reduced affinity towards alkali metal ions as ring system oxygen atoms were substituted by nitrogen or sulfur atoms.[79,97]

The development of efficient and reliable methods for the quantitative determination of stability constants for metal complexes has led to a great deal of interest in the binding affinities of many synthetic macrocyclic ligands systems with cations, anions and neutral molecules.[122] A variety of methods are now available for the determination of stability constants in both aqueous and non-aqueous solvent systems. These include calorimetry,[127-130] potentiometry (ion-selective electrodes),[128,131-136] nuclear magnetic resonance (n.m.r.) spectroscopy,[137-140] and ultraviolet spectroscopy.[141-143] Other techniques include, conductance,[128,144-146] pH-metric titrations (pH electrodes),[147-152] electrochemistry,[153,154] and fast atom bombardment (FAB) and electrospray ionisation (ESI) mass spectrometry.[155-159] The most viable method of choice usually depends on the nature of the ligand systems being studied, particularly with respect to the solubilities of these systems in appropriate solvent systems, and the availability of the equipment required for the analysis.[122]

3.3 The potentiometric titration technique

The most useful method for determining stability constants for the metal ion-macrocycle complexes relevant to this study was that of potentiometry utilizing a silver wire as a silver-ion selective electrode in non-aqueous media.

The thermodynamic stability constants (K_{th}) for the formation of a 1:1 metal ion-macrocycle complex is defined by Equation 3.3,

$$K_{th} = \frac{f_{ML}{}^{n+} [ML^{n+}]}{f_L [L] f_M{}^{n+} [M^{n+}]} \qquad \textbf{3.3}$$

where f_L, $f_M{}^{n+}$ and $f_{ML}{}^{n+}$ are the activity coefficients of the free ligand, the free metal ion, and the complex, respectively. When the ionic strength of the solution is maintained at a constant level throughout the titration, the activity co-efficients of the species are also held constant. Thus, provided the potentiometric titrations are carried out under conditions where the ionic strength of the supporting electrolyte is much greater than that of the species studied, changes in concentration of the titrated species parallel those of their

activities. This allows the stability constants to be quoted as those of concentration (K_S) alone (Equation 3.4).

$$K_s = K_{th} \frac{f_L \, f_M^{n+}}{f_{ML}^{n+}} = \frac{[[ML]^{n+}]}{[M^{n+}][L]} \qquad \textbf{3.4}$$

The technique of potentiometric titration using a silver-ion selective electrode involves a two-step process. The first step requires the determination of the stability constants ($K_S(Ag^+)$) of the silver(I)-ligand complexes. The determination of ($K_S(Ag^+)$) involves the direct potentiometric titration of a solution containing a known concentration of silver(I) ions with a ligand (L) solution, of known volume and concentration, in an appropriate solvent. The e.m.f. change (in mV) of the silver(I) ions is monitored throughout the titration by a silver-ion selective electrode. This allows the concentration of the free, solvated silver(I) ions at each point of the titration to be determined. The stability constants of the silver(I)-ligand complexes can then be calculated. This relationship is shown by Equations 3.5 and 3.6.

$$Ag^+ + L \underset{}{\overset{K_S(Ag+)}{\rightleftharpoons}} [AgL]^+ \qquad \textbf{3.5}$$

$$K_S(Ag^+) = \frac{[[AgL]^+]}{[Ag^+][L]} \qquad \textbf{3.6}$$

In calculating the stability constants of the silver(I)-complexes by this method, the electrode's response to the metal ion (Ag^+) concentration must also be investigated. This response is determined by an electrode calibration, which involves titrating a known volume of background electrolyte solution (0.050 M NEt_4ClO_4) with a solution of known concentration of silver(I) ions, usually in the form of silver nitrate, in an appropriate solvent. The electrode response to the metal ion concentration is measured, and is found to be pseudo-Nernstian (Equation 3.7).

$$E = E_0 + c \ln[M^{n+}] \qquad \textbf{3.7}$$

The constants E_0 and the slope c, required in the determination of the stability constants (K_S) can be determined simply from the plot of the potential E against the logarithm of the

free solvated metal ion concentration, $[Ag^+]$. In this study the values of E_0 and c were found to lie within the range of 100 - 300 and 19 - 28 (where the e.m.f. is measured in mV), respectively; values that are consistent with those quoted in the literature.[149] The results obtained from a calibration of the silver(I) ion selective electrode using a *N,N'*-dimethylformamide (DMF) solution of silver(I) ions are tabulated in Table 3.1 and plotted as shown in Figure 3.1 (Section 3.3.3).

An indirect, competitive titration method was employed in the determination of the stability constants ($K_S(M^+)$) of the metal complexes, where the metal ion is lead(II), zinc(II) or cadmium(II) ions. The direct method of analysis could not be applied in these cases as there were no ion selective electrodes available for these particular metal ions. The indirect method involves measuring the stability constant of the silver(I)-complex ($K_S(Ag^+)$) in the presence of a competing metal ion by titrating a solution of silver(I) ions with a solution containing the metal complex of known concentration. The change in e.m.f. observed (in mV) is attributed to the change in free silver(I) ion concentration in solution, as monitored by the silver(I) ion selective electrode. This equilibrium is shown in Equation 3.8,

$$[ML]^{n+} + Ag^+ \overset{K_e}{\rightleftharpoons} [AgL]^+ + M^{n+} \qquad \textbf{3.8}$$

where the equilibrium constant (K_e) for the competitive reaction is defined by Equation 3.9.

$$K_e = \frac{[[AgL]^+][M^{n+}]}{[[ML]^{n+}][Ag^+]} \qquad \textbf{3.9}$$

As the initial concentrations of metal complex, silver(I) and metal ions are known, and the equilibrium concentration of silver(I) is determined from the electrode potential of the silver(I)-ion electrode, the equilibrium concentrations of the species required to calculate K_e can also be determined. In these competitive titrations, the total metal ion concentrations of both silver(I) and metal ions were always greater than the total ligand

concentration, so that the concentration of the free ligand at equilibrium can be assumed to be negligible.

Finally, since the stability constant of the silver(I) complex, $K_S(Ag^+)$, is determined by a direct potentiometric titration, and the stability constant of the silver(I)-complex, K_e, in the presence of a competing metal ion of interest, is determined by a competitive titration, the stability constant of the particular metal complex, $K_S(M^{n+})$, where M^{n+} is either lead(II), zinc(II) or cadmium(II), is conveniently calculated using Equation 3.10.

$$K_s(M^{n+}) = \frac{K_s(Ag^+)}{K_e} = \frac{[[ML]^{n+}]}{[M^{n+}][L]} \qquad \textbf{3.10}$$

The stability constants of the lead(II), zinc(II) and cadmium(II) complexes in this study were determined by this method, which is viable provided that the silver(I)-complex is more stable than that of the other competing metal ion. If the reverse is true, the change in the concentration of the free, solvated silver(I) ions will be negligible, and immeasurable small changes to the electrode potential will be observed throughout the titration, thus rendering this method inapplicable for use in competitive equilibrium studies. It has been reported that for an accurate determination of the stability constant using competitive potentiometric titrations, the stability constants of the silver(I) and metal ion complexes must differ by a factor of at least 10 or more.[160]

The following sections describe in detail how stability constants for the formation of 1:1 metal complexes are extracted from the experimental potentiometric titration data. By the implementation of the FORTRAN-77 program called STAB,[161] the K_S values are derived according to the linear solution method, as described by Rossotti and Rossotti.[162] Examples of the potentiometric titration data that were obtained in our hands, for both direct and competitive titrations, are also included to further illustrate the method.

3.3.1 Direct titrations

Looking first at the direct potentiometric titration methods, the equilibrium constant K_S determined at each point i of the titration is given by,

$$K_s(i) = \frac{[[ML]^+(i)]}{[M^+(i)][L(i)]} \qquad \textbf{3.11}$$

Rearrangement of Equation 3.11 gives,

$$K_s(i)\,[L(i)] = \frac{[[ML]^+(i)]}{[M^+(i)]} \qquad \textbf{3.12}$$

or equivalently,

$$K_s(i)\,[L(i)] = \frac{1 - \alpha(i)}{\alpha(i)} \qquad \textbf{3.13}$$

where $\alpha(i) = \frac{[M^+(i)]}{[M^+(i)]_t}$ i.e. the proportion of total uncomplexed metal ion.

To determine the stability constants for complexes by a direct potentiometric titration method, the concentrations of all of the remaining parameters represented in Equation 3.12 must be calculated. These various concentrations, at each point i of the titration, are usually obtained from either known or measurable quantities.

By using the electrode calibration parameters, E_0 and c, and by rearrangement of Equation 3.7, the potential E(i) is related to the free metal ion concentration [$M^+(i)$] by Equation 3.14.

$$[M^+(i)] = \exp\frac{E(i) - E_0}{c} \qquad \textbf{3.14}$$

The concentrations [[ML]$^+(i)$] and [L(i)] are calculated from the mass balance Equations 3.15 and 3.16, respectively.

$$[M^+(i)]_t = [M^+(i)] + [[ML]^+(i)] \qquad \textbf{3.15}$$

$$[L(i)]_t = [L(i)] + [[ML]^+(i)] \qquad \textbf{3.16}$$

$[M^+(i)]_t$ and $[L(i)]_t$ represent the total silver(I) ion and ligand concentrations, respectively, and these values are calculated according to Equations 3.17 and 3.18, respectively. Equations 3.17 and 3.18 are used to determine the values corresponding to $[M^+(i)]_t$ and $[L(i)]_t$, respectively, from the known initial concentration of the ligand $[L]_{in}$ and the metal ion $[M^+]_{in}$.

$$[M^{+}(i)]_t = \frac{20 \times [M^{+}]_{in}}{20 + V_{titre}} \qquad \textbf{3.17}$$

$$[L(i)]_t = \frac{V_{titre} \times [L]_{in}}{20 + V_{titre}} \qquad \textbf{3.18}$$

By implementation of the STAB[161] program, the values for the required parameters described above can be calculated quite simply, and this in turn allows the values of $[L(i)]$ and $\frac{1 - \alpha(i)}{\alpha(i)}$ in Equation 3.13 to be calculated. By plotting the values of $[L(i)]$ versus $\frac{1 - \alpha(i)}{\alpha(i)}$, a straight line is obtained that passes through the origin with a slope K_S. All of the K_S values determined from the direct titrations performed in this study were analysed by this method.

3.3.2 Competitive titrations

When analysing competitive potentiometric titration data the following equations must be considered. By rearrangement of Equation 3.9, the following relationship holds where,

$$\frac{[[AgL]^{+}(i)]\,[M^{n+}(i)]}{[Ag^{+}(i)]} = K_e\,[[ML]^{n+}(i)] \qquad \textbf{3.19}$$

or similarly,

$$\frac{1 - \alpha(i)}{\alpha(i)}\,[M^{n+}(i)] = K_e\,[[ML]^{n+}(i)] \qquad \textbf{3.20}$$

where $\alpha(i) = \frac{[Ag^{+}(i)]}{[Ag^{+}(i)]_t}$, i.e. the mole fraction of the free solvated Ag^{+} ions.

Thus, to determine the stability constant (K_e) value for metal complexes of interest, the various concentrations of the parameters present in Equation 3.19 must be calculated. Once these concentrations have been deduced, the K_e value for complex can be obtained by plotting $\frac{1 - \alpha(i)}{\alpha(i)}\,[M^{+}(i)]$ versus $[[ML]^{n+}(i)]$, which gives a straight line with slope K_e.

Values for $[Ag^+(i)]$ are readily calculated from the measured e.m.f. values, as determined by an electrode calibration, using Equation 3.7. The concentrations of the remaining species in Equation 3.20 are calculated by using mass balance equations, which for competitive potentiometric titrations are as follows,

$$[Ag^+(i)]_t = [Ag^+(i)] + [AgL^+(i)] \quad \textbf{3.21}$$

$$[M^{n+}(i)]_t = [M^{n+}(i)] + [[ML]^{n+}(i)] \quad \textbf{3.22}$$

$$[L(i)]_t = [L(i)] + [[AgL]^+(i)] + [[ML]^{n+}(i)] \quad \textbf{3.23}$$

where $[Ag^+(i)]_t$, $[M^{n+}(i)]_t$ and $[L(i)]_t$ are the known total concentrations of silver(I), metal ion and ligand, respectively. However, since the total concentration of the both metal ions (Ag^+ and the M^{n+}) is always greater than the total ligand concentration, ($[M^{n+}]_t > [L]_t$), then the free ligand concentration [L] is negligible. Thus, Equation 3.23 can be simplified as follows,

$$[L(i)]_t = [[AgL]^+(i)] + [[ML]^{n+}(i)] \quad \textbf{3.24}$$

Values for $[Ag^+(i)]_t$, $[M^{n+}(i)]_t$ and $[L(i)]_t$ are determined according to the Equations 3.25, 3.26 and 3.27, respectively. V_{titre} (mL) represents the volume of complex solution added, at each point i of the titration, to the 20 mL solution of silver(I). $[Ag^+]_{in}$, $[M^{n+}]_{in}$ and $[L]_{in}$ are the known initial concentrations of silver(I), metal ion and ligand, respectively.

$$[Ag^+(i)]_t = \frac{20 \times [Ag^+]_{in}}{20 + V_{titre}} \quad \textbf{3.25}$$

$$[M^{n+}(i)]_t = \frac{V_{titre} \times [M^{n+}]_{in}}{20 + V_{titre}} \quad \textbf{3.26}$$

$$[L(i)]_t = \frac{V_{titre} \times [L]_{in}}{20 + V_{titre}} \quad \textbf{3.27}$$

As in the case of direct potentiometric titrations, the STAB program was implemented to calculate the values of $\frac{1 - \alpha(i)}{\alpha(i)}$ $[M^+(i)]$ and $[ML^{n+}(i)]$ using the equations discussed,

and subsequent plotting of $\frac{1 - \alpha(i)}{\alpha(i)}$ $[M^{n+}(i)]$ versus $[ML^{n+}(i)]$ yields a straight line with slope K_e. In both the direct and competitive titration methods, the stability constants, K_s and K_e, are determined by a linear regression of the slope.

Once K_e and $K_{s(Ag^+)}$ are determined, the stability constant for the competing metal ion, $K_{s(M^{n+})}$ can be determined simply by rewriting Equation 3.10 to give,

$$\log K_{s(M^{n+})} = \log K_{s(Ag^+)} - \log K_e \qquad \textbf{3.28}$$

3.3.3 Determination of stability constants by curve fitting

The method of curve fitting that is applied to confirm all values of stability constants, K_s for direct titrations or K_e for competitive titrations, relies upon the method described by Rossotti and Rossotti.[162] The FORTRAN-77 program VISP[161] calculates the theoretical titration curve which is a function of known concentrations, the calibrated electrode response and the stability constants, K_s or K_e. The derivation of this calculated curve is described below.

For direct potentiometric titrations, substitution of the mass balance Equations 3.15 and 3.16 into Equation 3.17 gives the following relationship,

$$K_s = \frac{[M^+(i)]_t - [M^+]}{([L(i)]_t - [M^+(i)]_t + [M^+(i)]) \times [M(i)]} \qquad \textbf{3.29}$$

If $[M^+(i)]_t = M_t$, $[L(i)]_t = L_t$ and $[M^+(i)] = M$, then Equation 3.29 can be simplified to give,

$$K_s = \frac{M_t - M}{(L_t - M_t + M) \times M} \qquad \textbf{3.30}$$

Rearrangement of Equation 3.30 gives the following quadratic equation,

$$K_sM^2 + (K_sL_t - K_sM_t + 1)M - M_t = 0 \qquad \textbf{3.31}$$

Solving this quadratic equation for M gives Equation 3.32,

$$M = \frac{-b \pm \sqrt{b^2 - 4ac}}{2a} \qquad \textbf{3.32}$$

where $a = K_s$, $b = (K_s L_t - K_s M_t + 1)$ and $c = -M_t$.

For competitive potentiometric titrations, substitution of the mass balance Equations 3.21, 3.22 and 3.23 in Equation 3.9 gives Equation 3.33,

$$K_e = \frac{([Ag^+(i)]_t - [Ag^+(i)]) \times ([M^{n+}(i)]_t - [L(i)]_t + [Ag^+(i)]_t - [Ag^+(i)]}{[Ag^+(i)] \times ([L(i)]_t - [Ag^+(i)]_t + [Ag^+(i)]} \qquad \textbf{3.33}$$

If $A_t = [Ag^+(i)]_t$, $M_t = [M^{n+}(i)]_t$, $L_t = [L(i)]_t$ and $A = [Ag^+(i)]$, then Equation 3.33 can be re-written as,

$$K_e = \frac{(A_t - A) \times (M_t - L_t + A_t - A)}{A \times (L_t - A_t + A)} \qquad \textbf{3.34}$$

Since the concentration of the silver(I) ions at each point of the titration, $[Ag^+(i)]$, is the experimentally determined variable, this value (A) can be determined by rearrangement of Equation 3.34 to give,

$$A^2(K_e - 1) + A(K_e L_t - K_e A_t + 2A_t - L_t + M_t) + A_t(L_t - M_t - A_t) = 0 \qquad \textbf{3.35}$$

Equation 3.35 can now be solved to give,

$$A = \frac{-b \pm \sqrt{b^2 - 4ac}}{2a} \qquad \textbf{3.36}$$

where $a = K_e - 1$, $b = K_e L_t - K_e A_t + 2A_t - L_t + M_t$ and $c = A_t(L_t - M_t - A_t)$.

In both the direct and competitive titrations, the conditions $b^2 - 4ac > 0$ and $0 < M < M_t$ or $0 < A < A_t$ must be satisfied. For both titration methods, the former is always satisfied under experimental conditions. The latter is usually satisfied by taking only the positive root of Equations 3.32 and 3.36, for direct and competitive titrations, respectively.

In summary, the VISP program generates a calculated titration curve (e.m.f. versus mL) by determining the free silver(I) ion concentration at each point of the titration, $[Ag^+(i)]$, whether it be for a direct (Equation 3.32) or a competitive (Equation 3.36) titration, and allows an initial estimate of K_s or K_e to be determined. By substitution of this concentration into Equation 3.7, a theoretical e.m.f. curve of the titration is obtained. By the systematic variation (by less than ± 1%) of these concentrations, in addition to the K_s

or K_e values obtained, the best possible fit between the experimental and calculated e.m.f. data is obtained.

A calibration of the silver(I) ion selective electrode using a DMF solution of silver(I) ions is presented as an example. The electrode potential versus the logarithm of the free solvated silver(I) concentrations obtained at each point of the titration appears in Table 3.1 and the plot of this data is presented in Figure 3.1. Examples of a direct and competitive titration are presented. The experimental and calculated data (as determined by the VISP program) for the direct stability constant determination of $[Ag\mathbf{6}]^+$ in DMF are presented in Table 3.2. The fit of the experimental e.m.f. values to the curve calculated by the VISP program for this system is shown in Figure 3.2. The straight line plot calculated by the STAB program is illustrated in Figure 3.3. The experimental and calculated data (as determined by the VISP program) for the competitive stability constant determination of $[Pb\mathbf{2}]^{2+}$ in DMF are presented in Table 3.4. The fit of the experimental e.m.f. values to the curve calculated by the VISP program for this system is shown in Figure 3.4. The straight line plot calculated by the STAB program is illustrated in Figure 3.5.

Table 3.1 *Experimental data and logarithm of the free solvated silver(I) concentrations ($ln[Ag^+]$) calculated for calibration of the silver(I) ion selective electrode using a DMF solution of silver(I) ions at 298.2 K and I = 0.050 M NEt_4ClO_4.*

titre (mL)	e.m.f. (mV)	$ln[Ag^+]$	titre (mL)	e.m.f. (mV)	$ln[Ag^+]$
0.22	-96.50	-9.81	2.12	-42.20	-7.63
0.33	-85.00	-9.42	2.22	-41.00	-7.59
0.42	-79.60	-9.17	2.32	-40.00	-7.55
0.52	-77.80	-9.05	2.42	-39.50	-7.51
0.62	-72.10	-8.79	2.52	-38.40	-7.48
0.72	-68.00	-8.65	2.62	-37.50	-7.44
0.82	-64.50	-8.52	2.72	-36.60	-7.41
0.92	-61.30	-8.41	2.82	-36.00	-7.38
1.02	-59.10	-8.31	2.92	-35.10	-7.35
1.12	-56.60	-8.23	3.02	-34.40	-7.32
1.22	-54.50	-8.14	3.12	-33.50	-7.29
1.32	-52.70	-8.07	3.22	-33.00	-7.26
1.43	-51.30	-8.00	3.32	-32.30	-7.24
1.52	-49.70	-7.94	3.42	-31.70	-7.21
1.62	-48.40	-7.88	3.52	-31.10	-7.19
1.72	-47.00	-7.82	3.62	-30.60	-7.16
1.82	-45.60	-7.77	3.72	-30.10	-7.14
1.92	-44.50	-7.72	3.82	-29.30	-7.12
2.02	-43.40	-7.68	3.92	-28.80	-7.10
2.12	-42.20	-7.63	4.02	-28.40	-7.08
2.22	-41.00	-7.59	4.12	-27.80	-7.06
2.32	-40.00	-7.55	4.22	-27.20	-7.04

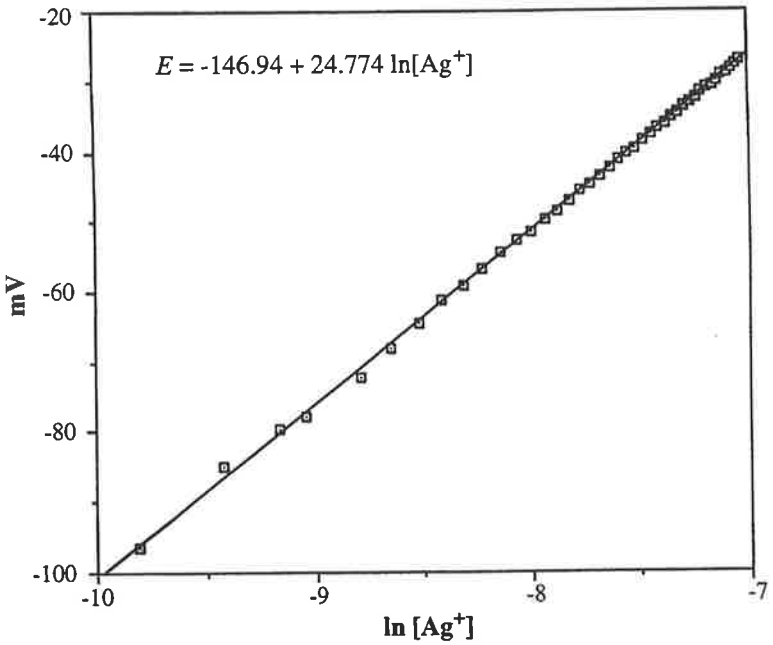

Figure 3.1 *Calibration of the silver(I) ion selective electrode with a DMF solution of silver(I) nitrate at 298.2 K and I = 0.050 M NEt_4ClO_4. A 20 mL solution of 5.000 x 10^{-2} M NEt_4ClO_4 (electrolyte) was titrated with a solution of 5.000 x 10^{-3} M $AgNO_3$. The parameters E_0 and c are equal to the y-intercept and the slope of the line, respectively (see Equation 3.7).*

Table 3.2 *Experimental and calculated e.m.f. titration data (as determined by the VISP program) for the determination of the stability constant of* $[Ag\mathbf{6}]^+$ *in DMF at 298.2 K and* $I = 0.050\ M\ NEt_4ClO_4$.

titre (mL)	expt. e.m.f. (mV)	calc. e.m.f. (mV)	titre (mL)	expt. e.m.f. (mV)	calc. e.m.f. (mV)
1.00	-65.00	-61.17	2.11	-150.00	-146.08
1.04	-65.80	-62.12	2.14	-168.30	-164.91
1.08	-65.80	-63.10	2.17	-185.20	-185.73
1.12	-66.40	-64.12	2.18	-196.70	-191.34
1.18	-66.80	-65.72	2.21	-205.30	-204.13
1.23	-67.40	-67.13	2.24	-213.60	-213.00
1.27	-68.50	-68.32	2.27	-219.00	-219.69
1.31	-69.80	-69.55	2.30	-222.00	-225.01
1.35	-71.10	-70.84	2.32	-227.00	-228.04
1.39	-71.60	-72.20	2.36	-232.20	-233.21
1.43	-72.50	-73.63	2.40	-237.20	-237.51
1.49	-73.70	-75.92	2.44	-240.50	-241.19
1.53	-75.90	-77.57	2.48	-243.60	-244.41
1.57	-77.00	-79.32	2.52	-246.60	-247.27
1.59	-79.10	-80.24	2.56	-248.50	-249.84
1.63	-80.60	-82.18	2.60	-251.80	-252.17
1.67	-82.30	-84.27	2.66	-254.60	-255.32
1.71	-85.40	-86.55	2.73	-258.20	-258.55
1.75	-88.50	-89.03	2.78	-260.20	-260.64
1.79	-90.90	-91.77	2.84	-263.00	-262.93
1.83	-94.50	-94.84	2.90	-265.40	-265.03
1.87	-99.50	-98.30	2.96	-267.50	-266.98
1.91	-103.00	-102.30	3.04	-270.00	-269.36
1.96	-110.10	-108.33	3.12	-272.30	-271.53
1.99	-116.10	-116.17	3.20	-274.80	-273.54
2.01	-119.90	-130.25	3.28	-276.50	-275.39
2.07	-133.70	-137.15	3.37	-278.50	-277.33
2.09	-141.00	-146.08	3.44	-280.40	-278.74

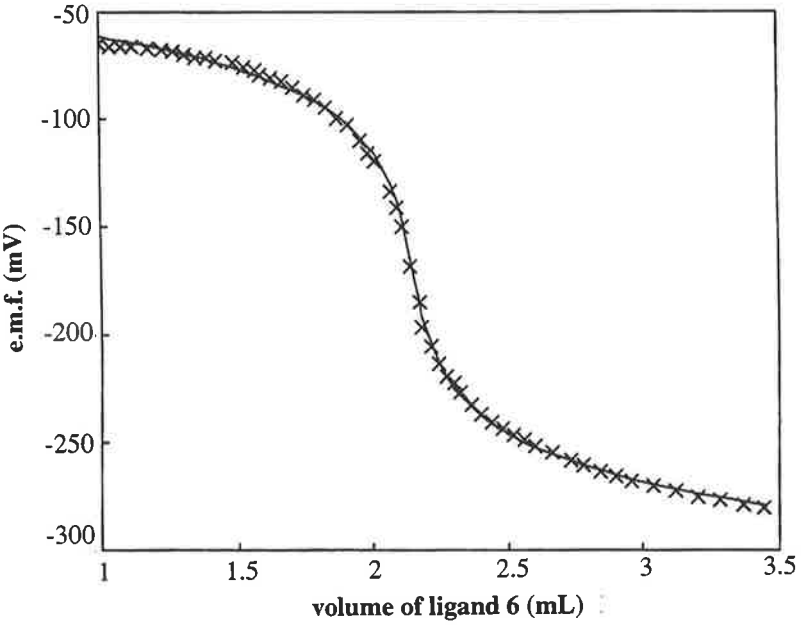

Figure 3.2 *Plot of experimental (x) and calculated (solid curve) e.m.f. versus titre for the direct titration of* ***6*** *with silver(I) in DMF solution at 298.2 K and I = 0.050 M* NEt_4ClO_4. *The log* $K_s = 7.52 \pm 0.01$.

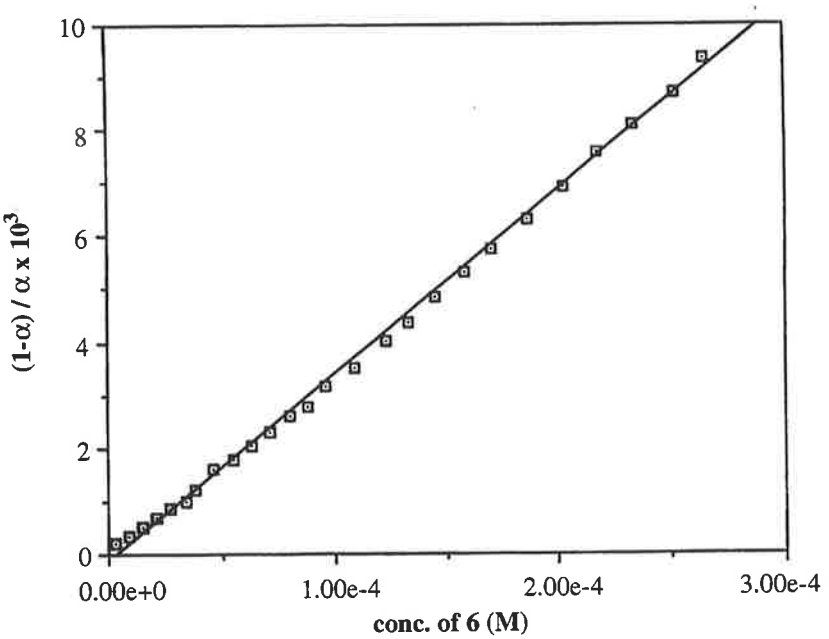

Figure 3.3 *Plot of 1-α / α versus [6] for the titration of* ***6*** *with silver(I) in DMF solution at 298.2 K and I = 0.050 M* (NEt_4ClO_4).

Table 3.4 *Experimental and calculated e.m.f. titration data (as determined by the VISP program) for the determination of the stability constant of* $[Pb2]^{2+}$ *in DMF solution at 298.2 K and I = 0.050 M* NEt_4ClO_4.

titre (mL)	expt. e.m.f. (mV)	calc. e.m.f. (mV)	titre (mL)	expt. e.m.f. (mV)	calc. e.m.f. (mV)
1.08	-83.70	-81.76	2.05	-180.50	-184.13
1.11	-83.90	-82.73	2.09	-198.20	-198.95
1.14	-84.50	-83.74	2.13	-209.80	-210.38
1.18	-85.30	-85.13	2.16	-217.30	-217.05
1.22	-86.20	-86.58	2.21	-225.90	-225.72
1.26	-87.80	-88.10	2.25	-231.20	-231.15
1.30	-89.10	-89.70	2.29	-236.30	-235.67
1.34	-91.70	-91.39	2.33	-240.50	-239.52
1.38	-93.20	-93.17	2.36	-244.60	-242.07
1.43	-95.60	-95.54	2.40	-247.40	-245.11
1.46	-97.00	-97.06	2.45	-250.80	-248.43
1.50	-99.50	-99.20	2.48	-252.30	-250.22
1.53	-101.30	-100.91	2.51	-253.60	-251.88
1.56	-104.90	-102.72	2.55	-255.30	-253.92
1.60	-107.10	-105.31	2.60	-257.20	-256.24
1.64	-109.90	-108.14	2.65	-257.60	-258.33
1.68	-110.30	-111.24	2.69	-258.80	-259.87
1.72	-115.40	-114.69	2.72	-259.50	-260.95
1.76	-118.80	-118.58	2.75	-260.70	-261.98
1.81	-123.70	-124.23	2.80	-262.50	-263.59
1.83	-127.70	-126.81	2.84	-263.30	-264.79
1.88	-135.40	-134.35	2.88	-264.30	-265.92
1.91	-141.30	-139.88	2.92	-266.00	-266.99
1.95	-149.60	-148.97	2.96	-267.70	-268.01
2.01	-167.40	-168.07			

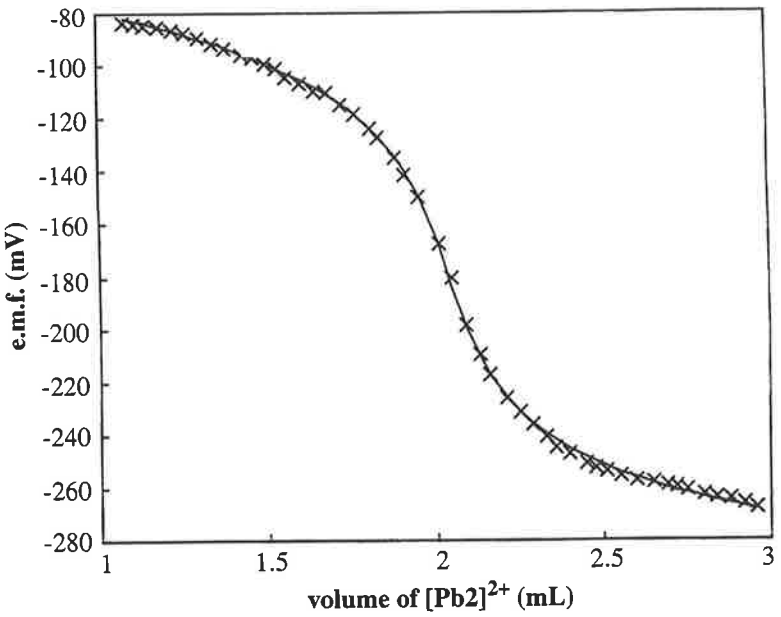

Figure 3.4 *Plot of experimental (x) and calculated (solid curve) e.m.f. versus titre for the titration of [Pb2]$^{2+}$ with silver(I) in DMF solution at 298.2 K and I = 0.050 M NEt_4ClO_4. The log K_s = 2.38 ± 0.21.*

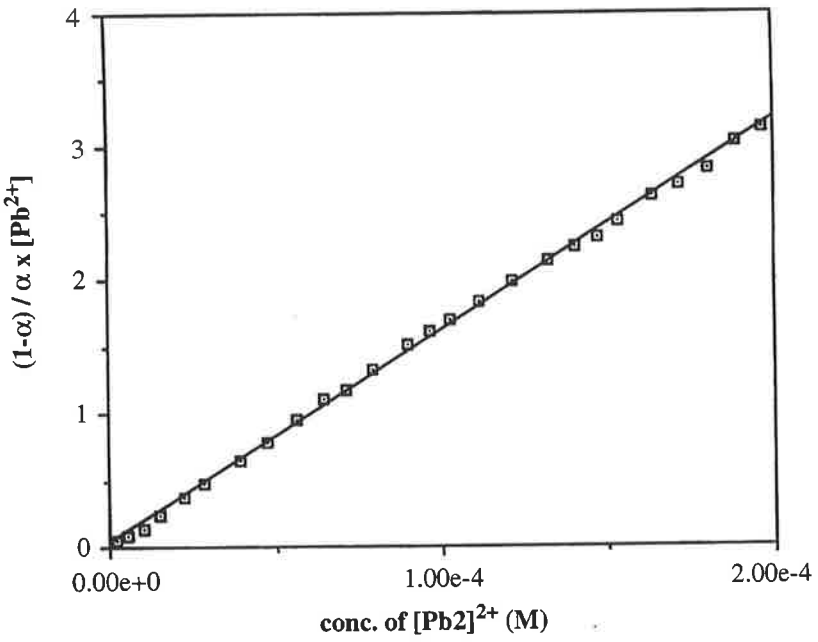

Figure 3.5 *Plot of 1-α / α x [Pb^{2+}] versus [Pb2]$^{2+}$ for the titration of [Pb2]$^{2+}$ with silver(I) in DMF solution at 298.2 K and I = 0.050 M NEt_4ClO_4.*

3.4 Results and Discussion

In this work, the stability constants (K_S) for $[ML]^{n+}$, where M^{n+} is silver(I), lead(II), zinc(II) and cadmium(II) ions and L is **1**, **2**, **5** and **6**, were determined by potentiometric methods using a silver(I)-ion selective electrode. The results obtained are summarized in Table 3.6. *N,N'*-dimethylformamide (DMF) was used as a solvent medium in our studies, as it allowed for a sufficient dissolution of the macrocyclic ligands at the concentrations required for the potentiometric analyses. The use of tetraethylammonium perchlorate (0.05 M) as a supporting electrolyte allowed the solutions under investigation to remain at a constant ionic strength throughout the length of the titration. As discussed in Section 3.3, this allows one to assess the stability constants of the metal-ligand systems in terms of concentration (K_S) alone, and no consideration of activity coefficients is required. A selectivity series for each ligand toward a particular metal ion could then be established.

The stability constants for the formation of the $[ML]^{n+}$ complexes where M^{n+} is lead(II), zinc(II), cadmium(II) and silver(I) ions, and L is **3** and **4** were not investigated by potentiometric methods. As described in Chapter 2, the syntheses of ligands **3** and **4** were quite extensive and laborious. Furthermore, ligands **3** and **4** exhibited a very low affinity toward lead(II), zinc(II) and cadmium(II) ions in the gas phase (Chapter 4). As a result, complexes of ligand **3** and **4** were not studied further by potentiometric analysis.

A plot of log K_S versus the macrocyclic ligand is presented in Figure 3.7. A selectivity series could not be determined for the interaction of these ligands with zinc(II) ions as only one ligand (namely, ligand **5**) appeared to form a stable zinc(II)-complex under our experimental conditions.

Table 3.6 *Apparent stability constants (log K_s) for the complexation of ligands **1**, **2**, **5** and **6** with silver(I), lead(II), zinc(II) and cadmium(II) ions in DMF solution at 298.2 K and I = 0.050 M NEt_4ClO_4.*

	Ligand **1**	Ligand **2**	Ligand **5**	Ligand **6**
Silver(I)	5.50 ± 0.04	6.49 ± 0.02	9.42 ± 0.13	7.52 ± 0.01
Lead(II)	2.62 ± 0.01	2.38 ± 0.21	6.71 ± 0.12	>7.52
Zinc(II)	< 2	< 2	4.30 ± 0.07	< 2
Cadmium(II)	< 2	< 2	5.92 ± 0.02	>7.52

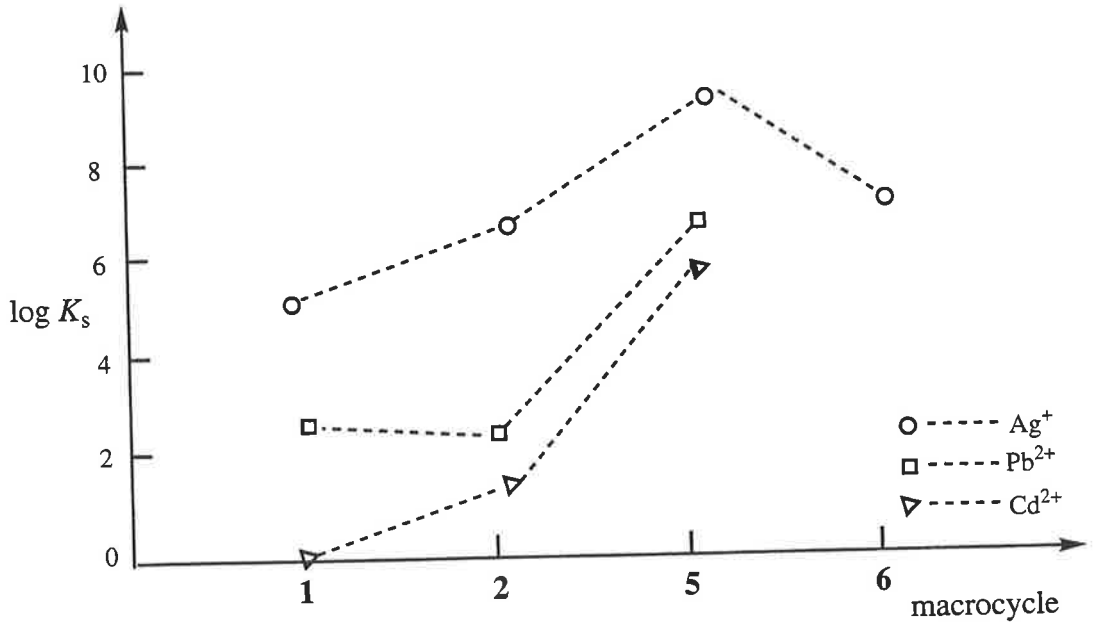

Figure 3.7

3.4.1 Complexation of ligands 1, 2, 5 and 6 with silver(I) ions.

The stability constants for the complexes of ligands **1**, **2**, **5**, and **6** with silver(I) ions were determined by direct potentiometric titrations. The highest stability constant was obtained for the $[Ag\mathbf{5}]^+$ complex, with a value of 9.42 ± 0.02 (Table 3.6). This experimental value was found to be in close agreement with that quoted in the literature,[163,164] for the formation of the $[Ag\mathbf{5}]^+$ complex under identical conditions. In contrast to the hard base oxygen donor atoms in crown polyethers, the presence of the softer base nitrogen donor atoms in ligand **5** tends to favour covalent bonding with the soft acid silver(I) ions. Indeed, crown polyamine derivatives, such as ligand **5**, show a marked selectivity toward transition and heavy metal ions, and a lower selectivity toward the alkali and alkaline earth metal ions.[69,97]

The formation of the $[Ag\mathbf{6}]^+$ complex was found to occur with a log $K_S = 7.52 \pm 0.01$. The $[Ag\mathbf{6}]^+$ complex was formed in DMF solution with a log K_S value which is two orders of magnitude lower than that of the $[Ag\mathbf{5}]^+$ complex (Table 3.6). As both ligands **5** and **6** contain the same number and type of donor atoms (two nitrogen and four oxygen) and the same eighteen-membered macrocyclic ring cavity, the decrease in log K_S as one moves from the $[Ag\mathbf{5}]^+$ complex to the $[Ag\mathbf{6}]^+$ complex must be attributed to the presence of the phenyl-hydroxyethyl pendant arms. The pendant arms of **6** do not facilitate the coordination of silver(I) ions, either because of the increase in steric hindrance introduced into the diaza-18-crown-6 moiety by the large pendant groups, or by the subsequent conformational distortion of the diaza-18-crown-6 macrocycle upon addition of the pendant groups.[160] This distortion may cause ligand **6** to move away from the conformation adopted by the unsubstituted diaza-18-crown-6 ligand **5**; an effect that may lead to a substantial decrease in the stability of the resulting silver(I) complex. Furthermore, since silver(I) tends to favour a linear coordination geometry,[165] it is feasible that the presence of the pendant arms causes sufficient distortion of the macrocycle to disrupt this mode of coordination. The lariat crown ethers **32** and **33**, with hydroxy- or methoxy-ethyl group functionality incorporated into the parent crown ether **5**, respectively,

have also been investigated for their binding affinities toward silver(I) ions in DMF solution. Similar decreases in stability were observed as one moves from the $[Ag\mathbf{5}]^+$ complex to the more highly substituted $[Ag\mathbf{32}]^+$ and $[Ag\mathbf{33}]^+$ complexes.[160,166]

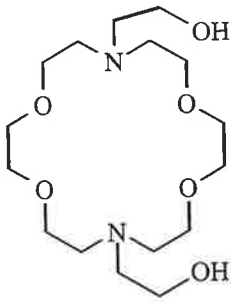

32

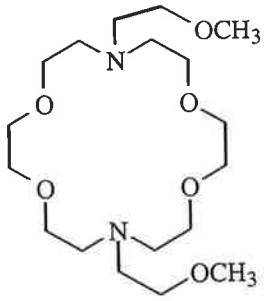

33

The tetrasulfide crown ether derivative **2** afforded a log K_S = 6.49 ± 0.02 for the corresponding silver(I) complex, $[Ag\mathbf{2}]^+$ (Table 3.6). It is well established that polysulfide macrocyclic ligands, where one or more oxygen donor atoms are replaced by sulfur atoms, show an increase in selectivity toward silver(I) ions.[76,81,97] This effect is most likely attributed to the soft base nature of the sulfur atoms, which favour the binding of soft acid silver(I) ions.

Of the four ligands studied in this series, the dipyridyl ligand **1** showed the lowest stability with silver(I) ions. The log K_S value for the $[Ag\mathbf{1}]^+$ complex was found to be 5.50 ± 0.04, considerably lower than the log K_S values of $[Ag\mathbf{5}]^+$, $[Ag\mathbf{6}]^+$ and $[Ag\mathbf{2}]^+$. Ligand **1** contains the same number and type of donor atoms as ligand **5** and **6** but, in addition, it also contains four extra methylene groups in its ring structure. Our results clearly demonstrate that as the cavity size of the macrocycle increases, from the diaza-18-crown-6 ring systems of ligands **5** and **6** to the 22-crown-6 ring system of ligand **1**, a lower affinity of the ligand toward silver(I) ions is observed. It is envisaged that macrocycle **1** would have to undergo quite significant conformational changes to accommodate the silver(I) ion within its cavity. The cavity radius of ligand **1** was estimated to be > 1.7 Å, as determined by the radius of the sphere which was able to be inserted into the intramolecular cavity of the space filling Corey-Pauling-Kolton (CPK) molecular models, without distortion of the ligand.[71,83] The cavity radii of ligands **5** and **6** were estimated to be ~1.3 Å by the same

method.[71,83] These results imply that the silver(I) ion, with an ionic radius of 1.15 Å,[167] is much better suited for accommodation by the smaller 18-crown-6 ring structures of ligands **5** and **6**.

One might envisage that the stability of ligand **1** toward silver(I) ions may be affected by the nature of nitrogen donor atoms, i.e. sp^2-hybridized pyridyl moieties, as opposed to the sp^3-hybridized amine groups of ligands **5** and **6**. However, many examples exist in the literature that demonstrate the high affinities of pyridino-aza-18-crown-6 derivatives toward silver(I) ions.[168] These studies demonstrate that the nature of nitrogen donors present in the ligand do not govern the overall stability of the silver(I) complex. It appears that the cavity size of the ligand is the most critical factor in complex stability.

In summary, the selectivity series of ligands **1**, **2**, **5**, and **6** toward silver(I) ions follows the order $[Ag\mathbf{5}]^+ > [Ag\mathbf{6}]^+ > [Ag\mathbf{2}]^+ > [Ag\mathbf{1}]^+$. The overall high stability observed by all four ligands with silver(I) ions is generally attributed to the appreciable covalent bonding that exists between the donor atoms (namely, nitrogen and sulfur) and the silver(I) ions.[69,97] Those ligands containing the four oxygen and two nitrogen donor atoms tend to show a greater selectivity toward silver(I) ions. The greater steric bulk of ligand **6**, when compared to **5**, causes a significant decrease in the stability of the corresponding silver(I)-complex. Ligand **1** possesses the same number and type of donor atoms as ligands **5** and **6**, but it is clear that its larger cavity size greatly lowers the stability of the corresponding $[Ag\mathbf{1}]^+$ complex. Ligand **2**, with its four soft sulfur atoms, shows a greater affinity toward the silver(I) ions than ligand **1**, but a significantly lower affinity when compared to ligands **5** and **6**.

3.4.2 Complexation of ligands 1, 2, 5 and 6 with lead(II) ions

The stability constants of the lead(II) complexes formed with ligands **1**, **2**, **5** and **6** with lead(II) ions (Table 3.6) decrease in the sequence $[Pb\mathbf{6}]^+ > [Pb\mathbf{5}]^+ >> [Pb\mathbf{1}]^+ \sim [Pb\mathbf{2}]^+$.

Despite the high stability of **6** toward lead(II) ions, the log K_s value for the $[Pb\mathbf{6}]^{2+}$ complex could not be determined. The technique of competitive potentiometric titrations

requires that the ligand possesses a greater stability toward the free metal ion (in this case, silver(I)) than any of the metal ions under investigation. This ensures that as the solution of the metal complex is added to the solution of free silver(I) ions, competition between the two metal ions for the ligand results in the significant displacement of the metal ions by the silver(I) ions. The change in the concentration of the free silver(I) ions is monitored by the silver(I) ion selective electrode. Thus, the greater the competition between the two metal ions for the ligand, the more significant the change in free silver(I) ion concentrations and the greater the change in electrode potential observed throughout the titration. This allows for an accurate determination of the log K_S value for the competitive titration. If the ligand is more stable with the metal ion, rather than the silver(I) ions, then the addition of the metal complex to the solution of free silver(I) ions causes negligible changes to the overall concentration of free silver(I) ions and, therefore, immeasurable changes in electrode potential are observed, at each point of the titration. This effect was observed in the case of **6** with lead(II) ions. A starting electrode potential of -61.2 mV was recorded, with systematic decreases in e.m.f. upon addition of the $[Pb\mathbf{6}]^{2+}$ complex at each point of the titration, resulting in a final electrode potential of -73.7 mV. Since very little change in the concentration of the free silver(I) ions was observed, ligand **6** clearly showed little affinity toward silver(I) ions in the presence of lead(II) ions. This implies that the $[Pb\mathbf{6}]^{2+}$ complex must be *more* stable than the competing $[Ag\mathbf{6}]^{+}$ complex. The log K_S value for the $[Pb\mathbf{6}]^{2+}$ complex cannot be determined by implementation of a competitive potentiometric titration method using a silver(I) selective electrode. What can be deduced, however, is that the $[Pb\mathbf{6}]^{2+}$ complex exists with a log K_S value $> 7.52 \pm 0.01$, i.e. greater than the log K_S value obtained for the $[Ag\mathbf{6}]^{+}$ complex under identical experimental conditions.

Lariat crown ether systems that are structurally related to **6** are known to display a high affinity toward lead(II) ions in aqueous media.[84,166,169] For example, ligand **32** was found to form a very stable complex with lead(II) ions (log K_S = 9.20).[166] The isomeric derivatives **33** and **34** were also found to coordinate lead(II) ions in aqueous media with a log K_S = 8.18[166] and log K_S = 8.57,[169] respectively. Inspection of these results clearly

shows that as the steric bulk of the lariat ether increases (by the incorporation of methyl substituents onto the pendant donor arms) an overall decrease in the stability of the resulting complex occurs in aqueous media. The complexation properties of these ligands with lead(II) ions in DMF solution have not been investigated to date.

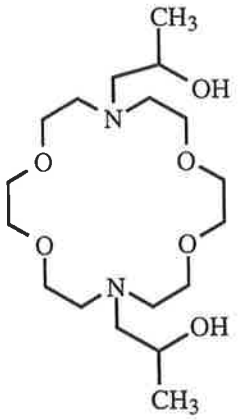

34

The stability of the $[Pb\mathbf{5}]^{2+}$ complex can be quantified by using a competitive potentiometric method in DMF solution. To date, little is known of the stability of ligand **5** with lead(II) ions, particularly under the conditions relevant to this study. $[Pb\mathbf{5}]^{2+}$ complexation has been reported in aqueous and methanol solvent systems with log K_s values of 6.90 and 9.48, respectively.[170,171] The large difference in these stabilities is attributed to the different solvation effects of the two media, and are readily explained by considering the Gutmann donor number (D_N) for each of the solvents. The D_N is a widely used parameter that expresses the donor strength of a solvent. It is generally defined as the magnitude of the negative enthalpy of complex formation (ΔH) between a donor solvent and the acceptor antimony(V) chloride ($SbCl_5$) in the inert medium 1,2-dichloromethane (Equation 3.37).[172,173]

$$\text{Solvent} + SbCl_3 \xrightarrow{ClCH_2CH_2Cl} \text{Solvent}\cdot SbCl_3 \qquad \textbf{3.37}$$

The D_N value of a solvent reflects its ability to act as a Lewis base in the presence of metal ions. Generally, the higher the D_N value of the solvent used for a potentiometric titration, the more strongly the solvent competes with the ligand of interest for coordination to the metal ion.[172,173] In the case of water and methanol, two D_N values are reported, namely

18 and 33 for water, and 19 and 23.5 for methanol.[174,175] The first value in each case is that obtained with dilute solutions of the protic solvent with 1,2-dichloromethane solution, and the second value is that obtained when neat protic solvent is used. The second of the D_N values has proved to be a more accurate measure of the donor ability of the respective solvents as it takes into consideration the intermolecular hydrogen-bonded structure of the protic solvents; this bonding is disrupted in the first case where the protic solvent is diluted in 1,2-dichloromethane.[176-178] Thus, if one considers the D_N values of water versus methanol, the much larger D_N for water implies that it solvates the lead(II) ions much more efficiently than the methanol and, therefore, it is harder for other ligands to displace the water molecules from the outer sphere of the lead(II) ions. This effect will in turn result in an overall lower stability for the $[Pb\mathbf{5}]^{2+}$ complex in aqueous media, when compared to the methanol solution.

The formation of the $[Pb\mathbf{6}]^{2+}$ complex occurred with a greater stability than that of the $[Pb\mathbf{5}]^{2+}$ complex (Table 3.6). This result was not unexpected. As previously mentioned, the incorporation of pendant arms, containing one or more neutral oxygen donor atoms, into crown ether ligands causes a marked increase in the selectivity of the lariat ethers toward larger metal ions, particularly lead(II) ions.[69,94,98,100,101,179] The origin of this selectivity may be that as one moves from the parent to the substituted ligand, the number of coordination sites that are available in the ligand increases from six to eight. Thus, the lariat ether ligand **6** allows for strong complexation with large metal ions that can achieve a coordination number of eight.[100] Furthermore, gas-phase studies have shown that the basicities of amines increase in the series, $NH_3 < RNH_2 < R_2NH < R_3N$ where R is an alkyl group.[98,180-182] Thus, it is envisaged that the slightly more basic nature of the tertiary nitrogen atom of ligand **6**, as compared to the secondary nitrogen atom of ligand **5**, would in part lead to an increase in the binding affinity of ligand **6** toward lead(II) ions.

The steric effects imposed on **6** by the presence of the phenyl-hydroxyethyl pendant arms must also be examined when considering the overall coordination properties of the ligand. It is feasible that the presence of the bulky pendant arms in **6** would sterically hinder the

coordination of the lead(II) ions. This effect should in turn lower the stability of the corresponding lead(II) complex. However, since this did not prove to be the case and, indeed, a large increase in the stability was observed as one moves from [Pb**5**]$^{2+}$ to [Pb**6**]$^{2+}$, it is clear that the steric effects are greatly outweighed by the favourable electronic properties of **6**. It can be concluded from this example that complex stability can be thought of as a delicate balance between both steric and electronic effects, each of which must be considered when a complex is modified by the addition of organic structural elements.[98]

The stability of the [Pb**2**]$^{2+}$ complex in DMF solution is low (log K_S = 2.38). This was unexpected particularly since macrocyclic ligands containing soft base sulfur atoms have been shown to exhibit a marked selectivity toward borderline hard acid lead(II) ions.[8,9,17,30] As described previously, the hard-soft acid-base (HSAB) character of both the donor atoms and the metal ion of interest is by no means the only parameter that governs metal-ligand reactions.[77] Solution studies have clearly demonstrated that as the number of large sulfur donor atoms increases in unsubstituted polysulfide macrocycles, the resulting ligand becomes substantially less flexible which, in turn, reduces the possible number of conformations the ligand can possess for metal ion incorporation.[81] Furthermore, X-ray diffraction studies of a number of these polyether ligands have shown that the sulfur atoms of the macrocyclic ring system are directed *out* of the ring cavity.[183,184] To our knowledge, related studies on the complexation behaviour of dibenzo-polysulfide macrocycles have not been reported previously, and so a direct comparison cannot be made with our work. It can be envisaged, however, that the presence of the four sulfur atoms and the two aryl groups of ligand **2** would certainly diminish its overall flexibility, and thus lead to the formation of metal complexes with low stability. Attempts at isolating suitable crystals of [Pb**2**]$^{2+}$ for X-ray crystallographic studies proved unsuccessful, however, *ab initio* calculations of [Pb**2**]$^{2+}$ were carried out to determine its gas phase structure (Chapter 4).

A low stability was also observed for the $[Pb\mathbf{1}]^{2+}$ complex. Even though **1** contains the same number and type of donor atoms as ligands **5** and **6**, namely two nitrogen and four oxygen atoms, its complexes do not exhibit the same stability with lead(II) ions (Table 3.6). The large cavity radius of the macrocycle **1** (> 1.7 Å)[77] is not suited for the complexation of lead(II) ions under the conditions employed in our study. It is envisaged that unfavourable conformational changes must occur for **1** to accommodate the lead(II) ions, with an ionic radius of 1.19 Å, within its macrocyclic ring cavity. To our knowledge, examples of the affinity of similarly sized macrocyclic crown ether systems of this type with lead(II) ions are unknown in the literature.

In conclusion, the stability constants obtained for the lead(II) complexes of ligands **1**, **2**, **5** and **6** decrease in the order: $[Pb\mathbf{6}]^{2+} > [Pb\mathbf{5}]^{2+} >> [Pb\mathbf{2}]^{2+} > [Pb\mathbf{1}]^{2+}$. The stability of the $[Pb\mathbf{6}]^{2+}$ complex could not be quantified by using the competitive potentiometric method as it possessed a higher stability than the corresponding $[Ag\mathbf{6}]^{+}$ complex. A low stability is demonstrated as one moves from the $[Pb\mathbf{6}]^{2+}$ to the $[Pb\mathbf{5}]^{2+}$ complex. In this case, the absence of the pendant donor arms decreases the affinity of the parent ligand **5** for lead(II) ions. Ligands **1** and **2** were found to exhibit low affinity for lead(II) ions.

3.4.3 Complexation of ligands 1, 2, 5 and 6 with zinc(II) ions

The results of the stability studies of ligands **1, 2, 5** and **6** with zinc(II) are summarized in Table 3.6. Of all four ligands investigated in this work, a stability constant could only be determined for the $[Zn\mathbf{5}]^{2+}$ complex. Ligands **1**, **2**, and **6** did not appear to form stable complexes with zinc(II) ions under our conditions.

In DMF solution, a log $K_s = 4.30 \pm 0.07$ was determined for the complex, $[Zn\mathbf{5}]^{2+}$ (Table 3.6). It has been demonstrated that the formation of this zinc(II) complex in methanol and in aqueous media occurs with a log $K_s = 4.84$ and a log $K_s = 3.1$, respectively.[84] Thus, the stability of the $[Zn\mathbf{5}]^{2+}$ complex increases as one moves from water to DMF to methanol solvent systems; a sequence which is in accordance with that expected from the solvent D_N

values where, in general, macrocyclic complex stabilities increase with a decrease in D_N.[172,173]

A low stability was observed for the $[Zn\mathbf{2}]^{2+}$ complex in DMF solution using competitive potentiometric methods. This result was expected. If one considers the HSAB characters of the donor atoms and metal ions involved, it is envisaged that ligand **2**, with its four soft base sulfur donor atoms, would not be particularly stable toward the borderline acid zinc(II) ions. The solvation of the zinc(II) ions must also be considered as a contributing factor that affects the stability of the $[Zn\mathbf{2}]^{2+}$ complex. DMF is considered to be a strong oxygen donor solvent (D_N = 26.6), and one would expect the small, borderline acid zinc(II) ions to be strongly solvated. Extensive solvation would lead to a lowering of the stability of the $[Zn\mathbf{2}]^{2+}$ complex, in spite of the favourable entropic drive associated with the "macrocyclic effect".[71,185]

All attempts at determining the stabilities of the $[Zn\mathbf{1}]^{2+}$ and $[Zn\mathbf{6}]^{2+}$ complexes by means of competitive potentiometric titration methods proved unsuccessful. Under the conditions of our study, no complex formation was observed between these ligands and zinc(II) ions. It can be assumed that if there exists no interaction between a ligand and a competing metal ion then the titration simply becomes a measure of the interaction between the ligand and the silver(I) ions. Indeed, when one compares the experimental data obtained for the competitive titration of ligand **1** (or **6**) with zinc(II) ions and the experimental data obtained for the direct titration of **1** (or **6**) with silver(I) ions, respectively, the competitive and direct titration data for the ligand are completely superimposable. This result clearly demonstrates that there is no interaction between either ligand **1** or **6** with zinc(II) ions and, indeed, the ligands are interacting exclusively with the silver(I) ions that are present in solution, as measured by the silver(I) ion selective electrode.

If one considers that ligand **1**, with a large cavity size of > 1.7 Å, is severely mis-matched for 1:1 encapsulation of a small zinc(II) ion (r = 0.74 Å), then complexation with a significant K_s value is unlikely. The complexation properties of **1** with zinc(II) ions were also investigated using UV-visible spectroscopy (Section 3.5.2) and electrospray ionisation

mass spectrometry (Section 4.2.1). In both cases, no evidence was obtained for the formation of the $[Zn\mathbf{1}]^{2+}$ complex.

Ligand **6** was not expected to form a stable complex with zinc(II) ions. Similar lariat ether systems, containing neutral oxygen donor atoms, have been found to be poorly selective for smaller metal ions such as zinc(II), and an increase in stability is observed with larger metal ions such as lead(II) and cadmium(II).[69,94,98,100,101]

In conclusion, a stability constant could only be determined for ligand **5** with zinc(II) ions in DMF solution using competitive potentiometric titration methods. The formation of the zinc(II) complex of ligand **2** was observed under our conditions, however, its stability was too low to be accurately quantified. No 1:1 complex formation was observed for ligands **1** and **6** with zinc(II) ions using potentiometric methods.

3.4.4 Complexation of ligands 1, 2, 5 and 6 with cadmium(II) ions

The stabilities of the complexes formed between ligands **1, 2, 5** and **6** with cadmium(II) ions are summarized in Table 3.6. The overall selectivity series for the ligands toward cadmium(II) ions follows the order: $[Cd\mathbf{6}]^{2+} > [Cd\mathbf{5}]^{2+} >> [Cd\mathbf{2}]^{2+} > [Cd\mathbf{1}]^{2+}$.

Even though the stability of $[Cd\mathbf{6}]^{2+}$ is high, it could not be quantified using a silver(I)-ion competitive potentiometric titration method. Throughout the titration, the systematic addition of a solution of $[Cd\mathbf{6}]^{2+}$ to the silver(I) solution caused very little change (< 15 mV) in the overall electrode potential of the system. Such a small change in electrode potential is observed when the addition of the competitive complex, in this case $[Cd\mathbf{6}]^{2+}$, causes negligible changes to the concentration of the free, solvated silver(I) ions, as monitored by the silver(I) ion electrode. This result is consistent with the poor competition that occurs between the silver(I) and cadmium(II) ions for ligand **6** and, therefore, it must have a greater affinity for cadmium(II) over silver(I). This phenomena, which is also observed for the determination of the stability constant of the $[Pb\mathbf{6}]^{2+}$ complex, renders our competitive potentiometric method inapplicable in determining the log K_S value of $[Cd\mathbf{6}]^{2+}$. It is accepted, however, that the formation of the $[Cd\mathbf{6}]^{2+}$ complex occurred with

a log K_s > 7.52, i.e. the log K_s value obtained for the [Ag**6**]$^+$ complex under identical conditions.

The binding affinities of related lariat crown ether systems **32**, **33** and **34** toward cadmium(II) ions have been studied by means of pH-potentiometric titration methods in aqueous media.[84,163,169] The stability constants for the [Cd**32**]$^{2+}$ and [Cd**34**]$^{2+}$ complexes were determined to be log K_s = 7.1 and log K_s = 7.64, respectively. The slight increase in stability as one moves from the [Cd**32**]$^{2+}$ to the [Cd**34**]$^{2+}$ complex is somewhat surprising when one considers that the lariat ether **34** is more sterically limited in its binding, attributed to presence of the methyl moieties on the chiral carbon atom of the pendant donor arm, than the unsubstituted ether **32**. However, one must also consider that the formation of the [Cd**34**]$^{2+}$ complex is enhanced by contributing electronic effects, imparted by the extra methyl group of the hydroxyethyl pendant arms in the lariat ether system, which appear to outweigh the steric effects and thus favour the formation of the resulting complex. Ligand **33** was also investigated for its affinity toward cadmium(II) ions in aqueous media.[166] A sharp decrease in the stability constant by a factor of three orders of magnitude was observed as one moves from the [Cd**32**]$^{2+}$ to the [Cd**33**]$^{2+}$ complex. This result clearly demonstrates that replacement of the simpler hydroxyethyl pendant arms of **32** with more substituted methoxyethyl groups causes a destabilizing effect on the coordination behaviour of the lariat ether **33** toward cadmium(II) ions.

The stability of the [Cd**5**]$^{2+}$ complex was calculated to be log K_s = 5.92 ± 0.02 (Table 3.6). No precedents exist in the literature that describe the affinity of ligand **5** toward cadmium(II) ions under similar conditions to those employed in this study. However, the formation of the [Cd**5**]$^{2+}$ complex is reported to occur in aqueous solution with a log K_s = 5.25, as observed using competitive pH-potentiometric titrations.[84] Therefore, an examination of the stability constants for [Cd**5**]$^{2+}$ complexation in water and DMF solvent systems reveals that the stability of the complex increases in the order DMF > water. This sequence is in accordance with that expected from the solvent D_N values, where in general complex stabilities increase with a decrease in D_N.[172,173]

An increase in stability is observed as one moves from the $[Cd\mathbf{5}]^{2+}$ complex to the $[Cd\mathbf{6}]^{2+}$ complex. As mentioned previously, the presence of the neutral oxygen donor atoms, in the form of phenyl-hydroxyethyl pendant arms, increases the affinity of **6** toward larger metal ions. A cadmium(II) ion, with an ionic radius of 0.95 Å, is sufficiently large enough to benefit from the two extra oxygen donors which supplement coordination by the macrocyclic ring donor atoms. Similar stabilizing factors may also apply to the formation of the $[Cd\mathbf{6}]^{2+}$ complex, as discussed for the $[Pb\mathbf{6}]^{2+}$ species in Section 3.4.2. Basically, the presence of the donor pendant arms of **6** causes an increase in the favourable electronic properties of the ligand, as compared to the unsubstituted parent crown ether **5**, and a subsequent increase in the binding affinity of **6** toward cadmium(II) ions is observed. By comparing the stability constants of the $[Cd\mathbf{5}]^{2+}$ and $[Cd\mathbf{6}]^{2+}$ complexes, the greater steric restraints expected of the lariat ether **6** do not significantly affect its coordination to cadmium(II). It is clear that in this system the stabilizing electronic factors associated with the pendant arms in ligand **6** outweigh any steric effects.

Under our conditions, ligand **2** was found to form weak complexes with cadmium(II), and a log $K_s < 2$ obtained for this system. One can invoke similar explanations to those described for the formation of the $[Pb\mathbf{2}]^{2+}$ complex in Section 3.4.2.

No 1:1 complexation was observed between ligand **1** and cadmium(II) ions in DMF solution. Examination of the experimental data obtained for the competitive titration of **1** with cadmium(II) ions were found to correspond exactly with those obtained for the direct titration of **1** with silver(I) ions. The macrocyclic cavity radius of ligand **1** is estimated to be > 1.7 Å,[71,83] and the ionic radius of cadmium(II), with a coordination number of six, is calculated to be 0.95 Å.[71,83] It is feasible that the significant mismatch between the size of the macrocyclic cavity of **1** and the ionic radius of the cadmium(II) ions is one of the major contributing factors that inhibits the formation of a stable $[Cd\mathbf{2}]^{2+}$ complex. This proposal is further supported if one examines the relative stabilities obtained for other complexes of ligand **1**, including those with silver(I), lead(II) and zinc(II) (Table 3.6). Under our conditions, the only stability constants that could be determined experimentally were those

for the $[Ag\mathbf{1}]^{2+}$ and $[Pb\mathbf{1}]^{2+}$ complexes. If one considers that silver(I), lead(II) and zinc(II) ions have ionic radii equal to 1.15 Å, 1.19 Å and 0.75 Å, respectively,[71,83] it is clear that the larger silver(I) and lead(II) ions tend to be better matched for inclusion within the macrocyclic cavity of ligand **1**.

3.5 UV-visible spectroscopy

The use of UV-visible spectroscopy as an alternative method for the determination of stability constants has been reported.[74,141-143] The basis of this technique involves measuring the change, either hypsochromic or bathochromic, in the absorbance maxima as one moves from the free ligand to the complex. One major advantage of this method over potentiometric methods is its increased sensitivity.

The first factor that must be established when pursuing K_S determinations using UV-visible spectroscopy is whether a significant shift in the absorbance maxima is observed as one moves from the free ligand to the complex. Using the experimental conditions discussed in Section 6.2.5, the UV-visible spectra of the solution of the free ligand **1**, and the solutions of **1** with excess lead(II), zinc(II), cadmium(II) and silver(I) ions, were recorded. The UV-visible spectra that were recorded are presented in Figures 3.5a-d. The UV-visible spectra obtained for the solution of the free ligand **2**, and the solutions of **2** with excess lead(II), zinc(II), cadmium(II) and silver(I) ions, are presented in Figures 3.6a-d. It is clear from the spectra that very little, if any, change in absorbance maxima occurred for any of the metal complexes formed from ligands **1** or **2**. The most significant change in absorbance maxima, in a bathochromic direction, was observed for the $[Ag\mathbf{1}]^{+}$ and $[Ag\mathbf{2}]^{+}$ complexes, as shown in Figures 3.5d and 3.6d, respectively. Regardless, in all cases studied, the minimal change in absorbance maxima for both ligands **1** and **2** (free and complexed) was not considered sufficient enough to allow stability constants to be determined with any great accuracy by this spectroscopic method.

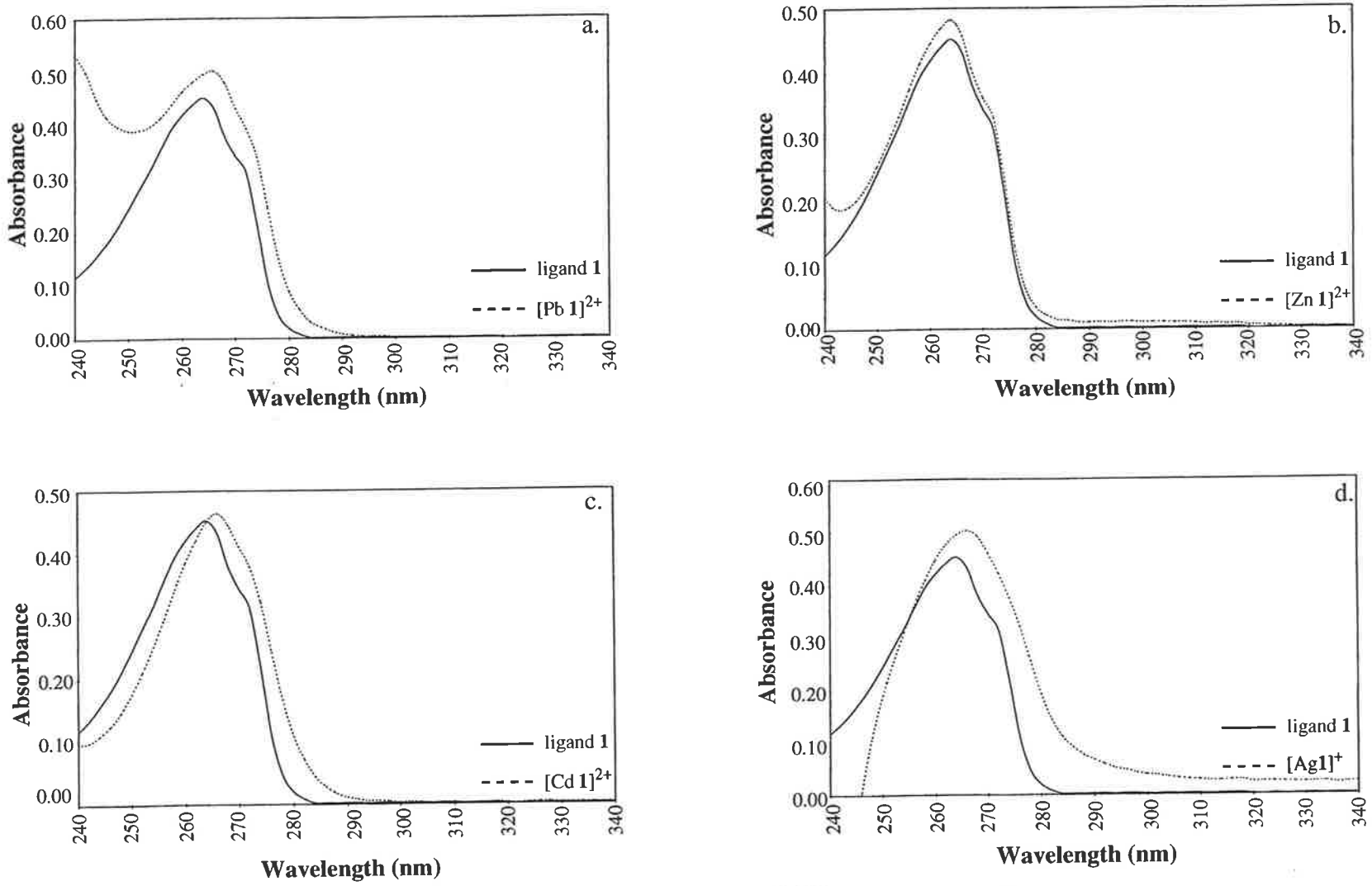

Figure 3.5 *UV-visible absorption spectra recorded for methanol solutions of ligand 1 in the absence (solid curve) and in the presence (dotted curve) of excess (a) lead(II), (b) zinc(II), (c) cadmium(II) and (d) silver(I) ions.*

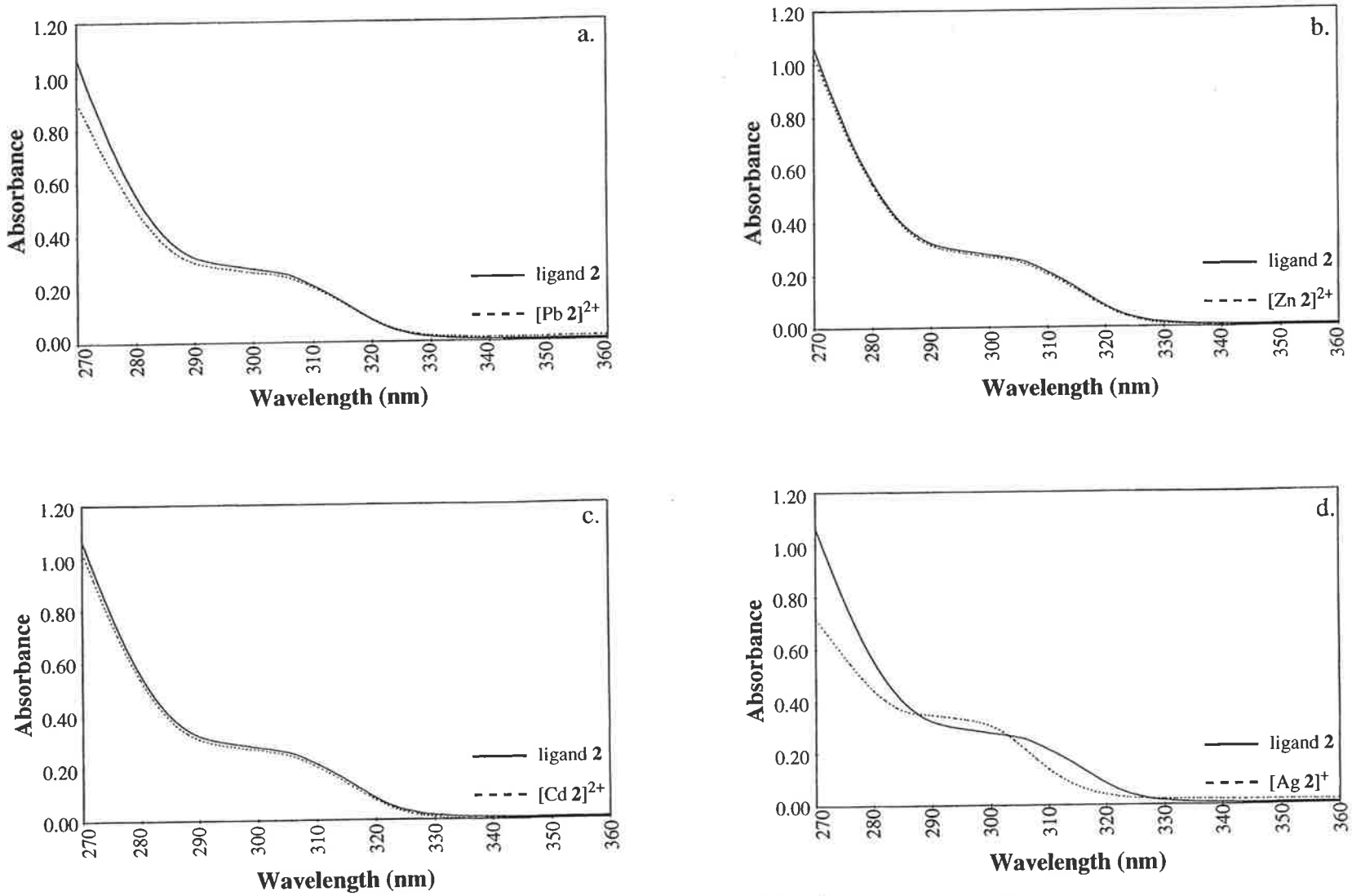

Figure 3.6 *UV-visible absorption spectra recorded for DMF solutions of ligand 2 in the absence (solid curve) and in the presence (dotted curve) of excess (a) lead(II), (b) zinc(II), (c) cadmium(II) and (d) silver(I) ions.*

3.6 Conclusions

By implementation of potentiometry, the coordination properties of ligands **1**, **2**, **5** and **6** with lead(II), zinc(II), cadmium(II) and silver(I) ions were investigated in DMF solution.

The results from our study show that the most stable lead(II) complex was formed with ligand **6**. Of the four ligands studied in this work, **6** appears to be the most likely prototype for the development of a lead(II)-ion specific probe. Additionally, since **6** does not form a stable complex with zinc(II) ions, a sufficient level of discrimination between zinc(II) and lead(II) ions exists. This discrimination is of relevance in the development of a target molecule that functions as a lead(II)-specific probe, particularly since zinc(II) ions are biologically prevalent cations that would possibly interfere with the monitoring of lead(II) levels in biological media. Ligand **6** was also found to form a stable complex with cadmium(II) ions in DMF solution. Unfortunately, since the K_S values for the complexation of **6** with cadmium(II) and lead(II) ions could not be differentiated using this potentiometric method, it remains unclear which of the two complexes is formed with a higher stability in DMF solution. In order to address this issue, the work described in Chapter 4 utilizes electrospray ionisation mass spectrometry (ESI-MS) for the determination of the relative stabilities of the complexes in the gas phase.

Ligand **5** was found to complex lead(II), zinc(II), cadmium(II) and silver(I) ions with moderate to high stabilities and thus, it exhibits little selectivity between these metal ions. The stability observed for $[Ag\mathbf{5}]^+$ was three orders of magnitude greater than that of the corresponding lead(II) complex. Ligand **5** also forms a stable complex with cadmium(II) and zinc(II) ions, but the resulting cadmium(II) and zinc(II) complexes were found to have a lower stability than that of the corresponding lead(II) complex.

For ligands **1** and **2**, low stability constants were determined for complexes with lead(II) ions. In both cases, sufficient discrimination was shown for lead(II) ions over

zinc(II) ions. However, it is acknowledged that since the lead(II) complexes of ligands **1** and **2** were formed with a very low stability, neither ligand is considered to be viable for development into a lead(II)-specific probe. The fact that ligand **2** proved to be a poor ligand for lead(II) in DMF solution, despite the incorporation of four soft base sulfur donor atoms, was somewhat surprising. This low stability of the $[Pb\mathbf{2}]^{2+}$ complex in solution is attributed to the free ligand conformation which appears unsuitable for coordinating lead(II) ions. The gas phase conformations of the free ligand and its corresponding lead(II) complex are presented in Chapter 4. Ligand **2** was found to interact very weakly with cadmium(II) ions in DMF solution. Ligand **1** did not complex cadmium(II) ions under our conditions, a phenomenon confirmed by comparison of the experimental results obtained for the competitive titration, in the presence of cadmium(II) ions, with those obtained for a direct titration of ligand **1** with silver(I) ions.

The following chapter details the use of electrospray ionisation mass spectrometry (ESI-MS) and *ab initio* calculations for investigating the complexation of ligands **1 - 6** with a series of metal ions in the gas phase. The results obtained from the ESI-MS studies should enable a thorough investigation of the coordination properties of ligands **1**, **2**, **5** and **6** to be established in both the solution and gas phase. It will be of interest to note whether any correlation in coordination behaviour is observed as one moves from the solution to the gas phase. ESI-MS methods will also offer valuable information into the coordination properties of ligands **3** and **4** with the series of relevant metal ions. *Ab initio* calculations will afford the optimized conformational geometries of the free ligands and the corresponding metal complexes.

4 Gas phase studies

Mass spectrometry and molecular modelling calculations are useful methods for probing metal-ligand interactions in the gas phase. This chapter is primarily concerned with the use of electrospray ionisation mass spectrometry (ESI-MS) for investigating the coordination properties of the macrocyclic ligands **1 - 6** with silver(I), lead(II), zinc(II) and cadmium(II) ions. The fundamental principles underlying the ESI-MS process are reviewed, particularly with reference to crown ether complexation reactions.

Complementary *ab initio* calculations utilising the Gaussian 94 suite of programs were performed on those species that were observed by ESI-MS methods. *Ab initio* calculations can afford the optimised conformational geometries of free ligands and the corresponding metal complexes. A brief overview of the underlying principles behind Gaussian 94 calculations is presented, and the limitations associated with these methods are also discussed.

4.1 Mass spectrometric methods for the assessment of metal complexation by crown ether ligands

Mass spectrometry has been shown to be a useful analytical tool in the assessment of metal-ligand interactions.[186] Mass spectrometric methods are considered to be particularly important when studying macrocyclic crown ethers and their derivatives, particularly since they allow the coordination properties of the ligands to be assessed in the absence of bulk solvent.[186] It is well established that a governing factor in the experimental assessment of metal ion complexation strengths and selectivities is the dependence of the complexation reaction on the solvent system in which the reaction is being studied.[69,71,77,83,186] Generally, the more polar the solvent used throughout the solution study, the greater the degree of solvation associated with the metal ion under investigation and subsequently, the interaction between the ligand and metal ion is diminished.[172,173]

Two prominent methods that exist for the analysis of metal-ligand interactions in the gas phase include fast atom bombardment mass spectrometry (FAB-MS) and ESI-MS. Both these methods have been found to be particularly serviceable analytical tools for the evaluation of the interactions between macrocyclic crown ether ligands, and their derivatives, with metal ions.[155-157,186-191]

The FAB-MS method is amenable to the study of molecular complexation as it involves the desorption of the substance(s) under study by low level energy transfer from the accelerated atoms that bombard the sample probe.[187] This energy transfer causes minimal fragmentation of the complexes under investigation. FAB ion sources operate with the substance under investigation being dispersed in a glycerol or *m*-nitrobenzyl alcohol matrix. Provided that adequate calibration is performed,[189] the mass spectral peak heights for the desorbed ionic species are proportional to the concentrations of these species in solution. Thus, comparisons of the relative intensities observed for each species will enable complex formation and stability to be assessed in the gas phase, at least on a semi-quantitative level. These results can be taken one step further and the gas phase stability constants (log K_S) for complex formation can be determined. Johnstone *et al.*[155,156,188,189] discuss in detail the use of FAB-MS for the determination of stability constants of the simple 18-crown-6 polyether ligand with sodium(I) and potassium(I) ions, by monitoring the change in concentration of the complex as the concentration of the metal ion present is systematically increased. These results clearly demonstrate that stability constants can be measured using FAB-MS. It was also suggested by the authors that, in this study, the results obtained were a good reflection of solution behaviour.[155,189] The importance of this pioneering method for the assessment of metal complexation is clear from a perusal of recent reports by Wang *et al.*,[187] Deaden *et al.*,[192] Brodbelt *et al.*,[190,193,194] and Bowers *et al.*[195]

The use of ESI-MS for studies of the interactions of macrocyclic ligands with metal ions is a technique that has only been investigated recently. Electrospray ionisation is considered to be a "softer" method for desorption than FAB, and it allows macrocyclic complexes to

be analysed with an even greater sensitivity than that of the FAB-MS method.[187] The formation of a metal complex under ESI-MS conditions is indicated by a positive ion signal observed at the relevant mass/charge (*m/z*) ratio. Measurements of the relative intensities of the positive ion signals observed by ESI-MS allows for the affinity of the ligand(s) toward the metal ion(s) to be assessed in the gas phase.

The use of ESI-MS for probing the interactions of various macrocyclic ligands with alkali, alkali earth, transition and heavy metal ions have featured predominantly in the recent literature.[157,186,187,191] Methods for the determination of gas phase stability constants for metal complexes are also discussed. In many cases, the stability constants obtained by means of gas phase investigations were found to be in good agreement with those obtained well-established solution methods.[157,186,187] Initially, many practitioners were wary of adapting the ESI-MS method to complexation studies because of the concern that the gas phase does not adequately reflect solution phenomena.[187,196,197] However, such correlations have been investigated in many cases where gas phase studies are conducted, and even though at times new trends have become apparent,[190] a sufficient number of examples show that gas phase results closely parallel those obtained from solution studies.[157,186,187]

The similarities that are found between the solution and gas phase data are generally attributed to the underlying methods of ESI-MS analysis. Even though ESI-MS is considered to be a technique for the determination of the complexation behaviour between macrocyclic ligand(s) and the metal ion(s) in the gas phase, the interaction between the two species occurs initially in the solution phase. A typical ESI-MS experiment involves the preparation of an analytical solution, containing both the host (macrocycle) and guest (metal ion) species, in an appropriate solvent system. This solution is equilibrated, and it is then introduced into the ESI mass spectrometer. The complexes are carefully transferred from the condensed phase into the gas phase as isolated entities. A more detailed explanation of the principles and practices of ESI-MS follows.

4.2 The electrospray ionisation mass spectrometry technique

The electrospray ionisation (ESI) technique involves the direct transfer of analyte species, which are ionized in the condensed phase, into the gas phase as isolated entities.[198] The electrospray technique is regarded as a much 'softer' method for desorption, as it allows the pre-existing ions to be gently transferred into the gas phase, thus resulting in minimal fragmentation.[191] When compared to conventional ionization mass spectrometry methods, such as electron ionization mass spectrometry (EI-MS), more severe ionization conditions are required for the conversion of neutral molecules into ions.

The mechanisms that govern the 'softer' ionization technique of ESI-MS can be divided into three stages: droplet formation, droplet shrinkage and gaseous ion formation.[198,199] A solution of the analyte is delivered to the tip of the electrospray capillary, where it experiences an electric field associated with the maintenance of the tip at high potential[198] (Figure 4.1). Assuming that positively-charged ions are to be analysed by ESI-MS, a high positive potential is applied, and the positive ions that are present in solution are found to accumulate at the surface of the electrospray capillary.

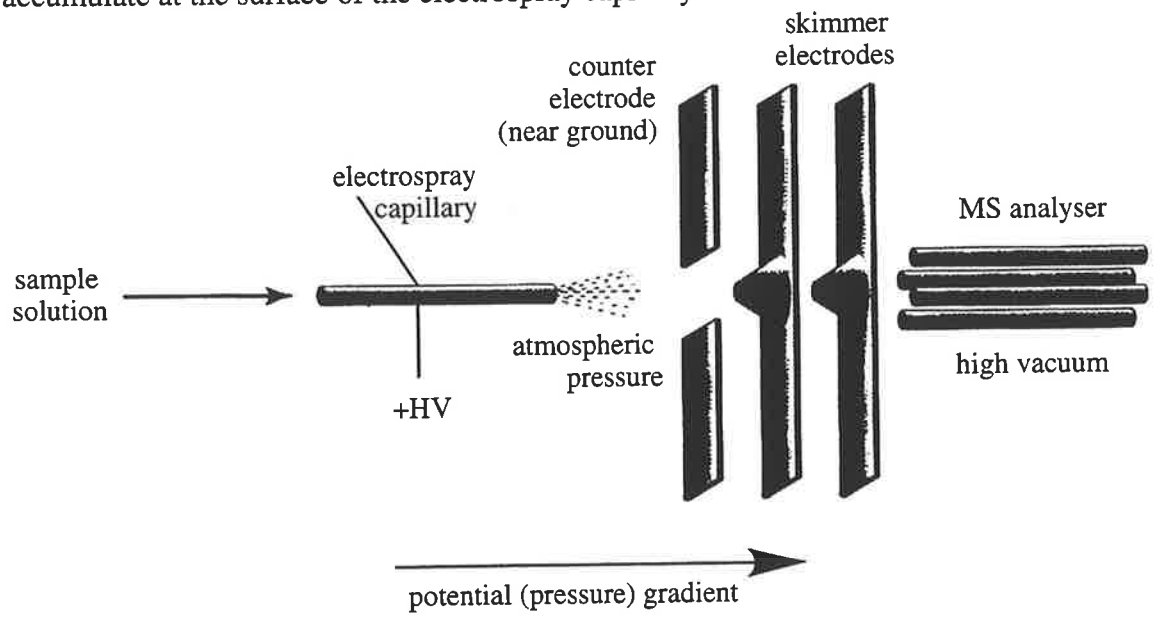

Figure 4.1 *The essential features of an electrospray interface.*[198]

The positive potential and pressure gradients force the solution of ions to be drawn out of the capillary in a downfield direction (Figure 4.1) to afford a 'Taylor cone' (Figure 4.2).

At a sufficiently high potential, the cone itself is drawn out to a filament which generates the mist of positively-charged droplets. This is known as the "budding process", and it will only occur when the surface tension of the droplets is exceeded by the applied electrostatic force. The diameter of the droplets formed by this process is influenced by a number of parameters, including the extent of the applied positive potential, the flow rate at which the solution is administered, and the properties of the solvent system used. This concludes the first stage for droplet formation.

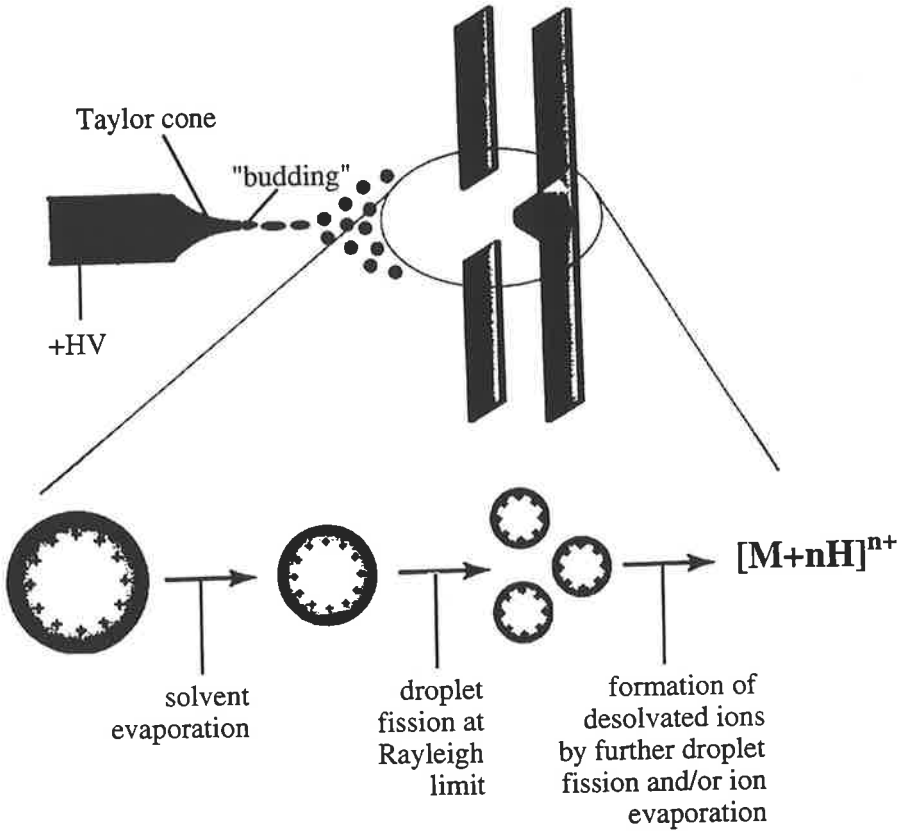

Figure 4.2 *Droplet production in the electrospray interface.*[198]

Once the droplets are released from the 'Taylor cone', they traverse a pressure gradient toward the analyser of the mass spectrometer, and evaporation of the solvent occurs. A reduction in the diameter of the droplets then ensues (Figure 4.2). Further shrinkage in the size of the droplets results from what is known as a 'Coulomb explosion'. A 'Coulomb explosion' causes the fission, or subdivision, of the droplets because of the increased charge density which is now present in the individual droplets as a result of the solvent evaporation. The 'Coulomb explosion' process will only occur when the magnitude of the

charge is sufficient to overcome the surface tension holding the droplet together. The point at which this occurs is known as the 'Rayleigh limit'. Thus, continuous depletion in the droplet size by evaporation and fission is thought to result ultimately in the formation of individual droplets that contain a single ion only. The final stage in this sequence involves the conversion of these solvated single ions into their related desolvated gaseous ion species. This process involves complete evaporation of the remaining solvent, a process thought to be aided by the activating collisions occurring between the charged ions at the electrospray interface.[198] Alternative mechanisms describing this ion evaporation process have featured prominently throughout the literature, and such mechanisms still remain a topic of wide interest.[198-202] Finally, the gaseous ions can enter the analyser of the mass spectrometer.

4.2.1 Results and Discussion

The positive ion ESI-MS method used for the determination of the binding affinities of the macrocyclic ligands **1 - 6** with silver(I), lead(II), zinc(II) and cadmium(II) ions follows the general procedure outlined by Young and co-workers.[157] Preliminary studies were commenced by recording an ESI spectrum for each ligand (**1 - 6**) in the presence of excess metal ion in methanol solution. In all cases, the metal ion of interest was maintained at much higher concentrations than the ligand concentration to ensure that complete complexation had occurred. Analysis of the sample solutions by ESI-MS allowed the nature of the cationic complexes formed in solution, and the relative intensities of these species, to be assessed. Once each ligand had been assessed for its selectivity toward individual metal ions, each of the ligands which had exhibited a strong affinity toward more than one metal ion was assessed by competitive ESI-MS experiments. In these experiments, a sample solution containing one ligand and *two* metal ions, in an appropriate solvent system, were assessed by ESI-MS. Comparisons of the relative intensities of each complex signal that was observed in the ESI mass spectrum enabled a relative stability series for the ligand toward two metal ions to be established. A more detailed explanation of the experimental conditions employed in this study is presented in Section 6.2.3.

In total, twenty-four sample solutions were investigated in this study. Very few solutions were found to produce strong cationic signals that represented a 1:1 metal-ligand complex under the conditions employed. All macrocyclic ligands (**1 - 6**) formed stable complexes with silver(I) ions under the conditions of the ESI-MS experiment. These results are tabulated in Table 4.1. Selected examples of the ESI spectra that were obtained are presented in Figures 4.3 and 4.4 which correspond to the $[Ag\mathbf{2}]^+$ and $[Ag\mathbf{6}]^+$ complexes, respectively. The isotopic distribution patterns produced in each case are consistent with the presence of the naturally occurring isotopes of the silver(I) ion, i.e. ^{107}Ag and ^{109}Ag. The strong positive ion signals observed for each silver(I)-ligand complex demonstrate that, under the conditions employed for ESI-MS, ligands **1 - 6** show a high affinity for silver(I) ions.

Table 4.1 *The positive m/z signals observed for $[ML]^{n+}$ complex formation between ligands L (**1 - 6**) and a series of metal ions M.*

Ligand	silver(I)	lead(II)	zinc(II)	cadmium(II)
1	*m/z* 589	-	-	-
2	*m/z* 559	*m/z* 330	-	-
3	*m/z* 465	-	-	-
4	*m/z* 705	-	-	-
5	*m/z* 370	-	-	*m/z* 187
6	*m/z* 609	*m/z* 355	-	*m/z* 373[a]

[a] *The molecular ion peak observed at m/z 373 corresponds to the solvated cadmium(II)-complex $[Cd\mathbf{6}]^{2+}.4MeOH$.*

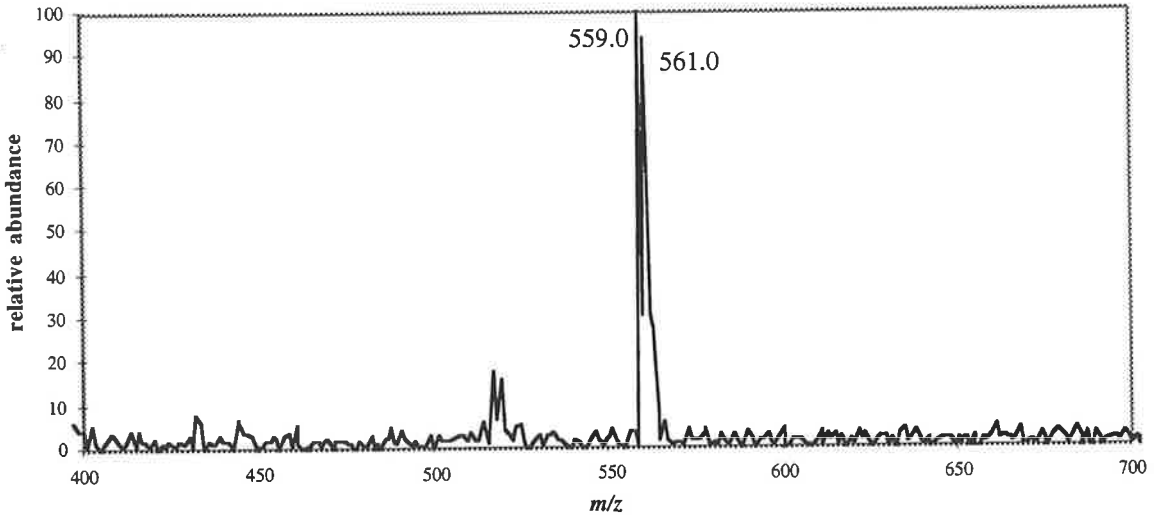

Figure 4.3 *ESI-MS of the [Ag2]$^+$ complex in methanol solution.*

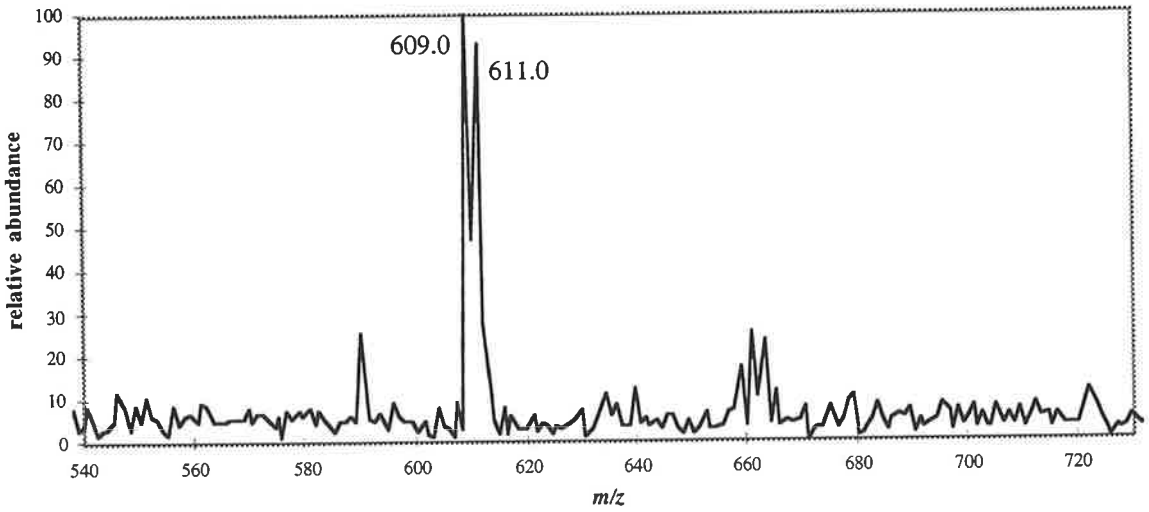

Figure 4.4 *ESI-MS of the [Ag6]$^+$ complex in methanol solution.*

Stable lead(II)-complexes were only observed for ligands **2** and **6** in the gas phase. The gas phase stability of the [Pb**2**]$^{2+}$ and [Pb**6**]$^{2+}$ species was demonstrated by the appearance of strong positive ion signals at *m/z* 330 and 355, respectively. These results are summarized in Table 4.1. It is clear when assessing these results that both ligands **2** and **6** show a significant affinity toward lead(II) ions under gas phase conditions.

Competitive ESI experiments were conducted on solutions that contained either ligand **2** or **6** with excess lead(II) and silver(I) ions. By a direct comparison of the relative intensity of the molecular ion peak for each complex, it is clear that the formation of [Ag**2**]$^+$ complex is favoured over the [Pb**2**]$^{2+}$ complex by a factor of approximately 3:1. This result

demonstrates that, under the conditions of this ESI study, ligand **2** has a significantly higher selectivity for silver(I) over lead(II) ions. In contrast, ligand **6** has a higher selectivity toward lead(II) ions under the same experimental conditions. Indeed, the intensity of the molecular ion peak for $[Pb\mathbf{6}]^{2+}$ was approximately 20 times greater than that of the $[Ag\mathbf{6}]^{+}$ peak. This result clearly demonstrates the highly selective nature of ligand **6** toward lead(II) ion over silver(I) ions. In each competitive experiment, there was no evidence for the formation of a mixed lead(II)-silver(I) species with either ligand **2** or **6**.

Stable complexes of ligands **5** and **6** with cadmium(II) ions were observed by ESI-MS. The ESI-MS spectrum confirmed the formation of the $[Cd\mathbf{5}]^{2+}$ complex by the appearance of a strong molecular ion cluster centred at *m/z* 187. The molecular ion cluster centred at *m/z* 307 was expected for the $[Cd\mathbf{6}]^{2+}$ complex. Instead, a strong molecular ion cluster centred at *m/z* 373 was observed in the ESI-MS spectrum, consistent with the formation of the $[Cd\mathbf{6}]^{2+}\cdot 4MeOH$ complex.

Competitive ESI-MS experiments were performed on solutions containing either ligand **5** or **6** with an excess of cadmium(II) and silver(I) ions. Under the conditions of our ESI-MS study, the formation of the $[Ag\mathbf{5}]^{+}$ complex was favoured over that of the $[Cd\mathbf{5}]^{2+}$ complex. This result confirms that ligand **5** is more selective toward silver(I) ions over cadmium(II) ions in the gas phase. Alternatively, the ESI-MS spectrum recorded for ligand **6** showed the exclusive formation of a cadmium(II)-complex, with no evidence for the formation of any silver(I) species. As described above, the expected molecular ion cluster for the $[Cd\mathbf{6}]^{2+}$ complex (centred at *m/z* 307) was not observed, but a strong molecular ion cluster centred at *m/z* 373 exhibits the characteristic isotopic distribution pattern that is indicative of cadmium.[203] This signal was attributed to the $[Cd\mathbf{6}]^{2+}\cdot 4MeOH$ species.

In chapter 3, solution studies were unable to confirm whether ligand **6** formed a more stable complex with lead(II) or cadmium(II) ions in DMF solution. The competitive ESI-MS spectrum (Figure 4.5) showed the presence of a strong cluster of signals centred at *m/z* 373, assigned to the $[Cd\mathbf{6}]^{2+}\cdot 4MeOH$ complex on the basis of characteristic isotopic

distribution pattern that is indicative of cadmium. A minor signal was also observed *m/z* 356, indicative of the $[Cd\mathbf{6}]^{2+}\cdot 3MeOH$ complex. The ESI-MS experiment did not provide any evidence of a $[Pb\mathbf{6}]^{2+}$. This competitive experiment clearly demonstrates that under the gas phase conditions employed for this study, ligand **6** is highly selective for cadmium(II) ions over lead(II) ions.

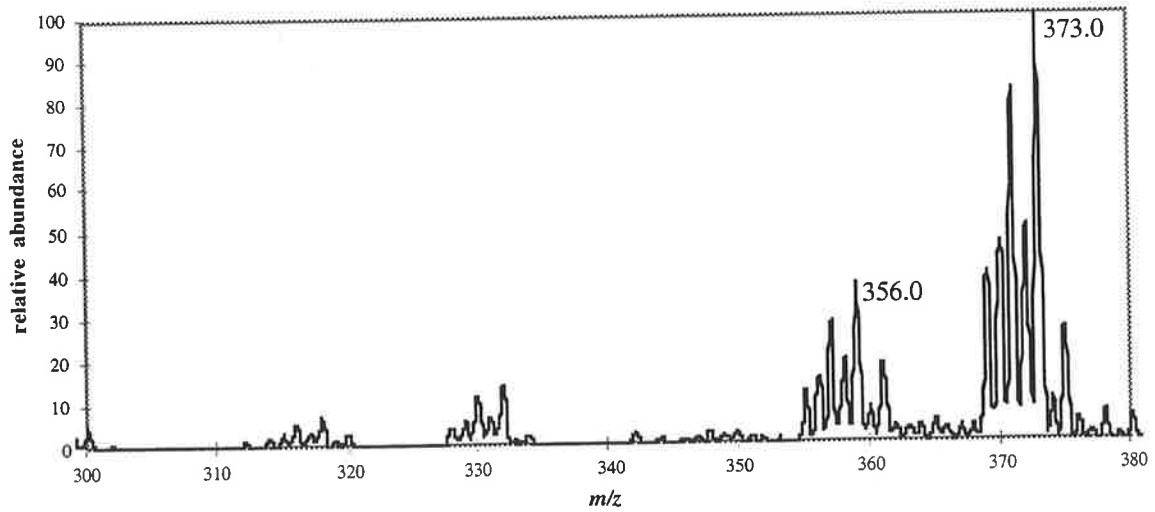

Figure 4.5 *ESI-MS of the $[Cd\mathbf{6}]^{2+}\cdot 4MeOH$ and $[Cd\mathbf{6}]^{2+}\cdot 3MeOH$ complexes at m/z 373 and 356, respectively, in methanol solution.*

None of the remaining sample solutions that were analysed by ESI-MS exhibited positive ion signals that were representative of a 1:1 metal-ligand complex, i.e. those solutions containing ligands **1**, **3**, **4** and **5** with lead(II) ions; ligands **1** - **6** with zinc(II) ions; and ligands **1** - **4** with cadmium(II) ions. It is possible that, under the conditions implemented in our study, the metal complexes may have formed in the gas phase but they were too unstable to be detected by ESI-MS methods. This phenomenon has been described previously by other workers who have probed the interactions of macrocyclic ligands with metal ions by means of mass spectrometric methods.[188,204]

The ESI-MS experiments suggest that ligands **3** and **4** have a low affinity for lead(II) and cadmium(II) in the gas phase. In contrast, ligands **5** and **6** formed stable complexes of cadmium(II) and, for the latter, lead(II). These results demonstrate that the steric effects and rigidity imposed by the aromatic groups within the ring systems of ligands **3** and **4** clearly diminish their complexation behaviour.[98,100,102] Furthermore, the reduced Lewis

basicity of the ring oxygen atoms, as a result of the adjacent aromatic groups, would contribute to the low stability of the complexes.[69] These factors appear to outweigh any stabilizing complexation effects of the pendant donor arms of ligand **4** (*cf.* ligand **6**).

In some cases, the expected metal complex was not detected and alternative complexation behaviour was observed. These results are summarized as follows.

In the ESI-MS spectrum of a solution of ligand **5** with lead(II) ions, a strong signal at *m/z* 285 was observed and is representative of the $[Na\mathbf{5}]^+$ complex. The precise origin of the sodium(I) ions is not clear. Since the ligand concentrations employed for ESI-MS analyses are very low ($\leq 10^{-6}$ M), the presence of sodium(I) as a laboratory contaminant may explain the formation of the $[Na\mathbf{5}]^+$ complex in solution.

Solutions of ligands **1** and **6** with zinc(II) ions gave rise to strong signals in the ESI-MS spectrum, at *m/z* 483 and *m/z* 503, corresponding to the protonated species $[H\mathbf{1}]^+$ and $[H\mathbf{6}]^+$, respectively. Furthermore, the ESI-MS spectrum of ligand **6** with zinc(II) ions showed a strong signal at *m/z* 525, corresponding to the $[Na\mathbf{6}]^+$ complex. When ligands **1** and **3** were assessed for their binding affinity toward cadmium(II) ions, strong signals were observed at *m/z* 483 and *m/z* 359, corresponding to the protonated species $[H\mathbf{1}]^+$ and $[H\mathbf{3}]^+$, respectively.

4.3 Gas phase versus solution phase studies

Some trends are evident if one compares the results of the ESI-MS analysis to those obtained for the related interactions in the solution phase (Chapter 3). All ligands that were studied in Chapter 3, i.e. **1**, **2**, **5** and **6**, formed relatively stable complexes with silver(I) ions in DMF solution (Table 3.5). Under ESI-MS conditions, ligands **1 - 6** were all found to interact strongly with silver(I) ions, a result which is consistent with the appearance of strong signals that are assigned to the silver(I) complexes (Table 4.1).

Stability constants were determined for the interaction of ligands **1**, **2**, **5** and **6** with lead(II) in DMF solution (Table 3.5). ESI-MS studies of these interactions confirmed the

formation of the $[Pb\mathbf{2}]^{2+}$ and $[Pb\mathbf{6}]^{2+}$ complexes in the gas phase. A competitive ESI-MS experiment clearly showed that the signal representing the $[Pb\mathbf{6}]^{2+}$ complex occurred with a higher relative intensity than that of the $[Pb\mathbf{2}]^{2+}$ complex. Thus, ESI-MS showed that ligand **6** has a higher stability with lead(II) than ligand **2**; a result that is in agreement with that observed in the solution studies. The inability to detect the $[Pb\mathbf{5}]^{2+}$ complex by ESI-MS was rather surprising when one considers the high stability observed for this complex in solution phase.

Solution studies demonstrated that ligands **5** and **6** produced relatively stable complexes with cadmium(II) ions (Table 3.5). These results were further confirmed by the appearance of the ESI-MS signals corresponding to the $[Cd\mathbf{5}]^{2+}$ and $[Cd\mathbf{6}]^{2+}\cdot 4MeOH$ complexes (Table 4.1). Competitive ESI-MS experiments demonstrated that the $[Ag\mathbf{5}]^{+}$ complex was formed with a higher stability than the $[Cd\mathbf{5}]^{2+}$ complex, a phenomenon that was also observed in DMF solution (Chapter 3). The formation of the $[Cd\mathbf{6}]^{2+}\cdot 4MeOH$ complex is clearly favoured over that of the $[Ag\mathbf{6}]^{+}$ species. Even though solution studies were primarily concerned with the stability of the $[Cd\mathbf{6}]^{2+}$ complex in DMF solution, the strong selectivity exhibited by ligand **6** toward cadmium(II) ions in the presence of silver(I) ions is clearly demonstrated in both the solution and gas phase.

ESI-MS proved to be a viable method for addressing a particular discrepancy that was encountered in our solution studies. Even though solution studies showed that ligand **6** formed highly stable complexes with lead(II) and cadmium(II) ions, its selectivity toward these metal ions could not be determined (Chapter 3). A competitive ESI-MS experiment demonstrated that ligand **6** was highly selective toward cadmium(II) ions over lead(II) ions in the gas phase, as confirmed by the formation of the $[Cd\mathbf{6}]^{2+}\cdot 4MeOH$ complex. Indeed, no evidence for a lead(II) complex of ligand **6** was observed in this ESI-MS competitive experiment.

Solution studies confirmed the very low stabilities of the $[Pb\mathbf{1}]^{2+}$, $[Zn\mathbf{2}]^{2+}$ and $[Cd\mathbf{2}]^{2+}$ complexes (Table 3.5). As expected, none of these complexes were observed under ESI-MS conditions. However, detection of the $[Pb\mathbf{2}]^{2+}$ complex by ESI-MS methods was

rather surprising as it possesses a low stability (log $K_s = 2.38 \pm 0.21$) in DMF solution. It is clear that the $[Pb\mathbf{2}]^{2+}$ species must be sufficiently stable in the gas phase for it to be detected by the mass analyser. Indeed, the absence of solvent would probably enhance the metal-ligand interaction in this complex to some degree.

4.4 *Ab initio* calculations

Electronic structure theory is a broad area within computational chemistry that is devoted to the structure of molecules and their reactivity.[205] Electronic structure methods use the theory of quantum mechanics as the basis for computations. Quantum mechanics states that the energy and other related properties of an atom or molecule may be obtained by solving the differential equation formulated by Schrödinger in the 1920's,

$$\mathbf{H}\Psi = E\Psi$$

where **H** is termed the Hamiltonian operator, E is the energy of the system, and Ψ is a wavefunction of the positions and momenta of all the particles.

The Schrödinger equation can be solved exactly for the hydrogen atom. Exact solutions to the Schrödinger equation for many-electron atoms and molecules (i.e. anything but the most trivial one-electron molecular system) are not possible. By implementation of a number of simplifying mathematical assumptions and procedures, however, electronic structure methods are able to offer an approximate solution of the Schrödinger equation for a large range of atoms and molecules.

Ab initio methods are a major class of electronic structure methods that use no empirical parameters in their computations other than physical constants, e.g. the speed of light, Planck's constant, and the masses and charges of electrons and nuclei.[205] Using these parameters, and a series of mathematical approximations, *ab initio* methods compute approximate solutions to the Schrödinger equation for a particular atom or molecule. In our study, the Gaussian 94[206] suite of programs approximates the atomic and molecular orbitals by implementation of the well-established Hartree-Fock method.[205,207,208]

Gaussian 94 is particularly useful for predicting the equilibrium structures of metal complexes such as those investigated in this work by the use of geometry optimization algorithms utilizing the LANL2DZ basis set. A basis set is the mathematical description of the molecular orbitals within a system, which combines to approximate the total electronic wavefunction used to perform the theoretical calculation.[205] Larger basis sets are better suited to approximate exact molecular orbitals as they impose fewer restrictions on the locations of the electron; an important consideration since the essence of the quantum mechanical picture of the atom is that electrons have a finite probability of existing in a certain region of space at any one time. A larger basis set is also desired for more accurate approximations of the atomic and molecular orbitals of larger atoms (i.e. post-Third Row atoms) and molecules, respectively.

The large LANL2DZ basis set implemented in our study requires considerably more computational resources than some of the simpler basis sets that are normally available to the computational chemist. Moreover, it offers the potential for more accurate estimations of the molecular orbitals of those molecules containing heavy atoms that are of relevance to our study. The LANL2DZ basis set includes effective core potential (ECP) approximations for the inner core electrons of large atoms. An ECP approximation is a means of treating valence electrons in a different manner to those lying closer to the nucleus of the atom. This is particularly important when one considers the relativistic effects associated with the core electrons.[205]

It is accepted that limitations do exist when applying computational methods for molecular modelling, particularly when applying high level *ab initio* theory. *Ab initio* methods have not always been particularly successful in representing equilibrium geometries of a number of molecules that incorporate transition and post-transition metals.[209] It has been shown that some discrepancies can appear due to limitations in either the Hartree-Fock approximation model or in the basis set used for calculations involving large metal ions.[209] Since this work is concerned with the gas phase interactions of macrocyclic ligands with

large metal ions, such as lead(II) and cadmium(II), limitations that exist in *ab initio* models with metal ions of high atomic number must be taken into consideration.

4.4.1 Results and Discussion

Complementary *ab initio* calculations were performed on the free ligands and the corresponding metal complexes that were observed by ESI-MS. The optimized structures of the free ligands **1 - 6** are shown in Figures 4.6 - 4.11, respectively. The optimized conformations of the free ligands confirm the flexible nature of these types of macrocyclic ligand systems.

In the gas phase, ligand **1** is shown to possess a boat-type conformation with the both the aromatic rings folded back toward each other (Figure 4.6). The nitrogen donor atoms point directly into the macrocyclic cavity, and are thus poised for an interaction with a metal ion. The oxygen donor atoms appear to be directed out of the ring cavity. The molecular structure of **1** (Appendix A), as determined by X-ray diffraction methods, clearly shows that the ligand possesses a chair-like conformation in the solid state. The two pyridyl rings occupy the same plane with a centre of inversion about a C_2 axis. Since there are no close intermolecular interactions observed in the solid state structure of **1**, the conformational differences between the gas phase and solid state geometries of the ligand may be attributed to crystal packing effects in the latter.

The optimized structure of ligand **2** (Figure 4.7) clearly shows that the four sulfur donor atoms are directed out of macrocyclic ring cavity. This conformation is reminiscent of related macrocyclic ligands which contain two-to-four sulfur atoms that are also directed out of the macrocyclic ring cavity.[183,184]

The dibenzo-diaza-18-crown-6 ligand **3** occupies a typical conformation exhibited by many of the simpler macrocyclic crown ethers (Figure 4.8). The nitrogen and oxygen donor atoms appear to occupy the same plane. Even though the oxygen atoms are positioned for coordination to the metal ion, the lone pairs of the nitrogen donor atoms are directed out of the macrocyclic cavity.

A comparison of the optimized structure of ligand **4** (Figure 4.9) to that obtained for ligand **3** (Figure 4.4) clearly shows the effect of the large pendant donor arms on the macrocyclic ring system. The pendant arms cause the two aromatic moieties of the ring structure to be folded back toward each other, resulting in a boat-like conformation for the ligand.

Ligand **5** is the least hindered of the macrocyclic ligands studied in this work. The optimized structure of **5** shows that the six donor atoms are not present in the same plane (Figure 4.10). The lone pair of electrons of each nitrogen atom is directed out of the macrocyclic cavity and thus, is considered to be inappropriately positioned for coordination to a metal ion.

The optimized structure of ligand **6** is presented in Figure 4.11. The steric strain and rigidity imparted onto the diaza-18-crown-6 ring system by the presence of the large pendant donor arms are clearly observed. The oxygen and nitrogen donor atoms of the ring no longer appear in the same plane, as observed for the parent crown ether. However, the side view of the molecule shows that the molecule distorts until the two aromatic rings become co-planar. The hydroxyl groups of the pendant arms lie directly above the ring structure, with one of the groups suitably positioned for subsequent 'capping' of the metal ion.

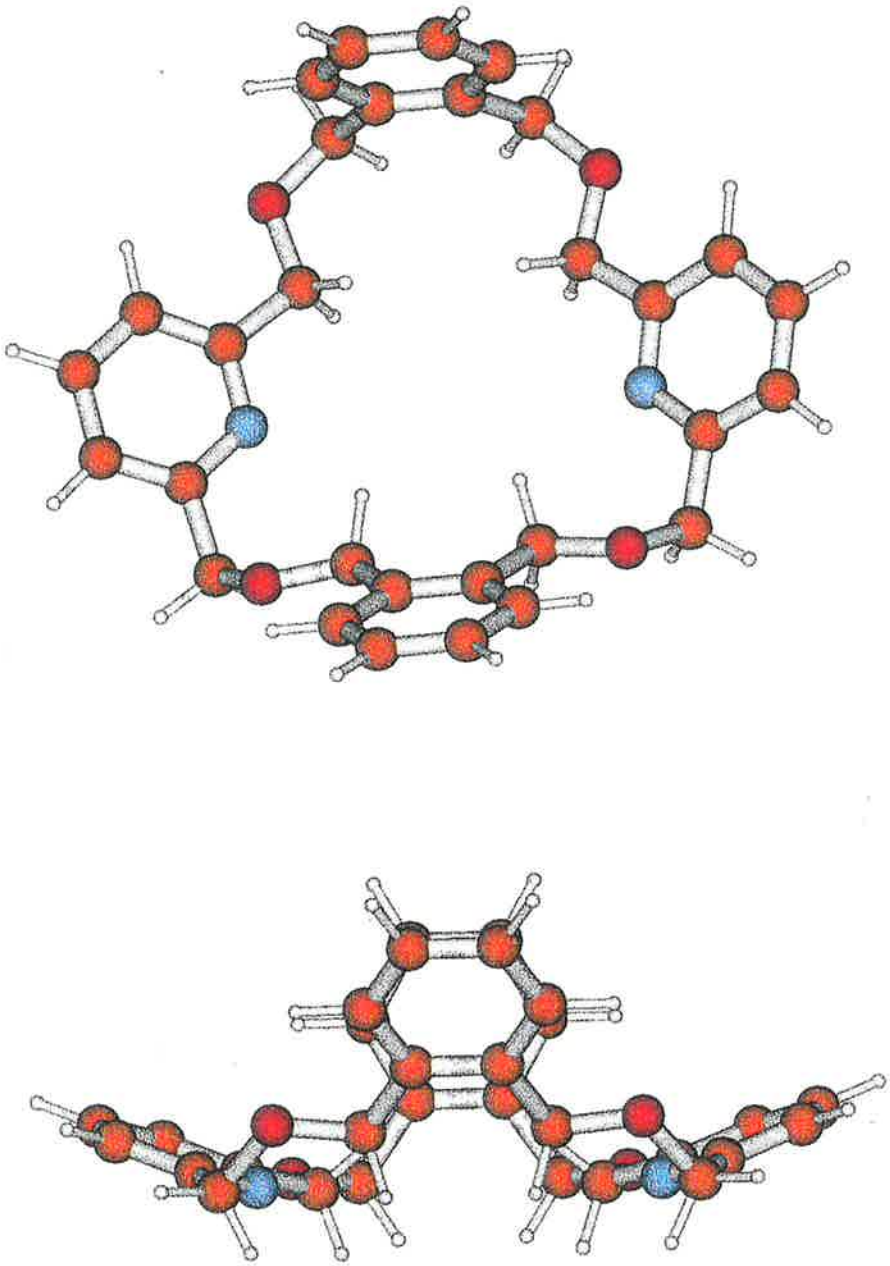

Figure 4.6 *Optimized gas phase geometry of ligand* ***1*** *as it appears in plan view (top) and in side view (bottom). (Blue = nitrogen; red = oxygen; orange = carbon; white = hydrogen).*

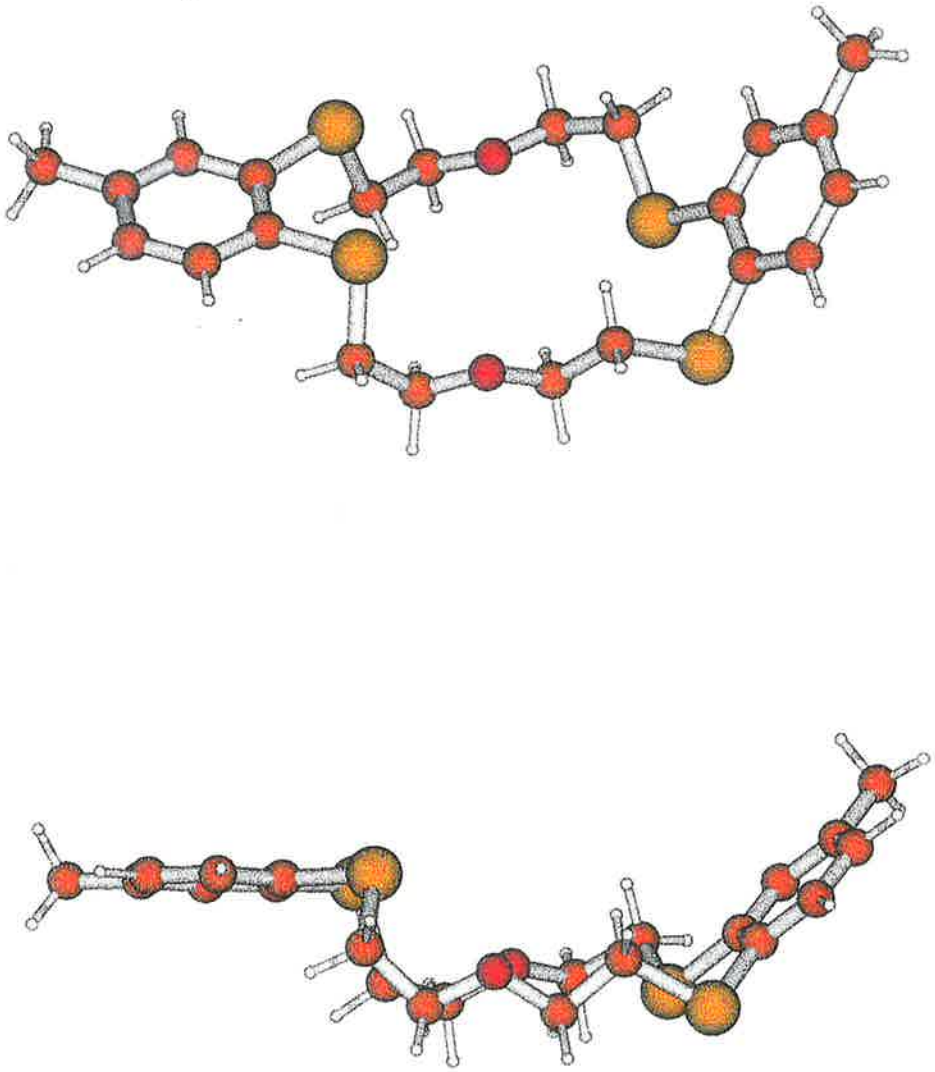

Figure 4.7 *Optimized gas phase geometry of ligand* **2** *as it appears in plan view (top) and in side view (bottom). (Yellow = sulfur; red = oxygen; orange = carbon; white = hydrogen).*

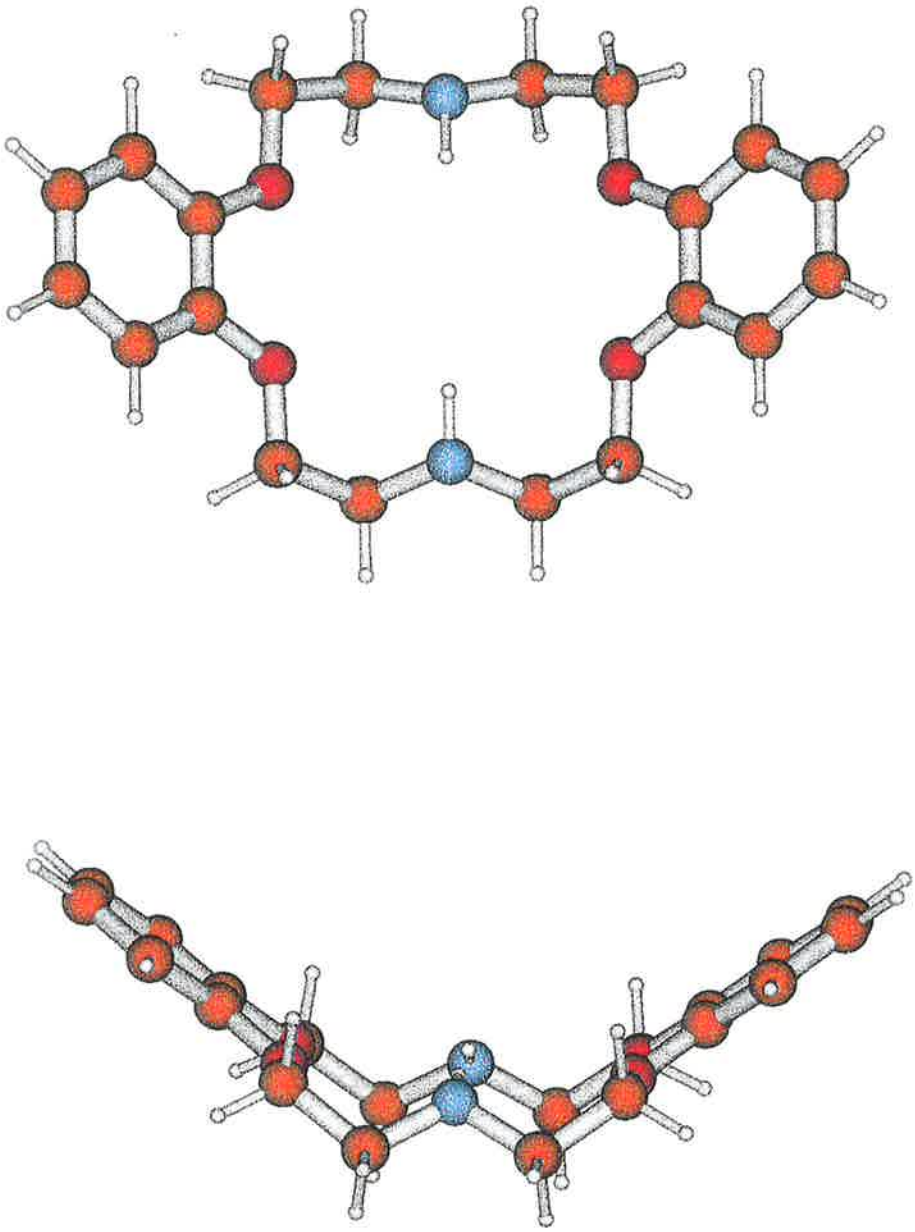

Figure 4.8 *Optimized gas phase geometry of ligand* **3** *as it appears in plan view (top) and in side view (bottom). (Blue = nitrogen; red = oxygen; orange = carbon; white = hydrogen).*

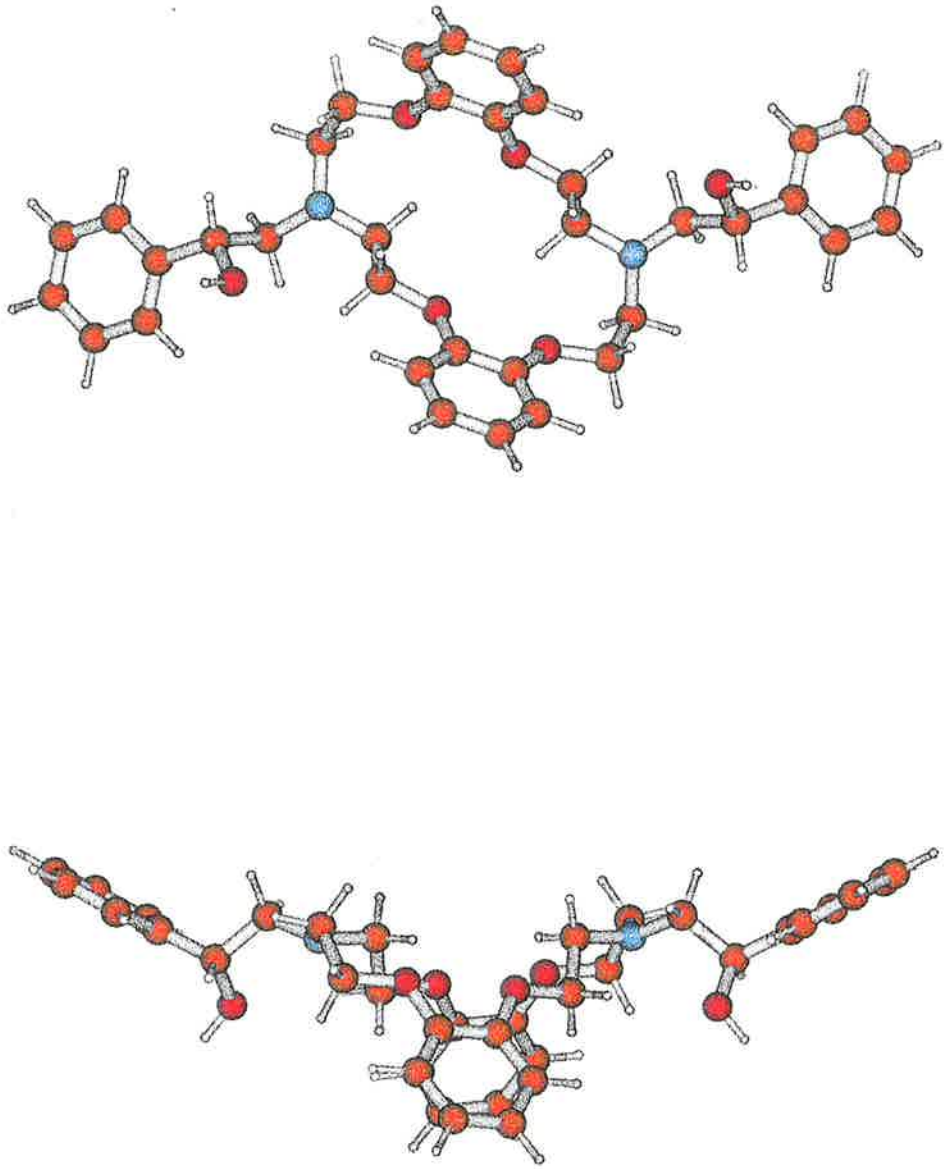

Figure 4.9 *Optimized gas phase geometry of ligand* ***4*** *as it appears in plan view (top) and in side view (bottom). (Blue = nitrogen; red = oxygen; orange = carbon; white = hydrogen).*

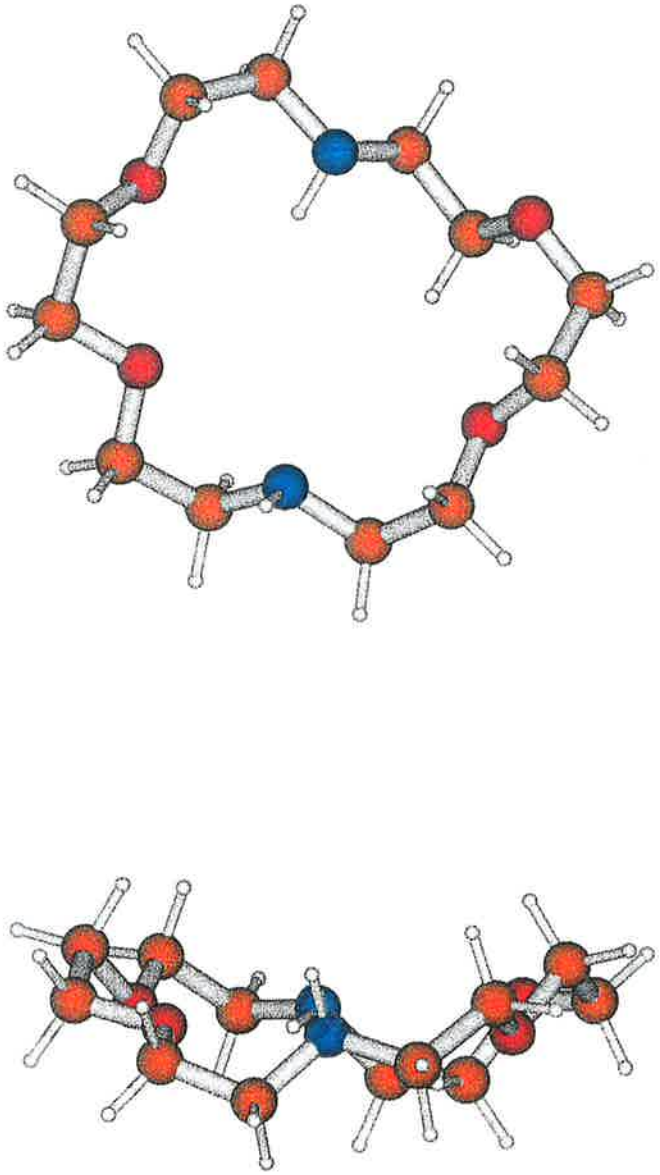

Figure 4.10 *Optimized gas phase geometry of ligand* **5** *as it appears in plan view (top) and in side view (bottom). (Blue = nitrogen; red = oxygen; orange = carbon; white = hydrogen).*

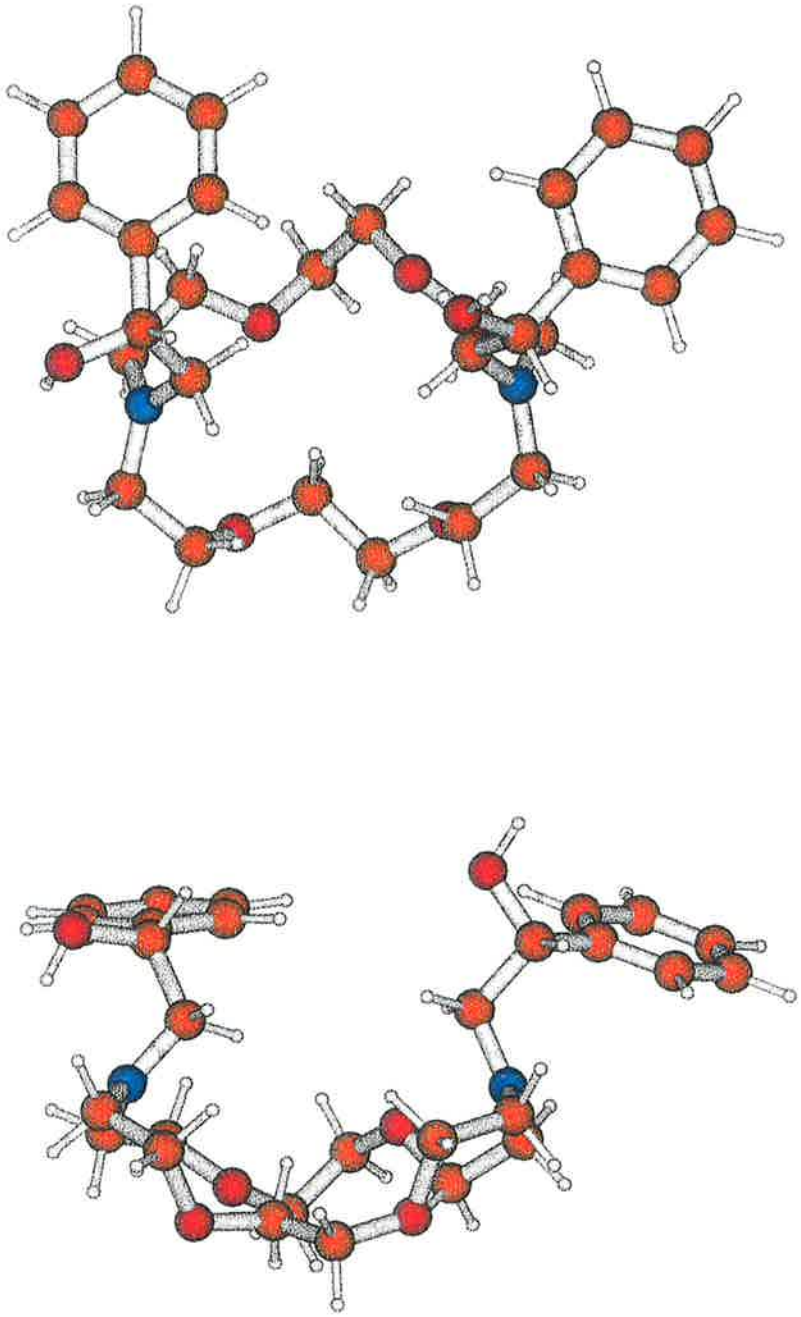

Figure 4.11 *Optimized gas phase geometry of ligand* ***6*** *as it appears in plan view (top) and in side view (bottom). (Blue = nitrogen; red = oxygen; orange = carbon; white = hydrogen).*

The optimized structures of the corresponding silver(I) complexes of ligands **1-6** are shown in Figures 4.12 - 4.17, respectively. It is apparent from these studies that, when compared to reported crystallographic data, *ab initio* calculations tend to elongate bond lengths between the metal ion and the ligand donor atoms. This may be due to a combination of effects including the limitations associated with the LANL2DZ basis set and the various approximations that are implemented in *ab initio* methods.[205,209] Other differences when one compares gas and solid phase metal-ligand interactions, e.g. crystal packing effects in the latter, should also be considered.

The calculated gas phase structure of $[Ag\mathbf{1}]^+$ is presented in Figure 4.12. Our results demonstrate that, in the gas phase, the silver(I) ion is surrounded by two mutually *trans* pyridyl nitrogen and ether oxygen atoms; the two remaining oxygen atoms are clearly directed out of the ring system and are too far removed for any interaction with the silver(I) ion. The average metal-ligand bond distances in the gas phase (d(Ag-O) = 2.56 Å; d(Ag-N) = 2.52 Å) are greater than the sum of the covalent radii of the atoms,[210,211] but the orientation of the donor atoms (two nitrogen and two oxygen) suggests that some weak interaction exists with the metal ion. The change in ligand conformation as one moves from the free ligand (Figure 4.6) to the silver(I) complex (Figure 4.12) shows that the boat conformation of the free ligand is significantly disrupted in the complex. The aryl rings remain almost parallel to each other regardless of the interaction with the metal ion.

The optimized structure of the $[Ag\mathbf{2}]^+$ complex appears in Figure 4.13. Despite the soft base nature of the sulfur atoms, little covalent interaction was observed between these donor atoms and the soft acid silver(I) ion. If one considers the average bond lengths observed between the silver(I) ion and the sulfur atoms (d(Ag-S) = 3.41 Å), and compares these distances to those calculated by using the sum of the covalent radii for each atom (d(Ag-S) = 2.54 Å),[210,211] it is clear that the donor atoms are too far away from the metal ion for any significant interaction to be observed. Indeed, if one compares the optimized geometry of the $[Ag\mathbf{2}]^+$ complex (Figure 4.13) to that of the free ligand (Figure 4.7), it is clear that very few conformational changes occur on metal binding, particularly with

respect to the orientation of the sulfur donor atoms, even in the presence of the silver(I) ion. The two oxygen donor atoms surround the silver(I) ion in a *trans* arrangement and appear to be favourably situated for interaction. The average bond lengths for the silver(I)-oxygen interactions in the gas phase (d(Ag-O) = 2.70 Å) were found to be greater than those determined by calculating the sum of the covalent radii of the atoms (d(Ag-O) = 2.20 Å).[210,211] It is postulated, therefore, that the ether oxygen atoms of ligand **2**, like other crown ethers, are weakly interacting with the silver(I) ion in a pseudo-linear arrangement. The average bond lengths for the silver(I)-oxygen and -nitrogen interactions in the gas phase were found to be longer than those determined crystallographically, namely (d(Ag-O) = 2.58 Å) and (d(Ag-S) = 2.54 Å);[212,213] a difference in part attributed to crystal packing effects in the solid state.

Ab initio calculations were performed on the [Ag**3**]$^+$ complex to afford its optimized structure presented in Figure 4.14. The silver(I) ion appears to rest in the centre of the macrocyclic cavity, resulting in significant distortion to the boat conformation of the free ligand **3** (Figure 4.8). The silver(I)-ligand interactions appear to be weak due to the large differences observed in the average silver(I)-oxygen and -nitrogen bond lengths (namely, d(Ag-O) = 2.59 Å; d(Ag-N) = 2.58 Å) when compared to the those calculated using the sum of the covalent radii of the individual atoms (d(Ag-O) = 2.20 Å; d(Ag-N) = 2.24 Å).[210,211] In this case, the silver(I)-oxygen bond lengths calculated in the gas phase (2.59 Å) appear to be in close agreement with those determined from crystallographic data (2.58 Å).[212,213]

The optimized structure of the [Ag**4**]$^+$ complex, as determined by *ab initio* methods, appears in Figure 4.15. The interactions observed between the silver(I) ion and the oxygen donor atoms (i.e. all four of the ether oxygen atoms and one of the oxygen atoms present on the pendant arm) appear to be primarily electrostatic in nature. Even though the average bond length for the silver(I)-oxygen interaction (d(Ag-O) = 2.55 Å) was found to be close to that determined crystallographically for a silver(I)-crown ether interaction (d(Ag-O) = 2.58 Å),[212,213] it was still found to be significantly longer than the sum of the

covalent radii of the two atoms (d(Ag-O) = 2.20 Å).[210,211] This result confirms that five of the six available oxygen atoms of ligand **4** are weakly coordinated to the silver(I) ion. Similarly, the distance between the silver(I) atom and the closest nitrogen atom was found to be equal to 2.68 Å and, at best, a weak electrostatic interaction between these atoms may be occurring. The remaining nitrogen atom and pendant arm oxygen atom are clearly too far removed for any significant interaction to occur with the silver(I) ion. The incorporation of the silver(I) ion into the macrocyclic cavity readily distorts the crown ether system away from the boat conformation exhibited by the free ligand (Figure 4.9).

The optimized structure of the silver(I) complex of the diaza-18-crown-6 ligand **5** is presented in Figure 4.16. The nitrogen donor atoms of the complex remain in similar positions to those observed for the free ligand **5** (Figure 4.10). It is apparent that the nitrogen atoms, with the lone pair of electrons directed out of the macrocyclic cavity, are not positioned appropriately for interaction with the silver(I) ion. Three of the oxygen and one of the nitrogen atoms do appear to be oriented appropriately for an electrostatic interaction with the metal ion.

The optimized structure of the [Ag**6**]$^+$ complex is presented in Figure 4.17. The incorporation of the silver(I) ion into the macrocyclic cavity appears to cause very little change in the overall conformation of the ligand structure, when compared to that calculated for the free ligand (Figure 4.11). The six ring donor atoms are oriented appropriately for an interaction with the metal ion. In particular, a large change in the orientation of one of the pendant donor arms as one moves from the free ligand to the complex allows for an interaction of one of the nitrogen atoms with the metal ion (d(Ag-N) = 2.52 Å). Neither of the pendant arm oxygen atoms appear to interact with the silver(I) ion in the gas phase.

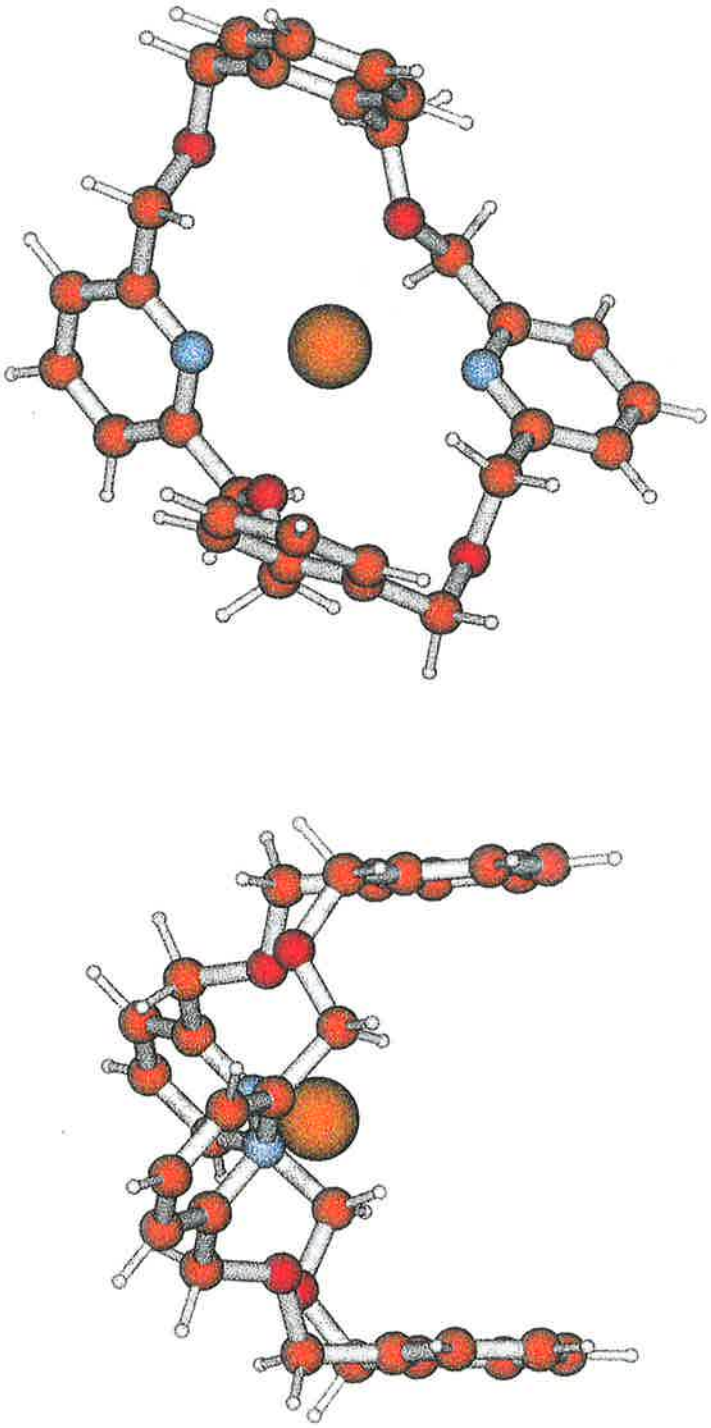

Figure 4.12 *Optimized gas phase geometry of [Ag**1**]$^+$ as it appears in plan view (top) and in side view (bottom). (Blue = nitrogen; red = oxygen; orange = carbon; white = hydrogen. Silver(I) ion appears as a large orange sphere).*

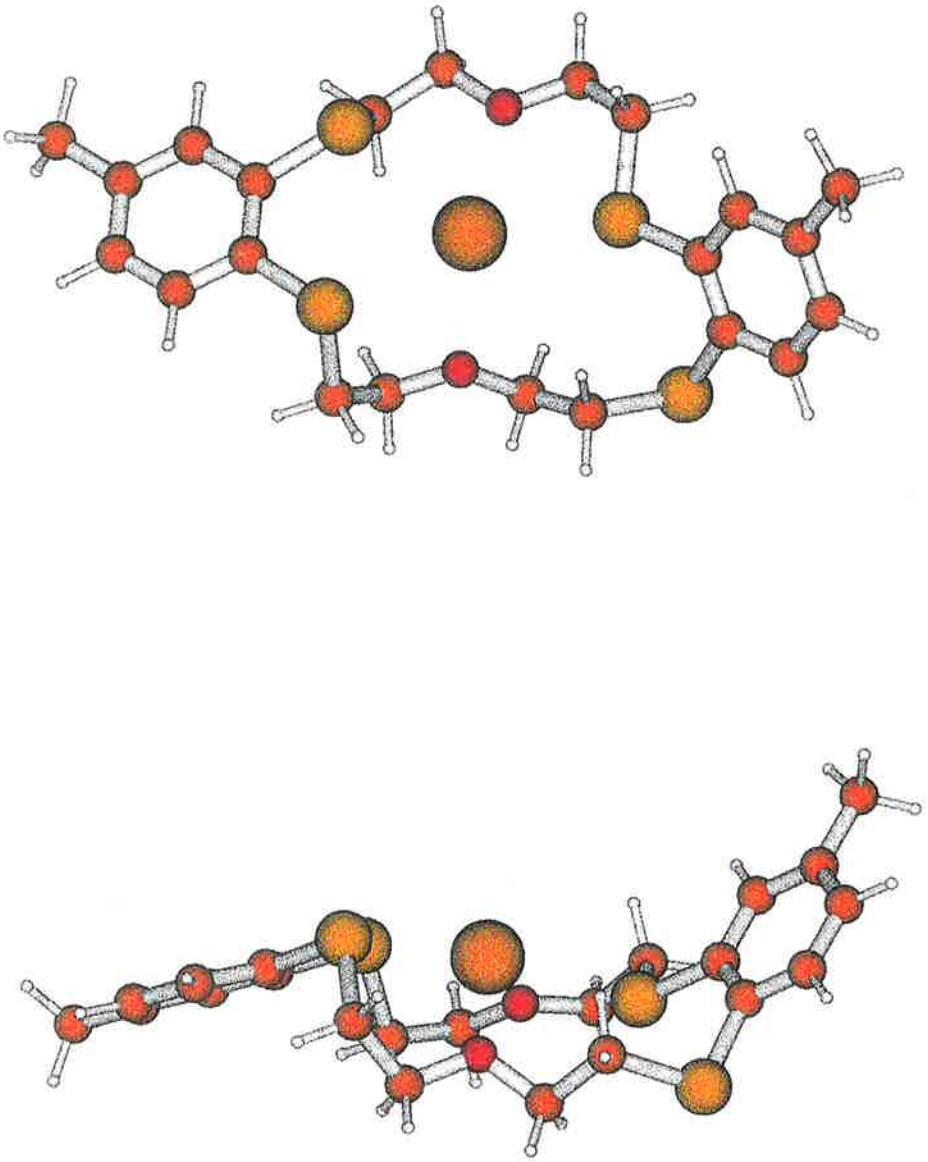

Figure 4.13 *Optimized gas phase geometry of [Ag2]$^+$ as it appears in plan view (top) and in side view (bottom). (Yellow = sulfur; red = oxygen; orange = carbon; white = hydrogen. Silver(I) ion appears as a large orange sphere).*

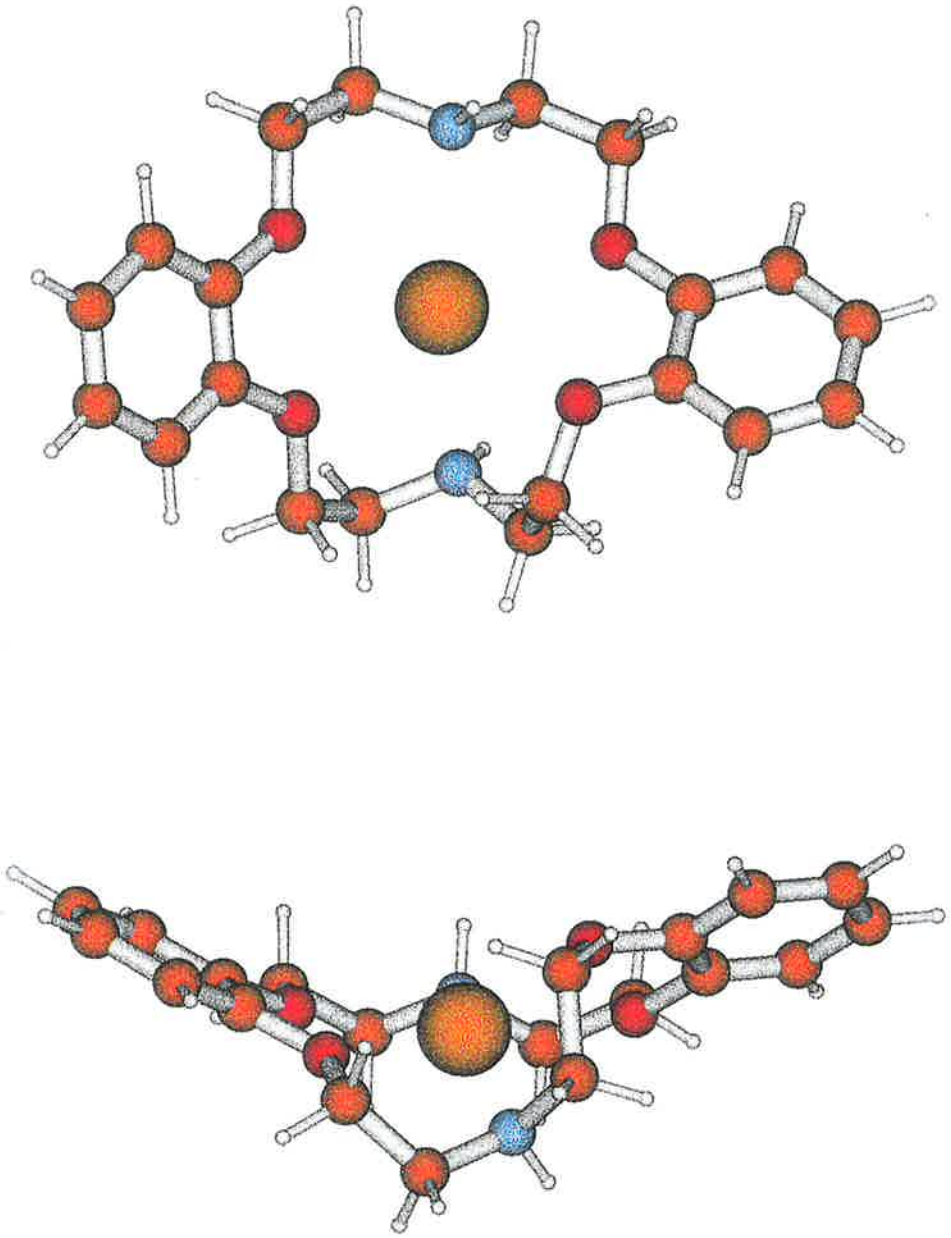

Figure 4.14 *Optimized gas phase geometry of [Ag3]$^+$ as it appears in plan view (top) and in side view (bottom). (Blue = nitrogen; red = oxygen; orange = carbon; white = hydrogen. Silver(I) ion appears as a large orange sphere).*

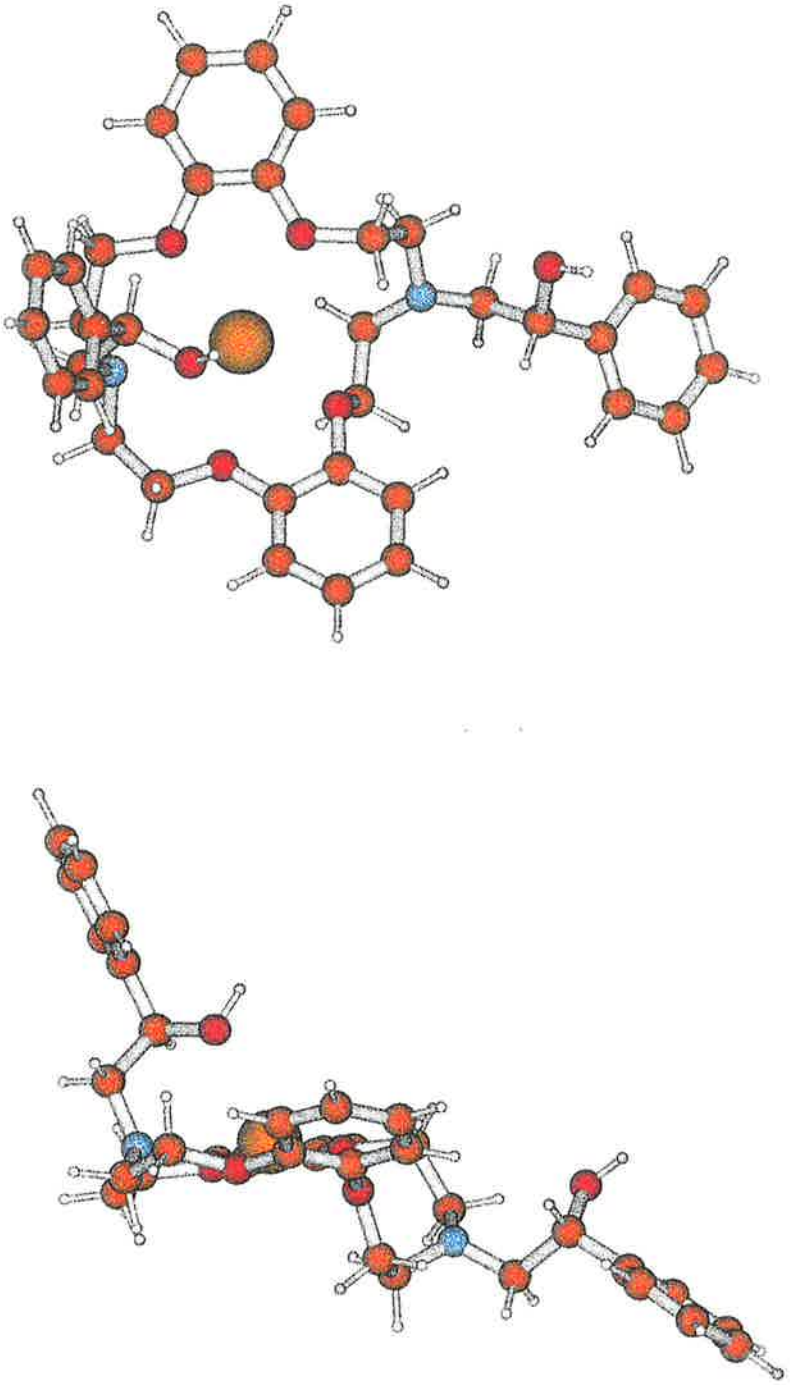

Figure 4.15 *Optimized gas phase geometry of [Ag**4**]$^+$ as it appears in plan view (top) and in side view (bottom). (Blue = nitrogen; red = oxygen; orange = carbon; white = hydrogen. Silver(I) ion appears as a large orange sphere).*

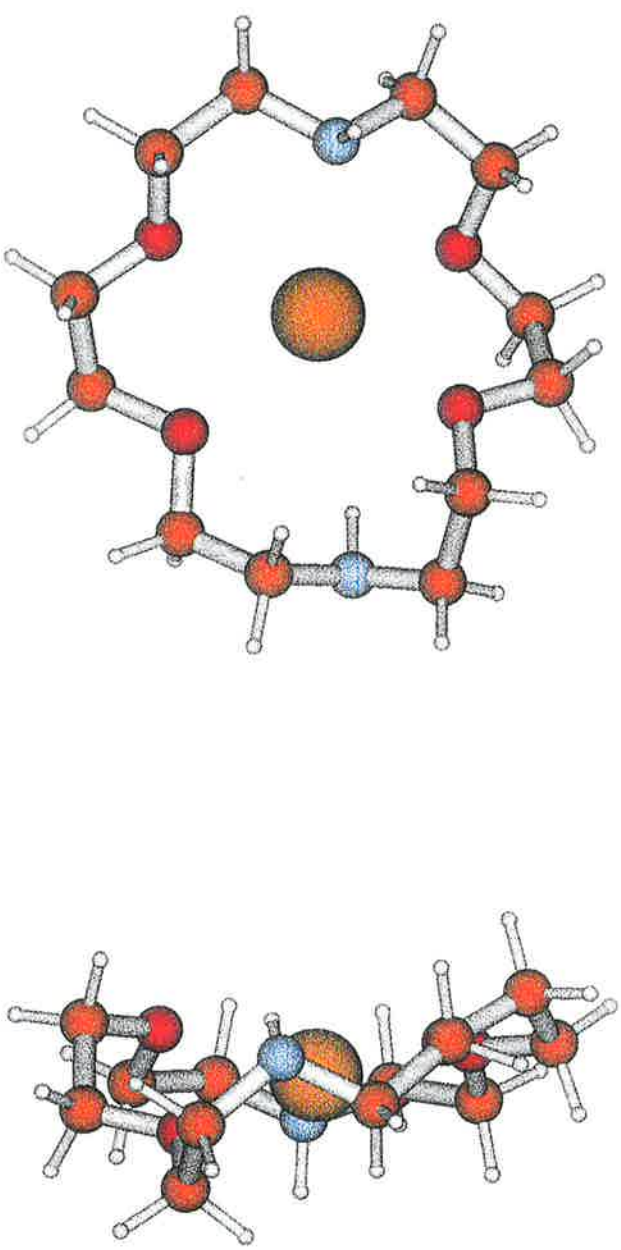

Figure 4.16 *Optimized gas phase geometry of [Ag**5**]$^+$ as it appears in plan view (top) and in side view (bottom). (Blue = nitrogen; red = oxygen; orange = carbon; white = hydrogen. Silver(I) ion appears as a large orange sphere).*

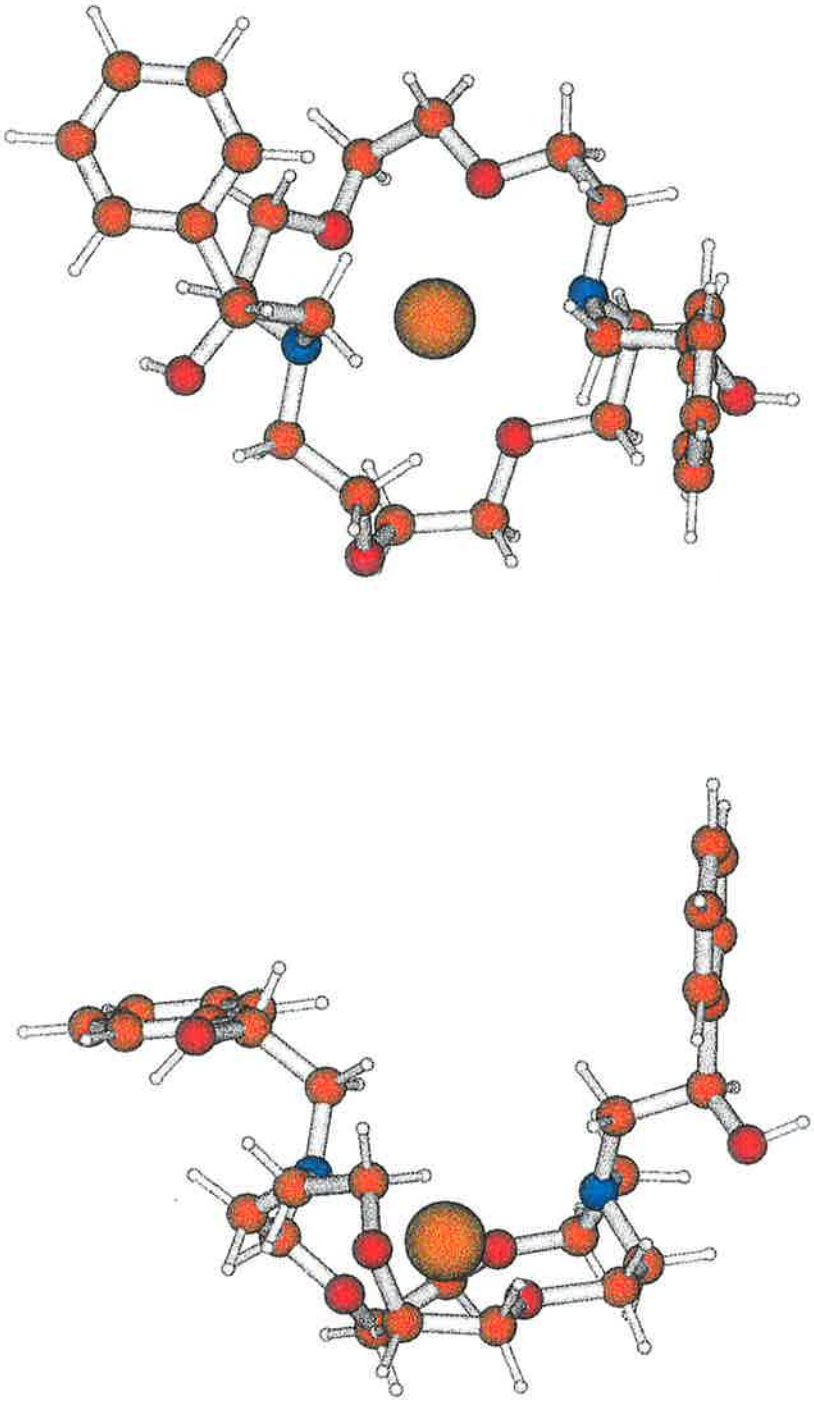

Figure 4.17 *Optimized gas phase geometry of [Ag6]$^+$ as it appears in plan view (top) and in side view (bottom). (Blue = nitrogen; red = oxygen; orange = carbon; white = hydrogen. Silver(I) ion appears as a large orange sphere).*

The optimized structures of the complexes $[Pb\mathbf{2}]^{2+}$ and $[Pb\mathbf{6}]^{2+}$ are presented in Figures 4.18 and 4.19, respectively.

In the $[Pb\mathbf{2}]^{2+}$ complex, little interaction occurs between the lead(II) ion and the sulfur donor atoms of the ring system as the average bond distances for the lead(II)-sulfur interactions were found to be extremely long (d(Pb-S) = 3.10 Å). Since this distance is much greater than the calculated sum of the covalent radii of the two atoms (d(Pb-S) = 2.17 Å),[210,211] it appears that very little interactions exist between metal and the sulfur atoms in the gas phase. Similarly, the average bond lengths for the lead(II)-oxygen interactions (d(Pb-O) = 2.58 Å) are longer than those expected (d(Pb-O) = 2.17 Å),[210,211] suggesting that the interaction between the lead(II) ion and the oxygen atoms are primarily electrostatic. The interaction of the macrocyclic ligand **2** with lead(II) causes significant distortion to the crown ether ring system, when compared to the free ligand (Figure 4.7), with the sulfur atoms directed out of the macrocyclic ring cavity.

The encapsulation of the lead(II) ion by ligand **6** results in a marked distortion of the crown ether ring system (Figure 4.19). Three of the oxygen and one of the nitrogen donor atoms in the ring structure are arranged around the lead(II) ion in a pseudo-tetrahedral geometry. The two remaining ring donor atoms (one oxygen and one nitrogen) are too far away from the metal for any significant covalent bonding interaction (d(Pb-O) = 4.33 Å; d(Pb-N) = 2.64 Å). The optimized structure of $[Pb\mathbf{6}]^{2+}$ (Figure 4.19) shows that the two neutral oxygen donor atoms, present on the pendant donor arms of **6**, are not suitably oriented for coordination to the metal centre. However, it is likely that in solution the pendant arms play an important role in the complexation reaction, as demonstrated by the significant increase in complex stability as one moves from ligand **5** to **6** (Section 3.4.2). There appears to be no evidence for the presence of a stereochemically-active lone pair on the lead(II) ion, although this result would need to be confirmed by X-ray crystallography.[99]

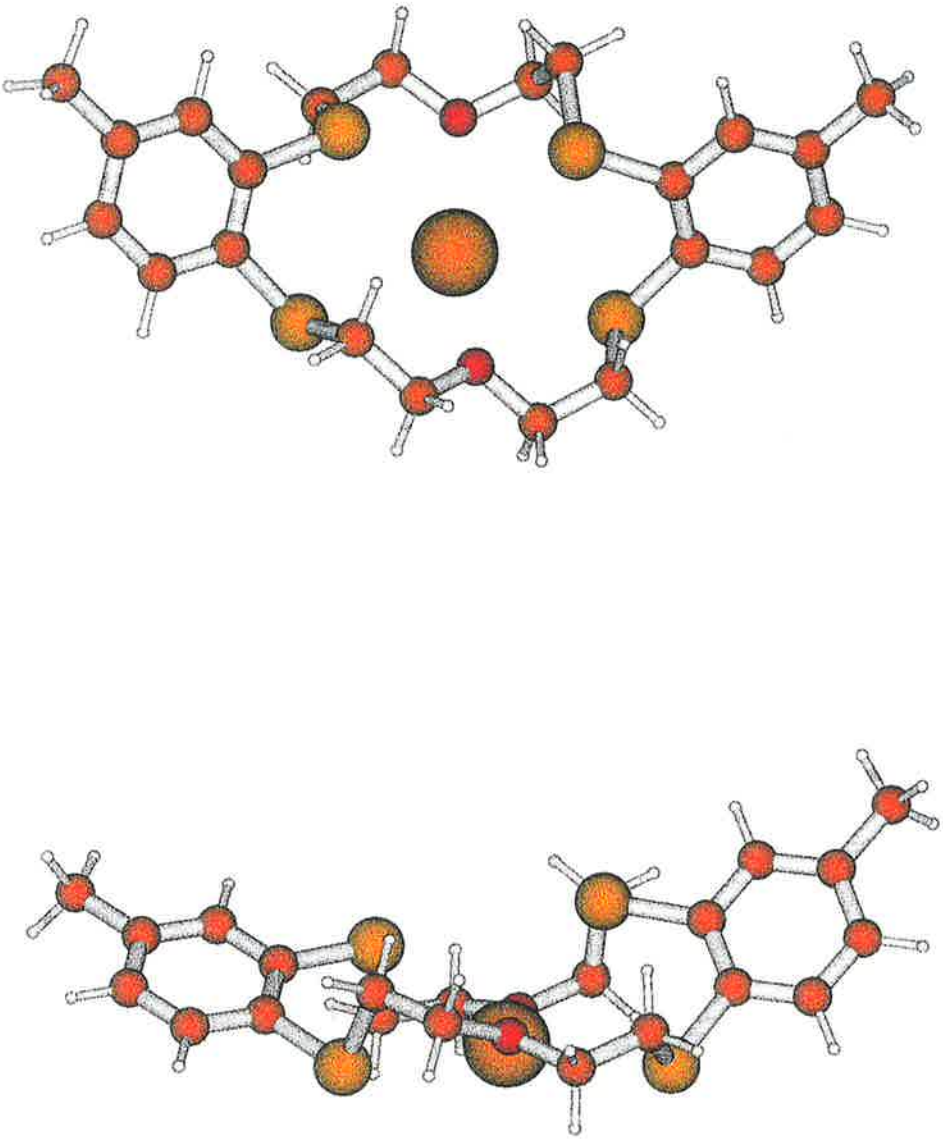

Figure 4.18 *Optimized gas phase geometry of* $[Pb2]^{2+}$ *as it appears in plan view (top) and in side view (bottom). (Yellow = sulfur; red = oxygen; orange = carbon; white = hydrogen. Lead(II) ion appears as a large orange sphere).*

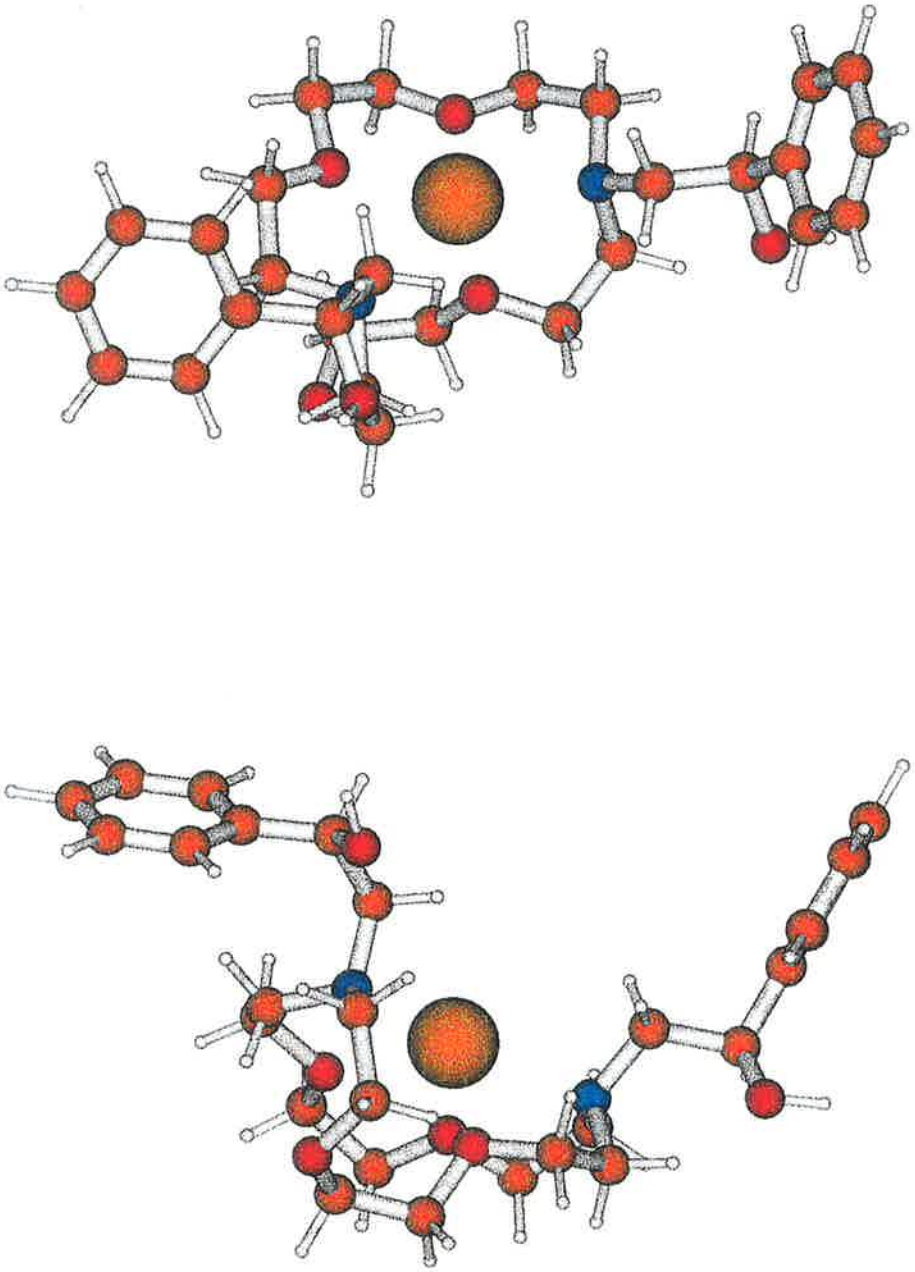

Figure 4.19 *Optimized gas phase geometry of* $[Pb\mathbf{6}]^{2+}$ *as it appears in plan view (top) and in side view (bottom). (Blue = nitrogen; red = oxygen; orange = carbon; white = hydrogen. Lead(II) ion appears as a large orange sphere).*

The optimized gas phase structures of complexes $[Cd\mathbf{5}]^{2+}$ and $[Cd\mathbf{6}]^{2+}$ are presented in Figures 4.20 and 4.21, respectively. In both complexes, the oxygen and nitrogen ring atoms appear to be oriented appropriately for interaction with the cadmium(II) ion. The cadmium(II)-oxygen and -nitrogen bond lengths (($[Cd\mathbf{5}]^{2+}$ d(Cd-O) = 2.37 Å; d(Cd-N) = 2.41 Å), ($[Cd\mathbf{6}]^{2+}$ d(Cd-O) = 2.22 Å; d(Cd-N) = 2.31 Å)) were found to be longer than those calculated by the sum of the covalent radii of the atoms (d(Cd-O) = 2.16 Å; d(Cd-N) = 2.20 Å),[210,211] confirming the electrostatic nature of these interactions in the gas phase. The two additional oxygen atoms that are present in the pendant arms of ligand **6** do not interact with cadmium(II) ion. Indeed, as the ring system closes in around the metal ion, the oxygen donor arms of the pendant arms appear to be pushed further out of the centre of the macrocycle. This distortion is clearly observed by comparing the optimized structure of the free ligand (Figure 4.11) with that of the corresponding cadmium(II) complex (Figure 4.21). However, as found for the complex $[Pb\mathbf{6}]^{2+}$, the increase in stability that is observed as one moves from the $[Cd\mathbf{5}]^{2+}$ to the $[Cd\mathbf{6}]^{2+}$ species clearly demonstrates the importance of these pendant donor arms for complexation in the solution phase (Section 3.4.4).

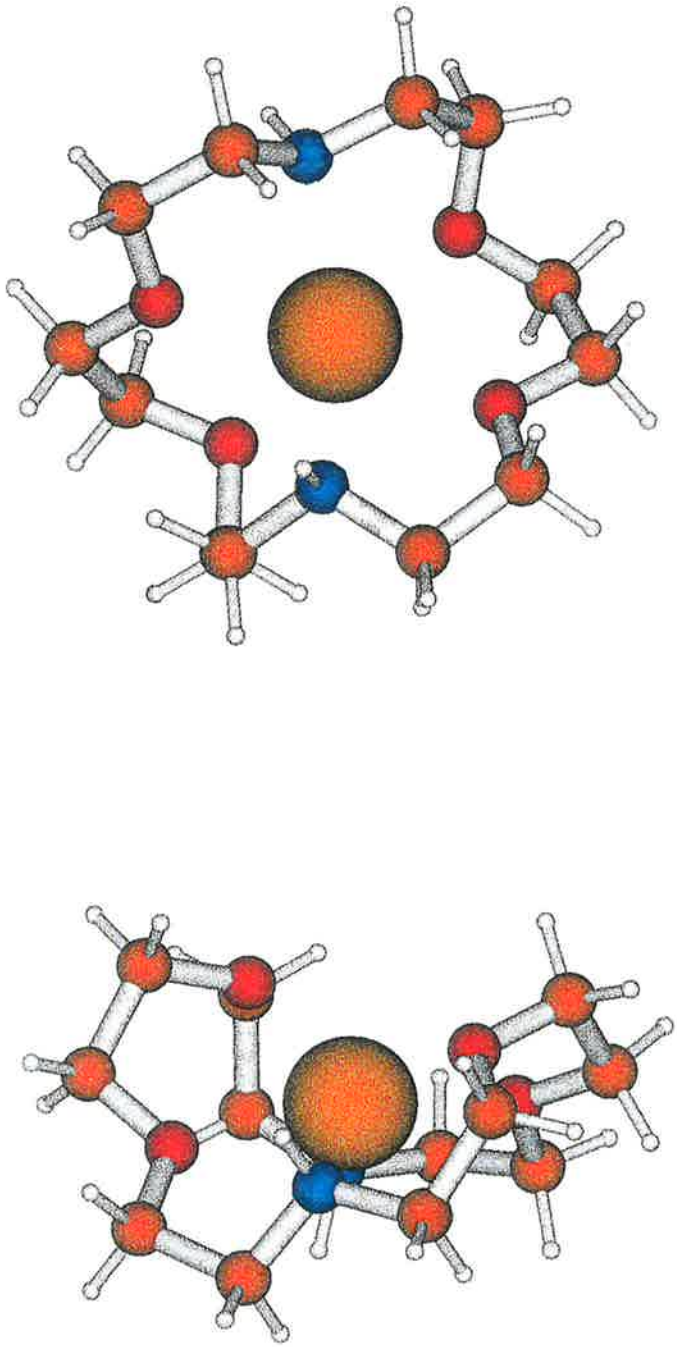

Figure 4.20 *Optimized gas phase geometry of* $[Cd5]^{2+}$ *as it appears in plan view (top) and in side view (bottom). (Blue = nitrogen; red = oxygen; orange = carbon; white = hydrogen. Cadmium (II) ion appears as a large orange sphere).*

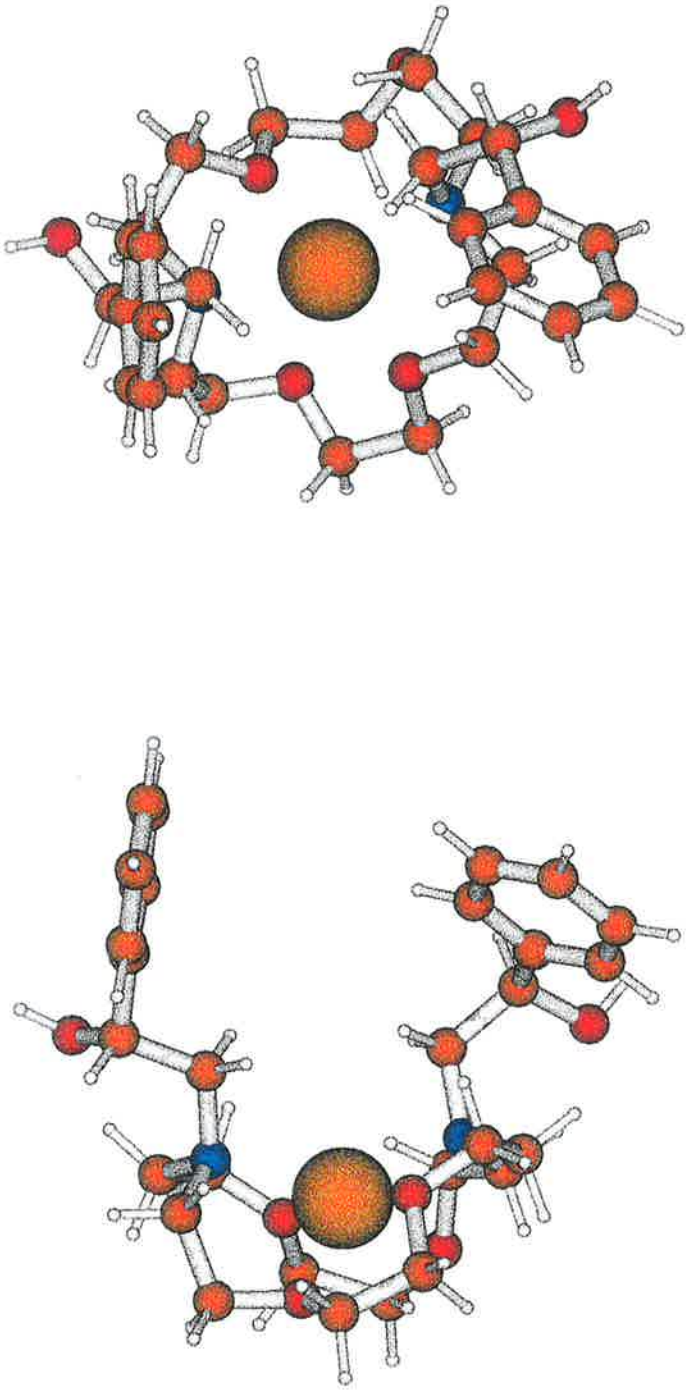

Figure 4.21 *Optimized gas phase geometry of* $[Cd6]^{2+}$ *as it appears in plan view (top) and in side view (bottom). (Blue = nitrogen; red = oxygen; orange = carbon; white = hydrogen. Cadmium (II) ion appears as a large red sphere).*

4.5 Conclusions

In this gas phase study, ESI-MS was used to probe the interactions of ligands **1 - 6** toward silver(I), lead(II), zinc(II) and cadmium(II) ions. The method has been shown to be a sensitive technique that allows the reaction between the macrocyclic ligands and metal ions to be monitored in the absence of bulk solvent. Analysis of the results from our solution phase investigations (Chapter 3) and our ESI-MS studies shows that the greater the stability of the metal complex in solution, the more likely the complex can be detected under ESI-MS conditions. In our hands, complexes that were formed with a low stability (i.e. log $K_s < 2$) in solution were not observed using ESI-MS methods. Indeed, the majority of the complexes observed using ESI-MS were all found to form relatively stable complexes in DMF solution. One exception is the $[Pb\mathbf{5}]^{2+}$ complex. This complex was formed in DMF solution with a relatively high stability, however, there appeared to be no evidence for its existence under ESI-MS conditions. The formation of the $[Pb\mathbf{2}]^{2+}$ complex occurs with a low stability in solution, however, this complex is observed by ESI-MS. This result may be attributed to the enhanced stability of the species in the gas phase where solvation effects play no role.

Complementary *ab initio* calculations afforded the optimized gas phase structures of the free ligands **1 - 6** and the corresponding metal complexes that were detected by ESI-MS experiments. Many of the optimized structures of the metal complexes possessed longer metal-ligand bond distances than those expected for a significant covalent interaction. This result may imply that the metal-ligand interactions that were observed are primarily electrostatic in nature, with very little covalent character. It is accepted that the limitations associated with *ab initio* calculations of large molecules incorporating heavy metals, particularly with reference to the approximations and the basis sets that were used, would significantly contribute to the longer than expected bond distances. Despite these shortcomings, *ab initio* methods were found to be particularly useful for investigating the changes in gas phase conformational geometry as one moves from the free ligand to the corresponding complex.

5 Summary and Conclusions

This thesis describes a comprehensive investigation of a select group of macrocyclic crown ether ligands that may potentially be used in the development of a lead(II)-ion specific probe for the detection and quantification of lead(II) concentrations in environmental and biological media.

The series of ligands chosen for this study contained a combination of oxygen, nitrogen and sulfur donor atoms. The dibenzo-dipyridyl-22-crown-6 derivative **1**, the bis(4-methylbenzo)tetrathia-18-crown-6 derivative **2**, and the dibenzo-diaza-18-crown-6 derivative **3** were prepared by a convergent synthetic strategy that culminated in the 1:1 condensation reaction between the appropriate components of the target macrocycle under low to moderate dilution conditions. The synthesis of ligand **1** was based on established literature methods, and its molecular structure was confirmed by X-ray crystallography. Attempts at the synthesis of macrocycles **2** and **3** by one-pot cyclization methods were found to be very low yielding. However, by implementation of multistep synthetic strategies, the yields of ligands **2** and **3** were improved. For example, ligand **2** has been synthesised previously by other workers in a 6% yield but, in our hands, a new reaction sequence afforded the target ligand in an overall yield of 20%.

The *N,N'*-phenylhydroxyethyl derivatives of dibenzo-diaza-18-crown-6 **4** and diaza-18-crown-6 **6** are new crown ether ligands which were obtained by a ring-opening reaction of *(R)*-styrene oxide with the parent crown ethers **3** and the commercially available diaza-18-crown-6 **5**, respectively. Interestingly, a lengthy reaction period of at least 10 days was required for the formation of ligand **4**, in stark contrast to the reaction time of 14 hours that was required for the formation of **6**. This phenomenon is most likely attributed to the steric bulk and inflexible nature of the parent crown ether **3**, as imposed by the aromatic moieties.

The solution and gas phase stabilities and selectivities of the series of crown ethers toward lead(II), zinc(II), and cadmium(II) and silver(I) ions were investigated by means of non-

aqueous potentiometry using an silver(I)-ion selective electrode, electrospray ionisation mass spectrometry and *ab initio* methods. Ligands **1** and **2** weakly complexed lead(II), cadmium(II) and zinc(II) ions in DMF solution, however ligand **2** formed a stable complex with lead(II) in the gas phase. Ligands **3** and **4** formed poorly stable complexes with lead(II), zinc(II) and cadmium(II) ions in the gas phase, and they were not studied further. Ligand **5** complexed lead(II) more strongly than cadmium(II) and zinc(II) ions in DMF solution, with only the cadmium(II) complex observed in the gas phase. The presence of *N,N'*-phenylhydroxyethyl pendant arms in ligand **6** substantially enhanced complexation of the heavy metal cations, with little affinity shown toward zinc(II) ions in both the solution and gas phase. The high affinity of ligands **1 - 6** toward silver(I) ions was observed in the gas phase. Ligands **1**, **2**, **5** and **6** were also found to form stable complexes with silver(I) ions in DMF solution.

The low stabilities of the complexes formed between ligand **1** and lead(II), zinc(II) and cadmium(II) ions are largely attributed to its considerable cavity size. Ligand **1** appears to be mismatched for metal ion encapsulation when one considers the sizes of even the larger metal ions studied in this work.

Ligand **2** formed complexes of low stability with lead(II), cadmium(II) and zinc(II) ions. The stabilities of the $[Cd\mathbf{2}]^{2+}$ and $[Pb\mathbf{2}]^{2+}$ complexes in DMF solution were somewhat unexpected, especially when one considers the soft base nature of the ligand sulfur atoms and the soft and borderline acid nature of the cadmium(II) and lead(II) ions, respectively. The orientation of the sulfur atoms which are directed out of the macrocyclic ring system, as demonstrated by *ab initio* calculations on the free ligand and the corresponding lead(II) complex, may in part contribute to the poor complex stability.

The gas phase complexation properties of the dibenzo-diaza-18-crown-6 ligand **3** were examined by means of ESI-MS. No evidence was obtained for the formation of lead(II), zinc(II) and cadmium(II) complexes, but the $[Ag\mathbf{3}]^{+}$ species was detected in the gas phase. The incorporation of pendant arms, containing neutral oxygen donor atoms, into the crown ether **3** was expected to enhance the selectivity and stability of the resulting lariat ether **4**

toward larger metal ions, such as lead(II) and cadmium(II). However, ESI-MS experiments confirmed that, under gas phase conditions, ligand **4** showed little affinity for these metal ions. This result was in contrast to that observed for the related $[Pb\mathbf{6}]^{2+}$ and $[Cd\mathbf{6}]^{2+}$ complexes. The steric effects associated with the aromatic rings, coupled with the considerable rigidity of the crown ether ring system of ligand **4**, would most likely diminish its interaction toward the metal ions studied in this work.

Ligand **5** was found to exhibit a particularly high stability toward silver(I) ions in both the solution and gas phase. A sharp decrease in stability was observed as one moves from the silver(I) complex of ligand **5** to the corresponding complex of ligand **6**. This result demonstrated that the pendant donor arms of **6** do not facilitate the complexation of the silver(I) ion, as supported by *ab initio* calculations.

Ligand **5** formed a stable complex with lead(II) ions in DMF solution, and sufficient discrimination was shown toward the larger metal ion over zinc(II) and cadmium(II). ESI-MS studies did not provide any evidence for the formation of the lead(II) or zinc(II) complex with this ligand, but the $[Cd\mathbf{5}]^{2+}$ species was observed in the gas phase.

The incorporation of pendant arms containing neutral oxygen donor atoms in the parent crown ether **5** was found to enhance significantly the stability of the lariat ether **6** toward the heavy metal ions lead(II) and cadmium(II). Ligand **6** was found to complex lead(II) and cadmium(II) ions with a higher stability than silver(I) ions in the solution phase, and thus an accurate determination of the stability constants for the $[Pb\mathbf{6}]^{2+}$ and $[Cd\mathbf{6}]^{2+}$ complexes was not possible by potentiometry using a silver(I)-ion selective electrode. However, competitive ESI-MS studies showed that ligand **6** exhibited a high selectivity toward cadmium(II) over lead(II) ions in the gas phase.

The work described in this thesis demonstrates that the potential development of ligand **6** into a heavy metal probe is feasible. This notion is supported by the clear discrimination of the ligand toward lead(II) and cadmium(II) over the biologically prevalent zinc(II) ions.

Further elaboration of ligand **6** is required in order to fully investigate its potential use as a fluorescent lead(II) specific probe. It is envisaged that the replacement of the phenyl rings in **6** with more highly conjugated groups, such as naphthalene or anthracene, will significantly enhance the optical properties of the ligand. This study has shown that the incorporation of simple aromatic groups *within* the crown ring structure is not facile, and quite extensive synthetic procedures need to be employed (e.g. the methods used for the preparation of ligands **3** and **4**). However, the relative ease of incorporating a chromophoric (or fluorophoric) moiety into the pendant arms of a simple, unsubstituted crown ether (such as ligand **5**) by means of an epoxide ring-opening reaction demonstrates the advantages of this method. Further elaboration of the target macrocycle with appropriate hydrophilic moieties will also be required in order to enhance the aqueous solubility of the ligand system, particularly since ligand **6** was found to be sparingly soluble in water.

6 Experimental

6.1 Synthetic Methods

6.1.1 General

Melting points (uncorrected) were recorded on a Kofler hot-stage apparatus equipped with a Reichert microscope. Microanalyses were performed by the Department of Chemistry, The University of Otago, Dunedin, New Zealand.

UV-visible spectra were recorded on a UV/VIS CARY 2200 spectrophotometer. Infrared spectra were recorded on a Hitachi 270-30 infrared spectrometer, as nujol mulls, liquid films or solutions as stated.

Electron impact mass spectra (EI-MS) and fast atom bombardment mass spectra (FAB-MS) were recorded on a Vacuum Generators ZAB 2HF mass spectrometer operating at 70 eV. Electrospray ionisation mass spectra (ESI-MS) were recorded using a Finnigan MAT ion trap LC-Q mass spectrometer, fitted with an electrospray ionisation source. Only the major fragmentations are given with their relative abundances shown in parentheses. High resolution mass spectrometry (HR-MS) was performed by the Department of Chemistry, The University of Tasmania, Hobart, Tasmania.

High field ^{1}H n.m.r. and ^{13}C n.m.r. spectra were recorded using either a 200 MHz or 300 MHz Gemini Varian spectrometer, as stated. All n.m.r. spectra were recorded as solutions of $CDCl_3$, unless otherwise stated, with tetramethylsilane (TMS) as an internal standard. All chemical shifts are quoted as δ in parts per million, and coupling constants J are given in Hertz. All multiplicities are abbreviated: s, singlet; d, doublet; t, triplet; q, quartet; m, multiplet; br, broad.

Analytical thin layer chromatography (t.l.c.) was carried out using Merck Kieselgel $60F_{254}$ on aluminium backed plates, and the t.l.c. chromatograms were visualised using UV light (254 nm). Flash chromatography[214] was performed using Amicon Matrix silica,

with a pore diameter of 60Å unless otherwise stated. Ion exchange chromatography was performed using Dowex AG 50W-X2 acidic cation-exchange resin.

All organic solvents and reagents were purified and dried using standard laboratory procedures.[215] Diethyl ether was distilled from sodium/benzophenone ketyl prior to use. Acetone, methanol and ethanol were distilled from anhydrous $CaSO_4$. Dichloromethane was distilled from P_2O_5. Light petroleum refers to the fraction with a boiling range 66° - 69°C. DMF was distilled from anhydrous $MgSO_4$. *n*-Butanol was dried with anhydrous $MgSO_4$, and distilled from sodium. Dimethyl sulfoxide and dimethoxyethane were distilled under reduced pressure from CaH_2. Pyridine was dried with sodium, followed by fractional distillation. All organic extracts are dried over anhydrous $MgSO_4$ or Na_2SO_4, as stated.

6.1.2 Syntheses

3,12,20,29-tetraoxa-35,36-diazapentacyclo[29.3.1.1.^{14,18}0$^{5-10}$0.^{22,27}]-hexatriaconta-1(35),5(10),6,8,14,16,18(36),22(27),23,25,31,33-dodecaene,[105] ***1***

2,6-(Dihydroxymethyl)pyridine, 7

Sodium borohydride (14.6 g, 384 mmol) was slowly added to a stirred solution of dimethyl 2,6-pyridinedicarboxylate (15 g, 77 mmol) in dry methanol (100 mL), and the resulting mixture refluxed for 14 h under an atmosphere of nitrogen. Upon cooling, the solvent was removed under reduced pressure and the crude material was dissolved in 10% sodium hydroxide solution (40 mL). The aqueous layer was extracted twice with tetrahydrofuran (2 x 60 mL) and the organic layers collected, dried ($MgSO_4$) and concentrated. The resulting solid was recrystallized from absolute ethanol to give **7** as white prisms (5.40 g, 50%), m.p. 114 - 116°C (lit.[111] 113°C). IR ν_{max} (nujol) 3364 (O-H), 2924, 2852, 1600 (C=N), 1464, 1378, 1348, 1082, 1022 cm^{-1}. ^1H n.m.r. (200 MHz) δ 2.85, br, 2H, 2 x OH; 4.74, s, 4H, 2 x CH_2; 7.27, d, *J* 7.7 Hz, 2 ArH; 7.71, t, *J* 7.7 Hz, ArH. MS *m/z* 139 ($M^{+\bullet}$, 50%), 138 (M-H, 100), 122 (M-OH, 70).

α,α'-Dibromo-o-xylene, 8

o-Xylene (10 g, 94 mmol) in dry carbon tetrachloride (20 mL) was added dropwise to a stirred solution of *N*-bromosuccinimide (34 g, 188 mmol) in dry carbon tetrachloride (80 mL). Benzoyl peroxide (0.31 g, 1.28 mmol) was added as a catalyst, and the solution was refluxed for 2 h under a nitrogen atmosphere. The resulting solution was filtered, and the solvent evaporated *in vacuo* to afford a pale yellow solid. The crude material was recrystallized from hexane to give **8** as fine white needles (14 g, 57%), m.p. 88 - 90°C (lit.[216] 98 - 99°C). ^{1}H n.m.r. (200 MHz) δ 4.67, s, 4H, 2 x CH_2; 7.34, m, 4 ArH. MS *m/z* 264 ($M^{+\bullet}$, 40%), 185 (M-Br, 100).

3,12,20,29-tetraoxa-35,36-diazapentacyclo[29.3.1.1.^{14,18}0.^{5,10}0.^{22,27}]-hexatriaconta-1(35),5(10),6,8,14,16,18 (36),22 (27),23,25,31,33-dodecaene, 1

2,6-(Dihydroxymethyl)pyridine **7** (5 g, 36 mmol) was added to a suspension of sodium hydride (1.90 g, 79 mmol) in dry dimethoxyethane (75 mL). A solution of α,α'-dibromo-*o*-xylene **8** (9.5 g, 36 mmol) in dry dimethoxyethane (55 mL) was added dropwise to the suspension, and the solution was stirred at room temperature for 1 h and then refluxed for 24 h. The reaction mixture was cooled, poured onto ice (200 mL) and extracted with chloroform (2 x 50 mL), giving upon concentration a white solid. Purification of the crude material by column chromatography (60% ethyl acetate/hexane) and recrystallization from absolute ethanol gave **1** as white crystals (6.07 g, 35%), m.p. 140 - 142°C (lit.[105] 142 - 143°C). ^{1}H n.m.r. (200 MHz) δ 4.55, s, 8H, 4 x OCH_2; 4.61, s, 8H, 4 x OCH_2; 7.25-7.62, m, 14H, CH. ^{13}C n.m.r. (200 MHz) δ 70.30, 73.40, 120.37, 128.16, 129.29, 136.9, 157.90, 168.51. FAB-MS *m/z* 483 ($(M+H)^+$, 100%), 307 (87), 289 (55).

2,3,11,12-Bis(4'-Methylbenzo)-1,4,10,13-tetrathia-7,16-dioxacycloocta-deca-2,11-diene, 2

2-(2'-Chloroethoxy)ethyl-2''-Tetrahydropyranyl ether, ***10***

2-(2'-Chloroethoxy)ethanol (6.2 mL, 58.7 mmol) was cooled to 0°C under an atmosphere of nitrogen. Neat dihydropyran (8.04 mL, 88 mmol) was slowly added to the solution, followed by one drop of concentrated HCl. The solution was allowed to warm to room temperature and stirred for 1 h. The solution was neutralised with triethylamine (~1 mL) and the resulting viscous oil was dissolved in dichloromethane (25 mL), and washed with water (2 x 20 mL) to remove the triethylamine hydrochloride salt by-product. The organic layers were combined, dried ($MgSO_4$), and evaporated, and the crude oil was purified by Kugelrohr distillation to afford the tetrahydropyranyl ether **10** as a colourless oil (8.36 g, 69%), b.p. 55°C / 0.02 mm Hg (lit.[112] b.p. 87 - 88°C / 0.5 mm Hg). ^{1}H n.m.r. (200 MHz) δ 1.53 - 1.81, m, 6H, 3 x CH_2(THP); 3.48 - 3.93, m, 5 x CH_2; 4.65, t, H, CH. FAB-MS *m/z* 209 ($(M+H)^+$, 33%), 85 ($M-C_4H_8O_2Cl$, 100).

2-{2-[(2-{[2-(2-hydroxyethoxy)ethyl]sulfanyl}-4-methylphenyl)-sulfanyl]-ethoxy}-1-ethanol, ***12***

To a solution of 3,4-dimercaptotoluene (3.3 mL, 22 mmol) in dry *n*-butanol (10 mL), was added solid sodium hydride (2.0 g, 49 mmol) and the solution was stirred for 20 min under a nitrogen atmosphere. 2-(2'-chloroethoxy)ethyl-2''-tetrahydropyranyl ether **10** (10.3 g, 49 mmol) in dry *n*-butanol (15 mL) was added dropwise over 1 h, and the solution was refluxed for 20 h. The reaction mixture was quenched with water (25 mL), and solvent was evaporated under reduced pressure. The remaining oily material was dissolved in dichloromethane (35 mL), washed with water (2 x 20 mL), and the organic layers were collected, dried ($MgSO_4$) and concentrated to afford the *O*-tetrahydropyranyl derivative as a pale yellow oil. The crude product was used without further purification.

The crude mixture (8.5 g, 17 mmol) was dissolved in *n*-butanol (10 mL). 1M HCl (60 mL, 68 mmol) was added, and the solution was stirred at room temperature. After 14 h, t.l.c. analysis (20% acetone / dichloromethane) showed that the reaction had not reached completion and thus, a further 2 equivalents of 1M HCl (29 mL, 34 mmol) was added, and the solution was heated at 80°C for a further 14 h. The reaction mixture was neutralised using 10% $NaHCO_3$ solution (25 mL), and the product was extracted with dichloromethane (3 x 25 mL). The organic fractions were combined, washed with water (30 mL), dried ($MgSO_4$) and evaporated *in vacuo*. After column chromatography of the residue (20% acetone / dichloromethane), the desired diol **12** was obtained as a pale, yellow oil (5.30 g, 73%). HR-MS Calcd for $C_{15}H_{24}S_2O_4$: *m/z* 332.11497. Found: *m/z* 332.11354. IR ν_{max} (neat) 3416 (O-H), 2924, 2860, 1640, 1586, 1460, 1384, 1356, 1292 (C-O), 1118, 1072, 868 cm^{-1}. ^1H n.m.r (300 MHz) δ 2.33, s, 3H, CH_3; 2.73, br, 2H, 2 x OH; 3.07 - 3.18, m 4H, 2 x CH_2S; 3.54 - 3.75, m, 12H, 6 x CH_2O; 6.96 - 7.29, m, 3 ArH. ^{13}C n.m.r. (300 MHz) δ 21.08, CH_3; 33.22, 33.83, 2 x CH_2S; 61.77, 61.78, 2 x CH_2OH; 69.38, 69.43, 2 x OCH_2CH_2OH; 72.15, 72.21, 2 x $SCH_2\mathbf{C}H_2O$; 127.56, 129.89, 131.08, 3 x CH; 132.62, 137.38, 137.75, 3 x C. MS *m/z* 332 ($M^{+\bullet}$, 40%), 271 (M-$C_2H_5O_2$, 56), 243 (M-$C_4H_9O_2$, 68), 167 (100), 154 (M-$C_8H_{18}O_4$, 73).

2-{2-[(5-methyl-2-{[2-(2-{[(4-methylphenyl)sulfonyl]oxy}-ethoxy)-ethyl]-sulfanyl}-phenyl)sulfanyl]ethoxy}ethyl-4-methyl-1-benzenesulfonate, ***13***

Under a nitrogen atmosphere, the diol **12** (1.0 g, 5.1 mmol) was dissolved in dry pyridine (10 mL) and cooled to -20°C. A solution of *p*-toluenesulfonyl chloride (4.83 g, 25 mmol) in dry pyridine (10 mL) was added dropwise to the cooled solution over 10 min, and the reaction mixture was maintained between -20°C and -10°C for 3 h. Upon completion, the mixture was warmed to room temperature, and the solvent was removed under reduced pressure. The remaining solid was taken up into dichloromethane (25 mL), washed with water (2 x 20 mL), and the organic fraction was collected, dried ($MgSO_4$) and concentrated to give a pale yellow oil. Purification by flash chromatography (30% ethyl acetate / hexane) afforded the desired product **13** as a viscous, colourless oil (2.45 g, 75%). Anal.

Calcd for $C_{29}H_{36}O_8S_4$: C, 54.35; H, 5.66%. Found: C, 54.51; H, 5.79%. ^{1}H n.m.r (300 MHz) δ 2.32, s, 3H, CH_3; 2.44, s, 6H,2 x CH_3; 2.94 - 3.06, m, 4H, 2 x CH_2S; 3.53 - 3.68, m, 8H, 4 x CH_2O; 4.12 - 4.18, m, 4H, 2 x CH_2OTs; 6.98 - 7.25, m, 3 ArH; 7.32, AA'BB', *J* 8Hz, 2 x CH; 7.79, AA'BB', *J* 8Hz, 2 x CH. ^{13}C n.m.r. (200 MHz) δ 20.88, CH_3; 21.45, 2 x $SO_2C_6H_5CH_3$; 32.33,32.92, 2 x SCH_2; 68,14, 68.19, 69.07, 69.51, 69.61, 6 x CH_2O; 127.32, 127.75, 129.40, 129.70, 130.71, 5 x CH; 132.10, 132.78, 137.16, 137.32, 144.72, 5 x C. MS *m/z* 640 ($M^{+\bullet}$, 6%), 469 (M-$C_7H_7SO_3$, 32), 199 (96), 91 (100).

1,2-di{[2-(2-chloroethoxy)ethyl]-sulfanyl}-4-methylbenzene, ***14***

The neat diol **12** (1.37 g, 4.1 mmol) was stirred under a nitrogen atmosphere and cooled to 0°C. Thionyl chloride (10 mL, 137 mmol) was added dropwise over 15 min, and the solution was warmed to room temperature and stirred for 14 h, followed by gentle heating at 80°C for 3 h. The excess thionyl chloride was removed under reduced pressure and the resulting brown oil was taken up in dichloromethane (40 mL), washed with 20% K_2CO_3 solution (20 mL), and water (20 mL). The organic layer was dried ($MgSO_4$) and concentrated *in vacuo* to afford a brown oily residue. Flash chromatography (1% acetone, dichloromethane) afforded the desired dichloride **14** as an orange oil, (0.37 g, 25%). HR-MS: Calcd for $C_{15}H_{22}S_2O_2Cl_2$: *m/z* 368.04720. Found: *m/z* 368.04548. IR ν_{max} (neat) 2920, 2856, 1586, 1462, 1362, 1298, 1260, 1200, 1114, 1038, 964, 746 (C-Cl), 666 (C-S) cm^{-1}. ^{1}H n.m.r. (300 MHz) δ 2.32, s, 3H, CH_3; 3.05-3.15, m, 4H, 2 x SCH_2; 3.58 - 3.75, m, 12H, 4 x OCH_2, 2xCH_2Cl; 6.95 - 7.28, m, 3 ArH. ^{13}C n.m.r. (200 MHz) δ 21.19, CH_3; 32.76, 33.38, 2 x CH_2S; 42.82, 42.85, 2 x CH_2Cl; 69.89, 69.97, 2 x SCH_2CH_2O; 71.12, 71.21, 2 x OCH_2CH_2Cl; 127.62, 129.88, 131.17, 3 x CH; 132.54, 137.49, 137.75, 3 x C. MS *m/z* 369 ($M^{+\bullet}$, 36%), 333.5 (M-Cl, 10), 298 (M-2Cl, 48), 186.7 (100).

2,3,11,12-Bis (4'-Methylbenzo)-1,4,10,13-tetrathia-7,16-dioxacyclo-octa-deca-2,11-diene, ***2***

Method 1

Solid sodium hydride (0.14 g, 3.4 mmol) was added to a solution of 3,4-dimercaptotoluene (0.23 mL, 1.6 mmol) in dry *n*-butanol (5 mL), and the solution was stirred at room temperature for 20 min under an atmosphere of nitrogen. The ditosylate **13** (1.0 g, 1.56 mmol) was dissolved in a 1:1 mixture of dry *n*-butanol and dry DMF (20 mL), and it was added to the solution over a 30 min period. The resulting mixture was heated to reflux for 24 h. The solvents were removed under reduced pressure, and the solid residue was dissolved in dichloromethane (25 mL) and washed with water (2 x 20 mL). The organic layer was dried ($MgSO_4$), and evaporated *in vacuo* to afford a pale yellow solid. The crude material was purified by flash chromatography (2% ethyl acetate / dichloromethane) and recrystallized (1:1 ethyl acetate / hexane) to afford the title compound **2** as fine, white needles (0.26 g, 36%), m.p. 140 - 144°C (lit.[76] 147°C). Anal. Calcd for $C_{22}H_{28}O_2S_4$: C, 58.37; H, 6.23%. Found: C, 58.21; H, 5.85%. UV λ_{max} (MeOH) 256 nm (lit.[76] 256 nm) ^{1}H n.m.r. (200 MHz) δ 2.29, s, 6H, 2 x CH_3; 3.00 - 3.12, m, 8H, 4 x CH_2S; 3.59 - 3.73, m, 8H, 4 x CH_2O; 6.91 - 7.26, m, 6ArH. ^{13}C n.m.r. (200 MHz) δ 21.12, CH_3; 33.40, 33.43, 33.91, 33.99, 4 x CH_2S; 69.35, 69.42, 69.52, 69.59, 4 x CH_2O; 127.64, 130.52, 131.82, 3 x CH; 133.03, 137.44, 138.32, 3 x CH. MS *m/z* 452 ($M^{+\bullet}$, 12%), 279 (21), 154 (100).

Method 2

3,4-Dimercaptotoluene (0.09 mL, 0.6 mmol) was dissolved in dry *n*-butanol (5 mL) under a nitrogen atmosphere. Solid sodium hydroxide (0.05 g, 1.3 mmol) was added to the solution, and it was warmed to 50°C for 60 min. The dichloride **14** (0.22 g, 0.6 mmol) was dissolved in dry *n*-butanol (10 mL), and added dropwise to the pale yellow solution over a 15 min period. The solution was then heated to reflux for 24 h. The *n*-butanol was removed under reduced pressure, and the remaining orange solid was dissolved in

dichloromethane (15 mL), washed with 10% NaOH solution (10 mL) and water (2 x 20 mL). The organic fraction was dried ($MgSO_4$), and concentrated *in vacuo*. Purification of the crude product by flash chromatography (30% ethyl acetate / hexane) and crystallization from 1:1 ethyl acetate / hexane afforded **2** as a white, crystalline solid (0.09 g, 33%), m.p. 141 - 144°C (lit.[76] m.p. 147°C). The spectroscopic data of the compound were identical to those quoted above (Method 1).

Attempted Synthesis of 7,16-Diaza-1,4,10,13-tetraoxa-2,3,11,12-dibenzo-cyclo-octadeca-2,11-diene, 3

N-bis(2-4'-methylphenylsulfonyloxy)ethyl-4'-methylphenylsulfonamide, ***16***

Diethanolamine (1.4 g, 13 mmol) was added dropwise to a stirred solution of *p*-toluenesulfonyl chloride (10 g, 52 mmol) in dry pyridine (30 mL) over a 30 min period. The solution was stirred for a further 3.5 h at room temperature. Water (70 mL) was then added, and the solution was stirred for a further 1.5 h at room temperature. The pale yellow precipitate was collected by vacuum filtration, washed with water (2 x 10 mL) and air-dried. Recrystallization of the crude product from methanol afforded the sulfonamide **16** as fine, white prisms (5.8 g, 78%), m.p. 98 - 100°C (lit.[49] m.p. 96 - 98°C). ^{1}H n.m.r. (200 MHz) δ 2.43, s, 3H, CH_3; 2.46, s, 6H, 2 x CH_3; 3.37, t, *J* 5.9 Hz, 4H, 2 x NCH_2; 4.11, t, *J* 5.9 Hz, 4H, 2 x OCH_2; 7.26 - 7.78, m, 12 ArH. FAB-MS *m/z* 568 ($(M+H)^+$, 19%), 396 (M-$C_7H_7SO_3$, 100), 155 (67).

8,19-di[(4-methylphenyl)sulfonyl]-7,8,9,10,18,19,20,21-octahydro-6H,17H-dibenzo[b,k][1,4,10,13,7,16]tetraoxadiazacyclo-octadecine, ***17***

Under a nitrogen atmosphere, solid potassium carbonate (3.7 g, 27 mmol) was added to a solution of pyrocatechol (1.0 g, 9 mmol) in dry DMF (25 mL). The sulfonamide **16** (5.15 g, 9 mmol), dissolved in dry DMF (40 mL), was added dropwise to the pyrocatechol solution over 20 min. The resulting mixture was refluxed at 80°C for 24 h and, upon

cooling, was added to ice-cold water (200 mL), and extracted with diethyl ether (3 x 20 mL). The organic layers were combined, dried ($MgSO_4$), and evaporated *in vacuo* to afford a white solid. T.l.c. analysis of the white solid (5% methanol / dichloromethane) showed that the crude residue contained an inseparable mixture of compounds **17** and **18**, m.p. 163 - 166°C (lit.[104] m.p. **17** 215-216°C; **18** 174 - 175°C). FAB-MS *m/z* 667 (**17** $(M+H)^+$, 18%), 334 (**18** $(M+H)^+$, 50%), 138 (55), 92(100).

7,16-Diaza-1,4,10,13-tetraoxa-2,3,11,12-dibenzo-cyclo-octadeca-2,11-diene, 3

Diethyl(o-phenylenedioxy)diacetate, 23

Solid potassium carbonate (75 g, 550 mmol) and ethyl bromoacetate (52.4 g, 310 mmol) were added to a solution of pyrocatechol (15 g, 140 mmol) in dry acetone (300 mL) and the mixture was refluxed for 48 h. The excess salts were removed by vacuum filtration and washed with acetone (2 x 20 mL). The acetone washes were combined with the filtrate and concentrated under *vacuo* to give an dark orange oil. The oil was taken up into diethyl ether (50 mL) and washed with 5% NaOH solution (2 x 20 mL), followed by water (2 x 20 mL). The organic layer was collected, dried ($MgSO_4$) and concentrated *in vacuo* to give a pale yellow oil. The crude extract was purified by Kugelrohr distillation to afford the product **23** as a colourless, viscous oil (21.7 g, 56%), b.p. 128°C / 0.08 mm. IR ν_{max} (nujol) 3524, 2932, 1756 (C=O), 1594, 1504, 1458, 1380, 1192, 1134, 1028, 834 cm^{-1}. ^1H n.m.r. (300 MHz) δ 1.29, t, *J* 10.5 Hz, 6H, 2 x $CH_2\mathbf{C}H_3$; 4.26, q, *J* 10.5 Hz, 4H, 2 x $\mathbf{C}H_2CH_3$; 4.72, s, 4H, 2 x CH_2; 6.93, m, 4 ArH. ^{13}C (300 MHz) δ 13.56, CH_3; 60.68, OCH_2; 66.18, $O\mathbf{C}H_2CH_3$; 115.21, 122.15, 2 x CH; 147.77, C; 168.72, CO. MS *m/z* 282 ($M^{+\bullet}$, 68%), 209 (M-$C_3H_5O_2$, 10), 135 (M-$C_6H_{10}O_4$, 25), 108 (48), 58 (100).

1,2-Bis-(2-hydroxyethoxy)benzene, ***24***

Method 1

Diethyl(*o*-phenylenedioxy)diacetate **23** (1.5 g, 5.3 mmol) was added dropwise to a stirred suspension of lithium aluminium hydride (0.8 g, 21 mmol) in dry diethyl ether (25 mL) and the mixture was stirred at room temperature for 16 h. The excess hydride was carefully quenched with water, and the excess salts were removed by vacuum filtration. The residues were washed with ethyl acetate (3 x 30 mL) and these washings, combined with the filtrate, were dried ($MgSO_4$) and evaporated under reduced pressure. The residue was crystallized from hexane to afford the desired compound **24** as white crystals (0.82 g, 78%), m.p. 79 - 80°C (lit.[120] m.p. 93 - 94°C). IR ν_{max} (nujol) 3504 (O-H), 2924, 2852, 1508, 1460, 1378, 1258 (C-O), 1220, 1080 cm^{-1}. ^1H n.m.r (200 MHz) δ 3.48 - 3.62, br, 2H, 2 x OH; 3.93 - 4.16, m, 8H, 2 x OCH_2CH_2OH; 7.00, s, 4 ArH. MS *m/z* 198 ($M^{+\bullet}$, 25%), 154 (M-C_2H_4O, 10), 109 (M-$C_4H_9O_2$, 100).

Method 2

Pyrocatechol (10 g, 90 mmol) and sodium hydroxide (8.7 g, 218 mmol) were stirred at room temperature in dry ethanol (50 mL) under a nitrogen atmosphere. A solution of 2-chloroethanol (14.5 mL, 218 mmol) in dry ethanol (50 mL) was then added dropwise over a 15 min period, and the resulting solution was refluxed for 24 h. The solvent was removed *in vacuo*, and the resulting dark orange oil was dissolved in chloroform (200 mL), and washed with 10% NaOH solution (3 x 100 mL), and water (2 x 100 mL). The organic layers were collected, dried ($MgSO_4$), and evaporated *in vacuo*. Crystallization of the crude product from benzene / petroleum ether afforded **24** as fine, white needles (9.0 g, 50%), m.p. 78 - 80°C (lit.[119]m.p. 78 - 80°C). The spectroscopic data obtained for the compound were identical to those quoted above.

*1.2-Bis-(2-p-tolyl-sulfonylethoxy)benzene, **20***

Method 1

Under a nitrogen atmosphere, 1,2-bis-(2-hydroxyethoxy)benzene **24** (4 g, 20 mmol) was dissolved in a solution of dry pyridine (30 mL) and cooled to 0°C. *p*-Toluenesulfonyl chloride (19.2 g, 100 mmol) in dry pyridine (50 mL) was then added dropwise to the solution over 0.5 h. The solution was allowed to warm to room temperature and it was stirred for a further 16 h. The reaction mixture was quenched with 10% $HCl_{(aq)}$ and extracted with ethyl acetate (2 x 30 mL). The organic layers were collected, washed with water (20 mL), dried ($MgSO_4$) and concentrated. The crude product was crystallized from ethyl acetate/hexane to afford **20** as white needles (5.7 g, 55%), m.p. 97 - 98°C (lit.[120] m.p. 95.5 - 97°C). ^1H n.m.r. (200 MHz) δ 2.45, s, 6H, 2 x CH_3; 4.18 - 4.33, m, 8H, 2 x CH_2OTs; 6.79 - 6.94, m, 4 ArH; 7.36, AA'BB', *J* 8 Hz, 2 x CH; 7.83, AA'BB', *J* 8 Hz, 2 x CH. FAB-MS *m/z* 507 ($(M+H)^+$, 8%), 197 ($M-C_{14}H_{14}S_2O_4$, 15), 154 (82), 93 (100).

Method 2

1,2-bis-(2-hydroxyethoxy)benzene **24** (7.0 g, 35 mmol) was suspended in dry dichloromethane (80 mL) under a nitrogen atmosphere, and the solution cooled to 0°C. Triethylamine (7.9 g, 77.7 mmol) was slowly added to the solution, and the temperature was maintained between 0 - 5°C. *p*-Toluenesulfonyl chloride (14.83 g, 77.7 mmol) in dry dichloromethane (110 mL) was then added dropwise over 30 min. The solution was then warmed to room temperature and stirred overnight. The precipitated triethylamine hydrochloride was removed by vacuum filtration, and the filtrate was evaporated *in vacuo* until a white solid appeared. Diethyl ether (200 mL) was then added to the remaining solution, and complete precipitation of the desired product occurred. The fine, white precipitate was collected by vacuum filtration, dissolved in dichloromethane (50 mL), and the organic layers washed with water (2 x 20 mL), dried ($MgSO_4$) and concentrated to afford the crude solid. Crystallisation from ethanol gave the desired product **20** as white

needles (15.5 g, 87%), m.p. 94.5 - 95.5°C (lit.[120] m.p. 95.5 - 97°C). The spectroscopic data obtained for the compound were identical to those quoted above.

*Catechol-bis-(2-azidoethylether), **25***

1,2-bis-(2-*p* -tolylsulfonylethoxy)benzene **20** (0.2 g, 0.4 mmol) was stirred with sodium azide (0.1 g, 1.6 mmol) in dry dimethyl sulfoxide (10 mL) for 24 h. The reaction mixture was poured into water (20 mL), and the product extracted into diethyl ether (2 x 20 mL). The organic layers were collected, dried ($MgSO_4$), evaporated *in vacuo*, and the residue was crystallized from ethanol to afford the product **25** as white crystals (0.092 g, 93%), m.p. 61 - 63°C (lit.[103] m.p. 86-88°C). IR ν_{max} (nujol) 2924, 2852, 2108 (N_3), 2068, 1506, 1456, 1380, 1290 (C-O), 1260 cm^{-1}. ^1H n.m.r (200 MHz) δ 3.53, t, *J* 5.2 Hz, 4H, 2 x CH_2N_3; 4.1, t, *J* 5.2 Hz, 4H, 2 x OCH_2; 6.86, s, 4 ArH. ^{13}C n.m.r. (300 MHz) δ 50.23, CH_2N_3; 68.13, CH_2O; 114.56, 122.08, 2 x CH; 148.55, C. MS *m/z* 248 ($M^{+\bullet}$, 30%), 136 (M-$C_2H_4N_6$, 55), 69 (100).

*2-[2-(2-amino-2-oxoethoxy)phenoxy]acetamide, **27***

Diethyl (*o*-phenylenedioxy)diacetate **23** (8.3 g, 29 mmol) was added dropwise to a rapidly stirred solution of concentrated aqueous ammonia (400 mL). Precipitation of the diamide product began immediately, and the solution was stirred for 14 h at room temperature. The resulting diamide was collected by vacuum filtration and washed thoroughly with water (2 x 20 mL). Recrystallization from methanol afforded the desired compound **27** as a white powder (2.64 g, 41%), m.p. 205 - 208°C (lit.[217] m.p. 206 - 208°C). IR ν_{max} (nujol) 3384 (N-H), 3188 (N-H), 2920, 2848, 1656 (C=O), 1504, 1462, 1380, 1314, 1292, 1264, 1190, 1124, 708 cm^{-1}. ^1H n.m.r (200 MHz, d_6-DMSO) δ 4.49, s, 4H, 2 x CH_2; 6.96, s, 4H, 4 ArH; 7.43, 4H, 2 x NH_2. ^{13}C n.m.r. (200 MHz) δ 67.07, CH_2; 113.43, CH; 120.89, CH; 140.02, C; 169.12, CO. FAB-MS *m/z* 225 ($(M+H)^+$, 12%), 154 (100), 136 (80), 77 (M-$C_4H_8N_2O_4$, 36).

*Catechol bis-(2-aminoethyl)ether, **26***

Under a nitrogen atmosphere, the diamide **27** (1 g, 4.46 mmol) was added to a stirred suspension of sodium borohydride (1.0 g, 27 mmol) in dry dimethoxyethane (30 mL). Boron trifluoride etherate (1.3 g, 9.0 mmol) was added dropwise to the solution over 1 h, and the resulting mixture was refluxed for 14 h. Once the reaction mixture had cooled to room temperature, 6 M HCl (10 mL) was added and the dimethoxyethane was removed *in vacuo*. Sodium hydroxide pellets were then added to the aqueous phase until the pH of the solution reached *ca.* 10. The aqueous layer was extracted with chloroform (2 x 30 mL), and the organic layers were dried (Na_2SO_4), and concentrated to afford the diamine **26** as a colourless oil (0.69 g, 80%), which was used without further purification. IR ν_{max} (neat) 3384 (N-H), 2928, 1592, 1504, 1456, 1254 (C-O), 1218, 1122, 1018, 744 cm^{-1}. ^1H n.m.r. (200 MHz) δ 1.76, br, 4H, 2 x NH_2; 3.10, t, *J* 5.14 Hz, 4H, 2 x CH_2N; 4.05, t, *J* 5.12 Hz, 4H, 2 x OCH_2; 6.95, s, 4 ArH. ^{13}C n.m.r. (200 MHz) δ 41.77, CH_2NH_2; 71.91, CH_2O; 114.88, CH; 121.76, CH; 149.22, C. FAB-MS *m/z* 197 ($(M+H)^+$, 64%), 153 ($M-C_2H_6N$, 20), 135 (30), 44 (100).

*Catechol bis-(N-ethoxycarbonyl-2-aminoethyl ether), **28***

Catechol bis-(2-aminoethyl)ether **26** (1.0 g, 5.1 mmol) was stirred in diethyl ether (10 mL) and water (10 mL) at 0°C under an atmosphere of nitrogen. Ethyl chloroformate (1.3 g, 12 mmol) in diethyl ether (5 mL) and sodium hydroxide (0.5 g, 12 mmol) in water (5 mL) were added, and the solution was allowed to warm to room temperature and stirred for 14 h. The organic layer was removed, and the aqueous layer was washed with diethyl ether (2 x 20 mL). The ether layers were combined, dried ($MgSO_4$) and evaporated to afford the crude product which, after column chromatography (2% methanol / dichloromethane) and crystallization from chloroform / hexane, afforded the product **28** as white crystals (1.3 g, 75%), m.p. 59 - 60°C (lit.[103] 60 - 61°C). ^1H n.m.r. (200 MHz) δ 1.25, t, *J* 7.2 Hz, 6H, 2 x CH_2CH_3; 3.56, q, *J* 5.1 Hz, 4H, 2 x CH_2N; 4.1, t, *J* 5.1Hz, 4H, 2 x OCH_2; 4.16, q, *J* 7.2

Hz, 4H, 2 x OCH_2CH_3; 5.58, br, 2H, 2 x NH; 6.95, s, 4 ArH. FAB-MS *m/z* 341 ($(M+H)^+$, 10%), 116 ($M-C_{11}H_{14}NO_4$, 100), 88 (55), 44 (48).

*Catechol bis-(N-benzyloxycarbonyl-2-aminoethyl ether), **21***

A solution of catechol bis-(2-aminoethyl ether) **26** (1.0 g, 5.1 mmol) in toluene (10 mL) and water (10 mL) was cooled to 0°C. Benzyl chloroformate in 50% toluene (3.7 mL, 13 mmol) and toluene (5 mL) were added dropwise to the cooled solution, followed by the addition of sodium hydroxide (0.86 g, 21 mmol) in water (10 mL). The solution was allowed to warm to room temperature and stirred for 24 h. Removal of the toluene under reduced pressure afforded a white suspension which was extracted with dichloromethane (3 x 30 mL). The organic extracts were combined, washed with 10% NaOH solution (2 x 20 mL) and water (30 mL), dried ($MgSO_4$) and evaporated *in vacuo*. The crude material was crystallized from 1:1 ethyl acetate / hexane to afford the benzyl carbamate **21** as a white crystalline solid (2.1 g, 89%) m.p. 102-104°C (lit.[103] 103-104°C). IR ν_{max} (nujol) 3344 (N-H), 2920, 2848, 1726 (C=O), 1686, 1592, 1546, 1428, 1378, 1294 (C-O), 1218, 1120, 1030, 948, 740 cm^{-1}. ^1H n.m.r. (200 MHz) δ 3.55, q, *J* 5 Hz, 4H, 2xCH_2N; 4.07, t, *J* 5 Hz, 4H, 2 x OCH_2; 5.09, s, 4H, 2 x CH_2Ph; 5.56, br, 2 x NH; 6.93, s, 4H, 4 ArH; 7.32, s, 10H, 10 ArH. ^{13}C n.m.r. (200 MHz) δ 40.58; 66.64; 68.85; 115.49; 122.28; 128.06; 128.45; 136.49; 148.82; 156.53. FAB-MS *m/z* 465 ($(M+H)^+$, 5%), 185 (44), 93 (100).

*N,N'-Bis-benzyloxycarbonyl-7,16-diaza-1,4,10,13-tetraoxa-2,3,11,12-dibenzo-octadeca-2,11-diene, **22***

Catechol bis-(*N*-benzyloxycarbonyl-2-aminoethyl ether) **21** (0.5 g, 1.1 mmol) in dry dimethyl sulfoxide (10 mL) was added dropwise to a suspension of sodium hydride (0.13 g, 5.4 mmol) in dry dimethyl sulfoxide (10 mL), and the solution was stirred at room temperature for 3 h. 1,2-Bis-(2-*p*-tolylsulfonylethoxy)benzene **20** (0.55 g, 1.1 mmol) in dimethyl sulfoxide (5 mL) was then added dropwise to the solution over a 0.5 h period, and

the mixture was stirred for a further 72 h at room temperature. The resulting solution was acidified to pH 1 using 10% $HCl_{(aq)}$ and extracted with chloroform (2 x 50 mL). The organic layers were washed with 10% K_2CO_3 solution (2 x 20 mL) and water (30 mL), dried ($MgSO_4$) and concentrated to afford the crude product as a white solid. Crystallization from chloroform / ether afforded the product **22** as white needles (0.36 g, 52%), m.p. 221 - 224°C (lit.[103] m.p. 221 - 224°C). IR ν_{max} (nujol) 2924, 2852, 1686 (C=O), 1592, 1506, 1456, 1366, 1256 (C-O), 1156, 1086, 994 cm^{-1}. ^1H n.m.r. (200 MHz) δ 3.90 - 4.21, m, 16H, 4 x NCH_2CH_2O; 5.15, s, 4H, 2 x CH_2Ph; 6.82, s, 8H, ArH; 7.35, s, 10H, ArH. ^{13}C n.m.r (300 MHz) δ 29.69; 47.89; 112.46; 121.12; 128.12; 128.57; 136.50; 148.46; 156.26. FAB-MS *m/z* 627 ($(M+H)^+$, 30%), 583 ($M-CO_2$, 44), 492 ($M-C_8H_7O_2$, 30), 446 (37), 154 (100).

7,16-Diaza-1,4,10,13-tetraoxa-2,3,11,12-dibenzocyclo-octa-deca-2,11-diene, 3

A solution of the carbamate derivative **22** (304 mg, 0.485 mmol) in acetic acid (2 mL) was heated with 50% hydrogen bromide in glacial acetic acid (4 mL) over a steam bath for 10 min. The mixture was diluted with water (20 mL) and extracted with chloroform (2 x 15 mL). The remaining aqueous layer was neutralised using 10% NaOH solution and extracted with chloroform (2 x 20 mL). The organic layers were collected, dried ($MgSO_4$) and evaporated *in vacuo* to afford the diamine **3** as a pale yellow oil (151 mg, 87%), which was used without further purification. IR ν_{max} (neat) 3326 (N-H), 2925, 2854, 2670, 2362, 2127, 2049, 1714, 1625, 1502, 1462, 1376, 1263 (C-O), 1124, 1043, 894, 744 cm^{-1}. ^1H n.m.r. (300 MHz) δ 2.55, br, 2H, 2 x NH; 3.16, t, *J* 5Hz, 8H, 4 x CH_2NH; 4.15, t, *J* 5Hz, 8H, 4 x CH_2O; 6.87, s, 8 ArH. ^{13}C (300 MHz) δ 22.03; 47.84; 67.58; 122.18; 148.57. FAB-MS *m/z* 359 ($(M+H)^+$, 62%), 154 (69), 136 ($M-C_{12}H_{18}N_2O_2$, 84), 55 (100).

2-[19-(2-hydroxy-2-phenylethyl)-7, 8, 9, 10, 18, 19, 20, 21-octahydro-6H, 17H-dibenzo[b, k][1,4,10,13,7,16]tetraoxadiazacyclooctadecin-8-yl]-1-phenyl-1-ethanol, 4

The dibenzo-diaza-18-crown-6 derivative **3** (210 mg, 0.59 mmol) was dissolved in dry DMF (5 mL) under a nitrogen atmosphere. *(R)*-Styrene oxide (700 mg, 5.9 mmol) was added dropwise over 15 min and the solution was heated to 100°C for 10 days. Removal of the solvent and excess *(R)*-styrene oxide under reduced pressure gave the desired product as a crude orange oil. Purification of the oil by flash chromatography (30% dichloromethane / 45% ethyl acetate / 20% ethanol / 5% $NH_{3(aq)}$), followed by trituration using a 1:10 DMF / water mixture afforded the desired product **4** as a pale orange powder, (55 mg, 16%). HR-MS Calcd for $C_{36}H_{42}N_2O_6$: *m/z* 599.30426. Found: *m/z* 599.31026. IR ν_{max} (nujol) 3356 (O-H), 2923, 2854, 1710, 1592, 1457, 1376, 1253 (C-O), 1222, 1045, 1027, 744, 698 cm^{-1}. ^1H n.m.r. (300 MHz) δ 2.59 - 2.63, m, 2H, NC**H**HCHR$_2$; 2.92 - 2.96, m, 2H, NCH**H**CHR$_2$; 3.30 - 3.35, m, 8H, 4 x NCH$_2$; 4.13 - 4.16, m, 8H, 4 x OCH$_2$; 4.65 - 4.67, m, 2H, CH$_2$C**H**R$_2$; 6.93, s, 8H, ArH; 7.26, s, 10H, ArH. ^{13}C n.m.r. (300 MHz) δ 54.20; 62.94; 67.08; 70.11; 113.04; 121.18; 125.92; 127.53; 128.37; 131.18; 148.61. ESI-MS *m/z* 621 ($(M+Na)^+$, 100%), 599 ($(M+H)^+$, 56%).

2-[16-(2-hydroxy-2-phenylethyl)-1,4,10,13-tetraoxa-7,16-diazacyclo-octadecanyl]-1-phenyl-1-ethanol, 6

(R)-styrene oxide (0.23 mL, 1.98 mmol) was added dropwise to a stirred solution of 1,10-diaza-18-crown-6 **5** (0.40 g, 0.76 mmol) in dry DMF (10 mL) and the solution was heated to 100°C for 24 h, under a nitrogen atmosphere. Removal of solvent and excess *(R)*-styrene oxide under reduced pressure afforded the crude product as an orange oil. Purification of the oil using ion exchange chromatography (50% ethyl acetate / 40% dichloromethane / 9% methanol / 1% $NH_{3(aq)}$) afforded the desired compound **6** as a pale yellow oil, (0.25 g, 66%). HR-MS Calcd for $C_{28}H_{42}N_2O_6$: *m/z* 503.30426. Found: *m/z* 503.31315. IR ν_{max} (neat) 3355 (O-H), 1708, 1461, 1376, 1259 (C-O), 1027, 744, 588 cm^{-1}. ^1H n.m.r. (200 MHz) δ 2.58-2.75, m, 8H, 4 x OCH$_2$C**H**$_2$N; 2.91-3.07, m, 4H, 2 x

$NCH_2CH(OH)Ph$; 3.57-3.76, m, 16H, 8 x OCH_2; 4.67-4.73, m, 1H,C**H**(OH)Ph; 7.23-7.40, m, 10H, 10 ArH. ^{13}C n.m.r. (200 MHz) δ 55.18; 64.42; 69.69; 70.51; 70.63; 125.96, 127.26, 128.21, 142.54. ESI-MS *m/z* 525 ($(M+Na)^+$, 100%), 503 ($(M+H)^+$, 8%).

6.2 Physical methods

6.2.1 Non-aqueous titrations

N,N'-dimethylformamide (DMF) was dried from $MgSO_4$, and purified by distillation from $MgSO_4$ and anhydrous $CuSO_4$. $CuSO_4$ was added to remove any dimethylamine impurity from the solvent. The DMF was stored under dry nitrogen. Silver(I) nitrate ($AgNO_3$) was commercially available and it was used without purification. It was dried under vacuum for 48 hours over P_2O_5 prior to use. The metal salts, lead perchlorate ($Pb(ClO_4)_2$), zinc nitrate ($Zn(NO_3)_2$), and cadmium perchlorate ($Cd(ClO_4)_2$) were commercially available and used without purification. All salts were dried over P_2O_5 for 24 hours.

Tetraethylammonium perchlorate (NEt_4ClO_4) was prepared by the addition of perchloric acid ($HClO_4$) to tetraethylammonium bromide (NEt_4Br). The resulting white precipitate was recrystallized from water until it was free from bromide and acid, and it was then dried under vacuum over P_2O_5.

All solutions were made up in dry DMF containing 0.050 M NEt_4ClO_4 supporting electrolyte under a stream of dry nitrogen. Titrations were carried out under dry nitrogen in a thermostatted (298.2 ± 0.01) reference vessel connected to a thermostatted titration vessel by a salt-bridge. The salt bridge was filled with a solution of dry DMF containing 0.050 M NEt_4ClO_4 supporting electrolyte. A stream of nitrogen gas was bubbled through the titration solution to remove any carbon dioxide from the system and prevent the ingress of atmospheric gases and moisture. The solutions were magnetically stirred for the duration of the titration. An Orion Research 720 digital analyser was used to measure the electrode potential during the titration. The reference electrode, which was used to monitor the change in concentration of free silver(I) ions throughout the course of the titration, consisted of a silver wire electrode. The reference solution was a 20 mL aliquot of 5×10^{-3} M $AgNO_3$ (in the reference vessel). All stability constants relevant to this study were determined by following these methods.

Stability constants for $[AgL]^+$ complexes, where L = **1**, **2**, **5** and **6**, were determined by direct potentiometric titrations. All titrations were performed in duplicate. For each titration, 20 mL of 5 x 10^{-4} M $AgNO_3$ solution (in the titration vessel) was titrated with 5 mL of 5 x 10^{-3} M L solution (in the burette). The results afforded the log K_s values for the $[Ag\mathbf{1}]^+$, $[Ag\mathbf{2}]^+$, $[Ag\mathbf{5}]^+$ and $[Ag\mathbf{6}]^+$ complexes, respectively. Stability constants for $[ML]^{n+}$ complexes, where L = **1**, **2**, **5** and **6** and M^{n+} = lead(II), zinc(II) and cadmium(II), were determined by competitive potentiometric titrations. For each competitive titration, 20 mL of 5 x 10^{-5} M $AgNO_3$ solution (in the titration vessel) was titrated with 5 mL of a solution of 5 x 10^{-3} M L and 2.5 x 10^{-2} M metal perchlorate (in the burette). The results afforded the log K_e values for the competitive titrations which allowed one to determine the log K_s values of the $[M\mathbf{1}]^{n+}$, $[M\mathbf{2}]^{n+}$, $[M\mathbf{5}]^{n+}$ and $[M\mathbf{6}]^{n+}$ complexes, where M^{n+} = lead(II), zinc(II) and cadmium(II).

The electrode response to the silver(I) ion concentration was determined by the titration of 20 mL of a 0.050 M $NEtClO_4$ solution (in the titration vessel) with 5 mL of 5 x 10^{-3} M $AgNO_3$ solution (in the burette), and measuring the corresponding change in potential. The electrode response to silver(I) ion concentration is pseudo-Nernstian and is given by Equation 3.7 (Chapter 3). The constants E_0 and c, required in the determination of the stability constants (K_S), can be determined simply from the plot of the potential E against the logarithm of the free solvated metal ion concentration, $\ln[M^+]$. The values of E_0 and c were found to lie within the range of 100 - 300 and 19 to 28 (where e.m.f is in mV), respectively; values that are consistent with those quoted in the literature.[149]

6.2.2 Standardisation of metal ion solutions

Prior to standardisation, the hygroscopic salts lead(II) perchlorate, zinc(II) nitrate, cadmium(II) perchlorate and silver(I) nitrate were dried for 48 hours under vacuum over P_2O_5. Deionised water was purified by means of a MilliQ Reagent system, boiled to expel dissolved gases, and protected from carbon dioxide by storage in a closed vessel under a drying tube of soda lime. Aqueous solutions of each metal salt were prepared to a final concentration of 0.1 M.

A Dowex AG 50W-X2 ion exchange column was washed twice with hydrochloric acid (0.1 M) to ensure complete protonation of the column, and rinsed thoroughly with Milli Q water. The column was then loaded with an aqueous solution of the metal salt (1.0 mL), and eluted with purified MilliQ water until an increase in the pH of the eluant occurred (from pH 1 to 6). Bromothymol blue (2 drops) was then added to the eluant, and the solution was titrated against sodium hydroxide (0.1 M) in order to determine the total number of moles of hydrochloric acid eluted from the column. This in turn allowed the number of moles of the metal ion to be determined accurately, since one mole of the metal(I) salt displaces one equivalent of protons from the column. Alternatively, one mole of metal(II) salt displaces two equivalents of protons from the column. Standardizations of each metal ion were conducted in triplicate.

The concentration of sodium hydroxide used in the above-mentioned titrations was determined accurately by standardisation against potassium hydrogen phthalate (10 mL, 5 x 10^{-2} M) using a Metrohm E665 Dosimat autoburette, an Orion SA720 potentiometer and an Orion 8172 Sure Flow Ross pH electrode. Titrations were controlled and the data collected by means of the computer program AUTOTIT7.

6.2.3 Electrospray ionisation mass spectrometry

The ESI-MS sample solutions were prepared by using HPLC grade methanol. Preliminary work involved the measurement of ESI-MS of the $[ML]^{n+}$ species prepared by addition of each of the macrocyclic ligands (**1 - 6**) to the metal ion of interest (i.e. lead(II), zinc(II), cadmium(II) and silver(I)). The lead(II) and cadmium(II) salts were in the form of their perchlorates, and the zinc(II) and silver(I) in the form of their nitrates. Each solution contained the ligand and the metal ion at a final concentration of 10^{-6} M and 10^{-4} M, respectively. The competitive ESI-MS experiments utilised solutions that were prepared in a similar manner to those described above, but each ligand solution contained two metals at a final concentration of 10^{-4} M.

A Finnigan MAT ion trap LC-Q (Finnigan, San Jose, CA, USA) octapole mass spectrometer fitted with an electrospray ionisation (ESI) source was used. Nitrogen was used as the nebulizing gas. The electrospray needle was maintained at 4.25 kV. The capillary temperature was maintained at 200°C. The tube lens offset was set at 30 V and the capillary voltage was maintained at 35 V. The sample solutions were introduced into the ESI source by infusion at flow rates of 12-18 μL per minute, with a syringe, in positive ion mode. Ions were detected by scanning the first quadrupole over the range *m/z* 200 ~ 800. At least 50 scans were averaged to obtain the representative spectra.

6.2.4 *Ab initio* calculations

The structure geometries of the macrocyclic crown ether complexes studied in this work were calculated using *ab initio* methods by means of GAUSSIAN 94 software[206] implemented on a Silicon Graphics Indigo^2 xZ workstation linked to a Silicon Graphics PowerChallenge supercomputer. The LANL2DZ basis set was used for all calculations. This basis set employs D95 methods (double-zeta splitting for hydrogenic and non-hydrogenic atoms) for elements up to the 3rd period, and Effective Core Potentials (ECPs) for elements past the 2nd period. Visualisation of molecules was accomplished by means of MOLDEN software (V3.0).

6.2.5 UV-visible spectroscopy

UV-visible spectra of the ligands (dibenzo-dipyridyl-22-crown-6 (**1**) and bis(4-methylbenzo)-tetrathia-18-crown-6 (**2**)) and their metal complexes (lead(II), zinc(II), cadmium(II) and silver(I)) were recorded using a Varian CARY 2000 spectrophotometer. The absorption spectra of the free ligands were recorded using sample solutions of either ligand **1** or **2** at concentrations of 10^{-4} M, in the presence of 0.05 M $NEtClO_4$ as supporting electrolyte, in methanol or DMF solution, respectively. The absorption spectra of the metal complexes were recorded using solutions of **1** or **2** that were prepared in a similar manner as above, but each solution contained the metal salt at 5 x 10^{-3} M concentration.

The lead(II) and cadmium(II) salts were in the form of their perchlorates and the silver(I) and zinc(II) were in the form of their nitrates.

All sample solutions were thermostatted to 298.2 ± 0.1 K by circulation of water through the cell compartment of the spectrometer using a Julabo P water pump. The absorption spectra of the solutions of ligands **1** and **2** were recorded over the wavelength range of 240 - 360 nm and 270 - 360 nm, respectively, sampling every 2 nm/sec. The bandwidth of the spectrometer was set to 1.0 nm and its slit height was set to 12 mm. The UV-visible spectra were measured and recorded by means of a IBM compatible personal computer. Baseline measurements were run for all spectra. The data were collated, and the plots of the absorption spectra were obtained by means of the computer programs Microsoft Excel 5.0 and MATLAB.

Appendix A *X-ray crystallographic data*

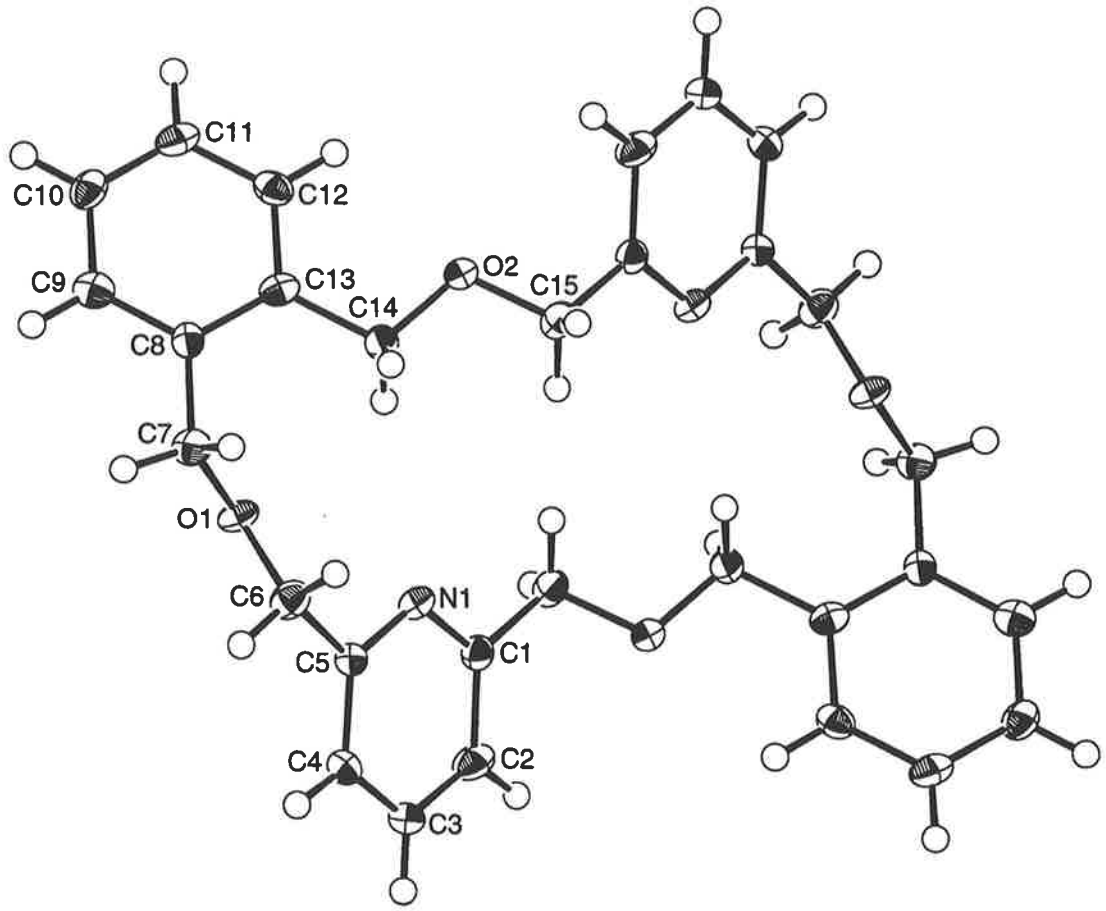

Figure A1 *Molecular structure of 3,12,20,29-Tetraoxa-35,36-diazapentacyclo-[29.3.1.1.^{14,18}0.^{5,10}-0.22,27]-hexatriaconta-1(35),6,8,14,16,18(36),22(27),23,25,31,33-dodecaene, 1.*

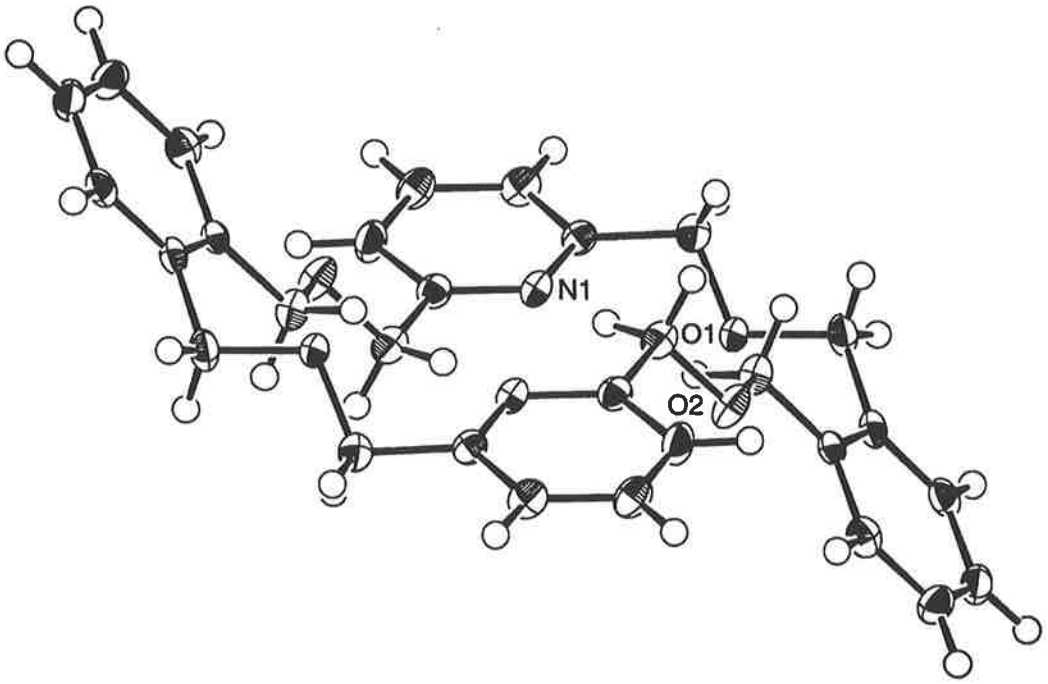

Figure A2 *Molecular structure of 1 (side view).*

atom	atom	distance	ADC(*)	atom	atom	distance	ADC(*)
O(1)	C(6)	1.428(5)	1	C(4)	C(5)	1.392(5)	1
O(1)	C(7)	1.446(5)	1	C(5)	C(6)	1.494(6)	1
O(2)	C(14)	1.416(5)	1	C(7)	C(8)	1.504(6)	1
O(2)	C(15)	1.423(5)	1	C(8)	C(9)	1.379(6)	1
N(1)	C(1)	1.346(5)	1	C(8)	C(13)	1.410(6)	1
N(1)	C(5)	1.342(5)	1	C(9)	C(10)	1.392(6)	1
C(1)	C(2)	1.408(6)	1	C(10)	C(11)	1.367(6)	1
C(1)	C(15)	1.485(6)	45503	C(11)	C(12)	1.403(6)	1
C(2)	C(3)	1.380(6)	1	C(12)	C(13)	1.408(6)	1
C(3)	C(4)	1.378(6)	1	C(13)	C(14)	1.500(6)	1

atom	atom	atom	angle	atom	atom	atom	angle
C(6)	O(1)	C(7)	112.1(3)	O(1)	C(7)	C(8)	110.0(4)
C(14)	O(2)	C(15)	112.3(3)	C(7)	C(8)	C(9)	119.7(4)
C(1)	N(1)	C(5)	118.9(4)	C(7)	C(8)	C(13)	120.4(4)
N(1)	C(1)	C(2)	121.5(4)	C(9)	C(8)	C(13)	119.9(4)
N(1)	C(1)	C(15)	117.2(4)	C(8)	C(9)	C(10)	120.9(4)
C(2)	C(1)	C(15)	121.3(4)	C(9)	C(10)	C(11)	120.2(4)
C(1)	C(2)	C(3)	119.1(4)	C(10)	C(11)	C(12)	120.3(4)
C(2)	C(3)	C(4)	119.1(4)	C(11)	C(12)	C(13)	119.9(4)
C(3)	C(4)	C(5)	119.3(4)	C(8)	C(13)	C(12)	118.8(4)
N(1)	C(5)	C(4)	122.2(4)	C(8)	C(13)	C(14)	121.2(4)
N(1)	C(5)	C(6)	115.9(4)	C(12)	C(13)	C(14)	120.2(4)
C(4)	C(5)	C(6)	121.7(4)	O(2)	C(14)	C(13)	110.3(4)
O(1)	C(6)	C(5)	109.0(4)	0(2)	C(15)	C(1)	108.2(4)

Torsion or Conformation Angles

(1)	(2)	(3)	(4)	angle	(1)	(2)	(3)	(4)	angle
O(1)	C(6)	C(5)	N(1)	54.3(5)	C(3)	C(4)	C(5)	C(6)	-175.9(5)
O(1)	C(6)	C(5)	C(4)	-129.9(4)	C(3)	N(1)	C(1)	C(15)	-178.0(4)
O(1)	C(7)	C(8)	C(9)	121.8(4)	C(5)	C(6)	O(1)	C(7)	-170.4(3)
O(1)	C(7)	C(8)	C(13)	-59.9(5)	C(6)	O(1)	C(7)	C(8)	150.7(3)
O(2)	C(14)	C(13)	C(8)	-175.9(4)	C(7)	C(8)	C(9)	C(10)	178.3(4)
O(2)	C(14)	C(13)	C(12)	3.8(6)	C(7)	C(8)	C(13)	C(12)	-178.5(4)
O(2)	C(15)	C(1)	N(1)	-129.2(4)	C(7)	C(8)	C(13)	C(14)	1.2(4)
O(2)	C(15)	C(1)	C(2)	48.9(6)	C(8)	C(9)	C(10)	C(11)	0.6(7)
N(1)	C(1)	C(2)	C(3)	-0.5(7)	C(8)	C(13)	C(12)	C(11)	0.0(6)
N(1)	C(5)	C(4)	C(3)	-0.3(7)	C(9)	C(8)	C(13)	C(12)	-0.2(6)
C(1)	N(1)	C(5)	C(4)	0.3(7)	C(9)	C(8)	C(13)	C(14)	179.5(4)
C(1)	N(1)	C(5)	C(6)	176.2(4)	C(9)	C(10)	C(11)	C(12)	-0.8(7)
C(1)	C(2)	C(3)	C(4)	0.6(7)	C(10)	C(9)	C(8)	C(13)	-0.1(7)
C(1)	C(15)	O(2)	C(14)	-163.0(3)	C(10)	C(11)	C(12)	C(13)	0.5(7)
C(2)	C(1)	N(1)	C(5)	0.1(7)	C(11)	C(12)	C(13)	C(14)	-179.7(4)
C(2)	C(3)	C(4)	C(5)	-0.2(7)	C(13)	C(14)	O(2)	C(15)	179.9(4)
C(3)	C(2)	C(1)	C(15)	177.5(4)					

Appendix B *Potentiometric titration data*

Table B.1 *Experimental and calculated e.m.f. titration data (as determined by the VISP program) for the determination of the stability constant of* $[AgI]^+$ *in DMF solution at 298.2 K and I = 0.050 M* NEt_4ClO_4.

titre (mL)	expt. e.m.f. (mV)	calc. e.m.f. (mV)	titre (mL)	expt. e.m.f. (mV)	calc. e.m.f. (mV)
1.02	-69.60	-70.86	1.98	-104.10	-105.34
1.07	-70.50	-71.90	2.02	-106.40	-107.74
1.10	-71.30	-72.54	2.06	-108.60	-110.17
1.14	-72.30	-73.43	2.10	-111.10	-112.59
1.18	-73.30	-74.35	2.14	-113.60	-114.98
1.22	-74.30	-75.31	2.18	-116.00	-117.31
1.26	-75.30	-76.30	2.22	-118.20	-119.55
1.30	-76.50	-77.35	2.27	-120.70	-122.22
1.34	-77.70	-78.41	2.30	-122.80	-123.74
1.38	-78.90	-79.54	2.34	-125.00	-125.68
1.42	-80.20	-80.72	2.38	-127.10	-127.51
1.46	-81.40	-81.95	2.42	-129.20	-129.24
1.50	-82.70	-83.24	2.46	-130.90	-130.88
1.54	-84.20	-84.60	2.50	-132.80	-132.42
1.58	-84.80	-86.03	2.54	-133.70	-133.89
1.62	-86.50	-87.54	2.58	-135.50	-135.27
1.66	-88.20	-89.13	2.62	-137.20	-136.58
1.70	-90.00	-90.81	2.68	-138.90	-138.43
1.74	-91.80	-92.59	2.74	-141.80	-140.15
1.78	-93.60	-94.47	2.80	-143.10	-141.75
1.82	-95.60	-96.45	2.86	-145.70	-143.26
1.86	-97.50	-98.53	2.92	-146.80	-144.66
1.90	-99.70	-100.72	2.98	-149.00	-145.99
1.94	-101.90	-102.99			

Table B.2 *Experimental and calculated e.m.f. titration data (as determined by the VISP program) for the determination of the stability constant of* $[Pb1]^{2+}$ *in DMF solution at 298.2 K and I = 0.050 M* NEt_4ClO_4.

titre (mL)	expt. e.m.f. (mV)	calc. e.m.f. (mV)	titre (mL)	expt. e.m.f. (mV)	calc. e.m.f. (mV)
1.50	-100.80	-102.10	2.20	-140.20	-140.45
1.54	-102.70	-103.61	2.24	-142.00	-142.60
1.56	-102.90	-104.39	2.28	-143.60	-144.61
1.60	-105.20	-106.03	2.32	-145.50	-146.49
1.64	-107.20	-107.75	2.36	-147.30	-148.24
1.68	-109.20	-109.58	2.40	-149.10	-149.87
1.74	-113.50	-112.53	2.44	-150.70	-151.39
1.78	-115.60	-114.64	2.48	-152.00	-152.81
1.83	-117.90	-117.15	2.52	-153.20	-154.14
1.86	-120.40	-119.20	2.56	-154.30	-155.38
1.88	-121.00	-120.41	2.60	-155.50	-156.56
1.90	-123.70	-121.65	2.64	-156.30	-157.64
1.94	-128.40	-124.18	2.68	-158.50	-158.67
1.96	-127.60	-125.47	2.72	-159.60	-159.64
1.98	-129.40	-126.77	2.76	-160.50	-160.57
2.01	-131.40	-128.73	2.80	-161.30	-161.44
2.05	-133.50	-131.33	2.84	-163.80	-162.25
2.08	-133.60	-133.26	2.88	-164.40	-163.04
2.12	-135.90	-135.76	2.92	-165.20	-163.78
2.16	-138.10	-138.17	2.98	-165.80	-164.84

Table B.3 *Experimental and calculated e.m.f. titration data (as determined by the VISP program) for the determination of the stability constant of* $[Ag\mathbf{2}]^+$ *in DMF solution at 298.2 K and I = 0.050 M* NEt_4ClO_4.

titre (mL)	expt. e.m.f. (mV)	calc. e.m.f. (mV)	titre (mL)	expt. e.m.f. (mV)	calc. e.m.f. (mV)
1.52	-103.56	-105.20	2.52	-251.30	-250.26
1.56	-106.94	-107.64	2.56	-255.66	-252.17
1.60	-108.80	-110.27	2.60	-257.28	-253.97
1.64	-110.93	-113.12	2.64	-258.69	-255.67
1.68	-114.01	-116.24	2.68	-259.84	-257.28
1.72	-116.93	-119.67	2.72	-261.46	-258.81
1.76	-120.18	-123.49	2.76	-263.34	-260.26
1.80	-122.31	-127.79	2.80	-263.77	-261.65
1.84	-126.52	-132.70	2.84	-263.81	-262.98
1.88	-132.10	-138.39	2.88	-265.31	-264.25
1.92	-139.74	-145.13	2.92	-266.08	-265.46
1.96	-149.02	-153.24	2.96	-267.13	-266.64
2.00	-161.43	-163.10	3.00	-268.61	-267.76
2.04	-177.45	-174.76	3.04	-269.25	-268.85
2.08	-192.43	-187.27	3.08	-270.25	-269.90
2.12	-204.23	-198.93	3.12	-270.88	-270.91
2.16	-212.60	-208.80	3.16	-271.99	-271.89
2.20	-219.65	-216.90	3.20	-272.94	-272.84
2.24	-225.39	-223.61	3.24	-273.66	-273.76
2.28	-230.09	-229.27	3.28	-274.68	-274.66
2.32	-234.08	-234.14	3.32	-275.63	-275.52
2.36	-235.62	-238.40	3.36	-275.55	-276.37
2.40	-239.40	-242.17	3.40	-276.38	-277.19
2.44	-242.61	-245.55	3.44	-277.16	-277.98
2.48	-244.74	-248.62	3.48	-277.94	-278.76

Table B.4 *Experimental and calculated e.m.f. titration data (as determined by the VISP program) for the determination of the stability constant of* $[Zn2]^{2+}$ *in DMF solution at 298.2 K and I = 0.050 M* NEt_4ClO_4.

titre (mL)	expt. e.m.f. (mV)	calc. e.m.f. (mV)	titre (mL)	expt. e.m.f. (mV)	calc. e.m.f. (mV)
1.12	-73.80	-74.25	2.16	-208.50	-211.37
1.16	-75.00	-75.99	2.20	-214.10	-216.19
1.20	-76.10	-78.00	2.24	-219.00	-220.07
1.24	-77.40	-78.56	2.28	-223.40	-223.31
1.28	-79.00	-80.12	2.33	-227.40	-226.70
1.32	-80.30	-80.43	2.36	-230.70	-228.48
1.36	-81.90	-82.24	2.40	-233.80	-230.60
1.44	-85.20	-86.40	2.44	-236.30	-232.50
1.48	-87.40	-88.90	2.48	-238.80	-234.21
1.52	-89.30	-91.31	2.52	-241.00	-239.98
1.56	-91.50	-93.26	2.56	-243.10	-244.80
1.60	-94.20	-95.37	2.62	-245.00	-245.92
1.64	-97.10	-97.71	2.68	-248.30	-249.13
1.68	-100.20	-100.30	2.74	-250.20	-250.53
1.72	-103.70	-103.22	2.81	-253.10	-252.10
1.76	-107.50	-106.56	2.86	-254.60	-253.90
1.80	-111.80	-110.47	2.92	-256.10	-255.12
1.85	-117.90	-116.51	2.98	-258.70	-257.38
1.88	-124.60	-121.08	3.04	-259.70	-258.13
1.92	-131.70	-128.98	3.12	-262.00	-263.10
1.96	-144.20	-140.68	3.20	-264.20	-264.89
2.00	-159.70	-159.91	3.28	-266.00	-266.91
2.04	-177.50	-182.18	3.36	-268.00	-268.16
2.08	-190.90	-196.23	3.44	-269.60	-269.96
2.12	-201.10	-205.09	3.52	-271.20	-270.84

Table B.5 *Experimental and calculated e.m.f. titration data (as determined by the VISP program) for the determination of the stability constant of* $[Cd2]^{2+}$ *in DMF solution at 298.2 K and I = 0.050 M* NEt_4ClO_4.

titre (mL)	expt. e.m.f. (mV)	calc. e.m.f. (mV)	titre (mL)	expt. e.m.f. (mV)	calc. e.m.f. (mV)
1.26	-73.50	-73.69	2.22	-170.00	-185.92
1.30	-74.80	-74.90	2.26	-186.30	-202.04
1.34	-76.20	-76.36	2.30	-199.10	-211.42
1.38	-77.30	-77.89	2.36	-209.30	-220.48
1.42	-78.80	-78.53	2.40	-217.40	-224.83
1.46	-80.20	-80.50	2.44	-223.80	-228.38
1.50	-81.80	-81.05	2.48	-228.80	-231.37
1.54	-83.40	-82.39	2.52	-232.20	-233.94
1.58	-85.10	-83.80	2.58	-237.20	-237.22
1.62	-86.90	-85.30	2.62	-241.10	-239.11
1.66	-88.90	-86.91	2.66	-243.90	-241.82
1.70	-90.80	-88.64	2.70	-246.40	-244.37
1.74	-93.30	-90.52	2.75	-248.80	-247.12
1.78	-96.00	-92.56	2.78	-250.80	-248.09
1.82	-98.60	-94.81	2.84	-252.50	-250.87
1.84	-98.70	-96.03	2.90	-256.30	-253.47
1.88	-101.70	-98.67	2.96	-257.80	-254.92
1.92	-105.00	-101.67	3.02	-260.40	-256.98
1.96	-108.50	-105.13	3.08	-261.80	-258.25
1.98	-112.70	-107.09	3.14	-263.00	-261.05
2.02	-117.90	-111.60	3.22	-266.00	-263.69
2.06	-124.10	-117.26	3.30	-266.90	-264.27
2.10	-132.50	-124.85	3.38	-268.80	-267.12
2.14	-142.20	-136.26	3.46	-270.50	-268.94
2.19	-155.90	-164.74	3.54	-272.40	-271.32

Table B.6 *Experimental and calculated e.m.f. titration data (as determined by the VISP program) for the determination of the stability constant of* $[Ag\mathbf{5}]^+$ *in DMF solution at 298.2 K and I = 0.050 M* NEt_4ClO_4.

titre (mL)	expt. e.m.f. (mV)	calc. e.m.f. (mV)	titre (mL)	expt. e.m.f. (mV)	calc. e.m.f. (mV)
1.50	-88.80	-87.42	2.20	-329.10	-346.26
1.54	-89.20	-89.22	2.22	-340.50	-353.88
1.58	-90.20	-91.14	2.24	-352.90	-359.83
1.62	-91.40	-93.20	2.26	-359.90	-364.70
1.66	-92.00	-95.43	2.28	-366.30	-368.82
1.70	-95.70	-97.84	2.30	-370.40	-372.40
1.74	-97.00	-100.47	2.32	-374.80	-375.56
1.76	-98.40	-101.89	2.34	-377.30	-378.39
1.80	-100.60	-104.96	2.36	-381.20	-380.95
1.86	-104.50	-110.31	2.40	-381.30	-385.45
1.90	-109.40	-114.56	2.44	-390.90	-389.30
1.94	-116.10	-119.57	2.48	-394.70	-392.67
1.98	-121.60	-125.70	2.52	-398.30	-395.67
2.02	-128.40	-133.62	2.58	-403.00	-399.62
2.06	-153.60	-144.79	2.64	-406.40	-403.07
2.08	-164.50	-152.75	2.70	-409.80	-406.13
2.10	-186.80	-164.04	2.76	-413.20	-408.88
2.12	-225.50	-183.64	2.84	-416.40	-412.15
2.14	-265.50	-259.78	2.92	-418.70	-415.08
2.16	-289.80	-317.88	3.00	-422.30	-417.71
2.18	-316.30	-335.62			

Table B.7 *Experimental and calculated e.m.f. titration data (as determined by the VISP program) for the determination of the stability constant of* $[Pb5]^{2+}$ *in DMF solution at 298.2 K and I = 0.050 M* NEt_4ClO_4.

titre (mL)	expt. e.m.f. (mV)	calc. e.m.f. (mV)	titre (mL)	expt. e.m.f. (mV)	calc. e.m.f. (mV)
1.02	-73.80	-75.07	1.78	-108.70	-107.44
1.06	-74.90	-76.17	1.82	-110.80	-109.86
1.10	-76.30	-77.32	1.86	-113.60	-112.28
1.14	-77.40	-78.52	1.91	-116.20	-114.95
1.18	-79.20	-79.77	1.94	-118.20	-116.97
1.22	-79.40	-81.08	1.98	-119.60	-119.21
1.27	-82.10	-82.62	2.02	-121.50	-121.34
1.30	-83.20	-83.87	2.06	-123.40	-123.37
1.34	-85.30	-85.37	2.10	-125.80	-125.28
1.38	-86.80	-86.95	2.14	-127.10	-127.08
1.42	-88.10	-88.60	2.18	-128.80	-128.78
1.46	-90.20	-90.34	2.22	-130.10	-130.36
1.50	-92.50	-92.17	2.26	-131.30	-131.85
1.54	-94.20	-94.09	2.30	-132.80	-133.25
1.58	-96.40	-96.10	2.34	-133.10	-134.56
1.62	-99.10	-98.21	2.38	-134.80	-135.80
1.66	-100.60	-100.41	2.42	-135.40	-136.96
1.70	-103.40	-102.70	2.48	-137.30	-138.58
1.74	-105.90	-105.05			

Table B.8 *Experimental and calculated e.m.f. titration data (as determined by the VISP program) for the determination of the stability constant of* $[Zn5]^{2+}$ *in DMF solution at 298.2 K and I = 0.050 M* NEt_4ClO_4.

titre (mL)	expt. e.m.f. (mV)	calc. e.m.f. (mV)	titre (mL)	expt. e.m.f. (mV)	calc. e.m.f. (mV)
1.52	-78.40	-78.00	2.54	-132.00	-138.56
1.56	-79.60	-79.02	2.56	-134.80	-143.03
1.60	-80.50	-80.06	2.58	-139.60	-148.32
1.64	-81.80	-81.15	2.60	-145.40	-154.74
1.69	-83.00	-82.43	2.62	-160.20	-162.80
1.72	-84.10	-83.45	2.64	-172.80	-173.22
1.76	-85.20	-84.68	2.67	-189.90	-189.94
1.80	-86.30	-85.95	2.70	-206.10	-212.60
1.84	-87.70	-87.28	2.72	-214.00	-221.93
1.88	-89.20	-88.68	2.74	-223.80	-229.16
1.93	-90.70	-90.52	2.78	-230.90	-239.76
1.96	-92.10	-91.69	2.82	-237.10	-247.35
2.00	-93.50	-93.32	2.86	-242.50	-253.21
2.04	-95.20	-95.04	2.90	-249.60	-257.96
2.08	-96.90	-96.88	2.93	-257.50	-261.00
2.12	-98.70	-98.85	2.96	-262.70	-263.70
2.16	-100.70	-100.95	3.00	-267.50	-266.88
2.20	-103.10	-103.23	3.04	-271.50	-269.67
2.24	-104.80	-105.71	3.08	-274.40	-272.16
2.28	-107.10	-108.42	3.12	-277.50	-274.41
2.33	-109.90	-111.82	3.18	-281.50	-277.39
2.36	-112.90	-114.78	3.25	-286.10	-280.42
2.40	-115.90	-118.59	3.32	-289.40	-283.07
2.44	-118.80	-123.01	3.40	-293.40	-285.73
2.49	-123.10	-128.98	3.48	-296.60	-288.08
2.52	-128.30	-134.69			

Table B.9 *Experimental and calculated e.m.f. titration data (as determined by the VISP program) for the determination of the stability constant of* $[Cd5]^{2+}$ *in DMF solution at 298.2 K and I = 0.050 M* NEt_4ClO_4.

titre (mL)	expt. e.m.f. (mV)	calc. e.m.f. (mV)	titre (mL)	expt. e.m.f. (mV)	calc. e.m.f. (mV)
1.00	-66.40	-69.95	1.92	-129.00	-129.63
1.08	-67.70	-72.07	1.94	-133.20	-132.55
1.12	-69.10	-73.21	1.96	-135.00	-135.35
1.16	-70.90	-74.40	1.98	-138.30	-138.00
1.20	-71.90	-75.65	2.02	-142.30	-142.80
1.24	-72.70	-76.97	2.04	-144.70	-144.96
1.28	-74.70	-78.37	2.08	-145.80	-148.81
1.32	-78.00	-79.85	2.12	-149.30	-152.14
1.36	-79.80	-81.43	2.14	-152.50	-153.64
1.40	-81.70	-83.12	2.18	-155.80	-156.36
1.44	-83.60	-84.93	2.22	-158.30	-158.75
1.48	-86.90	-86.89	2.26	-160.30	-160.89
1.52	-88.20	-89.02	2.30	-162.20	-162.81
1.56	-90.90	-91.35	2.34	-164.00	-164.54
1.60	-93.80	-93.92	2.38	-165.70	-166.13
1.65	-97.90	-97.16	2.42	-167.50	-167.57
1.68	-101.30	-99.98	2.46	-168.80	-168.91
1.72	-104.80	-103.61	2.52	-170.70	-170.73
1.76	-109.10	-107.75	2.58	-172.40	-172.36
1.78	-110.80	-110.04	2.64	-174.30	-173.84
1.81	-115.90	-113.11	2.70	-175.60	-175.19
1.84	-118.70	-117.82	2.76	-177.50	-176.42
1.86	-122.70	-120.69	2.82	-178.50	-177.56
1.88	-124.20	-123.65	2.88	-180.20	-178.61
1.90	-126.70	-126.65	2.94	-181.60	-179.90

Table B.10 *Experimental e.m.f. titration data obtained for the determination of the stability constant of* $[Pb\mathbf{6}]^{2+}$ *in DMF solution at 298.2 K and I = 0.050 M* NEt_4ClO_4.

titre (mL)	expt. e.m.f. (mV)	titre (mV)	expt. e.m.f. (mL)
0.00	-61.20	1.66	-68.40
0.10	-60.30	1.70	-68.70
0.20	-60.50	1.74	-68.80
0.30	-61.30	1.78	-69.00
0.40	-62.10	1.82	-69.10
0.50	-62.80	1.86	-69.30
0.60	-63.10	1.90	-69.40
0.70	-63.70	1.98	-69.70
0.80	-64.50	2.06	-70.00
0.91	-64.80	2.14	-70.10
0.94	-64.90	2.22	-70.30
0.98	-65.60	2.30	-70.80
1.02	-65.70	2.38	-71.00
1.06	-65.80	2.46	-71.10
1.10	-65.90	2.54	-71.30
1.14	-66.10	2.62	-71.50
1.18	-66.20	2.70	-71.80
1.22	-66.50	2.78	-71.90
1.26	-66.60	2.86	-72.10
1.28	-66.90	2.94	-72.30
1.32	-67.00	3.02	-72.50
1.36	-67.20	3.10	-72.50
1.42	-67.70	3.18	-72.70
1.46	-67.80	3.26	-73.00
1.50	-67.70	3.36	-73.00
1.54	-67.90	3.46	-73.20
1.58	-68.10	3.56	-73.50
1.62	-68.20	3.70	-73.70

Table B.11 *Experimental e.m.f. titration data obtained for the determination of the stability constant of* $[Cd\mathbf{6}]^{2+}$ *in DMF solution at 298.2 K and I = 0.050 M* NEt_4ClO_4.

titre (mL)	expt. e.m.f. (mV)	titre (mV)	expt. e.m.f. (mV)
0.00	-63.50	2.15	-69.10
0.14	-62.60	2.20	-69.20
0.24	-63.00	2.26	-69.50
0.34	-63.80	2.32	-69.70
0.44	-64.50	2.38	-69.70
0.54	-65.20	2.44	-69.90
0.64	-65.60	2.50	-70.00
0.74	-65.80	2.56	-70.20
0.84	-66.00	2.62	-70.30
0.88	-66.20	2.69	-70.80
0.92	-66.30	2.74	-71.00
0.96	-66.30	2.80	-71.20
1.02	-66.50	2.86	-71.30
1.06	-66.50	2.92	-71.40
1.10	-66.60	2.98	-72.80
1.14	-66.70	3.04	-73.00
1.18	-66.70	3.10	-73.10
1.24	-66.80	3.16	-73.20
1.30	-67.10	3.23	-73.50
1.36	-67.20	3.28	-73.70
1.42	-67.20	3.34	-74.00
1.49	-67.20	3.40	-74.20
1.54	-67.20	3.46	-74.10
1.60	-67.50	3.54	-74.50
1.66	-67.70	3.62	-75.00
1.72	-68.00	3.70	-75.40
1.78	-68.20	3.78	-75.60
1.84	-68.40	3.86	-76.00
1.90	-68.60	3.94	-76.20
1.96	-68.50	4.04	-76.40
2.02	-68.70	4.14	-76.80
2.08	-68.90		

References

1. Harrison, R. M.; Laxen, D. P. H. in *Lead Pollution, Causes and Control;* Chapman and Hall Ltd: London, 1981.

2. Ratcliffe, J. M. in *Lead in Man and the Environment;* Ellis Horwood Ltd: UK, 1981.

3. Barltrop, D. in *Poisoning: Diagnosis and Treatment;* Vale, J. A.; Meredith, T. J., Eds.; Update Books: New York, 1981.

4. Hamilton, A.; Hardy, H. L. in *Hamilton and Hardy's: Industrial Toxicology*; 4th Ed., John Wright PSG. Inc.: Massachusetts, 1983.

5. Mahaffey, K. R.; McKinney, J.; Reigart, J. R. in *Environmental Toxicants. Human Exposure and their Health Effects;* Van Nostrand Reinhold: New York, 1992; p 360.

6. Moore, J. W.; Ramamoorthy, S. in *Heavy Metals in Natural Waters. Applied Monitoring and Impact Assessment*; Springer-Verlag: New York, 1984.

7. Ho, T.-L. in *Hard and Soft Acids and Bases. Principle in Organic Chemistry;* Academic Press: London, 1977.

8. Pearson, R. G. *J. Am. Chem. Soc.* **1963**, *85*, 3533.

9. Pearson, R. G. in *Hard and Soft Acids and Bases;* John Wiley: New York, 1973.

10. Shriver, D. F.; Atkins, P.; Langford, C. H. in *Inorganic Chemistry;* 2nd Ed. W.H.Freeman and Company: New York, 1994; p 212.

11. Francis, B. M. in *Toxic Substances in the Environment*; John Wiley: New York, 1994.

12. Stubbs, R. L. in *Lead in the Environment;* Applied Science Publishers Ltd: UK, 1971.

13. White, J. M.; Harvey, D. R. *Nature* **1972**, *236*, 71.

14. Boggess, W. R.; Wixson, B. G. in *Lead in the Environment*; Castle House Publications, Ltd: London, 1979.

15. *Health and Environmental Lead in Australia;* Australian Academy of Science: Canberra, 1981.

16. Department of Health and Social Security in *Lead and Health*; Her Majesty's Stationary Office: London, 1980.

17. Abu-Dari, K.; Ekkehardt, H. F.; Raymond, K. N. *J. Am. Chem. Soc.* **1990**, *112*, 1519.

18. Vallee, B. L.; Ulmer, D. D., in *Biochemical Effects of Mercury, Cadmium and Lead;* John Wiley and Sons: New York, 1972.

19. Putnam, R. D. *Am. Ind. Hyg. Assoc. J* **1986**, *47*, 700.

20. Ochiai, E. -L. *Journal of Chemical Education* **1995**, *72*, 479.

21. McLaughlin, M. C. *New York J. Med.* **1956**, *56*, 3711.

22. Byers, R. K. *Pediatrics* **1959**, *23*, 559.

23. *Measuring Lead Exposure in Infants, Children and Other Sensitive Populations*; National Academy of Sciences: USA, 1993.

24. Needleman, H. L. in *Human Lead Exposure*; CRC Press Inc.: Florida., 1992.

25. Smith, M., in *The Lead Debate: The Environment, Toxicology and Child Health.;* Lansdown, R.;Yule, W., Eds.; Croom Helm Ltd: London, 1986.

26. Committee on Environmental Health *Pediatrics* **1993**, *92*, 176.

27. *Lead in Australian Children;* Australian Institute of Health and Welfare, 1996.

28. Needleman, H. L. *Science* **1985**, *227*, 701.

29. Hardy, H. L.; Bishop, R. C.; Maloof, C. C. *Arch. Ind. Hyg. Occup. Med.* **1951**, *3*, 267.

30. Abu-Dari, K.; Karpishin, T. B.; Raymond, K. N. *Inorg. Chem.* **1993**, *32*, 3052.

31. Wang, J. in *Stripping Analysis: Principles, Instrumentation and Application*; VCH Publishers: Weinheim, 1985.

32. Valenta, P.; Rutzel, H.; Nurnberg, H. W.; Stoeppler, M. Z. *Anal. Chem.* **1977**, *284*, 1.

33. Schroeder, H. A.; Nason, A. P. *Clin. Chem.* **1971**, *17*, 461.

34. Pinchin, M. J.; Newham, J. *Anal. Chim. Acta.* **1977**, *90*, 91.

35. Oehme, M. *Anal. Chem.* **1979**, *298*, 260.

36. Duic, L.; Szechter, S.; Srinivasan, S. *J. Electroanal. Chem.* **1973**, *41*, 83.

37. Morrell, G.; Giridhar, G. *Clin. Chem.* **1976**, *22*, 221.

38. Mason, W. T. in *Fluorescent and Luminescent Probes for Biological Activity;* Academic Press Ltd: London, 1993.

39. Fages, F.; Bodenant, B.; Weil, T. *J. Org. Chem.* **1996**, *61*, 3956.

40. Haugland, R. P. in *Handbook of Fluorescent Probes and Research Chemicals*; Molecular Probes: 1996.

41. Tsien, R. Y.; Minta, A.; Kao, J. P. Y. *J. Biol. Chem.* **1989**, *264*, 8171.

42. Tsien, R. Y.; Grynkiewicz, G.; Poenie, M. *J. Biol. Chem.* **1985**, *260*, 3440.

43. Tsien, R. Y. *Biochemistry* **1980**, *19*, 2396.

44. Czarnik, A. W. *Acc. Chem. Res.* **1994**, *27*, 302.

45. Morishima, Y.; Sato, T.; Kamachi, M. *Macromolecules* **1996**, *29*, 3960.

46. Andrianatoandro, H.; Barrans, Y.; Marsau, P. *Acta. Cryst.* **1995**, *B51*, 293.

47. Lehn, J.-M.; Fages, F.; Desvergne, J.-P.; Bouas-Laurent, H.; Marsau, P.; Kotzyba-Hilbert, F.; Albrecht-Gary, A.-M.; Al-Joubbeh, M. *J. Am. Chem. Soc* **1989**, *111*, 8672.

48. Sasaki, D. Y.; Schnek, D. R.; Pack, D. W.; Arnold, F. H. *Angew. Chem., Int. Ed. Engl.* **1995**, *34*, 905.

49. Bartsch, R. A.; Hallman, J. L.; Nabulsi, N. A. R.; Utterback, M. D.; Strzelbicka, B.; Porter, M. D.; Bastiaans, G. J.; Zak, J.; Vaidya, B. *Anal. Chem.* **1995**, *67*, 4101.

50. Fabbrizzi, L.; Licchelli, M.; Pallavicini, P.; Perotti, A.; Sacchi, D. *Angew. Chem., Int. Ed. Engl.* **1994**, *33*, 1975.

51. Czarnik, A. W.; Chae, M.-Y.; Cherian, X. M. *J. Org. Chem.* **1993**, *58*, 5797.

52. Czarnik, A. W.; Yoon, J.; Ohler, N. E.; Vance, D. H.; Aumiller, W. D. *Tetrahedron Letters* **1997**, *36*, 3845.

53. Lincoln, S. F.; Hendrickson, K. M.; Rodopoulous, T.; Pittet, P.-A.; Mahadevan, I.; Ward, A. D.; Kurucsev, T.; Duckworth, P. A.; Forbes, I. J.; Zalewski, P. D.; Betts, W. H. *J. Chem. Soc., Dalton Trans.* **1997**, 3879.

54. Tsien, R. Y. *Annu. Rev. Biophys. Bioeng.* **1983**, *12*, 91.

55. Tsien, R. Y.; Pozzan, T.; Rink, T. J. *Trends Biochem. Sci.* **1984**, 263.

56. Tsien, R. Y.; Pozzan, T.; Rink, T. J. *J. Cell Biol.* **1982**, *94*, 325.

57. Carron, K.; Crane, L. G.; Wang, D.; Sears, L. M.; Heyns, B. *Anal. Chem* **1995**, *67*, 360.

58. Kramer, R. *Angew. Chem., Int. Ed. Engl.* **1998**, *37*, 772.

59. Sammes, P. G.; Yahioglu, G. *Natural Product Reports* **1996**, 1.

60. Schneider, H.-J.; Durr, R. S. *Frontiers in Supramolecular Organic Chemistry and Photochemistry;* VCH publishers: Weinheim, 1991; p 29.

61. Kaim, W.; Schwederski, B. in *Bioinorganic Chemistry: Inorganic Elements in the Chemistry of Life*; Wiley: New York, 1994.

62. Vallee, B. L.; Auld, D. S. *Acc. Chem. Res.* **1993**, *26*, 543.

63. Fausto da Silva, J. J. R.; Williams, R. J. P. in *The Biological Chemistry of the Elements*; Oxford University Press: Oxford, 1992.

64. Vallee, B. L.; Auld, D. S. *Proc. Natl. Acad. Sci. USA* **1990**, *87*, 220.

65. Cunane, S. C. in *Zinc: Clinical and Biochemical Significance*; CRC Press: Boca Raton, Florida, 1988.

66. Williams, R. J. P. *Polyhedron* **1987**, *6*, 61.

67. Czarnik, A. W.; Huston, M. E.; Haider, K. W. *J. Am. Chem. Soc.* **1988**, *110*, 4460.

68. Dietrich, B.; Viout, P.; Lehn, J.-M. in *Macrocyclic Chemistry: Aspects of Organic and Inorganic Supramolecular Chemistry;* VCH Publishers: New York, 1993; p 203.

69. Lindoy, L. F. in *The Chemistry of Macrocyclic Ligand Complexes*; Cambridge University Press: Cambridge, 1989.

70. Boucher, L. J., in *Coordination Chemistry of Macrocyclic Compounds;* Melson, G. A., Ed.; Plenum Press: New York, 1979.

71. Gokel, G. in *Crown Ethers and Cryptands*; The Royal Society of Chemistry: Cambridge, 1991.

72. Hiraoka, M. in *Crown Compounds: Their Characteristics and Applications;* Elsevier Science Publishing: Amsterdam, 1982.

73. Cram, D. J.; Cram, J. M. in *Container Molecules and Their Guests*; The Royal Society of Chemistry: Cambridge, 1994.

74. Pederson, C. J. *J. Am. Chem. Soc.* **1967**, *89*, 7017.

75. Pederson, C. J. *J. Am. Chem. Soc.* **1967**, *89*, 2495.

76. Pedersen, C. J. *J. Org. Chem.* **1971**, *36*, 254.

77. Izatt, R. M.; Christensen, J. J.; Eatough, D. J. *Chem. Rev.* **1974**, *74*, 351.

78. Lehn, J.-M. *Structure and Bonding* **1973**, *16*, 1.

79. Frensdorff, H. K.; Pederson, C. J. *Angew. Chem., Int. Ed. Engl.* **1972**, *11*, 16.

80. Izatt, R. M.; Rytting, J. H.; Nelson, D. P.; Haymore, B. L.; Christensen, J. J. *J. Am. Chem. Soc.* **1971**, *93*, 1619.

81. Bradshaw, J. S.; Hui, J. Y. *J. Heterocyclic Chem.* **1974**, *11*, 649.

82. Lindoy, L. F. *Chem. Soc. Rev.* **1975**, *4*, 421.

83. Izatt, R. M.; Bradshaw, J. S.; Nielsen, S. A.; Lamb, J. D.; Christensen, J. J.; Sen, D. *Chem. Rev.* **1985**, *85*, 271.

84. Izatt, R. M.; Pawlak, K.; Bradshaw, J. S.; Bruening, R. L. *Chem. Rev.* **1991**, *91*, 1721.

85. Hancock, R. D.; Martell, A. E. *Chem. Rev.* **1989**, *89*, 1875.

86. Lindoy, L. F. *Chem. in Aust.* **1991**, *58*, 157.

87. Sousa, L. R.; Larson, J. M. *J. Am. Chem. Soc.* **1977**, *99*, 307.

88. Bouas-Laurent, H. J.; Lehn, J.-M.; Marsau, P.; Kotzyba-Hibert, F.; Desvergne, J.-P.; Fages, F.; Albrecht-Gary, A.-M.; Al-Joubbeh, M. *J. Am. Chem. Soc.* **1989**, *111*, 6872.

89. Bouas-Laurent, H. J.; Lehn, J.-M.; Konopelski, J. P.; Kotzyba-Hibert, F.; Desvergne, J.-P.; Fages, F.; Castellan, A. *J. Chem. Soc., Chem. Commun.* **1985**, 1709.

90. Wolfbeis, O. S.; Offenbacher, H. *Monatsch. Chem.* **1984**, *115*, 647.

91. de Silva, A. P.; de Silva, S. A. *J. Chem. Soc. Chem. Commun.* **1986**, 1709.

92. Street, K. W.; Krause, S. A. *Anal. Lett.* **1986**, *19*, 735.

93. Czarnik, A. W.; Huston, M. E.; Haider, K. W. *J. Am. Chem. Soc.* **1988**, *110*, 4460.

94. Hancock, R. D.; Bhavan, R.; Wade, P. W.; Boeyens-Jan, C. A.; Dobson, S. M. *Inorg. Chem.* **1989**, *28*, 187.

95. Lindoy, L. F. in *Synthesis of Macrocycles: The Design of Selective Complexing Agents. Progress in Macrocyclic Chemistry;* Izatt, R. M.; Christensen, J. J., Eds.; John Wiley and Sons: New York, 1987; p 53.

96. Stephen, W. I. in *The Determination of Trace Metals in Natural Waters*; Blackwell Scientific: Oxford, 1988.

97. Frensdorff, H. K. *J. Am. Chem. Soc.* **1971**, *93*, 600.

98. Hancock, R. D. *Pure & Appl. Chem.* **1986**, *58*, 1445.

99. Hancock, R. D.; Shaikjee, M. S.; Dobson, S. M.; Boeyens-Jan, C. A. *Inorg. Chim. Acta* **1988**, *154*, 229.

100. Alexander, V. *Chem. Rev.* **1995**, *95*, 281.

101. Hancock, R. D.; Damu, K. V.; Shaikjee, M. S.; Michael, J. P.; Howard, A. S. *Inorg. Chem.* **1986**, *25*, 3879.

102. Bradshaw, J. S.; Pastushok, V. N.; Bordunov, A. V.; Izatt, R. M. *J. Org. Chem* **1996**, *61*, 6888.

103. Hodgkinson, L. C.; Johnson, M. R.; Leigh, S. J.; Spencer, N.; Sutherland, I. O. *J. Chem. Soc., Perkin Trans. I* **1979**, 2193.

104. Hogberg, S. A. G.; Cram, D. J. *J. Org. Chem.* **1975**, *40*, 151.

105. Newkome, G. R.; Robinson, J. M. *J. Chem. Soc. Chem. Comm.* **1973**, 831.

106. Amabilino, D. B.; Preece, J. A.; Stoddart, J. F. in *Macrocyclic Synthesis: A Practical Approach;* Parker, D.; Harwood, L. M.;Moody, C. J., Eds.; Oxford University Press: New York, 1996 .

107. Perry, J. J. B.; Kilburn, J. D. in *Synthetic Developments in Host-Guest Chemistry*; 4th. Ed.; Vol. 1; John Wiley: New York, 1994.

108. Curtis, N. F.; Curtis, Y. M.; Powell, H. K. J. *J. Chem. Soc.* **1966**, 1015.

109. Curtis, N. F. *J. Chem. Soc.* **1960**, 4409.

110. Anderson, S.; Anderson, H. L.; Sanders, J. M. *Acc. Chem. Res.* **1993**, *26*, 469.

111. Shimamoto, T.; Ishikawa, M.; Ishikawa, H.; Inoue, M. *Chem. Abs.* **1968**, *68*, 2810.

112. Kyba, E. P. *J. Am. Chem. Soc.* **1977**, *99*, 2564.

113. Greene, T. W.; Wuts, P. G. M. in *Protective Groups in Organic Synthesis*; John Wiley: New York, 1991.

114. Kemp, W. in *Organic Spectroscopy*; The Macmillan Press: London, 1975.

115. Bradshaw, J. S.; Krakowiak, K. E.; Maas, G. E.; Hathaway, J. K.; Izatt, R. M. *J. Heterocyclic Chem.* **1995**, *32*, 179.

116. Bartsch, R. A.; Chapoteau, E.; Czech, B. P.; Krzykawski, J.; Kumar, A.; Robison, T. W. *J. Org. Chem.* **1993**, *58*, 4681.

117. Closson, W. D.; Wriede, P.; Bank, S. *J. Am. Chem. Soc.* **1966**, *88*, 1581.

118. Ji, S.; Gortler, L. B.; Waring, A.; Battisti, A.; Sank, S.; Closson, W. D. *J. Am. Chem. Soc.* **1967**, *89*, 5311.

119. Landini, D.; Montanari, F.; Rolla, F. *Synthesis* **1978**, 223.

120. Hodgkinson, L. C.; Sutherland, I. O. *J. Chem. Soc. Perkin Trans I* **1979**, 1908.

121. Rolla, F. *J. Org. Chem.* **1982**, *47*, 4327.

122. Martell, A. E.; Montekaitis, R. J. in *The Determination and Use of Stability Constants*; VCH Publishers: New York, 1988.

123. Izatt, R. M.; Rytting, J. H.; Nelson, D. P.; Haymore, B. L.; Christensen, J. J. *Science* **1969**, *164*, 443.

124. Izatt, R. M.; Christen, J. J. in *Synthetic Multidentate Macrocyclic Compounds*; Academic Press: 1978.

125. Wong, K. H.; Koniser, G.; Smid, J. *J. Am. Chem. Soc.* **1970**, *92*, 666.

126. Pederson, C. J. *Aldrichim. Acta.* **1971**, *4*, 1.

127. Buschmann, H.-J. *J. Solution Chem.* **1986**, *15*, 453.

128. Buschmann, H.-J. *Inorg. Chim. Acta.* **1992**, *195*, 91.

129. Buschmann, H.-J.; Benken, R. *Inorg. Chim. Acta.* **1987**, *134*, 49.

130. Cox, B. G.; Firman, P.; Horst, H.; Schneider, H. *Polyhedron* **1983**, *2*, 343.

131. Arnold, K. A.; Gokel, G. W. *J. Org. Chem.* **1986**, *51*, 5015.

132. Nakamura, T.; Yumoto, Y.; Izutsu, K. *Bull. Chem. Soc. Jpn.* **1982**, *55*, 1850.

133. Buschmann, H. J. *Inorg. Chim. Acta.* **1986**, *120*, 125.

134. Gatto, V. J.; Arnold, K. A.; Viscariello, A. M.; Miller, S. R.; Morgan, C. R.; Gokel, G. W. *J. Org. Chem.* **1986**, *51*, 5373.

135. Gokel, G. W.; White, B. D.; Arnold, K. A. *Tetrahedron Lett.* **1987**, *28*, 1749.

136. Gokel, G. W.; Arnold, K. A.; Echegoyen, L.; Fronczek, F. R.; Gandour, R. D.; Gatto, V. J.; White, B. D. *J. Amer. Chem. Soc.* **1987**, *109*, 3716.

137. Cahen, Y. M.; Dye, J. L.; Popov, A. I. *J. Phys. Chem.* **1975**, *79*, 1289.

138. Mei, E.; Liu, L.; Dye, J. L.; Popov, A. I. *J. Solution Chem.* **1977**, *6*, 771.

139. Popov, A. I.; Shamsipur, M. *Inorg. Chim. Acta.* **1980**, *43*, 243.

140. Popov, A. I.; Lee, Y. C.; Allison, J. *Polyhedron* **1985**, *4*, 441.

141. Lagrange, J.; Metabanzoulou, J. P.; Fux, P.; Lagrange, P. *Polyhedron* **1989**, *8*, 2251.

142. Cazaux, L.; Duriez, M. C.; Picard, C.; Tisnes, P. *Tetrahedron Lett.* **1989**, *30*, 1369.

143. Valente, J. V. Ph.D. Thesis, *Synthetic studies towards potential lead(II) specfic fluorescent probes;* The University of Adelaide, 1998.

144. Chen, L.; Bos, M.; Grootenhuis, P. D. J.; Christenhusz, A.; Hoogendam, E.; Reinhoudt, D. N.; van der Linden, W. E. *Anal. Chim. Acta.* **1987**, *201*, 117.

145. Takeda, Y.; Katsuta, K.; Inoue, Y.; Hakushi, T. *Bull. Chem. Soc. Jpn.* **1988**, *61*, 627.

146. Zollinger, D. P.; Bulten, E.; Christenhusz, A.; Bos, M.; van der Linden, W. E. *Anal. Chim. Acta.* **1987**, *198*, 207.

147. Lehn, J.-M.; Sauvage, J.-P. *J. Chem. Soc., Chem. Commun.* **1971**, 440.

148. Clarke, P.; Gulbis, J. M.; Lincoln, S. F.; Tiekink, E. R. T. *Inorg. Chem.* **1992**, *31*, 3398.

149. Lehn, J.-M.; Sauvage, J.-P. *J. Am. Chem. Soc* **1975**, *97*, 6700.

150. Lindoy, L. F.; Adam, K. R.; Leong, A. J.; Hendry, P.; Smith, S. V.; Yellowless, D. J. *J. Coord. Chem.* **1988**, *19*, 189.

151. Delgado, R.; Siegfried, L. C.; Kaden, T. A. *Helv. Chim. Acta.* **1990**, *73*, 140.

152. Chang, C. A.; Chang, P. H. L.; Manachanda, V. K.; Kasprzyk, S. P. *Inorg. Chem.* **1988**, *27*, 3786.

153. Lee, E. L.; Gansow, O. A.; Weaver, M. J. *J. Am. Chem. Soc.* **1980**, *102*, 2278.

154. Stroka, J.; Cox, B. G.; Schneider, H. *J. Electroanal. Chem.* **1989**, *266*, 337.

155. Johnstone, R. A. W.; Lewis, I. A. S. *Int. J. Mass Spectrom.* **1983**, *46*, 451.

156. Johnstone, R. A. W.; Lewis, I. A. S. *J. Chem. Soc., Chem. Commun.* **1984**, 1268.

157. Young, D. S.; Hung, H. Y.; Liu, L. K. *Rapid Commun. Mass Spectrom.* **1997**, 11, 769.

158. Bonas, G.; Bosso, C.; Vignon, M. R. *J. Inclusion Phenom. Mol. Recognit. Chem.* **1989**, *7*, 637.

159. Man, V. F.; Lin, J. D. *J. Am. Chem. Soc.* **1985**, *107*, 4635.

160. Rodopoulous, T. Ph.D. Thesis, *An Equilibrium and Kinetic Study of Cryptand, Lariat Ether and Fluorescent Zinc(II) Complexes;* The University of Adelaide, 1993.

161. Clarke, P. Ph.D. Thesis, *STAB program*, The University of Adelaide, 1992.

162. Rossotti, F. J. C.; Rossotti, H. in *The Determination of Stability Constants*; McGraw-Hill: New York, 1961.

163. Kulstad, S.; Malmsten, L. A. *J. Inorg. Nucl. Chem.* **1981**, *43*, 1299.

164. Izutsu, K.; Ito, M.; Sarai, E. *Anal. Sci.* **1985**, *1*, 341.

165. Cotton, F. A.; Wilkinson, G. in *Advanced Inorganic Chemistry*; 3rd Ed.; Interscience: New York, 1980.

166. Lucas, J. Ph.D. Thesis, *Reaction Dynamics of Some Pendant Arm Macrocycles;* The University of Adelaide, 1994.

167. Shannon, R. D. *Acta. Cryst.* **1976**, *A32*, 751.

168. Bradshaw, J. S.; Bordunov, A. V.; Hellier, P. C.; Dalley, N. K.; Kou, X.; Zhang, X. X.; Izatt, R. M. *J. Org. Chem.* **1995**, *60*, 6097.

169. Hancock, R. D.; Bhavan, R.; Shaikjee, M. S.; Wade, P. W.; Hearn, A. *Inorg. Chim. Acta.* **1986**, *112*, L23.

170. Spiess, B.; Arnaud-Neu, F.; Schwing-Weill, M. J. *J. Helv. Chim. Acta.* **1980**, *63*, 2287.

171. Buschmann, H. J. *Inorg. Chim. Acta.* **1985**, *98*, 43.

172. Gutmann, V. in *Coordination Chemistry in Non-Aqueous Systems;* Springer-Verlag: Vienna, 1968.

173. Gutmann, V.; Wychera, E. *Inorg. Nucl. Chem. Lett.* **1966**, 2, 257.

174. Popov, A. I.; DeWitte, W. J. *J. Solution Chem.* **1976**, *5*, 231.

175. Popov, A. I.; Erlich, R. H.; Roach, E. *J. Am. Chem. Soc.* **1970**, *92*, 4989.

176. Lincoln, S. F.; Abou-Hamdan, A. *Inorg. Chem.* **1991**, *30*, 462.

177. Lincoln, S. F.; Abou-Hamdan, A. *Inorg. Chem.* **1990**, *29*, 3584.

178. Lincoln, S. F.; Brereton, I. M.; Spotswood, T. M. *J. Am. Chem. Soc.* **1986**, *108*, 8134.

179. Chang, C. A.; Rowland, M. E. *J. Am. Chem. Soc.* **1983**, *22*, 3866.

180. Kappes, M. M.; Stanley, R. H. *J. Am. Chem. Soc.* **1982**, *104*, 1819.

181. Kappes, M. M.; Stanley, R. H. *J. Am. Chem. Soc.* **1982**, *104*, 1813.

182. Munson, M. S. B. *J. Am. Chem. Soc.* **1965**, *87*, 2332.

183. Christensen, J. J.; Dalley, N. K.; Larson, S. B.; Smith, J. S.; Matheson, K. L.; Izatt, R. M. *J. Heterocyclic Chem.* **1981**, *18*, 463.

184. Dalley, N. K.; Smith, J. S.; Larson, S. B.; Matheson, K. L.; Christensen, J. J.; Izatt, R. M. *J. Chem. Soc., Chem. Commun.* **1975**, 84.

185. Hancock, R. D.; McDougall, G. J. *J. Am. Chem. Soc.* **1980**, *102*, 6551.

186. Wang, K.; Han, X.; Gross, R. W.; Gokel, G. W. *J. Am. Chem. Soc.* **1995**, *117*, 7680.

187. Wang, K.; Gokel, G. W. *J. Org. Chem.* **1996**, *61*, 4693.

188. Johnstone, R. A. W.; Rose, M. E. *J. Chem. Soc., Chem. Commun.* **1983**, 1268.

189. Johnstone, R. A. W.; Lewis, I. A. S.; Rose, M. E. *Tetrahedron* **1983**, *39*, 1597.

190. Brodbelt, J. S.; Liou, C.-C. *J. Am. Soc. Mass Spectrom.* **1992**, *3*, 543.

191. Colton, R.; Mitchell, S.; Traeger, J. C. *Inorg. Chim. Acta* **1995**, *231*, 87.

192. Dearden, D. V.; Leming, S.; Chu, I.-H.; Zhang, H. *J. Am. Chem. Soc.* **1991**, *113*, 7415.

193. Brodbelt, J. S.; Maleknia, S. *J. Am. Chem. Soc.* **1992**, *114*, 4295.

194. Brodbelt, J. S.; Wu, H.-F. *J. Am. Chem. Soc.* **1994**, *116*, 6418.

195. Bowers, M. T.; Wyttenbach, v. H., G.; Lee, S. *J. Am. Chem. Soc.* **1995**, *117*, 10159.

196. Grossel, M. C.; Hamilton, D. G.; Langley, G. J. *J. Chem. Soc., Perkin Trans.* **1995**, 2, 929.

197. Wang, G.; Cole, R. B. *Org. Mass Spectrom.* **1994**, *29*, 419.

198. Gaskell, S. J. *J. Mass Spectrom.* **1997**, *32*, 677.

199. Kebarle, P.; Tang, L. *Anal. Chem.* **1993**, *65*, 972A.

200. Fenn, J. B. *J. Am. Soc. Mass Spectrom.* **1993**, *4*, 524.

201. Iribarne, J. V.; Thompson, B. A. *J. Chem. Phys.* **1976**, *64*, 2287.

202. Iribarne, J. V.; Thompson, B. A. *J. Chem. Phys.* **1979**, *71*, 4451.

203. Emsley, J. in *The Elements*; Oxford University Press Inc.: New York, 1998.

204. Lincoln, S. F.; May, B. *Personal communication.*

205. Foresman, J. B.; Frisch, A. in *Exploring Chemistry with Electronic Structure Methods: A Guide to Using Gaussian.*; 2nd Ed.; Gaussian Inc.: Pittsburgh, 1993.

206. Frisch, M. J.; Trucks, G. W.; Schlegel, H. B.; Gill, P. M. W.; Johnson, B. G.; Robb, M. A.; Cheeseman, J. R.; Keith, T.; Petersson, G. A.; Montgomery, J. A.; Raghavachari, K.; Al-Laham, M. A.; Zakrzewski, V. G.; Ortiz, J. V.; Foresman, J. B.; Cioslowski, J.; Stefanov, B. B.; Nanayakkara, A.; Challacombe, M.; Peng, C. Y.; Ayala, P. Y.; Chen, W.; Wong, M. W.; Andres, J. L.; Replogle, E. S.; Gomperts, R.; Martin, R. L.; Fox, D. J.; Binkley, J. S.; Defrees, D. J.; Baker, J.; Stewart, J. P.; Head-Gordon, M.; Gonzalez, C.; Pople, J. A. *Gaussian 94;* Revision D.3, Pittsburgh, PA, 1995.

207. Grant, G. H.; Richards, W. G. in *Computational Chemistry*; Oxford University Press: Oxford, 1995.

208. Hehre, W. J.; Radom, L.; Schleyer, P. R.; Pople, J. A. in *Ab initio Molecular Orbital Theory*; John Wiley: New York, 1986.

209. *MacSpartan Plus: Tutorial and User's Guide*; Wavefunction: California, 1996.

210. Mackay, K. M.; Mackay, R. A. in *Introduction to Modern Inorganic Chemistry*; 4th Ed.; Prentice-Hall: New Jersey, 1989.

211. West, A. R. in *Basic Solid State Chemistry*; John Wiley: New York, 1984.

212. Orpen, A. G.; Brammer, L.; Allen, F. H.; Kennard, O.; Watson, D. G.; Taylor, R. *J. Chem. Soc., Dalton Trans.* **1989**, S1.

213. Jones, P. G.; Gries, T.; Grutzmacher, H.; Roesky, H. W.; Schimkowiak, J.; Sheldrick, G. M. *Angew. Chem., Int. Ed. Engl.* **1984**, *23*, 376.

214. Still, W.; Kahn, M.; Mitra, A. *J. Org. Chem* **1978**, *43*, 2923.

215. Perrin, D. D.; Armarego, W. L. F.; Perrin, D. R. in *Purification of Laboratory Chemicals; 3rd ed.*; Pergamon Press: Oxford, 1988.

216. Wenner *J. Org. Chem.* **1952**, *17*, 523.

217. Lin, W. O.; Altoe, A. P. *Monatsh. Chem.*, **1982**, *113*, 101.